NASA Technical Paper 3628

Static Investigation of a Multiaxis Thrust-Vectoring Nozzle With Variable Internal Contouring Ability

David J. Wing, Charles T. L. Mills, and Mary L. Mason
Langley Research Center • Hampton, Virginia

National Aeronautics and Space Administration
Langley Research Center • Hampton, Virginia 23681-0001

June 1997

Acknowledgments

The research presented in this report is the result of a cooperative effort of Pratt & Whitney, Government Engines & Space Propulsion, United Technologies Corporation; Lockheed Martin Tactical Aircraft Systems (formerly Lockheed Aeronautical Systems Company); and the Langley Research Center. The design and development of the nozzle concept and test hardware were performed by Pratt & Whitney. Additional engineering and test support was provided by Lockheed Martin.

Available electronically at the following URL address: http://techreports.larc.nasa.gov/ltrs/ltrs.html

Printed copies available from the following:

NASA Center for AeroSpace Information
800 Elkridge Landing Road
Linthicum Heights, MD 21090-2934
(301) 621-0390

National Technical Information Service (NTIS)
5285 Port Royal Road
Springfield, VA 22161-2171
(703) 487-4650

Summary

The thrust efficiency and vectoring performance of a convergent-divergent nozzle were investigated at static conditions in the model preparation area of the Langley 16-Foot Transonic Tunnel. The diamond-shaped nozzle was capable of varying the internal contour of each quadrant individually by using cam mechanisms and retractable drawers to produce pitch and yaw thrust vectoring. Pitch thrust vectoring was achieved by either retracting the lower drawers to incline the throat or varying the internal flow-path contours to incline the throat. Yaw thrust vectoring was achieved by reducing flow area left of the nozzle centerline and increasing flow area right of the nozzle centerline; a skewed throat deflected the flow in the lateral direction.

The peak thrust efficiency of the unvectored nozzle was approximately 1 to 2 percent lower than that of most high-performance exhaust nozzles. Losses were attributed to underexpanded flow conditions near the nozzle centerline and recirculation regions near the sidewalls. Pitch thrust vectoring was limited in magnitude and unfavorable in its performance trend in that low thrust-vector angles occurred at the lower pressure ratios typical of high-performance maneuvers. Yaw thrust-vector angles of nearly 11° were achieved at low pressure ratios. Yaw thrust-vector angle decreased as nozzle pressure ratio was increased and sometimes reversed direction at higher pressure ratios.

Introduction

An extensive effort has been underway to develop a database of convergent-divergent nozzle designs for advanced aircraft engines. The joint effort by industry and the Langley Research Center has generally been oriented toward providing multifunctional capabilities to nozzles such as variable throat and exit areas, single or multiaxis thrust vectoring, and thrust reversing. Simultaneously, an attempt has been made to minimize any adverse impact on the overall aircraft by maintaining high cruise thrust efficiency and to provide suitable airframe integration characteristics by minimizing nozzle system weight and blending with the aerodynamic external lines.

The means by which the aforementioned parameters are varied have covered a wide range of concepts. Some of these concepts are depicted conceptually in figure 1. The axisymmetric nozzle typically achieves throat area control with a set of hydraulic piston actuators distributed around the nozzle and tied to both the convergent and divergent surfaces (a set of overlapping leaves). Thrust vectoring of axisymmetric nozzles can be achieved by a hydraulically driven synchronization ring attached to the divergent flaps (refs. 1 and 2) or by a gimbal mechanism (ref. 3). The nonaxisymmetric or two-dimensional nozzle (not shown in fig. 1) typically has hydraulic piston actuators attached individually to hinged convergent and divergent surfaces to allow independent control of throat and exit areas. This arrangement also permits synchronized deflection of divergent flaps for providing thrust vectoring (ref. 4). Many other concepts for thrust vectoring that have been studied include postexit vanes (refs. 5 and 6), deployable deflectors imbedded in the divergent flaps (ref. 7), and skewed-throat hinge lines (ref. 8). Through these and other studies, it has been learned that significant thrust vectoring with minimal thrust losses is best achieved by subsonic flow turning. Skewing the minimum area plane (forcing the aerodynamic throat to form at an oblique angle to the nozzle thrust axis) was found to be an effective means of achieving subsonic flow turning (ref. 8). Development of this concept has resulted in axisymmetric and rectangular nozzle designs which can provide pitch and yaw thrust vectoring in either direction by using the skewed-throat technique.

The current investigation examines a new multiaxis thrust-vectoring nozzle concept based on this skewed-throat technique. The concept is referred to as the "variable internal contour (VIC) nozzle," and the design is intended to provide multiaxis thrust vectoring with relatively low losses in thrust efficiency to a nozzle with advanced airframe integration characteristics.

The convergent-divergent VIC nozzle concept has the ability to vary its internal contour to promote pitch or yaw thrust vectoring. It can transition between dry power and afterburning power settings (i.e., vary the throat, or minimum flow, area) by the translation of nozzle components along inclined planes. This translation feature can also be used to generate thrust vectoring. The internal contouring and translation features are presented in more detail in the section "Nozzle Conceptual Design and Model Description." The nozzle incorporates a diamond cross section and scarfed trailing edges; this allows better integration with most advanced airframe afterbodies than nozzles with axisymmetric or rectangular cross sections. This multiaxis thrust-vectoring nozzle concept represents a new mechanical technique for achieving throat area and thrust-vectoring control.

The purpose of this investigation was to evaluate at static conditions (no external flow) the thrust efficiency of the unvectored VIC nozzle concept and the vectoring performance and the impact of vectoring on thrust efficiency for two pitch thrust-vectoring techniques and one yaw thrust-vectoring technique. Two basic nozzle trailing-edge geometries were also studied. Nozzle pressure ratio (NPR) was varied from 2 to as high as 10 in

some configurations. Measurements of three components of force and internal static pressure distributions were obtained at each test condition. A surface flow visualization technique was used to aid in analyzing the flow field.

Symbols

D_l lower drawer position (retracted, partial, extended)

D_u upper drawer position (retracted, partial, extended)

F_A measured axial-force component, lb

F_i ideal isentropic thrust,

$$w_p\sqrt{\frac{R_j T_{t,j}}{g^2}\frac{2\gamma}{\gamma-1}\left[1-\left(\frac{p_a}{p_{t,j}}\right)^{(\gamma-1)/\gamma}\right]},\ \text{lb}$$

F_N measured normal-force component, positive upward, lb

F_r resultant gross thrust, $\sqrt{F_A^2+F_N^2+F_S^2}$, lb

F_r/F_i resultant thrust ratio

F_S measured side-force component, positive to right, lb

g gravitational acceleration, 32.174 ft/sec^2

h_{peak} peak height of throat insert on inboard (nozzle centerline) face, in. (see fig. 6(b))

I_{ll} lower left throat insert identification number (see table in fig. 6(b) for throat insert identification numbers)

I_{lr} lower right throat insert identification number (see table in fig. 6(b))

I_{ul} upper left throat insert identification number (see table in fig. 6(b))

I_{ur} upper right throat insert identification number (see table in fig. 6(b))

L length of nozzle with no drawer retraction, 7.875 in. (see figs. 5 and 10)

NPR nozzle pressure ratio, $\frac{p_{t,j}}{p_a}$

p internal static pressure, psi

p_a atmospheric pressure, psi

$p_{t,j}$ jet total pressure, psi

R_j gas constant for air ($\gamma = 1.3997$), 1716 ft^2/sec^2-°R

$T_{t,j}$ jet total temperature, °R

w width of nozzle aft of transition section, 5.130 in.

w_p measured air weight-flow rate, lb/sec

x distance downstream from transition section, in. (see fig. 5)

x_{peak} longitudinal distance from upstream face of throat insert to ridge line, measured on inboard face (nozzle centerline), in. (see fig. 6(b))

y lateral distance from nozzle centerline, in.

δ_p resultant pitch thrust-vector angle, positive downward, $\tan^{-1}\frac{F_N}{F_A}$, deg

δ_y resultant yaw thrust-vector angle, positive to left, $\tan^{-1}\frac{F_S}{F_A}$, deg

γ ratio of specific heats, 1.3997 for air

Abbreviations:

a.h. arrowhead

2D two-dimensional

CD convergent-divergent

Ext. extended

I configuration designation for interfairing installed (e.g., configuration 1-I is configuration 1 with the interfairing installed)

I-F interfairing installation

LL lower left (nozzle quadrant)

LR lower right (nozzle quadrant)

Par. partial

Ret. retracted

sta. model station, in.

s.t. swallowtail

T.E. trailing-edge geometry

T.S. throat strip installed

UL upper left (nozzle quadrant)

UR upper right (nozzle quadrant)

VIC variable internal contour

WL water line, in.

Apparatus and Procedures

Test Facility

The test was performed in the model preparation area of the Langley 16-Foot Transonic Tunnel, an area normally used for model setup and calibration before entrance into the wind tunnel. The model preparation area has a high-pressure air supply and a data acquisition system; therefore, it is occasionally used to test the internal performance of nozzles at wind-off conditions.

The air system uses the same supply of clean, dry air used in the wind tunnel propulsion simulations and the same valves, filters, and heat exchanger to provide air at a constant total temperature of about 530°R. The model was mounted on a sting-strut support system in a soundproof room with an air exhaust collector duct downstream of the jet. The control room is adjacent to the test area, and a window between the rooms allows for model observation during testing. Reference 9 provides further details of the facility.

Single-Engine Propulsion Simulation System

A sketch of the air-powered, single-engine propulsion simulation system on which the nozzle configurations were statically tested is presented in figure 2. The propulsion simulation system is shown with a typical nozzle configuration installed. As shown in figure 2, air is supplied through six lines in the support strut to an annular nonmetric (not supported by the force balance) high-pressure plenum. The air flows radially out the high-pressure plenum through eight equally spaced sonic nozzles into a metric low-pressure plenum. This nonmetric-to-metric flow transfer design (perpendicular to the nozzle axis) minimizes the tare force on the balance caused by axial momentum transfer of the flow across the force balance. Flexible bellows act as seals between the metric and nonmetric portions of the model and minimize forces caused by pressurization. The air passes through a choke plate for flow straightening, through an instrumentation section, through a circular-to-rectangular transition section, and into the nozzle; the air then exhausts to atmospheric pressure.

Nozzle Conceptual Design and Model Description

The variable internal contour (VIC) nozzle is a convergent-divergent nozzle with three-dimensional internal geometry. Photographs of some of the model configurations are shown in figures 3 and 4. Sketches of the nozzle geometry are shown in figure 5. When configured for unvectored thrust, the nozzle is symmetric about the vertical and horizontal planes. The cross-sectional shape of the nozzle is rectangular at the entrance station (sta. 44.589, downstream of the circular-to-rectangular transition section, fig. 2) and changes to diamond shaped or hexagonal, depending on the configuration, in the converging section; a diamond or hexagonal cross section is then maintained to the nozzle exit.

The geometric throat is formed by ridges in each quadrant which are oriented, when viewed as a group in planform, in a vee with a forward-pointing vertex and a 60° half-angle. (See throat ridge lines in fig. 5, view A-A.) The contour of the ridge (referred to hereafter as “the throat ridge”) and the surrounding converging and diverging surfaces are smooth and continuous, and the throat ridge (i.e., contour peak) height of each quadrant can be varied independently. In the full-scale, operational nozzle concept, these throat ridges are formed by cams supporting flexible skins, as shown in figure 6(a). The throat ridge height and axial position are controlled by rotating the cam. For the model used in this test, interchangeable, solid throat inserts were used to simulate the cam mechanism. Combinations of five throat inserts with different throat ridge heights, shown in figure 6(b), were used in this test. As can be seen in the figure, longitudinal location of the throat ridge was varied with throat ridge height to simulate a cam operation. During the test, a set of 1/8-in-diameter half-round rods referred to as “throat strips” were installed along the throat ridges of inserts 1 and 2 on some configurations as a means for potentially improving the thrust-vectoring performance. Photographs of inserts with the throat strips installed are shown in figure **7**. More detailed information on the reasons for installing these throat strips can be found in the section “Discussion of Results.”

Two concepts for pitch thrust vectoring were studied and are depicted in figure 8. The concept in figure 8(a) takes advantage of the longitudinal throat ridge translation when the ridge height is changed. The throat ridge on the lower half is higher and therefore farther forward than the throat ridge on the upper half. This concept is based on the assumption that the aerodynamic throat will still form between the upper and lower ridges and will therefore be deflected as shown in the sketch. It would be necessary in such a concept to balance the changes in upper and lower ridge heights such that the total flow area seen by the engine remains constant so that the engine operation is not adversely impacted.

The second concept, shown in figure 8(b), takes advantage of the fact that the upper and lower halves of the nozzle are mounted on inclined planes on the transition section; translation of either the upper or lower half along these planes results in the throat ridges moving forward and apart from their counterparts on the opposite half. The full-scale concept for this translation is the retraction of drawers into the bulkhead of the transition section; on the model, exchangeable spacer blocks referred to as “drawers” are used to simulate this retraction. As shown in figure 8(b), the lower half of the nozzle is translated forward along the inclined plane relative to the upper half to produce pitch thrust vectoring. This thrust-vectoring concept is also based on the assumption that the aerodynamic throat will still form between the upper and lower pairs of ridges; this results in a deflected throat and therefore pitch thrust vectoring. Once again, maintaining constant total flow area for the engine is necessary for full-scale application, although this

consideration was not modeled for the test of this nozzle concept.

The concept for yaw thrust vectoring is shown in figure 9. By increasing the height of the left-side (as shown) throat ridges, the flow area on that side is reduced, and the reduction forces most of the flow to pass through the right-side throat. As a result of the vee throat-ridge orientation, the right-side throat is skewed such that the flow should be turned to the left, thus resulting in positive yaw thrust vectoring (side force to the right). The translation concept of nozzle quadrants used for pitch thrust vectoring was not investigated for yaw thrust vectoring.

As shown in figure 10, simultaneous forward translation of the upper and lower nozzle halves results in an increase in geometric throat area (corresponding to an increase in power setting) as the throat ridges move apart. The nozzle exit cross-sectional geometry becomes hexagonal as the flat sidewalls are exposed to the exhaust flow. Three drawer positions—extended (no retraction), partial retraction, and full retraction—were tested to simulate dry power, partial afterburning power, and full afterburning power modes of operation. Typical dry power configurations are shown in figures 3(b) and 4(c). Typical full afterburning power configurations are shown in figures 3(f) and 4(f).

As shown in figure 5, two geometries of the nozzle exit trailing edges were tested and are referred to as the "swallowtail" and "arrowhead" configurations. The trailing edge of the arrowhead configuration forms a vee with an aft-pointing vertex. The trailing edge of the swallowtail configuration has the opposite orientation, a vee with a forward-pointing vertex. The swallowtail sidewalls completely contain the flow in the lateral direction; the forward-pointing vee of the upper and lower flap trailing edge provides ventilation for the flow in the vertical direction. (See fig. 5(a).) Conversely, the arrowhead configuration contains the flow in the vertical direction and allows ventilation in the lateral direction. (See fig. 5(b).) The trailing-edge pieces begin aft of the throat inserts, and their surfaces are neither divergent nor convergent (i.e., parallel to the nozzle centerline). The sidewalls of both configurations are also scarfed and terminate at the trailing edge (i.e., the sidewalls for the swallowtail and arrowhead configurations are of different lengths). However, the sidewalls are not exposed to the flow downstream of the throat ridge line unless some or all drawers are retracted.

Some configurations were tested with an additional external component installed that represents part of the interfairing which would likely be present in a twin-engine installation. This interfairing was attached to the left sidewall and can be seen in several of the photographs of figures 3 and 4. (For example, see fig. 3(e).) A description of all configurations is presented in table 1.

Instrumentation

A six-component strain-gauge balance was used to measure forces and moments on the model; the moment data are not included in this report but were used for balance-interactions corrections. Jet total pressure was calculated by averaging total pressure measurements from nine individual pitot probes located at a fixed station in the instrumentation section. (See fig. 2.) A thermocouple was also positioned in the instrumentation section to measure jet total temperature. The weight-flow rate w_p of the high-pressure air supplied to the nozzle was measured by a multiple critical venturi located in the air system upstream of the model.

The internal surface static pressure distribution was measured for each test configuration. Each nozzle quadrant was instrumented with five rows of pressure orifices oriented longitudinally. Additionally, one sidewall was instrumented with orifices on the centerline. Representative locations of static pressure orifices are shown in figure 11 and detailed locations are tabulated in table 2. The x/L location of each pressure measurement is given for five constant span locations ($y/(w/2)$ = 0.058, 0.275, 0.491, 0.708, and 0.924) where $y/(w/2)$ is the span location normalized by the nozzle half-width.

Data Reduction

Every data point used in the computations was the average of 50 frames of data recorded at a rate of 10 frames/sec. With the exception of resultant gross thrust F_r, all thrust data in this report are referenced to the model centerline. Four basic performance parameters are used in the presentation of results: resultant thrust ratio F_r/F_i, axial thrust ratio F_A/F_i, resultant pitch thrust-vector angle δ_p, and resultant yaw thrust-vector angle δ_y. Reference 10 presents a detailed description of the data reduction procedures used for the current investigation.

The resultant thrust ratio F_r/F_i, the resultant gross thrust divided by the ideal isentropic thrust, is used as a measure of nozzle thrust efficiency. Resultant gross thrust is obtained from the axial, normal, and side components of the jet thrust measured by the force balance. (See section "Symbols.") Ideal isentropic thrust F_i is based on measured air weight-flow rate w_p, jet total pressure $p_{t,j}$, and jet total temperature $T_{t,j}$ and assumes fully expanded isentropic flow. (See section "Symbols" for the equation.)

The axial thrust ratio F_A/F_i is the ratio of the measured nozzle thrust along the model centerline to the ideal nozzle thrust. As can be seen from the definitions of

F_A and F_r, the thrust F_A along the model centerline reflects the geometric loss that results from turning the thrust vector away from the axial direction; the resultant gross thrust F_r does not.

The angles δ_p and δ_y are the calculated angles in the pitch and yaw thrust-vector planes at which the resultant gross thrust is deflected from the nozzle axis. As indicated in the section "Symbols," these angles are calculated from the measured normal, side, and axial forces produced by the jet and would increase with either an increase in normal or side force or a decrease in axial force.

Corrections were applied to all balance measurements before they were entered in the calculation of performance parameters. Each balance component was initially corrected for model weight tares and isolated balance interactions. Because the bellows (fig. 2) create a restraint on the installed balance, the balance was recalibrated after installation in the model and corrections resulting from additional component interactions were computed. Besides providing a set of assembly interaction corrections, the recalibration also accounts for the effects of pressurization (nozzle pressure ratio) and momentum (weight flow). The bellows in the air pressurization system were designed to eliminate pressure and momentum interactions with the balance. However, residual tares still exist and result from a small pressure differential between the ends of the bellows when air system internal velocities are high and from small differences in the spring constants of the forward and aft bellows when pressurized. The residual tares were determined by testing a set of reference calibration nozzles with known performance over a range of expected internal pressures, weight-flow rates, and external forces and moments. The procedures for determining and computing the tares are discussed in references 9 and 10.

Uncertainty Analysis

An uncertainty analysis of the results presented was performed based on a propagation of bias uncertainties of actual measurements through the data reduction equations. The analysis assumes that bias errors are dominant over precision errors and is based on the method presented in reference 11. This method uses the first-order terms in a Taylor series expansion of the data reduction equations to estimate the uncertainty contributions of each measurement. With this technique, the contribution of each measurement would be the measurement uncertainty multiplied by the derivative of the data reduction equation with respect to that measurement. The total uncertainty of the final calculated result is estimated as the root-sum-square of the individual contributions with 95 percent confidence.

The analysis accounted for the uncertainties of the following measurements: jet total pressure, jet total temperature, atmospheric pressure, venturi weight-flow rate, and three components of force. The analysis also accounted for the beneficial effect of averaging multiple measurements of the same quantity, such as the total pressure in the instrumentation section.

The results of the analysis for the range of test conditions indicate that the uncertainties in F_r/F_i, F_A/F_i, δ_p, and δ_y are essentially independent of nozzle pressure ratio. The uncertainties of the thrust ratios F_r/F_i and F_A/F_i are approximately ±0.006. The uncertainty of δ_p is approximately ±1.2 percent of measured value, and the uncertainty of δ_y is approximately ±1.1 percent of measured value.

Flow Visualization

Surface flow visualization was performed for various configurations at a limited number of test conditions by using a paint flow technique. In this technique, an oil-based paint with fluorescent dye is applied to the model surfaces in a pattern of dots. Operating the jet at a specified condition causes dye streaks to form and dry on the model, which indicates some flow features and directions. The model is then disassembled and photographed under ultraviolet light to show maximum detail.

Discussion of Results

The discussion of the performance and flow characteristics of the VIC nozzle is divided into sections on the unvectored nozzle, the pitch thrust-vectoring configurations, and the yaw thrust-vectoring configurations. Each section has separate discussions for the configurations with swallowtail geometry and with arrowhead geometry.

The thrust performance for each configuration is tabulated in tables 3 through 24. The internal static pressure ratios for each configuration are tabulated in tables 25 through 46. Only two quadrants of pressure data per configuration were included in the data tabulations because of model symmetry (upper left and upper right for unvectored and yaw thrust-vectoring configurations; upper left and lower left for pitch thrust-vectoring configurations). As can be seen in the pressure ratio data plots, the pressure data for the lower left quadrant is missing for some configurations because of instrumentation failure during the test.

Unvectored Performance

Swallowtail geometry. The performance of the unvectored swallowtail nozzle is shown in figure 12. Performance data are presented for the extended drawer

configuration (configuration 1, corresponding to dry power mode) and for the retracted drawer configuration (configuration 2, corresponding to afterburning power mode). Additionally, data are presented for the extended drawer configuration with the interfairing installed (configuration 1-I).

Despite the complex internal geometry and trailing-edge flap design of the VIC nozzle, the performance curves for each configuration shown are characteristic of nozzles with simple geometry in that peak performance occurs at a single, distinct nozzle pressure ratio (NPR) and significant overexpansion and underexpansion losses occur at NPRs below and above this condition, respectively. Additional flow expansion on the trailing-edge pieces (conversion of pressure thrust to momentum thrust for reduced underexpansion losses) at NPRs greater than this value does not occur because the trailing-edge pieces are not divergent surfaces and therefore no acceleration is induced. Nonzero pitch thrust-vector angles at low NPR is likely the result of either balance uncertainties or small irregularities in the model fabrication.

The distribution of internal static pressure ratio $p/p_{t,j}$ at NPR = 4 is presented in figure 13. Pressure distributions for each of the four nozzle quadrants are presented; each quadrant has five longitudinal rows of pressure orifices, each row at a different spanwise location (fig. 11) denoted by $y/(w/2)$. Two relevant pressure ratios are indicated with dashed lines. The pressure ratio $p/p_{t,j} = 0.528$ represents the condition for sonic flow. One can determine the approximate orientation of the sonic plane (locus of points in the flow field where the local Mach number is unity) by observing the relative locations (x/L and $y/(w/2)$) where the pressure distributions first reach this value. As shown in figure 13, all pressure distributions passed through this value at approximately the same longitudinal location, $x/L = 0.4$; this indicates that the throat (sonic plane) was neither inclined (indicated by a difference in sonic x/L between upper and lower quadrants) nor skewed (indicated by a difference in sonic x/L between different orifice rows across the nozzle width). The other dashed line labeled $p_a/p_{t,j}$ indicates the value of atmospheric pressure, or the pressure ratio of fully expanded flow. The value of $p_a/p_{t,j}$ is the inverse of NPR. The usefulness of this value is demonstrated in the following discussion of losses affecting peak resultant thrust ratio F_r/F_i.

As shown in figure 12, the peak thrust ratio for configuration 1 occurred at NPR = 4 and had a value of 0.974, about 1 to 2 percent below typical peak thrust ratios of two-dimensional–convergent-divergent (2D–CD) and axisymmetric CD nozzles (refs. 1 through 4). The static pressure distribution in the nozzle at this condition gives some insight into the factors affecting the thrust level and is presented in figure 13. The static pressure ratio $p/p_{t,j}$, when compared with the inverse of the nozzle pressure ratio (labeled on all pressure plots as $p_a/p_{t,j}$), indicates the degree of expansion of the flow. As mentioned, a static pressure ratio equal to the inverse of NPR ($p_a/p_{t,j} = 0.25$ for NPR = 4, in fig. 13) indicates fully expanded flow, as seen, for example, at the trailing edges of the nozzle (last pressure orifices in each row) at $y/(w/2) = 0.491$ and 0.924. A static pressure ratio greater than the inverse of NPR, such as at the trailing edge at $y/(w/2) = 0.058$ (near the nozzle centerline), indicates a region of underexpanded flow. Losses in thrust efficiency resulting from underexpanded flow are caused by not converting all available potential energy (i.e., pressure) into kinetic energy (i.e., velocity).

To estimate the maximum probable effect on thrust ratio, the static pressure ratio close to the centerline trailing edge ($x/L = 0.592$, $y/(w/2) = 0.058$), $p/p_{t,j} = 0.369$, is inverted to give the nozzle pressure ratio which would result in fully expanded flow at that location (rather than underexpanded flow) or NPR = 2.71. This operating condition would be the design NPR for a CD nozzle with an expansion ratio (exit area divided by throat area) of approximately 1.06 (determined from one-dimensional nozzle theory, ref. 12). The effect on thrust efficiency of operating such a nozzle at the underexpanded condition of NPR = 4 (an underexpanded condition for this hypothetical nozzle) can then be estimated with basic nozzle theory. The result would be a reduction in thrust ratio of 0.008 or nearly 1 percent, which would partly account for the reduced value of peak thrust efficiency of the VIC nozzle as compared with typical axisymmetric and 2D–CD nozzles. Although not all exhaust flow is as underexpanded as the nozzle center region flow, most of the exhaust flow passes through this region as a result of the diamond geometry; therefore, the flow field of this region is dominant.

The internal static pressure distributions in figure 13 indicate an additional potential source of inefficiency at the condition of peak thrust ratio. At $y/(w/2) = 0.924$ (near the sidewall), an area of assumed constant pressure between $x/L = 0.592$ and 0.681 (upstream portion of the trailing-edge piece; fig. 11(a)) suggests a region of possible flow separation. Surface flow visualization was performed at this condition on configuration 1-I (same as configuration 1 but with the interfairing installed) by using the paint flow technique described in the section "Apparatus and Procedures." Flow visualization photographs of configuration 1-I at NPR = 4 are shown in figure 14. The end view of the assembled configuration in figure 14(a) shows no significant external flow entrainment over the interfairing; this indicates that the effect of the interfairing on the nozzle performance was negligible. The photographs of the disassembled nozzle in

figures 14(b) and 14(c), showing the upper and lower nozzle surfaces, respectively, reveal significant regions of recirculation near the nozzle sidewalls. The location of these recirculation regions corresponds to the previously discussed location of constant pressure shown in figure 13, except that the regions extend upstream farther into the nozzle. These regions of recirculation probably account for some of the loss in peak thrust efficiency.

As can be seen in figure 14(c), which shows the lower nozzle surface and one sidewall, the recirculation region begins where the upper and lower nozzle throat ridge lines met and the exhaust flow ceases to wash the sidewall surface. This location is the termination of the nozzle transition from rectangular cross section to diamond cross section. By this point the flow area near the sidewall has been greatly reduced and most of the sidewall flow must turn inboard. The pressure distribution shown in figure 13 indicates that the recirculation is bounded on the downstream end by a high-pressure region starting at $x/L = 0.770$ because the flow expanding around the recirculation encounters the sidewall and pressurizes that region of the nozzle.

The sidewalls for configuration 2, an afterburning configuration, are not terminated by the upper and lower nozzle surfaces as are those of the dry power configurations, 1 and 1-I. In the transition to the afterburning configuration, the drawers are retracted (i.e., removed from the model hardware, fig. 10) and the upper and lower nozzle surfaces slide forward and apart from each other, exposing the sidewall to exhaust flow downstream of the throat ridge line. Therefore no recirculation region is expected for the afterburning configurations. Although no flow visualization was obtained for this configuration, the internal pressure distribution, presented in figure 15 at the condition of peak thrust ratio, NPR = 3, shows no regions of constant pressure near the sidewall ($y/(w/2) = 0.924$); this indicates that a recirculation region (separation) probably does not exist. Comparison of the peak resultant thrust ratios shown in figure 12 for configurations 1 and 2 indicates an increase in thrust efficiency of 0.008, or nearly 1 percent, by retracting the drawers. This increase in efficiency is probably the result of eliminating the recirculation region.

An additional effect of retracting the drawers should be noted. As shown in figure 12, the NPR of peak thrust efficiency shifts from approximately NPR = 4 in dry power mode to a value of approximately NPR = 3.25 in afterburning mode. This shift indicates a reduction in the effective expansion ratio (exit area divided by throat area) which may be related to two factors. First, retracting the drawers to increase the vertical throat height also increases the exit height by the same amount. The result is a reduction in the expansion ratio. However, this process does not account for the entire shift. When the nozzle centerline duct height dimensions are used to approximate the geometric expansion ratio, the expansion ratios of configurations 1 and 2 are approximately 1.174 and 1.125, respectively, corresponding to design NPRs (theoretical condition of peak performance) of 3.65 and 3.26. This reduction in NPR of approximately 0.4 is less than the measured reduction of approximately 0.75. The second factor affecting the NPR shift is probably the set of recirculation regions. The disappearance of the recirculation regions probably results in a larger effective throat area, which causes an additional decrease in expansion ratio and thus a decrease in NPR for peak thrust efficiency.

The effect on performance of the interfairing is also presented in figure 12. The data indicate a reduction in peak thrust efficiency of approximately 0.003 as a result of interfairing installation. However, as shown in figure 14(a), no flow entrainment or impingement on the interfairing was evident in surface flow visualization. The apparent reduction in peak thrust ratio is within the uncertainty band of ±0.006 and may therefore not be significant.

Arrowhead geometry. The internal performance of the arrowhead VIC nozzle is presented in figure 16. The trends and levels are similar to those of the swallowtail configuration, shown in figure 12. The largest differences in thrust efficiency between the two geometries occurred at overexpanded conditions (NPR below that of peak thrust ratio) where the arrowhead configurations had slightly higher performance at equivalent nozzle pressure ratios. The similarities in performance levels and trends indicate that the internal performance of the VIC nozzle is primarily driven by nozzle geometry upstream of the triangular trailing-edge pieces.

The internal pressure distributions of the dry and afterburning (drawers extended and retracted) arrowhead configurations are presented in figures 17 and 18 at the NPR for peak thrust ratio. Comparisons with the swallowtail pressure distributions in figure 13 (drawers extended or dry power) and figure 15 (drawers retracted or afterburning power) reveal that the distributions were essentially the same up to the beginning of the trailing-edge pieces ($x/L = 0.57$ in figs. 13 and 17 and $x/L = 0.47$ in figs. 15 and 18). The similarity in pressure distributions upstream of the trailing-edge pieces probably indicates a similarity in causes for thrust loss. For example, for the arrowhead geometry, the static pressure ratio at $y/(w/2) = 0.058$ and $x/L = 0.592$ (fig. 17, UL) at $\mathrm{NPR} \approx 4$ was 0.387. The flow at this location near the centerline of the nozzle was therefore underexpanded, as was the flow in the similar location for the swallowtail configuration. This behavior was identified earlier as a

probable cause for losses in peak thrust ratio. Although this location is not at the arrowhead nozzle exit, the trailing-edge pieces are not divergent, and no further thrust is extracted from the underexpanded flow.

An additional similarity can be seen in the flow visualization photographs of configuration 3 at NPR = 4, shown in figure 19, where a separation region is indicated near the sidewall at the trailing edge. This location corresponds to the recirculation region shown in figure 14 for the swallowtail configuration, and the effect on performance was probably similar as well.

Pitch Thrust Vectoring

The intention, once again, for the VIC nozzle concept is to achieve significant levels of multiaxis thrust vectoring with minimal degradation in nozzle thrust efficiency. The skewed-throat technique is employed such that flow turning would occur at subsonic conditions, and the nozzle would therefore not incur the significant thrust losses associated with turning supersonic flow. At least 15° of pitch or yaw thrust vectoring is generally desired for maneuvering, although the requirements are typically reduced at higher NPRs because tight maneuvers tend to occur more often at low NPRs. During thrust vectoring, a limited reduction in thrust efficiency of perhaps 2 percent could probably be tolerated with the assumption that thrust vectoring is typically employed for only brief periods of time.

Swallowtail geometry. Two methods of pitch vectoring were studied for the swallowtail configuration. (See fig. 8.) The data for both methods are presented in figure 20. The first method used the variable internal contouring mechanism to incline the throat. As discussed previously, the throat ridge in each quadrant could be varied in height and longitudinal location by a cam mechanism in the surfaces of a conceptual full-scale nozzle. (See fig. 6(a).) For the scale model tested, solid internal flow-path inserts were exchanged to simulate the cam operation. Insert 1 represents the lowest peak height and most aft peak location. The inserts then progress successively to 5, which represents the highest and most forward peak. (See fig. 6(b).) By combining different inserts on the upper and lower flow-path surfaces, the geometric throat can be inclined with respect to the nozzle centerline with the intent of providing pitch thrust vectoring with minimal losses in thrust efficiency. Note that the terms “inclined throat” and “skewed throat” are both used in this report but refer to different effects. An inclined throat is oriented such that the sonic line (intersection of the sonic plane with the nozzle surface) on the upper surface is aft of the sonic line on the lower surface. A skewed throat is oriented such that, when the nozzle flow field is viewed in planform, the right- or left-side sonic line is aft of the opposing side (to generate yaw thrust vectoring).

Configuration 5 incorporated insert 2 on the upper surface and insert 3 on the lower surface such that the geometric throat was inclined downward. As shown in figure 20(a), essentially no pitch thrust vectoring was generated by this configuration. A reduction in thrust efficiency of about 1 percent at underexpanded conditions relative to the baseline unvectored nozzle (configuration 1) is also indicated.

By inspecting the location of sonic flow on the upper and lower surfaces ($p/p_{t,j}$ = 0.528) in the pressure distributions shown in figure 21 (at NPR ≈ 6), one can determine that the throat was not inclined in the pitch direction. In fact, similar to the unvectored configuration shown in figure 13, the throat did not form along the skewed throat ridge lines but was relatively planar at about x/L = 0.41. It was surmised that the inserts with the smaller ridges (inserts 1 and 2) did not have peaks sufficient to force the location of the throat. A modification to these inserts was made and is shown in figure 7. Half-round, 1/8-in-diameter rods, called throat strips, were attached to the inserts along the throat ridge lines (contour peaks). Configuration 6 incorporated these throat strips on both the upper (insert 1) and lower (insert 2) surfaces.

As shown in figure 20(a), configuration 6 exhibited a marked reduction in thrust efficiency as compared with the baseline configuration without the throat strips; this result is not surprising because the throat strip constitutes a large obstruction to the flow. However, no positive pitch thrust vectoring was observed despite this attempt to force the throat inclination. The pressure distributions shown in figure 22 indicate that sonic flow did occur approximately along the throat ridge line as desired (indicated by a spanwise variation on each flap of sonic flow which corresponds to the ridge location) and that sonic flow on the upper surface was downstream of that on the lower surface, an indication of a positively deflected throat. However, the pressure distributions also indicate generally higher pressures on the lower surface than on the upper surface, which would result in a negative (downward) normal force offsetting the positive (upward) normal force generated from the positively deflected flow. The flow was probably turned toward the lower surface but was forced to change direction parallel to the centerline. This change in direction for supersonic flow would result in an oblique shock and an associated thrust loss. The pressure distributions in figure 22 indicate possible evidence of such an oblique shock on the lower surface (step pressure increases between the first and second pressure orifices downstream of the throat strips). Additionally, the extreme drop in pressure across

the throat strips acting on their aft-projected area would result in an additional loss in thrust efficiency. The data indicate that forcing the throat, and therefore the flow, to deflect by using the throat strips as tested was unsuccessful in producing the desired thrust vectoring.

The second method investigated for pitch thrust vectoring involved longitudinally displacing the throat ridge lines by retracting only the lower drawers. Configuration 7 consisted of insert 3 with extended upper drawers and partially retracted lower drawers. The lower drawers were then fully retracted to produce configuration 8. The performance data shown in figure 20(b) indicate the generation of positive pitch thrust-vector angles, although the magnitudes were small when compared with other thrust-vectoring concepts (refs. 1 through 8). At NPR = 7, partial retraction resulted in about 4° of thrust vectoring and full retraction resulted in about 6° of thrust vectoring. Pitch thrust-vector angles of these magnitudes may be sufficient for trim but would be insufficient for maneuvering (at least 15° is generally desired). In addition to this result, this thrust-vectoring technique has three limitations. First, the pitch thrust-vector angle decreased with decreasing NPR such that no thrust vectoring was generated at NPR = 2.5; high thrust-vector angles are desired at low NPR (corresponding to low vehicle speed) because many air-to-air combat maneuvers occur in this regime. Second, retracting the drawers for thrust vectoring simultaneously increases the throat area and, therefore, the nozzle power setting; the desire is that thrust vectoring and power setting be independently controllable. Third, once maximum afterburning power is required by the pilot during combat (both drawers retracted), pitch thrust-vectoring capability with this technique is lost. Nevertheless, this technique would still be viable for dry power thrust vectoring if an alternate means to generate thrust vectoring for afterburning power were available.

The internal pressure distributions at NPR $\approx$ 7, shown for configurations 7 and 8 in figures 23 and 24, respectively, reveal complex patterns where higher pressures prevail on either the upper or lower surfaces, depending on location. The pressure distributions indicate that the angles δ_p were limited because the throat was not inclined to the nozzle centerline. The pitch thrust vectoring was entirely generated by unequal upper and lower flap areas. The greater surface area of the upper surface (fig. 8(b)) results in a net upward load and a positive pitch thrust-vector angle.

Surface flow visualization photographs in figure 25 of configuration 8 at NPR = 8 show relatively smooth flow throughout the nozzle (no separation regions are evident). As seen in figure 25(a), flow near the sidewall turns inward and then outward as a result of the upper and lower surfaces closing together. The outward-turned flow is then redirected aft by the sidewall, generating an oblique shock indicated in the flow visualization by a change in paint streak direction. Although this shock system probably resulted in some thrust loss to the nozzle, the translation concept (configurations 7 and 8) appears to have the highest thrust efficiency of the two pitch thrust-vectoring concepts tested on the VIC nozzle. (See fig. 20.) The resultant thrust ratio comparison between the unvectored and vectored configurations indicates both an increase in thrust efficiency at low NPR and a reduction to a lower NPR of peak performance; identical effects were seen in the transition from dry power to afterburning power with drawer retraction. The causes identified for the performance changes with power setting changes (the elimination of the separation regions and an effective decrease in expansion ratio) are also applicable for the vectoring performance changes.

Arrowhead geometry. The drawer retraction method of pitch vectoring was also evaluated with the arrowhead trailing-edge geometry. Thrust performance is presented in figure 26 for configurations 9 (lower drawers partially retracted) and 10 (lower drawers fully retracted). The comparison with the unvectored configuration in figure 26(a) indicates the same trends in thrust efficiency as seen for the swallowtail configuration. Pitch thrust-vector angles at NPR = 7 of approximately 2° and 4° were generated by these configurations. As can be seen in figure 26(b), pitch thrust-vectoring characteristics were similar in trend but smaller in magnitude than those of the swallowtail configuration. This result was expected because the trailing-edge pieces of the arrowhead configuration restrict flow from turning in the pitch direction, whereas the swallowtail trailing-edge geometry provides a ventilated region for flow turning. Ventilation in the intended direction of vectoring is beneficial to thrust vectoring because it prevents the plume from pressurizing the surface which offsets the vectoring force.

The pressure distributions of configurations 9 and 10 are shown in figures 27 and 28, respectively. Complex pressure distributions similar to those seen for the swallowtail configuration can be seen. Again, the greater surface area of the upper surface results in a net upward normal force and a positive pitch thrust-vector angle.

Flow visualization photographs of configuration 10 at NPR = 6 are shown in figure 29. Flow near the trailing edge turns outboard as the underexpanded flow expands without sidewall containment. Because the peak resultant thrust ratios of the swallowtail and arrowhead configurations were approximately equal (fig. 26(b)), the resultant thrust lost as a result of this flow angularity must be approximately equal to the thrust lost in the swallowtail

configuration as the sidewalls redirect the supersonic flow aft through oblique shocks, as discussed earlier.

Yaw Thrust Vectoring

Swallowtail geometry. The yaw thrust-vectoring technique investigated for the VIC nozzle involved reducing the flow area on one side of the nozzle and increasing the area on the other side by installing appropriate throat inserts into the model. (See fig. 9.) As tested, the majority of the flow would pass on the right side of the nozzle and should be deflected to the left by the skewed throat ridge line.

The internal thrust efficiency and yaw thrust-vectoring performance of several swallowtail configurations are presented in figure 30. Each configuration contained insert 5 on the left side (highest peak height, smallest flow area) and insert 1 on the right side (lowest peak height, largest flow area). Configuration 11 had no throat strips installed, whereas configuration 12 had throat strips installed on insert 1. (See fig. 7.) Configurations 11-I and 12-I were the same as configurations 11 and 12 except for the addition of an interfairing. The negligible effect of the interfairing was the same as for the unvectored nozzle.

As shown in figure 30, the thrust efficiency of configuration 11 as compared with the unvectored configuration was relatively low with a peak value of 0.952. The pressure distributions for configuration 11 at NPR = 3 and NPR ≈ 6 are shown in figure 31. As stated earlier, the missing data in the lower left quadrant are the result of instrumentation failure during the test. By inspecting the spanwise locations of sonic flow ($p/p_{t,j} = 0.528$), one can see that, for each NPR, the sonic line formed with a skewed orientation similar to that of the throat ridge line, although the right side was less skewed (approximately 15°) than the left, which appeared to be coincident with the throat ridge line (a skew angle of 30°). The opposite orientations of the right and left sonic lines indicate that flows from each side were directed toward each other; the nozzle thrust efficiency was therefore probably reduced as the two supersonic streams interacted and adjusted direction. The low static pressures downstream of the left-side sonic line acting on the aft-facing surface further reduced the thrust efficiency of the nozzle and suggest that either little flow passed on the left side as intended or the flow was significantly accelerated. Comparison of the pressure distribution with the flow visualization of configuration 12 given later will help to establish that the low pressure probably indicates reduced flow passage rather than accelerated flow.

As shown in figure 30, the yaw thrust-vector angle for configuration 11 was essentially constant (near 2°) above NPR = 2. Comparison of the pressure distributions shown in figure 31 reveals that the flow fields at NPR = 3 and NPR ≈ 6 were essentially the same up to $x/L = 0.55$; this indicates that conditions upstream of this location are dominant in determining the yaw thrust-vector angle.

The low value of yaw thrust-vector angle can be attributed to three factors. First, the deflection angle of the right-side sonic line was only about 15°, less than the skew angle of 30° on the right-side throat ridge line. Second, the interaction from the oncoming left-side flow would also reduce the overall thrust-vector angle. Lastly, the swallowtail design of the nozzle would inhibit yaw thrust vectoring because the trailing-edge sections block lateral flow expansion and turning. The pressure distributions in figure 31 show that pressures on the nozzle surfaces aft of $x/L = 0.6$ were generally higher on the left side than on the right; this acts to reduce the yaw thrust-vector angle. Ventilating this region may result in an increased yaw thrust-vector angle.

Installing the throat strips on insert 1 (right side) significantly affected the nozzle performance. As shown in figure 30, the thrust-vector angle of configuration 12 was not constant but varied from positive values at greatly overexpanded conditions (NPR significantly below that for peak thrust efficiency) to negative values at near-design and underexpanded conditions. Overall thrust efficiency was also reduced and effective nozzle expansion ratio was increased (peak thrust efficiency shifted to a higher NPR).

The pressure distributions shown in figure 32 for configuration 12 at NPR ≈ 3 ($\delta_y = 4.5$) and NPR = 6 ($\delta_y = -0.4$) indicate that the throat location does not vary with NPR and that the right-side sonic line is coincident with the throat strip. As NPR is increased from 3 to 6, static pressures downstream of the throat on the right side are significantly reduced, whereas the pressures on the left side are only slightly reduced. Comparison of the right-side pressure distributions with atmospheric pressure ($p_a/p_{t,j}$) indicates that the right side has a separation-dominated flow field; the left-side flow field is dominated by the jet, and therefore the pressure distributions on that side tend to track changes in the jet total pressure. The result is a reduction in positive side force and yaw thrust-vector angle with increases in NPR.

Different combinations of throat inserts for yaw thrust vectoring of the swallowtail configuration were studied, and the performance data for each are presented in figure 33. Throat strips were installed on all inserts 1 and 2. The effect of increasing the flow area on the right side while holding the left side fixed is seen by comparing configuration 14 with configuration 13. The yaw thrust-vector angle is increased in magnitude (absolute

value), but the increase is small, generally less than 1°. The difference between these configurations, however, is only an approximate 5-percent increase in flow area on the right side for configuration 14, which may not be enough of a change to significantly improve thrust vectoring.

The effect of reducing the flow area on the left side while holding the right side fixed is seen by comparing configuration 12 with configuration 14. By replacing insert 4 of configuration 14 with insert 5, the left-side flow area is reduced by approximately 36 percent. However, this change also resulted in only a small increase in thrust-vector angle of about 2° across the NPR range. The amount of thrust vectoring is apparently less dependent on the inserts than it is on the skewed orientation of the throat ridges.

Flow visualization photographs of configuration 12 at NPR = 3 and 6 are shown in figures 34 and 35, respectively. At both conditions, the flow patterns downstream of the throat ridge lines on both the right and left sides indicate separated flow. Previous pressure data have shown that a well-defined throat ridge, such as that provided by either the highly contoured inserts 4 and 5 or the installed throat strips, is required to force the sonic line to form along the skewed throat ridge lines. Unfortunately, the abrupt divergent geometry of such well-defined throat ridges appears to also produce a poor downstream flow field and low thrust performance.

As mentioned earlier in the discussion of configuration 11, low static pressures downstream of the left throat ridge line either indicated reduced flow or greatly accelerated flow on that side. Configuration 12 is identical to configuration 11 on the left side (throat insert 5). The pressure distributions for configuration 12 shown in figure 32 indicate a similar low-pressure region as that seen for configuration 11. The flow visualization photographs of configuration 12 in figure 34 indicate a recirculation (separated) region downstream of the throat ridge line. This flow separation establishes that the low pressure for both configurations was the result of reduced flow, rather than accelerated flow, which would be indicated by straight, axial paint streaks, not the more random or circulatory patterns that are shown.

Arrowhead geometry. The thrust efficiency and vectoring performance of the yaw thrust-vectored arrowhead VIC nozzle are shown in figure 36. Similar to the swallowtail configuration, thrust efficiency is significantly reduced when the internal contours are set for yaw thrust vectoring. Causes identified for the swallowtail thrust loss are applicable for the arrowhead geometry as well: the interaction between opposed right- and left-side flows and the pressure drop across the throat strips. The arrowhead configuration produced larger yaw thrust-vector angles than did the swallowtail configuration (fig. 36(b)); this was expected because of the increased lateral ventilation of the arrowhead trailing-edge pieces. Nearly 11° of yaw thrust vectoring was produced at NPR = 2 by configuration 16 (inserts 1 and 5), although yaw thrust-vector angle was again quickly reduced as NPR was increased. The effect of reducing the left-side flow area (by replacing insert 4 with insert 5) was more beneficial for the arrowhead geometry (configurations 15 and 16) than it was for the swallowtail geometry (configurations 14 and 12); the benefit of ventilated sidewall regions is again illustrated.

The pressure distributions for configurations 15 and 16 at $\mathrm{NPR} \approx 3$ are shown in figures 37 and 38, respectively. The distributions on the right-side quadrants of the two configurations are nearly equivalent. The distributions of the left-side quadrants, however, differ throughout each nozzle. The most notable difference is the orientation of the throat. The locations of the sonic line for configurations 12, 15, and 16 at $\mathrm{NPR} \approx 3$ were estimated from the pressure distributions and transposed onto sketches of the hardware, as shown in figure 39. The sonic line on the left side of configuration 15 (center sketch) was approximately perpendicular to the nozzle centerline (constant x/L of about 0.37) out to the fourth row of pressure orifices from the sidewall ($y/(w/2)$ = 0.708). For configuration 16 (lower sketch), the right-side sonic line orientation extends past the centerline and intersects the left-side throat ridge line at approximately the second pressure orifice row from the centerline ($y/(w/2)$ = 0.275) before reorienting along the left-side ridge line. In this case, a larger portion of the sonic line is skewed relative to the nozzle centerline as compared with configuration 15; this results in a larger thrust-vector angle. This behavior indicates a strong sensitivity of the sonic line orientation near the nozzle centerline to the left-side throat-ridge geometry and that significant reduction in left-side flow area near the nozzle centerline is necessary to generate significant thrust-vector angles by ensuring that the majority of the nozzle flow passes through the highly skewed right-side throat geometry.

A comparison of the sonic line orientations of configurations 12 (swallowtail) and 16 (arrowhead) in figure 39 indicates a similar flow field where the right-side sonic line orientation carries past the centerline until intersecting with the left-side throat ridge line. The swallowtail configuration, however, produced a smaller thrust-vector angle as a result of the containment provided by the outboard trailing-edge pieces. Flow visualization photographs of configuration 16 are shown in figures 40 and 41. A comparison of these photographs with those of configuration 12 in figures 34 and 35

reveals the effect of lateral ventilation on the flow path as indicated by the direction of the paint streaks at the nozzle trailing edge; the arrowhead configuration allows the flow to exhaust in a more lateral direction than the swallowtail configuration and, therefore, generates larger thrust-vector angles.

Conclusions

The thrust efficiency and vectoring performance of a convergent-divergent nozzle were investigated at static conditions in the model preparation area of the Langley 16-Foot Transonic Tunnel. The diamond-shaped nozzle was capable of varying the internal contour of each quadrant individually by using cam mechanisms and retractable drawers to change nozzle power setting and also to produce pitch and yaw thrust vectoring. Pitch thrust vectoring was achieved by either retracting the lower drawers to incline the throat or varying the internal flow-path contours to incline the throat. Yaw thrust vectoring was achieved by reducing flow area left of the nozzle centerline and increasing flow area right of the nozzle centerline, where a skewed throat deflected the flow in the lateral direction. Based on the discussion of results, the following conclusions are highlighted:

1. The peak thrust efficiency of the unvectored nozzle was approximately 1 to 2 percent lower than that of most high-performance exhaust nozzles. Losses were attributed to underexpanded flow conditions near the nozzle centerline and recirculation or separation regions on the upper and lower flaps near the sidewalls. The latter was eliminated in the transition to the afterburning power setting by separating the upper and lower nozzle surfaces from each other.

2. The orientation of the scarfed trailing edges (swallowtail versus arrowhead) had no appreciable effect on unvectored thrust performance but did affect thrust vectoring as a result of the ventilated regions inherent in the two configurations. Pitch thrust-vector angle was greater for the swallowtail orientation (ventilated centerline region on upper and lower flaps), and yaw thrust-vector angle was greater for the arrowhead orientation (ventilated lateral regions).

3. Pitch thrust-vector angle was less than 7° throughout the test range of nozzle pressure ratios and was unfavorable in its performance trend in that the largest pitch thrust-vector angles occurred at higher nozzle pressure ratios. Most thrust-vectoring maneuvers requiring significant thrust-vector angles occur at low nozzle pressure ratios.

4. Yaw thrust-vector angles of nearly 11° were achieved at low pressure ratios. Yaw thrust-vector angle decreased with increasing nozzle pressure ratio and sometimes reversed direction at higher pressure ratios.

NASA Langley Research Center
Hampton, VA 23681-0001
December 19, 1996

References

1. Wing, David J.; and Capone, Francis J.: *Performance Characteristics of Two Multiaxis Thrust-Vectoring Nozzles at Mach Numbers up to 1.28*. NASA TP-3313, 1993.

2. Carson, George T., Jr.; and Capone, Francis J.: *Static Internal Performance of an Axisymmetric Nozzle With Multiaxis Thrust-Vectoring Capability.* NASA TM-4237, 1991.

3. Berrier, Bobby L.; and Taylor, John G.: *Internal Performance of Two Nozzles Utilizing Gimbal Concepts for Thrust Vectoring*. NASA TP-2991, 1990.

4. Re, Richard J.; and Leavitt, Laurence D.: *Static Internal Performance Including Thrust Vectoring and Reversing of Two-Dimensional Convergent-Divergent Nozzles*. NASA TP-2253, 1984.

5. Mason, Mary L.; and Berrier, Bobby L.: *Static Performance of Nonaxisymmetric Nozzles With Yaw Thrust-Vectoring Vanes.* NASA TP-2813, 1988.

6. Asbury, Scott C.; and Capone, Francis J.: *Multiaxis Thrust-Vectoring Characteristics of a Model Representative of the F-18 High-Alpha Research Vehicle at Angles of Attack From 0° to 70°*. NASA TP-3531, 1995.

7. Asbury, Scott C.: *Effects of Internal Yaw-Vectoring Devices on the Static Performance of a Pitch-Vectoring Nonaxisymmetric Convergent-Divergent Nozzle*. NASA TP-3369, 1993.

8. Wing, David J.: *Static Performance Investigation of a Skewed-Throat Multiaxis Thrust-Vectoring Nozzle Concept*. NASA TP-3411, 1994.

9. Staff of the Propulsion Aerodynamics Branch: *A User's Guide to the Langley 16-Foot Transonic Tunnel Complex, Revision 1*. NASA TM-102750, 1990. (Supersedes NASA TM-831186, compiled by Kathryn H. Peddrew, 1981.)

10. Mercer, Charles E.; Berrier, Bobby L.; Capone, Francis J.; and Grayston, Alan M.: *Data Reduction Formulas for the 16-Foot Transonic Tunnel—NASA Langley Research Center, Revision 2*. NASA TM-107646, 1992. (Supersedes NASA TM-86319, Rev. 1.)

11. Coleman, Hugh W.; and Steele, W. Glenn, Jr.: *Experimentation and Uncertainty Analysis for Engineers*. John Wiley & Sons, 1989.

12. Hunter, Craig A.: *An Approximate Theoretical Method for Modeling the Static Thrust Performance of Non-Axisymmetric Two-Dimensional Convergent-Divergent Nozzles*. NASA CR-195050, 1995.

Table 1. Description of Configurations

Configuration	Vectoring	Trailing-edge geometry	Throat inserts				Drawers		Interfairing	Throat strips
			UL	UR	LL	LR	Upper	Lower		
1	None	Swallowtail	3	3	3	3	Extended	Extended	Not installed	Not installed
1-I									Installed	
2							Retracted	Retracted	Not installed	
3		Arrowhead					Extended	Extended		
3-I									Installed	
4							Retracted	Retracted	Not installed	
5	Pitch	Swallowtail	2	2			Extended	Extended		
6			1	1	2	2				Installed
7			3	3	3	3		Partial		Not installed
8								Retracted		
9		Arrowhead						Partial		
10								Retracted		
11	Yaw	Swallowtail	5	1	5	1		Extended		
11-I									Installed	
12									Not installed	Installed
12-I									Installed	
13			4	2	4	2			Not installed	
14				1		1				
15		Arrowhead								
15-I									Installed	
16			5		5				Not installed	
16-I			5		5				Installed	

Table 2. Locations x/L of Pressure Orifices for Each Set of Configurations

Configurations 1, 1-I — UL

x/L for $y/(w/2)$ of —				
-0.058	-0.275	-0.491	-0.708	-0.924
0.068	0.322	0.068	0.403	0.068
0.230	0.360	0.236	0.441	0.236
0.281	0.398	0.362	0.479	0.444
0.319	0.464	0.400	0.540	0.482
0.357	0.540	0.438		0.592
0.417		0.488		0.681
0.481		0.540		0.770
0.540		0.592		0.858
0.592		0.681		0.947
		0.770		

UR

x/L for $y/(w/2)$ of —				
0.058	0.275	0.491	0.708	0.924
0.068	0.322	0.068	0.403	0.068
0.230	0.360	0.236	0.441	0.236
0.281	0.398	0.362	0.479	0.444
0.319	0.464	0.400	0.540	0.482
0.357	0.540	0.438		0.592
0.417		0.488		0.681
0.481		0.540		0.770
0.540		0.592		0.858
0.592		0.681		0.947
		0.770		

Configuration 2 — UL

x/L for $y/(w/2)$ of —				
-0.058	-0.275	-0.491	-0.708	-0.924
0.137	0.228	0.142	0.310	0.142
0.188	0.266	0.269	0.348	0.350
0.226	0.304	0.307	0.386	0.388
0.264	0.371	0.345	0.447	0.498
0.324	0.447	0.395		0.587
0.387		0.447		0.676
0.447		0.498		0.765
0.498		0.587		0.854
		0.676		

UR

x/L for $y/(w/2)$ of —				
0.058	0.275	0.491	0.708	0.924
0.137	0.228	0.142	0.310	0.142
0.188	0.266	0.269	0.348	0.350
0.226	0.304	0.307	0.386	0.388
0.264	0.371	0.345	0.447	0.498
0.324	0.447	0.395		0.587
0.387		0.498		0.676
0.447		0.587		0.765
0.498		0.676		0.854

Configurations 3, 3-I — UL

x/L for $y/(w/2)$ of —				
-0.058	-0.275	-0.491	-0.708	-0.924
0.068	0.322	0.068	0.403	0.068
0.230	0.360	0.236	0.441	0.236
0.281	0.398	0.362	0.479	0.444
0.319	0.464	0.400	0.540	0.482
0.357	0.540	0.438		0.592
0.417		0.488		
0.481		0.540		
0.540		0.592		
0.592		0.681		
0.681		0.770		
0.770				
0.897				

UR

x/L for $y/(w/2)$ of —				
0.058	0.275	0.491	0.708	0.924
0.068	0.322	0.068	0.403	0.068
0.230	0.360	0.236	0.441	0.236
0.281	0.398	0.362	0.479	0.444
0.319	0.464	0.400	0.540	0.482
0.357	0.540	0.438		0.592
0.417		0.488		
0.481		0.540		
0.540		0.592		
0.592		0.681		
0.681		0.770		
0.770				
0.897				

Configuration 4 — UL

x/L for $y/(w/2)$ of —				
-0.058	-0.275	-0.491	-0.708	-0.924
0.137	0.228	0.142	0.310	0.142
0.188	0.266	0.269	0.348	0.350
0.226	0.304	0.307	0.386	0.388
0.264	0.371	0.345	0.447	0.498
0.324	0.447	0.395		
0.387		0.447		
0.447		0.498		
0.498		0.587		
0.587		0.676		
0.676				
0.803				

UR

x/L for $y/(w/2)$ of —				
0.058	0.275	0.491	0.708	0.924
0.137	0.228	0.142	0.310	0.142
0.188	0.266	0.269	0.348	0.350
0.226	0.304	0.307	0.386	0.388
0.264	0.371	0.345	0.447	0.498
0.324	0.447	0.395		
0.387		0.447		
0.447		0.498		
0.498		0.587		
0.587		0.676		
0.676				
0.803				

Table 2. Continued

Configuration 5 UL

x/L for $y/(w/2)$ of —				
-0.058	-0.275	-0.491	-0.708	-0.924
0.068	0.304	0.068	0.385	0.068
0.263	0.361	0.236	0.442	0.236
0.320	0.399	0.345	0.480	0.426
0.358	0.472	0.402	0.540	0.483
0.415	0.540	0.440		0.592
0.477		0.490		0.681
0.540		0.540		0.770
0.592		0.592		0.858
		0.681		0.947
		0.770		

LL

x/L for $y/(w/2)$ of —				
-0.058	-0.275	-0.491	-0.708	-0.924
0.068	0.322	0.068	0.403	0.068
0.230	0.360	0.236	0.441	0.236
0.281	0.398	0.362	0.479	0.444
0.319	0.464	0.400	0.540	0.482
0.357	0.540	0.438		0.592
0.417		0.488		0.681
0.481		0.540		0.770
0.592		0.592		0.858
		0.681		0.947
		0.770		

Configuration 6 UL

x/L for $y/(w/2)$ of —				
-0.058	-0.275	-0.491	-0.708	-0.924
0.068	0.271	0.068	0.419	0.068
0.233	0.338	0.210	0.483	0.210
0.297	0.402	0.379	0.521	0.460
0.361	0.440	0.442		0.524
0.399	0.490	0.480		0.592
0.439	0.540	0.540		0.681
0.490		0.592		0.770
0.540		0.681		0.858
0.592		0.770		0.947

LL

x/L for $y/(w/2)$ of —				
-0.058	-0.275	-0.491	-0.708	-0.924
0.068	0.304	0.068	0.385	0.236
0.263	0.361	0.236	0.442	0.426
0.320	0.399	0.345	0.480	0.483
0.358	0.472	0.402	0.540	0.592
0.415	0.540	0.440		0.681
0.477		0.490		0.770
0.540		0.540		0.858
0.592		0.592		0.947
		0.681		
		0.770		

Configuration 7 UL

x/L for $y/(w/2)$ of —				
-0.058	-0.275	-0.491	-0.708	-0.924
0.068	0.322	0.068	0.403	0.068
0.230	0.360	0.236	0.441	0.236
0.281	0.398	0.362	0.479	0.444
0.319	0.464	0.400	0.540	0.482
0.357	0.540	0.438		0.592
0.417		0.488		0.681
0.481		0.540		0.770
0.540		0.592		0.858
0.592		0.681		0.947
		0.770		

LL

x/L for $y/(w/2)$ of —				
-0.058	-0.275	-0.491	-0.708	-0.924
0.014	0.268	0.014	0.349	0.014
0.177	0.306	0.182	0.388	0.182
0.227	0.344	0.309	0.426	0.390
0.266	0.411	0.347	0.487	0.428
0.304	0.487	0.385		0.538
0.364		0.435		0.627
0.427		0.487		0.716
0.487		0.627		0.805
0.538		0.716		0.894

Configuration 8 UL

x/L for $y/(w/2)$ of —				
-0.058	-0.275	-0.491	-0.708	-0.924
0.068	0.322	0.068	0.403	0.068
0.230	0.360	0.236	0.441	0.236
0.281	0.398	0.362	0.479	0.444
0.319	0.464	0.400	0.540	0.482
0.357	0.540	0.438		0.592
0.417		0.488		0.681
0.481		0.540		0.770
0.540		0.592		0.858
0.592		0.681		0.947
		0.770		

LL

x/L for $y/(w/2)$ of —				
-0.058	-0.275	-0.491	-0.708	-0.924
0.137	0.228	0.142	0.310	0.142
0.188	0.266	0.269	0.348	0.350
0.226	0.304	0.307	0.386	0.388
0.264	0.371	0.345	0.447	0.498
0.324	0.447	0.395		0.587
0.387		0.447		0.676
0.447		0.498		0.765
0.498		0.587		0.854
		0.676		

Table 2. Continued

Configuration 9 UL

x/L for $y/(w/2)$ of —				
-0.058	-0.275	-0.491	-0.708	-0.924
0.068	0.322	0.068	0.403	0.068
0.230	0.360	0.236	0.441	0.236
0.281	0.398	0.362	0.479	0.444
0.319	0.464	0.400	0.540	0.482
0.357	0.540	0.438		0.592
0.417		0.488		
0.481		0.540		
0.540		0.592		
0.592		0.681		
0.681		0.770		
0.770				
0.897				

LL

x/L for $y/(w/2)$ of —				
-0.058	-0.275	-0.491	-0.708	-0.924
0.014	0.268	0.014	0.349	0.014
0.177	0.306	0.182	0.388	0.182
0.227	0.344	0.309	0.426	0.390
0.266	0.411	0.385	0.487	0.428
0.304	0.487	0.435		0.538
0.364		0.487		
0.427		0.538		
0.487		0.627		
0.538		0.716		
0.627				
0.716				
0.843				

Configuration 10 UL

x/L for $y/(w/2)$ of —				
-0.058	-0.275	-0.491	-0.708	-0.924
0.068	0.322	0.068	0.403	0.068
0.230	0.360	0.236	0.441	0.236
0.281	0.398	0.362	0.479	0.444
0.319	0.464	0.400	0.540	0.482
0.357	0.540	0.438		0.592
0.417		0.488		
0.481		0.540		
0.540		0.592		
0.592		0.681		
0.681		0.770		
0.770				
0.897				

LL

x/L for $y/(w/2)$ of —				
-0.058	-0.275	-0.491	-0.708	-0.924
0.137	0.228	0.142	0.310	0.142
0.188	0.266	0.269	0.348	0.350
0.226	0.304	0.345	0.386	0.388
0.264	0.371	0.395	0.447	0.498
0.324	0.447	0.447		
0.387		0.498		
0.447		0.587		
0.498		0.676		
0.587				
0.676				
0.803				

Configurations 11, 11-I, 12, 12-I UL

x/L for $y/(w/2)$ of —				
-0.058	-0.275	-0.491	-0.708	-0.924
0.068	0.253	0.068	0.334	0.068
0.212	0.291	0.210	0.372	0.210
0.250	0.355	0.294	0.436	0.375
0.314	0.418	0.332	0.540	0.413
0.377	0.477	0.395		0.540
0.439	0.540	0.464		0.592
0.490		0.540		0.681
0.540		0.592		0.770
0.592		0.681		0.858
		0.770		0.947

UR

x/L for $y/(w/2)$ of —				
0.058	0.275	0.491	0.708	0.924
0.068	0.271	0.068	0.419	0.068
0.233	0.338	0.210	0.483	0.210
0.297	0.402	0.379	0.521	0.460
0.361	0.440	0.442		0.524
0.399	0.490	0.480		0.592
0.439	0.540	0.540		0.681
0.490		0.592		0.770
0.540		0.681		0.858
0.592		0.770		0.947

Configuration 13 UL

x/L for $y/(w/2)$ of —				
-0.058	-0.275	-0.491	-0.708	-0.924
0.068	0.285	0.068	0.366	0.068
0.244	0.323	0.236	0.404	0.236
0.282	0.374	0.325	0.455	0.407
0.333	0.440	0.363	0.540	0.445
0.402	0.540	0.414		0.540
0.472		0.477		0.592
0.540		0.540		0.681
0.592		0.592		0.770
		0.681		0.858
		0.770		0.947

UR

x/L for $y/(w/2)$ of —				
0.058	0.275	0.491	0.708	0.924
0.068	0.304	0.068	0.385	0.236
0.263	0.361	0.236	0.442	0.426
0.320	0.399	0.345	0.480	0.483
0.358	0.472	0.402	0.540	0.592
0.415	0.540	0.440		0.681
0.477		0.490		0.770
0.540		0.540		0.858
0.592		0.592		0.947
		0.681		
		0.770		

Table 2. Concluded

Configuration 14 UL

x/L for $y/(w/2)$ of —				
-0.058	-0.275	-0.491	-0.708	-0.924
0.068	0.285	0.068	0.366	0.068
0.244	0.323	0.236	0.404	0.236
0.282	0.374	0.325	0.455	0.407
0.333	0.440	0.363	0.540	0.445
0.402	0.540	0.414		0.540
0.472		0.477		0.592
0.540		0.540		0.681
0.592		0.592		0.770
		0.681		0.858
		0.770		0.947

UR

x/L for $y/(w/2)$ of —				
0.058	0.275	0.491	0.708	0.924
0.068	0.271	0.068	0.419	0.068
0.233	0.338	0.210	0.483	0.210
0.297	0.402	0.379	0.521	0.460
0.361	0.440	0.442		0.524
0.399	0.490	0.480		0.592
0.439	0.540	0.540		0.681
0.490		0.592		0.770
0.540		0.681		0.858
0.592		0.770		0.947

Configurations 15, 15-I UL

x/L for $y/(w/2)$ of —				
-0.058	-0.275	-0.491	-0.708	-0.924
0.068	0.285	0.068	0.366	0.068
0.244	0.323	0.236	0.404	0.236
0.282	0.374	0.325	0.455	0.407
0.333	0.440	0.363	0.540	0.445
0.402	0.540	0.414		0.540
0.472		0.477		0.592
0.540		0.540		
0.592		0.592		
0.681		0.681		
0.770		0.770		
0.897				

UR

x/L for $y/(w/2)$ of —				
0.058	0.275	0.491	0.708	0.924
0.068	0.271	0.068	0.419	0.068
0.233	0.338	0.210	0.483	0.210
0.297	0.402	0.379	0.521	0.460
0.361	0.440	0.442		0.524
0.399	0.490	0.480		0.592
0.439	0.540	0.540		
0.490		0.592		
0.540		0.681		
0.592		0.770		
0.681				
0.770				
0.897				

Configurations 16, 16-I UL

x/L for $y/(w/2)$ of —				
-0.058	-0.275	-0.491	-0.708	-0.924
0.068	0.253	0.068	0.334	0.068
0.212	0.291	0.210	0.372	0.210
0.250	0.355	0.294	0.436	0.375
0.314	0.418	0.332	0.540	0.413
0.377	0.477	0.395		0.540
0.439	0.540	0.464		0.592
0.490		0.540		
0.540		0.592		
0.592		0.681		
0.681		0.770		
0.770				
0.897				

UR

x/L for $y/(w/2)$ of —				
0.058	0.275	0.491	0.708	0.924
0.068	0.271	0.068	0.419	0.068
0.233	0.338	0.210	0.483	0.210
0.297	0.402	0.379	0.521	0.460
0.361	0.440	0.442		0.524
0.399	0.490	0.480		0.592
0.439	0.540	0.540		
0.490		0.592		
0.540		0.681		
0.592		0.770		
0.681				
0.770				
0.897				

Swallowtail sidewall centerline

x/L for —	
Left	Right
0.262	0.262
0.401	0.401
0.541	0.541
0.770	0.770
0.947	0.947

Arrowhead sidewall centerline

x/L for —	
Left	Right
0.262	0.262
0.401	0.401
0.541	0.541

Table 3. Internal Static Performance Data for Configuration 1

NPR	F_r/F_i	F_A/F_i	δ_p, deg	δ_y, deg
2.011	0.9382	0.9381	0.77	-0.21
2.513	0.9560	0.9559	0.52	-0.16
2.993	0.9671	0.9671	0.38	-0.13
3.492	0.9723	0.9723	0.32	-0.16
4.003	0.9742	0.9742	0.26	-0.21
4.504	0.9738	0.9738	0.25	-0.18
4.995	0.9722	0.9721	0.20	-0.21
5.998	0.9680	0.9680	0.14	-0.19
7.987	0.9582	0.9582	0.07	-0.15
9.998	0.9486	0.9486	0.04	-0.12

Table 4. Internal Static Performance Data for Configuration 1-I

NPR	F_r/F_i	F_A/F_i	δ_p, deg	δ_y, deg
2.007	0.9365	0.9364	0.80	-0.16
2.493	0.9526	0.9526	0.58	-0.06
3.009	0.9636	0.9636	0.43	-0.05
3.509	0.9697	0.9697	0.34	-0.13
3.999	0.9711	0.9711	0.28	-0.12
4.498	0.9716	0.9715	0.24	-0.16
4.997	0.9698	0.9698	0.19	-0.14
6.009	0.9662	0.9662	0.16	-0.16
7.998	0.9570	0.9570	0.08	-0.13
9.991	0.9482	0.9482	0.09	-0.11

Table 5. Internal Static Performance Data for Configuration 2

NPR	F_r/F_i	F_A/F_i	δ_p, deg	δ_y, deg
2.009	0.9658	0.9657	0.43	-0.04
2.507	0.9778	0.9778	0.26	-0.03
3.005	0.9818	0.9818	0.19	-0.08
3.497	0.9817	0.9817	0.11	-0.07
4.001	0.9798	0.9798	0.06	-0.06
4.998	0.9752	0.9752	0.05	0.01
5.984	0.9678	0.9678	0.01	0.04

Table 6. Internal Static Performance Data for Configuration 3

NPR	F_r/F_i	F_A/F_i	δ_p, deg	δ_y, deg
1.996	0.9531	0.9530	0.85	-0.28
2.500	0.9617	0.9616	0.75	-0.06
3.003	0.9707	0.9706	0.58	-0.09
3.517	0.9730	0.9729	0.50	-0.08
3.992	0.9741	0.9741	0.44	-0.11
4.479	0.9738	0.9737	0.35	-0.07
5.039	0.9701	0.9701	0.28	-0.08
6.037	0.9665	0.9665	0.28	-0.16
6.983	0.9621	0.9621	0.25	-0.17
7.977	0.9572	0.9572	0.22	-0.12
9.962	0.9480	0.9480	0.24	-0.09

Table 7. Internal Static Performance Data for Configuration 3-I

NPR	F_r/F_i	F_A/F_i	δ_p, deg	δ_y, deg
2.019	0.9532	0.9530	0.88	0.00
2.502	0.9610	0.9609	0.69	0.14
3.001	0.9695	0.9694	0.56	0.11
3.508	0.9713	0.9712	0.47	-0.20
3.997	0.9725	0.9725	0.39	-0.21
4.515	0.9715	0.9715	0.34	-0.22
5.007	0.9691	0.9690	0.27	-0.22
5.980	0.9652	0.9652	0.22	-0.19
6.995	0.9604	0.9604	0.19	-0.14
7.974	0.9549	0.9549	0.18	-0.13
9.998	0.9471	0.9471	0.23	-0.10

Table 8. Internal Static Performance Data for Configuration 4

NPR	F_r/F_i	F_A/F_i	δ_p, deg	δ_y, deg
2.010	0.9655	0.9655	0.50	0.28
2.505	0.9733	0.9733	0.34	0.22
3.009	0.9796	0.9796	0.21	0.07
3.496	0.9793	0.9793	0.12	0.05
4.008	0.9776	0.9776	0.03	-0.02
4.502	0.9756	0.9756	0.03	0.01
4.996	0.9731	0.9731	0.03	0.03
6.006	0.9664	0.9664	0.00	0.08

Table 9. Internal Static Performance Data for Configuration 5

NPR	F_r/F_i	F_A/F_i	δ_p, deg	δ_y, deg
2.001	0.9434	0.9434	0.62	-0.06
2.501	0.9605	0.9604	0.37	-0.17
3.004	0.9677	0.9677	0.31	0.00
3.495	0.9713	0.9713	0.25	0.01
4.005	0.9728	0.9728	0.23	0.06
4.503	0.9718	0.9718	0.18	0.06
5.012	0.9696	0.9696	0.15	0.04
6.017	0.9643	0.9643	0.13	0.04
8.002	0.9526	0.9526	0.06	0.03
9.998	0.9412	0.9412	0.01	0.07

Table 10. Internal Static Performance Data for Configuration 6

NPR	F_r/F_i	F_A/F_i	δ_p, deg	δ_y, deg
2.009	0.8881	0.8880	-0.91	0.11
2.504	0.9035	0.9032	-1.25	0.79
2.986	0.9175	0.9174	-0.93	0.22
4.008	0.9342	0.9342	-0.36	0.04
4.496	0.9366	0.9366	-0.27	0.00
5.014	0.9393	0.9393	-0.30	-0.03
6.047	0.9395	0.9395	-0.28	-0.01
7.034	0.9368	0.9368	-0.29	0.01
8.003	0.9347	0.9347	-0.31	0.04

Table 11. Internal Static Performance Data for Configuration 7

NPR	F_r/F_i	F_A/F_i	δ_p, deg	δ_y, deg
2.031	0.9482	0.9481	-0.49	-0.24
2.489	0.9657	0.9657	0.13	-0.12
2.991	0.9731	0.9730	0.75	-0.18
3.491	0.9764	0.9762	1.33	-0.17
3.986	0.9761	0.9755	1.94	-0.17
4.530	0.9748	0.9739	2.47	-0.13
4.989	0.9727	0.9715	2.85	-0.11
6.014	0.9680	0.9662	3.47	-0.08
6.945	0.9626	0.9604	3.87	-0.04
7.989	0.9572	0.9545	4.25	-0.02

Table 12. Internal Static Performance Data for Configuration 8

NPR	F_r/F_i	F_A/F_i	δ_p, deg	δ_y, deg
2.005	0.9614	0.9613	-0.74	0.00
2.498	0.9729	0.9729	0.27	0.03
2.977	0.9771	0.9769	1.24	0.03
3.523	0.9782	0.9774	2.20	-0.01
3.980	0.9778	0.9764	3.05	-0.03
4.521	0.9752	0.9729	3.94	-0.08
4.987	0.9738	0.9708	4.56	-0.08
5.972	0.9692	0.9647	5.54	-0.08
6.984	0.9634	0.9575	6.34	-0.08
7.539	0.9612	0.9546	6.74	-0.07

Table 13. Internal Static Performance Data for Configuration 9

NPR	F_r/F_i	F_A/F_i	δ_p, deg	δ_y, deg
2.016	0.9619	0.9617	0.93	0.16
2.497	0.9729	0.9727	1.10	-0.06
3.001	0.9787	0.9786	0.95	-0.08
3.503	0.9782	0.9780	1.17	-0.09
4.002	0.9778	0.9775	1.46	-0.10
4.499	0.9754	0.9749	1.72	-0.10
5.014	0.9706	0.9701	1.95	-0.11
6.000	0.9669	0.9662	2.19	-0.11
6.981	0.9602	0.9593	2.43	-0.03
8.028	0.9548	0.9537	2.71	-0.01
8.921	0.9508	0.9496	2.92	0.03

Table 14. Internal Static Performance Data for Configuration 10

NPR	F_r/F_i	F_A/F_i	δ_p, deg	δ_y, deg
2.000	0.9696	0.9694	1.12	0.32
2.488	0.9761	0.9759	1.16	0.19
3.010	0.9794	0.9793	1.02	0.11
3.500	0.9788	0.9785	1.43	0.05
4.018	0.9757	0.9750	2.15	-0.14
4.504	0.9751	0.9741	2.61	-0.15
4.988	0.9737	0.9725	2.88	-0.08
5.983	0.9680	0.9661	3.65	-0.09
6.986	0.9616	0.9589	4.28	-0.06
7.365	0.9596	0.9566	4.51	-0.03

Table 15. Internal Static Performance Data for Configuration 11

NPR	F_r/F_i	F_A/F_i	δ_p, deg	δ_y, deg
2.024	0.8907	0.8906	0.45	0.71
2.499	0.9107	0.9104	0.63	1.52
2.997	0.9265	0.9260	0.57	1.72
3.497	0.9364	0.9359	0.36	1.70
4.007	0.9438	0.9434	0.19	1.69
5.028	0.9506	0.9501	-0.12	1.77
5.994	0.9520	0.9515	-0.07	1.86
8.011	0.9491	0.9486	-0.21	1.80
9.985	0.9434	0.9429	-0.14	1.81

Table 16. Internal Static Performance Data for Configuration 11-I

NPR	F_r/F_i	F_A/F_i	δ_p, deg	δ_y, deg
2.014	0.8954	0.8947	0.80	2.06
2.532	0.9069	0.9064	0.55	1.76
3.014	0.9247	0.9241	0.51	1.86
3.504	0.9351	0.9347	0.32	1.81
3.991	0.9428	0.9423	0.30	1.75
4.485	0.9471	0.9467	0.01	1.80
5.015	0.9504	0.9498	0.13	1.89
6.011	0.9517	0.9512	-0.02	1.86
7.993	0.9485	0.9480	-0.02	1.81
9.984	0.9428	0.9423	-0.03	1.78

Table 17. Internal Static Performance Data for Configuration 12

NPR	F_r/F_i	F_A/F_i	δ_p, deg	δ_y, deg
2.010	0.8749	0.8683	0.96	6.98
2.507	0.8871	0.8824	0.68	5.90
3.011	0.9004	0.8976	0.83	4.51
3.506	0.9100	0.9080	0.48	3.72
4.005	0.9164	0.9151	0.33	2.96
4.503	0.9213	0.9207	0.19	2.06
4.999	0.9253	0.9251	0.05	1.04
6.002	0.9307	0.9307	-0.11	-0.37

Table 18. Internal Static Performance Data for Configuration 12-I

NPR	F_r/F_i	F_A/F_i	δ_p, deg	δ_y, deg
1.994	0.8641	0.8568	0.54	7.42
2.498	0.8804	0.8756	0.74	5.95
3.003	0.8976	0.8947	0.83	4.54
3.507	0.9083	0.9063	0.52	3.77
3.995	0.9149	0.9136	0.31	3.01
4.508	0.9213	0.9207	0.16	2.09
5.006	0.9255	0.9254	0.06	1.10
5.992	0.9302	0.9302	-0.11	-0.28
6.993	0.9334	0.9332	-0.15	-1.08
8.010	0.9330	0.9327	-0.13	-1.61

Table 19. Internal Static Performance Data for Configuration 13

NPR	F_r/F_i	F_A/F_i	δ_p, deg	δ_y, deg
2.025	0.9083	0.9049	1.22	4.75
2.496	0.9123	0.9108	1.06	3.07
3.010	0.9211	0.9207	0.79	1.58
3.500	0.9310	0.9308	0.32	0.98
3.998	0.9388	0.9388	0.29	0.50
5.002	0.9470	0.9470	0.06	-0.74
5.996	0.9521	0.9517	0.06	-1.64
6.992	0.9520	0.9513	0.03	-2.13
7.979	0.9502	0.9494	0.05	-2.34

Table 20. Internal Static Performance Data for Configuration 14

NPR	F_r/F_i	F_A/F_i	δ_p, deg	δ_y, deg
1.995	0.9138	0.9096	0.26	5.50
2.509	0.9183	0.9161	0.91	3.87
3.029	0.9255	0.9242	0.74	2.97
3.493	0.9326	0.9319	0.64	2.23
4.019	0.9371	0.9369	0.29	1.29
4.532	0.9415	0.9415	0.10	0.21
4.999	0.9432	0.9431	0.12	-0.62
5.991	0.9460	0.9455	0.09	-1.83
7.018	0.9465	0.9456	0.02	-2.50
8.003	0.9441	0.9430	0.01	-2.78

Table 21. Internal Static Performance Data for Configuration 15

NPR	F_r/F_i	F_A/F_i	δ_p, deg	δ_y, deg
2.003	0.9053	0.9010	0.86	5.50
2.479	0.9114	0.9073	0.48	5.43
3.009	0.9217	0.9180	0.34	5.10
3.494	0.9285	0.9256	0.33	4.50
4.005	0.9339	0.9313	0.33	4.24
4.491	0.9374	0.9349	0.15	4.16
4.992	0.9389	0.9368	0.21	3.88
5.998	0.9404	0.9387	0.10	3.46
6.994	0.9397	0.9382	-0.03	3.24
8.029	0.9388	0.9374	0.02	3.19

Table 22. Internal Static Performance Data for Configuration 15-I

NPR	F_r/F_i	F_A/F_i	δ_p, deg	δ_y, deg
2.004	0.9044	0.9003	0.84	5.39
2.502	0.9126	0.9086	0.46	5.36
3.004	0.9232	0.9195	0.32	5.18
3.502	0.9307	0.9278	0.27	4.48
3.993	0.9358	0.9334	0.30	4.16
4.492	0.9400	0.9375	0.17	4.16
4.993	0.9426	0.9405	0.20	3.88
6.996	0.9415	0.9400	-0.01	3.26
7.982	0.9401	0.9387	-0.04	3.17
9.999	0.9323	0.9309	-0.03	3.20

Table 23. Internal Static Performance Data for Configuration 16

NPR	F_r/F_i	F_A/F_i	δ_p, deg	δ_y, deg
1.990	0.8637	0.8484	1.12	10.77
2.510	0.8826	0.8697	0.58	9.80
3.007	0.8971	0.8867	0.31	8.73
3.501	0.9062	0.8979	0.19	7.74
4.003	0.9126	0.9055	0.24	7.14
4.497	0.9173	0.9110	0.18	6.70
4.979	0.9210	0.9156	0.19	6.19
6.005	0.9237	0.9196	0.17	5.40
7.007	0.9257	0.9225	0.06	4.73
7.973	0.9258	0.9230	0.04	4.48
10.056	0.9229	0.9204	0.00	4.23

Table 24. Internal Static Performance Data for Configuration 16-I

NPR	F_r/F_i	F_A/F_i	δ_p, deg	δ_y, deg
2.003	0.8596	0.8443	0.94	10.80
2.518	0.8802	0.8668	0.41	10.01
3.012	0.8946	0.8839	0.12	8.85
3.500	0.9056	0.8975	0.14	7.70
4.007	0.9115	0.9045	0.36	7.13
4.514	0.9160	0.9098	0.17	6.68
5.009	0.9202	0.9149	0.25	6.16
6.060	0.9234	0.9194	0.06	5.36
7.000	0.9252	0.9218	-0.01	4.88
7.985	0.9258	0.9229	-0.06	4.58
9.981	0.9231	0.9206	-0.08	4.29

Table 25. Nozzle Internal Static Pressure Ratios for Configuration 1

UL quadrant: $y/(w/2) = -0.058$

	$p/p_{t,j}$ at x/L of—								
NPR	0.068	0.230	0.281	0.319	0.357	0.417	0.481	0.540	0.592
2.011	0.952	0.811	0.749	0.685	0.613	0.498	0.458	0.414	0.532
2.513	0.950	0.811	0.750	0.685	0.613	0.498	0.458	0.399	0.381
2.993	0.951	0.811	0.750	0.685	0.612	0.498	0.458	0.398	0.366
3.492	0.951	0.811	0.751	0.684	0.611	0.498	0.457	0.417	0.369
4.003	0.951	0.811	0.750	0.684	0.611	0.498	0.457	0.419	0.369
4.504	0.950	0.811	0.750	0.683	0.610	0.498	0.457	0.420	0.368
4.995	0.950	0.811	0.750	0.683	0.610	0.498	0.457	0.420	0.369
5.998	0.949	0.810	0.750	0.682	0.609	0.498	0.458	0.420	0.369
7.987	0.949	0.809	0.748	0.680	0.606	0.498	0.456	0.419	0.369
9.998	0.948	0.808	0.748	0.678	0.604	0.497	0.456	0.419	0.372

UL quadrant: $y/(w/2) = -0.275$

	$p/p_{t,j}$ at x/L of—				
NPR	0.322	0.360	0.398	0.464	0.540
2.011	0.681	0.615	0.534	0.419	0.463
2.513	0.680	0.615	0.534	0.420	0.396
2.993	0.680	0.616	0.535	0.420	0.396
3.492	0.680	0.616	0.535	0.420	0.387
4.003	0.680	0.616	0.536	0.420	0.387
4.504	0.680	0.616	0.536	0.420	0.387
4.995	0.679	0.616	0.536	0.420	0.387
5.998	0.679	0.616	0.536	0.419	0.388
7.987	0.677	0.615	0.535	0.418	0.388
9.998	0.676	0.614	0.535	0.417	0.387

UL quadrant: $y/(w/2) = -0.491$

	$p/p_{t,j}$ at x/L of—									
NPR	0.068	0.236	0.362	0.400	0.438	0.488	0.540	0.592	0.681	0.770
2.011	0.961	0.834	0.592	0.511	0.424	0.336	0.492	0.511	0.419	0.487
2.513	0.961	0.833	0.591	0.511	0.423	0.337	0.316	0.431	0.371	0.385
2.993	0.961	0.833	0.592	0.511	0.423	0.337	0.317	0.297	0.373	0.290
3.492	0.960	0.834	0.592	0.511	0.423	0.337	0.317	0.288	0.373	0.258
4.003	0.960	0.833	0.593	0.512	0.423	0.337	0.318	0.288	0.374	0.253
4.504	0.960	0.834	0.592	0.512	0.423	0.337	0.318	0.288	0.375	0.253
4.995	0.960	0.833	0.592	0.512	0.423	0.338	0.319	0.288	0.376	0.253
5.998	0.959	0.833	0.592	0.511	0.422	0.338	0.319	0.287	0.378	0.254
7.987	0.959	0.832	0.591	0.511	0.421	0.337	0.320	0.287	0.379	0.256
9.998	0.958	0.831	0.590	0.511	0.419	0.337	0.320	0.286	0.380	0.257

Table 25. Continued

UL quadrant: $y/(w/2) = -0.708$

NPR	$p/p_{t,j}$ at x/L of— 0.403	0.441	0.479	0.540
2.011	0.478	0.346	0.261	0.429
2.513	0.478	0.346	0.262	0.328
2.993	0.476	0.345	0.263	0.280
3.492	0.476	0.345	0.264	0.245
4.003	0.476	0.345	0.264	0.236
4.504	0.475	0.344	0.264	0.230
4.995	0.474	0.344	0.265	0.227
5.998	0.474	0.343	0.265	0.218
7.987	0.473	0.342	0.266	0.206
9.998	0.472	0.341	0.266	0.204

UL quadrant: $y/(w/2) = -0.924$

NPR	$p/p_{t,j}$ at x/L of— 0.068	0.236	0.444	0.482	0.592	0.681	0.770	0.858	0.947
2.011	0.971	0.910	0.370	0.395	0.384	0.359	0.438	0.532	0.511
2.513	0.969	0.911	0.371	0.208	0.276	0.263	0.359	0.441	0.406
2.993	0.971	0.910	0.371	0.139	0.230	0.231	0.370	0.396	0.338
3.492	0.970	0.910	0.371	0.134	0.221	0.224	0.365	0.343	0.287
4.003	0.970	0.910	0.371	0.135	0.223	0.222	0.361	0.336	0.236
4.504	0.970	0.910	0.372	0.136	0.225	0.222	0.357	0.336	0.204
4.995	0.970	0.910	0.372	0.136	0.227	0.221	0.355	0.337	0.201
5.998	0.970	0.909	0.372	0.138	0.230	0.219	0.348	0.340	0.203
7.987	0.969	0.908	0.372	0.140	0.234	0.221	0.339	0.338	0.205
9.998	0.968	0.907	0.372	0.142	0.236	0.218	0.334	0.336	0.206

UR quadrant: $y/(w/2) = 0.058$

NPR	$p/p_{t,j}$ at x/L of— 0.068	0.230	0.281	0.319	0.357	0.417	0.481	0.540	0.592
2.011	0.952	0.809	0.748	0.687	0.614	0.494	0.460	0.444	0.541
2.513	0.951	0.809	0.748	0.687	0.614	0.493	0.459	0.415	0.381
2.993	0.951	0.810	0.747	0.686	0.614	0.493	0.458	0.404	0.374
3.492	0.951	0.809	0.747	0.686	0.614	0.493	0.456	0.401	0.370
4.003	0.951	0.807	0.747	0.686	0.613	0.493	0.456	0.398	0.369
4.504	0.951	0.807	0.746	0.686	0.613	0.493	0.456	0.394	0.369
4.995	0.951	0.807	0.746	0.686	0.612	0.492	0.456	0.391	0.369
5.998	0.951	0.806	0.745	0.685	0.611	0.492	0.456	0.386	0.369
7.987	0.950	0.805	0.744	0.683	0.610	0.491	0.454	0.383	0.368
9.998	0.949	0.803	0.742	0.682	0.608	0.490	0.453	0.380	0.370

UR quadrant: $y/(w/2) = 0.275$

NPR	$p/p_{t,j}$ at x/L of— 0.322	0.360	0.398	0.464	0.540
2.011	0.684	0.616	0.535	0.420	0.459
2.513	0.683	0.617	0.535	0.420	0.405
2.993	0.682	0.617	0.535	0.420	0.405
3.492	0.683	0.617	0.535	0.420	0.396
4.003	0.683	0.617	0.535	0.420	0.397
4.504	0.682	0.617	0.535	0.420	0.397
4.995	0.682	0.616	0.535	0.420	0.397
5.998	0.681	0.616	0.535	0.420	0.397
7.987	0.680	0.613	0.533	0.419	0.397
9.998	0.678	0.612	0.533	0.418	0.397

Table 25. Concluded

UR quadrant: $y/(w/2) = 0.491$

NPR	$p/p_{t,j}$ at x/L of— 0.068	0.236	0.362	0.400	0.438	0.488	0.540	0.592	0.681	0.770
2.011	0.960	0.832	0.587	0.514	0.423	0.337	0.490	0.512	0.415	0.486
2.513	0.961	0.831	0.586	0.514	0.423	0.337	0.321	0.436	0.360	0.385
2.993	0.961	0.831	0.586	0.514	0.424	0.338	0.322	0.308	0.370	0.288
3.492	0.962	0.831	0.586	0.514	0.424	0.338	0.322	0.294	0.365	0.259
4.003	0.962	0.831	0.586	0.514	0.424	0.338	0.322	0.294	0.364	0.253
4.504	0.961	0.831	0.586	0.514	0.424	0.338	0.322	0.294	0.364	0.253
4.995	0.961	0.830	0.585	0.514	0.424	0.338	0.323	0.294	0.364	0.254
5.998	0.961	0.830	0.585	0.513	0.424	0.339	0.323	0.294	0.366	0.257
7.987	0.961	0.828	0.583	0.512	0.423	0.339	0.323	0.293	0.369	0.265
9.998	0.960	0.827	0.582	0.512	0.422	0.339	0.324	0.292	0.368	0.263

UR quadrant: $y/(w/2) = 0.708$

NPR	$p/p_{t,j}$ at x/L of— 0.403	0.441	0.479	0.540
2.011	0.470	0.354	0.262	0.412
2.513	0.470	0.354	0.263	0.325
2.993	0.469	0.355	0.264	0.269
3.492	0.469	0.355	0.264	0.224
4.003	0.469	0.355	0.264	0.217
4.504	0.469	0.355	0.264	0.213
4.995	0.469	0.355	0.265	0.213
5.998	0.468	0.355	0.265	0.219
7.987	0.467	0.355	0.266	0.225
9.998	0.466	0.354	0.266	0.202

UR quadrant: $y/(w/2) = 0.924$

NPR	$p/p_{t,j}$ at x/L of— 0.068	0.236	0.444	0.482	0.592	0.681	0.770	0.858	0.947
2.011	0.971	0.908	0.367	0.403	0.385	0.363	0.434	0.530	0.512
2.513	0.971	0.908	0.367	0.197	0.279	0.266	0.349	0.439	0.408
2.993	0.970	0.908	0.368	0.140	0.231	0.232	0.360	0.401	0.336
3.492	0.971	0.907	0.368	0.135	0.219	0.224	0.359	0.350	0.284
4.003	0.971	0.907	0.369	0.137	0.218	0.224	0.360	0.335	0.241
4.504	0.971	0.907	0.369	0.137	0.217	0.226	0.361	0.331	0.200
4.995	0.971	0.907	0.370	0.138	0.218	0.229	0.360	0.327	0.195
5.998	0.970	0.906	0.370	0.140	0.221	0.235	0.349	0.325	0.195
7.987	0.969	0.905	0.370	0.144	0.228	0.238	0.335	0.327	0.198
9.998	0.969	0.904	0.370	0.148	0.230	0.233	0.334	0.325	0.199

Table 26. Nozzle Internal Static Pressure Ratios for Configuration 1-I

UL quadrant: $y/(w/2) = -0.058$

NPR	$p/p_{t,j}$ at x/L of— 0.068	0.230	0.281	0.319	0.357	0.417	0.481	0.540	0.592
2.007	0.949	0.810	0.750	0.684	0.612	0.497	0.454	0.422	0.537
2.493	0.948	0.812	0.749	0.684	0.612	0.497	0.454	0.417	0.379
3.009	0.950	0.811	0.750	0.683	0.611	0.497	0.454	0.417	0.371
3.509	0.950	0.811	0.750	0.683	0.610	0.498	0.455	0.418	0.369
3.999	0.949	0.811	0.750	0.683	0.610	0.497	0.455	0.418	0.369
4.498	0.950	0.811	0.750	0.682	0.609	0.498	0.455	0.418	0.369
4.997	0.950	0.810	0.750	0.682	0.609	0.498	0.456	0.419	0.369
6.009	0.949	0.810	0.749	0.681	0.608	0.498	0.456	0.419	0.369
7.998	0.948	0.809	0.748	0.680	0.606	0.497	0.456	0.419	0.371
9.991	0.948	0.809	0.748	0.678	0.605	0.497	0.456	0.418	0.373

UL quadrant: $y/(w/2) = -0.275$

NPR	$p/p_{t,j}$ at x/L of— 0.322	0.360	0.398	0.464	0.540
2.007	0.682	0.614	0.533	0.418	0.458
2.493	0.681	0.615	0.534	0.419	0.385
3.009	0.681	0.615	0.534	0.419	0.386
3.509	0.680	0.615	0.535	0.419	0.386
3.999	0.680	0.615	0.535	0.419	0.387
4.498	0.680	0.615	0.535	0.419	0.387
4.997	0.679	0.616	0.535	0.419	0.387
6.009	0.679	0.615	0.535	0.419	0.387
7.998	0.677	0.615	0.535	0.418	0.388
9.991	0.676	0.614	0.535	0.417	0.388

UL quadrant: $y/(w/2) = -0.491$

NPR	$p/p_{t,j}$ at x/L of— 0.068	0.236	0.362	0.400	0.438	0.488	0.540	0.592	0.681	0.770
2.007	0.961	0.832	0.591	0.509	0.422	0.336	0.490	0.513	0.421	0.487
2.493	0.960	0.832	0.591	0.510	0.422	0.336	0.315	0.426	0.371	0.383
3.009	0.960	0.832	0.592	0.510	0.422	0.336	0.316	0.289	0.374	0.291
3.509	0.960	0.833	0.591	0.511	0.422	0.336	0.317	0.287	0.376	0.258
3.999	0.960	0.833	0.592	0.511	0.422	0.337	0.318	0.287	0.377	0.253
4.498	0.960	0.833	0.592	0.511	0.422	0.337	0.318	0.287	0.377	0.253
4.997	0.960	0.832	0.592	0.511	0.422	0.337	0.319	0.287	0.379	0.253
6.009	0.960	0.833	0.592	0.511	0.421	0.337	0.319	0.287	0.379	0.254
7.998	0.959	0.832	0.591	0.511	0.420	0.337	0.320	0.287	0.378	0.256
9.991	0.958	0.831	0.590	0.511	0.420	0.337	0.320	0.286	0.380	0.257

Table 26. Continued

UL quadrant: $y/(w/2) = -0.708$

NPR	$p/p_{t,j}$ at x/L of— 0.403	0.441	0.479	0.540
2.007	0.478	0.346	0.262	0.427
2.493	0.476	0.346	0.262	0.328
3.009	0.476	0.345	0.263	0.268
3.509	0.475	0.345	0.264	0.230
3.999	0.475	0.344	0.264	0.221
4.498	0.475	0.344	0.264	0.215
4.997	0.474	0.343	0.265	0.209
6.009	0.474	0.343	0.265	0.204
7.998	0.473	0.342	0.266	0.205
9.991	0.472	0.341	0.266	0.201

UL quadrant: $y/(w/2) = -0.924$

NPR	$p/p_{t,j}$ at x/L of— 0.068	0.236	0.444	0.482	0.592	0.681	0.770	0.858	0.947
2.007	0.970	0.908	0.370	0.393	0.387	0.360	0.436	0.532	0.513
2.493	0.970	0.910	0.370	0.205	0.281	0.264	0.355	0.441	0.411
3.009	0.970	0.910	0.370	0.137	0.232	0.227	0.362	0.395	0.337
3.509	0.970	0.910	0.370	0.135	0.224	0.221	0.359	0.344	0.287
3.999	0.970	0.910	0.371	0.135	0.225	0.220	0.356	0.336	0.235
4.498	0.970	0.909	0.371	0.136	0.226	0.220	0.353	0.336	0.204
4.997	0.970	0.909	0.372	0.137	0.228	0.219	0.350	0.338	0.203
6.009	0.970	0.909	0.372	0.138	0.231	0.219	0.345	0.339	0.204
7.998	0.969	0.907	0.372	0.140	0.233	0.220	0.339	0.338	0.205
9.991	0.968	0.907	0.372	0.142	0.235	0.218	0.335	0.337	0.206

UR quadrant: $y/(w/2) = 0.058$

NPR	$p/p_{t,j}$ at x/L of— 0.068	0.230	0.281	0.319	0.357	0.417	0.481	0.540	0.592
2.007	0.951	0.808	0.748	0.686	0.613	0.493	0.455	0.447	0.540
2.493	0.951	0.808	0.748	0.686	0.614	0.492	0.454	0.422	0.382
3.009	0.952	0.808	0.747	0.686	0.613	0.492	0.454	0.408	0.372
3.509	0.952	0.808	0.748	0.686	0.613	0.492	0.454	0.400	0.371
3.999	0.952	0.807	0.746	0.686	0.613	0.492	0.454	0.395	0.370
4.498	0.951	0.807	0.746	0.685	0.613	0.491	0.454	0.391	0.370
4.997	0.951	0.807	0.746	0.685	0.612	0.491	0.455	0.388	0.369
6.009	0.951	0.806	0.745	0.684	0.611	0.491	0.454	0.384	0.370
7.998	0.950	0.805	0.744	0.683	0.610	0.490	0.454	0.382	0.370
9.991	0.949	0.803	0.742	0.682	0.609	0.489	0.453	0.379	0.370

UR quadrant: $y/(w/2) = 0.275$

NPR	$p/p_{t,j}$ at x/L of— 0.322	0.360	0.398	0.464	0.540
2.007	0.684	0.614	0.534	0.419	0.457
2.493	0.683	0.615	0.534	0.420	0.395
3.009	0.682	0.615	0.535	0.420	0.396
3.509	0.683	0.615	0.535	0.420	0.396
3.999	0.682	0.615	0.535	0.420	0.396
4.498	0.682	0.615	0.535	0.420	0.397
4.997	0.681	0.615	0.534	0.420	0.397
6.009	0.681	0.614	0.534	0.419	0.397
7.998	0.680	0.613	0.533	0.419	0.398
9.991	0.678	0.612	0.533	0.418	0.398

Table 26. Concluded

UR quadrant: $y/(w/2) = 0.491$

NPR	$p/p_{t,j}$ at x/L of— 0.068	0.236	0.362	0.400	0.438	0.488	0.592	0.681	0.770
2.007	0.960	0.831	0.587	0.513	0.423	0.335	0.512	0.416	0.486
2.493	0.962	0.830	0.587	0.513	0.422	0.336	0.435	0.360	0.384
3.009	0.962	0.830	0.587	0.513	0.423	0.337	0.297	0.366	0.291
3.509	0.962	0.831	0.586	0.513	0.423	0.337	0.292	0.365	0.259
3.999	0.961	0.830	0.586	0.513	0.424	0.338	0.292	0.366	0.253
4.498	0.961	0.830	0.586	0.513	0.424	0.338	0.293	0.367	0.252
4.997	0.961	0.830	0.586	0.513	0.424	0.338	0.293	0.367	0.252
6.009	0.961	0.830	0.585	0.512	0.423	0.338	0.293	0.365	0.255
7.998	0.961	0.828	0.584	0.512	0.423	0.339	0.293	0.369	0.264
9.991	0.960	0.827	0.582	0.511	0.422	0.339	0.292	0.367	0.261

UR quadrant: $y/(w/2) = 0.708$

NPR	$p/p_{t,j}$ at x/L of— 0.403	0.441	0.479	0.540
2.007	0.472	0.353	0.262	0.411
2.493	0.472	0.354	0.263	0.326
3.009	0.470	0.354	0.263	0.261
3.509	0.469	0.355	0.264	0.213
3.999	0.469	0.355	0.264	0.203
4.498	0.469	0.355	0.264	0.199
4.997	0.469	0.355	0.264	0.196
6.009	0.468	0.355	0.265	0.199
7.998	0.467	0.355	0.266	0.219
9.991	0.466	0.355	0.266	0.201

UR quadrant: $y/(w/2) = 0.924$

NPR	$p/p_{t,j}$ at x/L of— 0.068	0.236	0.444	0.482	0.592	0.681	0.770	0.858	0.947
2.007	0.969	0.908	0.368	0.402	0.386	0.364	0.435	0.530	0.513
2.493	0.970	0.908	0.368	0.194	0.281	0.267	0.349	0.440	0.411
3.009	0.970	0.907	0.368	0.137	0.230	0.229	0.359	0.399	0.335
3.509	0.970	0.907	0.369	0.137	0.220	0.222	0.358	0.347	0.284
3.999	0.971	0.907	0.368	0.138	0.220	0.222	0.357	0.336	0.237
4.498	0.970	0.907	0.370	0.139	0.221	0.222	0.356	0.335	0.203
4.997	0.971	0.907	0.370	0.140	0.221	0.223	0.358	0.334	0.198
6.009	0.970	0.906	0.370	0.141	0.220	0.228	0.355	0.325	0.195
7.998	0.969	0.905	0.370	0.145	0.229	0.238	0.335	0.327	0.198
9.991	0.969	0.904	0.370	0.148	0.230	0.232	0.335	0.325	0.199

Table 27. Nozzle Internal Static Pressure Ratios for Configuration 2

UL quadrant: $y/(w/2) = -0.058$

	$p/p_{t,j}$ at x/L of—							
NPR	0.137	0.188	0.226	0.264	0.324	0.387	0.447	0.498
2.009	0.757	0.705	0.648	0.585	0.488	0.471	0.456	0.455
2.507	0.757	0.706	0.648	0.584	0.488	0.472	0.457	0.410
3.005	0.757	0.706	0.647	0.584	0.489	0.472	0.457	0.404
3.497	0.758	0.706	0.646	0.583	0.489	0.473	0.458	0.404
4.001	0.758	0.705	0.646	0.583	0.489	0.473	0.459	0.404
4.998	0.757	0.705	0.645	0.582	0.489	0.473	0.459	0.405
5.984	0.757	0.706	0.645	0.581	0.489	0.474	0.459	0.406

UL quadrant: $y/(w/2) = -0.275$

	$p/p_{t,j}$ at x/L of—				
NPR	0.228	0.266	0.304	0.371	0.447
2.009	0.648	0.592	0.523	0.435	0.434
2.507	0.647	0.592	0.525	0.435	0.435
3.005	0.647	0.593	0.525	0.435	0.436
3.497	0.647	0.593	0.525	0.435	0.437
4.001	0.646	0.593	0.526	0.435	0.437
4.998	0.646	0.593	0.526	0.435	0.437
5.984	0.645	0.593	0.526	0.435	0.438

UL quadrant: $y/(w/2) = -0.491$

	$p/p_{t,j}$ at x/L of—								
NPR	0.142	0.269	0.307	0.345	0.395	0.447	0.498	0.587	0.676
2.009	0.771	0.578	0.517	0.452	0.389	0.398	0.362	0.526	0.507
2.507	0.771	0.579	0.518	0.452	0.390	0.399	0.363	0.365	0.419
3.005	0.773	0.579	0.518	0.452	0.390	0.399	0.363	0.364	0.325
3.497	0.772	0.578	0.519	0.452	0.391	0.400	0.363	0.363	0.293
4.001	0.773	0.579	0.519	0.451	0.391	0.400	0.363	0.363	0.287
4.998	0.772	0.579	0.519	0.451	0.391	0.401	0.363	0.363	0.285
5.984	0.772	0.579	0.519	0.450	0.391	0.401	0.363	0.363	0.284

Table 27. Continued

UL quadrant: $y/(w/2) = -0.708$

NPR	$p/p_{t,j}$ at x/L of— 0.310	0.348	0.386	0.447
2.009	0.496	0.427	0.364	0.322
2.507	0.495	0.426	0.365	0.324
3.005	0.494	0.426	0.366	0.325
3.497	0.494	0.425	0.367	0.326
4.001	0.493	0.425	0.367	0.326
4.998	0.493	0.425	0.368	0.327
5.984	0.492	0.424	0.368	0.327

UL quadrant: $y/(w/2) = -0.924$

NPR	$p/p_{t,j}$ at x/L of— 0.142	0.350	0.388	0.498	0.587	0.676	0.765	0.854
2.009	0.832	0.399	0.317	0.258	0.473	0.530	0.518	0.500
2.507	0.831	0.400	0.319	0.253	0.375	0.461	0.448	0.379
3.005	0.831	0.399	0.319	0.253	0.361	0.441	0.374	0.307
3.497	0.832	0.400	0.319	0.253	0.356	0.442	0.369	0.272
4.001	0.832	0.399	0.320	0.252	0.351	0.443	0.369	0.267
4.998	0.831	0.399	0.320	0.252	0.340	0.445	0.370	0.267
5.984	0.831	0.399	0.321	0.252	0.331	0.446	0.371	0.267

UR quadrant: $y/(w/2) = 0.058$

NPR	$p/p_{t,j}$ at x/L of— 0.137	0.188	0.226	0.264	0.324	0.387	0.447	0.498
2.009	0.756	0.702	0.649	0.586	0.484	0.473	0.474	0.459
2.507	0.755	0.703	0.650	0.587	0.484	0.472	0.453	0.413
3.005	0.755	0.702	0.649	0.587	0.484	0.472	0.442	0.406
3.497	0.754	0.701	0.650	0.586	0.484	0.472	0.434	0.405
4.001	0.754	0.700	0.649	0.586	0.484	0.472	0.429	0.406
4.998	0.753	0.701	0.649	0.585	0.483	0.472	0.424	0.406
5.984	0.753	0.700	0.648	0.585	0.483	0.472	0.421	0.406

UR quadrant: $y/(w/2) = 0.275$

NPR	$p/p_{t,j}$ at x/L of— 0.228	0.266	0.304	0.371	0.447
2.009	0.649	0.594	0.526	0.437	0.446
2.507	0.649	0.593	0.526	0.437	0.447
3.005	0.649	0.593	0.526	0.437	0.448
3.497	0.648	0.593	0.527	0.437	0.448
4.001	0.647	0.593	0.527	0.437	0.448
4.998	0.647	0.593	0.527	0.437	0.449
5.984	0.647	0.592	0.526	0.437	0.449

Table 27. Concluded

UR quadrant: $y/(w/2) = 0.491$

NPR	$p/p_{t,j}$ at x/L of— 0.142	0.269	0.307	0.345	0.395	0.498	0.587	0.676
2.009	0.771	0.573	0.521	0.448	0.390	0.371	0.530	0.507
2.507	0.769	0.575	0.521	0.450	0.390	0.371	0.376	0.425
3.005	0.769	0.573	0.521	0.450	0.390	0.372	0.373	0.324
3.497	0.769	0.573	0.521	0.451	0.391	0.372	0.373	0.288
4.001	0.769	0.572	0.521	0.451	0.391	0.372	0.373	0.280
4.998	0.768	0.571	0.521	0.451	0.391	0.372	0.371	0.278
5.984	0.767	0.572	0.520	0.450	0.391	0.372	0.370	0.278

UR quadrant: $y/(w/2) = 0.708$

NPR	$p/p_{t,j}$ at x/L of— 0.310	0.348	0.386	0.447
2.009	0.491	0.432	0.363	0.322
2.507	0.490	0.434	0.365	0.322
3.005	0.488	0.434	0.365	0.323
3.497	0.489	0.435	0.366	0.323
4.001	0.488	0.434	0.366	0.323
4.998	0.487	0.435	0.366	0.323
5.984	0.487	0.434	0.367	0.323

UR quadrant: $y/(w/2) = 0.924$

NPR	$p/p_{t,j}$ at x/L of— 0.142	0.350	0.388	0.498	0.587	0.676	0.765	0.854
2.009	0.829	0.399	0.336	0.290	0.459	0.529	0.517	0.498
2.507	0.828	0.401	0.338	0.255	0.380	0.457	0.447	0.379
3.005	0.827	0.401	0.339	0.255	0.367	0.436	0.376	0.304
3.497	0.828	0.401	0.340	0.255	0.363	0.437	0.370	0.267
4.001	0.827	0.401	0.340	0.255	0.357	0.438	0.369	0.261
4.998	0.827	0.401	0.341	0.254	0.344	0.440	0.371	0.261
5.984	0.826	0.402	0.342	0.254	0.331	0.442	0.371	0.261

Table 28. Nozzle Internal Static Pressure Ratios for Configuration 3

UL quadrant: $y/(w/2) = -0.058$

	$p/p_{t,j}$ at x/L of—											
NPR	0.068	0.230	0.281	0.319	0.357	0.417	0.481	0.540	0.592	0.681	0.770	0.897
1.996	0.951	0.813	0.751	0.688	0.613	0.498	0.510	0.630	0.606	0.551	0.514	0.502
2.500	0.951	0.813	0.751	0.687	0.613	0.498	0.456	0.419	0.557	0.515	0.442	0.372
3.003	0.950	0.813	0.752	0.687	0.613	0.499	0.457	0.419	0.387	0.494	0.418	0.357
3.517	0.951	0.813	0.751	0.687	0.612	0.499	0.457	0.420	0.387	0.334	0.414	0.319
3.992	0.950	0.813	0.751	0.687	0.611	0.500	0.458	0.420	0.387	0.332	0.361	0.302
4.479	0.950	0.813	0.751	0.686	0.611	0.499	0.458	0.420	0.387	0.332	0.290	0.308
5.039	0.951	0.813	0.751	0.686	0.611	0.499	0.458	0.421	0.386	0.332	0.279	0.312
6.037	0.950	0.812	0.751	0.685	0.610	0.499	0.458	0.421	0.386	0.333	0.279	0.274
6.983	0.950	0.812	0.751	0.685	0.609	0.499	0.458	0.421	0.387	0.333	0.278	0.250
7.977	0.949	0.812	0.750	0.684	0.608	0.499	0.458	0.421	0.386	0.333	0.278	0.237
9.962	0.949	0.811	0.749	0.682	0.607	0.498	0.458	0.421	0.386	0.333	0.277	0.232

UL quadrant: $y/(w/2) = -0.275$

	$p/p_{t,j}$ at x/L of—				
NPR	0.322	0.360	0.398	0.464	0.540
1.996	0.685	0.616	0.531	0.421	0.624
2.500	0.684	0.616	0.533	0.421	0.384
3.003	0.683	0.617	0.533	0.421	0.384
3.517	0.683	0.617	0.534	0.421	0.384
3.992	0.682	0.617	0.535	0.421	0.384
4.479	0.681	0.617	0.535	0.421	0.384
5.039	0.682	0.617	0.535	0.421	0.385
6.037	0.681	0.617	0.535	0.421	0.385
6.983	0.680	0.617	0.536	0.421	0.385
7.977	0.679	0.616	0.536	0.421	0.385
9.962	0.677	0.616	0.535	0.420	0.385

UL quadrant: $y/(w/2) = -0.491$

	$p/p_{t,j}$ at x/L of—									
NPR	0.068	0.236	0.362	0.400	0.438	0.488	0.540	0.592	0.681	0.770
1.996	0.960	0.834	0.596	0.511	0.423	0.452	0.583	0.575	0.527	0.506
2.500	0.960	0.834	0.594	0.510	0.422	0.337	0.417	0.507	0.465	0.416
3.003	0.961	0.834	0.595	0.511	0.422	0.337	0.317	0.444	0.386	0.393
3.517	0.961	0.835	0.594	0.511	0.422	0.337	0.317	0.309	0.383	0.308
3.992	0.960	0.834	0.595	0.511	0.422	0.338	0.318	0.289	0.392	0.305
4.479	0.960	0.835	0.594	0.511	0.422	0.338	0.318	0.288	0.382	0.309
5.039	0.960	0.835	0.595	0.511	0.421	0.338	0.318	0.288	0.362	0.313
6.037	0.960	0.834	0.594	0.511	0.421	0.338	0.319	0.288	0.306	0.313
6.983	0.960	0.834	0.594	0.511	0.420	0.338	0.319	0.288	0.284	0.311
7.977	0.960	0.834	0.593	0.511	0.420	0.338	0.319	0.288	0.281	0.309
9.962	0.959	0.833	0.592	0.511	0.418	0.338	0.319	0.287	0.275	0.300

Table 28. Continued

UL quadrant: $y/(w/2) = -0.708$

NPR	$p/p_{t,j}$ at x/L of— 0.403	0.441	0.479	0.540
1.996	0.480	0.344	0.433	0.498
2.500	0.479	0.343	0.260	0.381
3.003	0.477	0.343	0.261	0.326
3.517	0.477	0.343	0.262	0.285
3.992	0.477	0.342	0.262	0.200
4.479	0.477	0.342	0.262	0.186
5.039	0.476	0.342	0.262	0.186
6.037	0.476	0.342	0.262	0.186
6.983	0.476	0.342	0.262	0.186
7.977	0.475	0.341	0.263	0.187
9.962	0.474	0.340	0.263	0.187

UL quadrant: $y/(w/2) = -0.924$

NPR	$p/p_{t,j}$ at x/L of— 0.068	0.236	0.444	0.482	0.592
1.996	0.970	0.912	0.367	0.455	0.455
2.500	0.971	0.912	0.368	0.304	0.358
3.003	0.971	0.911	0.368	0.232	0.297
3.517	0.971	0.911	0.369	0.161	0.253
3.992	0.971	0.912	0.369	0.123	0.221
4.479	0.971	0.911	0.369	0.123	0.193
5.039	0.971	0.911	0.368	0.123	0.172
6.037	0.971	0.910	0.369	0.124	0.148
6.983	0.970	0.910	0.369	0.125	0.130
7.977	0.970	0.909	0.368	0.127	0.117
9.962	0.970	0.908	0.368	0.129	0.101

UR quadrant: $y/(w/2) = 0.058$

NPR	$p/p_{t,j}$ at x/L of— 0.068	0.230	0.281	0.319	0.357	0.417	0.481	0.540	0.592	0.681	0.770	0.897
1.996	0.946	0.811	0.749	0.687	0.612	0.493	0.510	0.633	0.607	0.550	0.518	0.504
2.500	0.947	0.810	0.748	0.687	0.612	0.493	0.455	0.432	0.556	0.515	0.447	0.375
3.003	0.946	0.810	0.748	0.687	0.611	0.493	0.455	0.432	0.384	0.494	0.422	0.359
3.517	0.947	0.810	0.748	0.687	0.611	0.493	0.455	0.433	0.384	0.334	0.419	0.320
3.992	0.947	0.809	0.747	0.687	0.612	0.493	0.455	0.433	0.383	0.332	0.374	0.307
4.479	0.947	0.810	0.747	0.687	0.613	0.493	0.455	0.434	0.383	0.332	0.294	0.309
5.039	0.947	0.809	0.746	0.687	0.613	0.493	0.455	0.434	0.383	0.332	0.284	0.308
6.037	0.946	0.808	0.746	0.686	0.613	0.493	0.455	0.435	0.383	0.332	0.283	0.303
6.983	0.948	0.807	0.745	0.686	0.612	0.493	0.454	0.435	0.382	0.332	0.283	0.247
7.977	0.946	0.807	0.745	0.685	0.611	0.492	0.454	0.434	0.381	0.332	0.283	0.236
9.962	0.946	0.806	0.743	0.684	0.610	0.491	0.453	0.434	0.380	0.331	0.283	0.232

UR quadrant: $y/(w/2) = 0.275$

NPR	$p/p_{t,j}$ at x/L of— 0.322	0.360	0.398	0.464	0.540
1.996	0.686	0.616	0.536	0.419	0.622
2.500	0.684	0.616	0.537	0.419	0.395
3.003	0.684	0.616	0.536	0.419	0.396
3.517	0.684	0.616	0.537	0.419	0.395
3.992	0.684	0.616	0.537	0.420	0.395
4.479	0.684	0.615	0.537	0.419	0.396
5.039	0.683	0.615	0.537	0.419	0.396
6.037	0.683	0.615	0.536	0.419	0.396
6.983	0.682	0.615	0.536	0.419	0.396
7.977	0.682	0.614	0.535	0.418	0.396
9.962	0.680	0.613	0.534	0.417	0.397

Table 28. Concluded

UR quadrant: $y/(w/2) = 0.491$

NPR	$p/p_{t,j}$ at x/L of— 0.068	0.236	0.362	0.400	0.438	0.488	0.540	0.592	0.681	0.770
1.996	0.960	0.831	0.587	0.516	0.425	0.431	0.585	0.580	0.524	0.511
2.500	0.960	0.831	0.587	0.515	0.425	0.338	0.395	0.516	0.466	0.422
3.003	0.961	0.831	0.587	0.515	0.425	0.338	0.322	0.438	0.380	0.404
3.517	0.961	0.832	0.586	0.515	0.426	0.338	0.323	0.300	0.388	0.318
3.992	0.960	0.831	0.586	0.515	0.426	0.338	0.323	0.290	0.390	0.313
4.479	0.960	0.831	0.585	0.515	0.426	0.340	0.323	0.290	0.373	0.319
5.039	0.960	0.830	0.586	0.515	0.426	0.340	0.323	0.291	0.347	0.326
6.037	0.960	0.830	0.585	0.515	0.426	0.341	0.324	0.291	0.303	0.322
6.983	0.960	0.830	0.584	0.515	0.426	0.341	0.324	0.291	0.298	0.322
7.977	0.959	0.829	0.584	0.514	0.425	0.341	0.324	0.291	0.298	0.310
9.962	0.959	0.829	0.582	0.513	0.424	0.341	0.325	0.290	0.297	0.278

UR quadrant: $y/(w/2) = 0.708$

NPR	$p/p_{t,j}$ at x/L of— 0.403	0.441	0.479	0.540
1.996	0.472	0.356	0.420	0.496
2.500	0.472	0.356	0.264	0.386
3.003	0.471	0.356	0.265	0.326
3.517	0.471	0.357	0.265	0.274
3.992	0.471	0.357	0.265	0.192
4.479	0.470	0.357	0.265	0.192
5.039	0.470	0.357	0.265	0.192
6.037	0.470	0.357	0.266	0.193
6.983	0.469	0.357	0.266	0.193
7.977	0.469	0.357	0.266	0.194
9.962	0.467	0.356	0.267	0.195

UR quadrant: $y/(w/2) = 0.924$

NPR	$p/p_{t,j}$ at x/L of— 0.068	0.236	0.444	0.482	0.592
1.996	0.966	0.910	0.373	0.455	0.462
2.500	0.968	0.908	0.371	0.239	0.367
3.003	0.967	0.908	0.372	0.150	0.308
3.517	0.967	0.908	0.372	0.135	0.262
3.992	0.967	0.908	0.373	0.136	0.231
4.479	0.967	0.908	0.374	0.137	0.207
5.039	0.967	0.908	0.374	0.138	0.184
6.037	0.967	0.908	0.374	0.141	0.154
6.983	0.967	0.907	0.374	0.143	0.139
7.977	0.967	0.906	0.374	0.145	0.124
9.962	0.967	0.905	0.372	0.148	0.107

Table 29. Nozzle Internal Static Pressure Ratios for Configuration 3-I

UL quadrant: $y/(w/2) = -0.058$

NPR	$p/p_{t,j}$ at x/L of— 0.068	0.230	0.281	0.319	0.357	0.417	0.481	0.540	0.592	0.681	0.770	0.897
2.019	0.952	0.812	0.752	0.688	0.614	0.498	0.479	0.627	0.604	0.547	0.508	0.498
2.502	0.951	0.812	0.752	0.687	0.614	0.498	0.456	0.419	0.555	0.514	0.443	0.372
3.001	0.950	0.813	0.752	0.687	0.613	0.498	0.457	0.419	0.387	0.492	0.418	0.356
3.508	0.950	0.812	0.752	0.686	0.612	0.498	0.457	0.420	0.387	0.333	0.413	0.318
3.997	0.950	0.812	0.752	0.686	0.612	0.499	0.457	0.420	0.387	0.332	0.359	0.302
4.515	0.950	0.812	0.751	0.686	0.612	0.499	0.457	0.420	0.387	0.332	0.296	0.307
5.007	0.949	0.812	0.752	0.685	0.611	0.499	0.458	0.420	0.387	0.332	0.279	0.311
5.980	0.950	0.812	0.751	0.685	0.610	0.499	0.458	0.421	0.387	0.333	0.278	0.276
6.995	0.949	0.812	0.750	0.684	0.609	0.499	0.458	0.421	0.387	0.333	0.278	0.250
7.974	0.949	0.811	0.750	0.683	0.608	0.499	0.458	0.421	0.386	0.333	0.278	0.238
9.998	0.948	0.811	0.749	0.682	0.607	0.498	0.458	0.421	0.386	0.333	0.277	0.232

UL quadrant: $y/(w/2) = -0.275$

NPR	$p/p_{t,j}$ at x/L of— 0.322	0.360	0.398	0.464	0.540
2.019	0.683	0.616	0.534	0.421	0.620
2.502	0.681	0.616	0.535	0.421	0.384
3.001	0.682	0.616	0.535	0.421	0.384
3.508	0.681	0.617	0.536	0.421	0.384
3.997	0.681	0.617	0.536	0.421	0.385
4.515	0.680	0.617	0.536	0.421	0.384
5.007	0.680	0.617	0.536	0.421	0.385
5.980	0.680	0.617	0.537	0.421	0.385
6.995	0.679	0.617	0.537	0.421	0.385
7.974	0.678	0.616	0.536	0.421	0.385
9.998	0.677	0.616	0.536	0.420	0.385

UL quadrant: $y/(w/2) = -0.491$

NPR	$p/p_{t,j}$ at x/L of— 0.068	0.236	0.362	0.400	0.438	0.488	0.540	0.592	0.681	0.770
2.019	0.959	0.835	0.596	0.510	0.423	0.409	0.576	0.572	0.522	0.499
2.502	0.959	0.834	0.594	0.510	0.422	0.337	0.410	0.505	0.466	0.414
3.001	0.959	0.835	0.594	0.511	0.422	0.337	0.317	0.433	0.387	0.391
3.508	0.959	0.835	0.594	0.510	0.421	0.337	0.317	0.302	0.384	0.308
3.997	0.959	0.835	0.594	0.511	0.422	0.337	0.318	0.288	0.391	0.304
4.515	0.959	0.835	0.594	0.511	0.421	0.338	0.318	0.288	0.386	0.307
5.007	0.959	0.835	0.594	0.511	0.421	0.338	0.319	0.288	0.368	0.311
5.980	0.959	0.835	0.594	0.511	0.420	0.338	0.319	0.288	0.310	0.311
6.995	0.959	0.834	0.593	0.511	0.419	0.338	0.319	0.288	0.284	0.308
7.974	0.959	0.834	0.593	0.511	0.419	0.338	0.319	0.288	0.281	0.308
9.998	0.958	0.833	0.592	0.511	0.417	0.338	0.319	0.288	0.275	0.297

Table 29. Continued

UL quadrant: $y/(w/2) = -0.708$

NPR	$p/p_{t,j}$ at x/L of— 0.403	0.441	0.479	0.540
2.019	0.480	0.341	0.425	0.488
2.502	0.479	0.341	0.260	0.379
3.001	0.477	0.340	0.260	0.321
3.508	0.477	0.340	0.260	0.283
3.997	0.477	0.340	0.260	0.204
4.515	0.477	0.340	0.260	0.186
5.007	0.477	0.340	0.261	0.186
5.980	0.476	0.339	0.261	0.187
6.995	0.476	0.339	0.261	0.187
7.974	0.475	0.339	0.262	0.187
9.998	0.474	0.339	0.262	0.188

UL quadrant: $y/(w/2) = -0.924$

NPR	$p/p_{t,j}$ at x/L of— 0.068	0.236	0.444	0.482	0.592
2.019	0.970	0.912	0.368	0.448	0.449
2.502	0.970	0.912	0.369	0.298	0.356
3.001	0.969	0.912	0.369	0.233	0.294
3.508	0.969	0.911	0.368	0.161	0.249
3.997	0.969	0.911	0.368	0.124	0.221
4.515	0.969	0.911	0.369	0.122	0.196
5.007	0.969	0.911	0.368	0.123	0.177
5.980	0.969	0.911	0.369	0.124	0.147
6.995	0.969	0.910	0.369	0.125	0.127
7.974	0.969	0.909	0.369	0.126	0.114
9.998	0.968	0.909	0.368	0.128	0.101

UR quadrant: $y/(w/2) = 0.058$

NPR	$p/p_{t,j}$ at x/L of— 0.068	0.230	0.281	0.319	0.357	0.417	0.481	0.540	0.592	0.681	0.770	0.897
2.019	0.946	0.812	0.749	0.687	0.615	0.494	0.480	0.629	0.605	0.546	0.512	0.501
2.502	0.946	0.810	0.748	0.687	0.615	0.493	0.456	0.430	0.555	0.514	0.448	0.376
3.001	0.946	0.811	0.748	0.687	0.614	0.493	0.455	0.431	0.384	0.489	0.422	0.360
3.508	0.946	0.810	0.748	0.687	0.614	0.494	0.455	0.432	0.384	0.333	0.418	0.320
3.997	0.947	0.809	0.747	0.687	0.614	0.494	0.455	0.432	0.384	0.331	0.371	0.306
4.515	0.946	0.809	0.746	0.687	0.613	0.493	0.455	0.432	0.384	0.331	0.292	0.309
5.007	0.946	0.809	0.746	0.686	0.613	0.493	0.455	0.433	0.383	0.332	0.284	0.310
5.980	0.946	0.808	0.746	0.686	0.613	0.493	0.455	0.434	0.383	0.332	0.283	0.304
6.995	0.946	0.808	0.745	0.685	0.612	0.493	0.455	0.434	0.383	0.332	0.283	0.251
7.974	0.946	0.807	0.744	0.685	0.611	0.492	0.454	0.434	0.382	0.331	0.283	0.237
9.998	0.945	0.806	0.743	0.684	0.610	0.492	0.453	0.434	0.380	0.331	0.282	0.232

UR quadrant: $y/(w/2) = 0.275$

NPR	$p/p_{t,j}$ at x/L of— 0.322	0.360	0.398	0.464	0.540
2.019	0.688	0.617	0.536	0.420	0.619
2.502	0.686	0.617	0.536	0.419	0.395
3.001	0.685	0.617	0.537	0.420	0.395
3.508	0.684	0.616	0.537	0.419	0.395
3.997	0.684	0.616	0.536	0.419	0.395
4.515	0.683	0.616	0.536	0.419	0.395
5.007	0.683	0.616	0.536	0.419	0.395
5.980	0.683	0.615	0.536	0.419	0.396
6.995	0.682	0.615	0.536	0.419	0.396
7.974	0.682	0.614	0.535	0.418	0.396
9.998	0.681	0.613	0.534	0.417	0.397

Table 29. Concluded

UR quadrant: $y/(w/2) = 0.491$

NPR	$p/p_{t,j}$ at x/L of— 0.068	0.236	0.362	0.400	0.438	0.488	0.540	0.592	0.681	0.770
2.019	0.962	0.833	0.588	0.516	0.425	0.381	0.578	0.578	0.519	0.505
2.502	0.960	0.833	0.588	0.516	0.425	0.339	0.391	0.516	0.466	0.423
3.001	0.961	0.832	0.586	0.516	0.425	0.339	0.323	0.438	0.380	0.404
3.508	0.961	0.832	0.586	0.516	0.425	0.339	0.323	0.299	0.387	0.318
3.997	0.961	0.831	0.586	0.516	0.426	0.340	0.323	0.290	0.389	0.314
4.515	0.960	0.832	0.585	0.516	0.425	0.340	0.323	0.291	0.371	0.320
5.007	0.960	0.832	0.585	0.516	0.426	0.340	0.324	0.291	0.348	0.327
5.980	0.960	0.831	0.584	0.515	0.426	0.341	0.324	0.291	0.305	0.323
6.995	0.960	0.831	0.584	0.515	0.425	0.341	0.324	0.291	0.298	0.322
7.974	0.959	0.830	0.583	0.514	0.425	0.341	0.324	0.291	0.298	0.312
9.998	0.958	0.829	0.582	0.513	0.424	0.341	0.325	0.291	0.298	0.278

UR quadrant: $y/(w/2) = 0.708$

NPR	$p/p_{t,j}$ at x/L of— 0.403	0.441	0.479	0.540
2.019	0.474	0.356	0.398	0.488
2.502	0.473	0.356	0.264	0.386
3.001	0.471	0.356	0.265	0.326
3.508	0.472	0.356	0.265	0.273
3.997	0.471	0.356	0.265	0.193
4.515	0.471	0.356	0.266	0.192
5.007	0.470	0.357	0.266	0.192
5.980	0.470	0.357	0.266	0.193
6.995	0.469	0.357	0.266	0.193
7.974	0.468	0.357	0.266	0.194
9.998	0.467	0.356	0.267	0.195

UR quadrant: $y/(w/2) = 0.924$

NPR	$p/p_{t,j}$ at x/L of— 0.068	0.236	0.444	0.482	0.592
2.019	0.966	0.910	0.371	0.449	0.455
2.502	0.966	0.910	0.372	0.236	0.367
3.001	0.965	0.909	0.372	0.149	0.308
3.508	0.966	0.908	0.372	0.135	0.261
3.997	0.966	0.909	0.373	0.137	0.230
4.515	0.966	0.909	0.373	0.137	0.205
5.007	0.966	0.908	0.373	0.139	0.185
5.980	0.966	0.908	0.373	0.141	0.155
6.995	0.966	0.907	0.373	0.143	0.140
7.974	0.966	0.907	0.373	0.145	0.124
9.998	0.966	0.906	0.371	0.148	0.107

Table 30. Nozzle Internal Static Pressure Ratios for Configuration 4

UL quadrant: $y/(w/2) = -0.058$

	$p/p_{t,j}$ at x/L of—										
NPR	0.137	0.188	0.226	0.264	0.324	0.387	0.447	0.498	0.587	0.676	0.803
2.010	0.761	0.706	0.651	0.589	0.491	0.475	0.459	0.428	0.560	0.519	0.498
2.505	0.762	0.708	0.651	0.589	0.490	0.475	0.459	0.428	0.377	0.417	0.397
3.009	0.762	0.707	0.651	0.588	0.491	0.476	0.461	0.428	0.377	0.347	0.361
3.496	0.762	0.707	0.651	0.588	0.492	0.476	0.461	0.428	0.377	0.347	0.340
4.008	0.761	0.707	0.650	0.588	0.492	0.476	0.461	0.428	0.377	0.348	0.317
4.502	0.761	0.708	0.650	0.587	0.492	0.476	0.461	0.428	0.377	0.348	0.313
4.996	0.761	0.708	0.649	0.586	0.492	0.476	0.461	0.428	0.377	0.348	0.311
6.006	0.761	0.707	0.649	0.586	0.492	0.476	0.462	0.428	0.377	0.348	0.308

UL quadrant: $y/(w/2) = -0.275$

	$p/p_{t,j}$ at x/L of—				
NPR	0.228	0.266	0.304	0.371	0.447
2.010	0.650	0.595	0.526	0.437	0.437
2.505	0.650	0.595	0.527	0.437	0.438
3.009	0.649	0.596	0.527	0.437	0.438
3.496	0.649	0.596	0.528	0.438	0.439
4.008	0.649	0.596	0.528	0.437	0.439
4.502	0.648	0.596	0.529	0.437	0.440
4.996	0.648	0.596	0.529	0.437	0.440
6.006	0.647	0.596	0.529	0.437	0.440

UL quadrant: $y/(w/2) = -0.491$

	$p/p_{t,j}$ at x/L of—								
NPR	0.142	0.269	0.307	0.345	0.395	0.447	0.498	0.587	0.676
2.010	0.774	0.581	0.519	0.453	0.392	0.401	0.423	0.545	0.505
2.505	0.775	0.581	0.520	0.453	0.393	0.401	0.369	0.455	0.392
3.009	0.775	0.582	0.521	0.453	0.393	0.402	0.369	0.370	0.363
3.496	0.776	0.582	0.521	0.453	0.394	0.403	0.369	0.368	0.323
4.008	0.776	0.581	0.521	0.453	0.394	0.403	0.369	0.367	0.315
4.502	0.775	0.582	0.521	0.452	0.394	0.403	0.369	0.367	0.314
4.996	0.776	0.582	0.521	0.452	0.394	0.403	0.369	0.366	0.314
6.006	0.775	0.581	0.521	0.451	0.394	0.403	0.369	0.365	0.314

Table 30. Continued

UL quadrant: $y/(w/2) = -0.708$

NPR	$p/p_{t,j}$ at x/L of— 0.310	0.348	0.386	0.447
2.010	0.497	0.430	0.367	0.324
2.505	0.495	0.429	0.368	0.325
3.009	0.495	0.429	0.368	0.325
3.496	0.495	0.429	0.369	0.325
4.008	0.495	0.429	0.369	0.326
4.502	0.494	0.428	0.369	0.326
4.996	0.494	0.428	0.369	0.326
6.006	0.493	0.427	0.370	0.326

UL quadrant: $y/(w/2) = -0.924$

NPR	$p/p_{t,j}$ at x/L of— 0.142	0.350	0.388	0.498
2.010	0.835	0.375	0.294	0.455
2.505	0.835	0.375	0.294	0.359
3.009	0.834	0.378	0.294	0.275
3.496	0.834	0.378	0.293	0.258
4.008	0.834	0.379	0.292	0.256
4.502	0.834	0.380	0.292	0.256
4.996	0.834	0.382	0.290	0.256
6.006	0.833	0.388	0.289	0.256

UR quadrant: $y/(w/2) = 0.058$

NPR	$p/p_{t,j}$ at x/L of— 0.137	0.188	0.226	0.264	0.324	0.387	0.447	0.498	0.587	0.676	0.803
2.010	0.760	0.707	0.651	0.590	0.487	0.476	0.470	0.425	0.560	0.523	0.499
2.505	0.759	0.707	0.653	0.591	0.487	0.475	0.471	0.425	0.377	0.414	0.399
3.009	0.759	0.706	0.653	0.590	0.487	0.476	0.472	0.426	0.377	0.352	0.367
3.496	0.759	0.706	0.653	0.591	0.487	0.476	0.472	0.426	0.377	0.352	0.331
4.008	0.758	0.705	0.652	0.591	0.487	0.476	0.473	0.426	0.377	0.352	0.314
4.502	0.757	0.705	0.652	0.590	0.487	0.476	0.473	0.426	0.377	0.353	0.313
4.996	0.756	0.704	0.652	0.590	0.487	0.475	0.474	0.426	0.377	0.353	0.313
6.006	0.756	0.704	0.652	0.589	0.486	0.475	0.474	0.426	0.376	0.353	0.312

UR quadrant: $y/(w/2) = 0.275$

NPR	$p/p_{t,j}$ at x/L of— 0.228	0.266	0.304	0.371	0.447
2.010	0.651	0.595	0.529	0.439	0.448
2.505	0.651	0.596	0.529	0.439	0.448
3.009	0.651	0.595	0.529	0.439	0.449
3.496	0.650	0.595	0.529	0.439	0.449
4.008	0.650	0.595	0.529	0.439	0.450
4.502	0.650	0.595	0.529	0.439	0.450
4.996	0.649	0.595	0.529	0.438	0.450
6.006	0.649	0.595	0.529	0.438	0.450

Table 30. Concluded

UR quadrant: $y/(w/2) = 0.491$

NPR	$p/p_{t,j}$ at x/L of— 0.142	0.269	0.307	0.345	0.395	0.447	0.498	0.587	0.676
2.010	0.774	0.575	0.524	0.453	0.392	0.406	0.485	0.543	0.508
2.505	0.772	0.577	0.524	0.453	0.393	0.406	0.372	0.467	0.395
3.009	0.773	0.575	0.524	0.453	0.393	0.406	0.372	0.396	0.370
3.496	0.772	0.575	0.524	0.454	0.394	0.407	0.372	0.388	0.327
4.008	0.772	0.574	0.524	0.454	0.394	0.407	0.372	0.386	0.318
4.502	0.771	0.574	0.524	0.453	0.394	0.407	0.372	0.385	0.317
4.996	0.772	0.574	0.524	0.453	0.394	0.407	0.372	0.385	0.317
6.006	0.771	0.573	0.524	0.453	0.394	0.408	0.372	0.383	0.316

UR quadrant: $y/(w/2) = 0.708$

NPR	$p/p_{t,j}$ at x/L of— 0.310	0.348	0.386	0.447
2.010	0.494	0.436	0.367	0.326
2.505	0.494	0.436	0.368	0.326
3.009	0.492	0.437	0.369	0.326
3.496	0.491	0.437	0.369	0.326
4.008	0.491	0.437	0.369	0.326
4.502	0.491	0.437	0.369	0.326
4.996	0.490	0.436	0.370	0.326
6.006	0.489	0.436	0.370	0.326

UR quadrant: $y/(w/2) = 0.924$

NPR	$p/p_{t,j}$ at x/L of— 0.142	0.350	0.388	0.498
2.010	0.832	0.405	0.341	0.475
2.505	0.831	0.406	0.342	0.365
3.009	0.831	0.405	0.343	0.282
3.496	0.831	0.407	0.344	0.258
4.008	0.830	0.406	0.344	0.257
4.502	0.830	0.406	0.344	0.257
4.996	0.830	0.406	0.345	0.257
6.006	0.829	0.405	0.344	0.257

Table 31. Nozzle Internal Static Pressure Ratios for Configuration 5

UL quadrant: $y/(w/2) = -0.058$

NPR	$p/p_{t,j}$ at x/L of— 0.068	0.263	0.320	0.358	0.415	0.477	0.540	0.592
2.001	0.945	0.784	0.708	0.636	0.532	0.444	0.444	0.531
2.501	0.945	0.784	0.709	0.634	0.533	0.443	0.443	0.399
3.004	0.946	0.784	0.709	0.633	0.533	0.443	0.443	0.392
3.495	0.946	0.784	0.709	0.633	0.533	0.444	0.443	0.392
4.005	0.946	0.784	0.709	0.633	0.533	0.443	0.444	0.392
4.503	0.945	0.783	0.709	0.632	0.533	0.442	0.443	0.392
5.012	0.945	0.783	0.708	0.632	0.533	0.442	0.443	0.392
6.017	0.944	0.783	0.708	0.632	0.532	0.442	0.443	0.391
8.002	0.944	0.782	0.706	0.632	0.531	0.441	0.443	0.390
9.998	0.944	0.781	0.706	0.632	0.531	0.441	0.443	0.390

UL quadrant: $y/(w/2) = -0.275$

NPR	$p/p_{t,j}$ at x/L of— 0.304	0.361	0.399	0.472	0.540
2.001	0.730	0.639	0.567	0.418	0.415
2.501	0.729	0.639	0.568	0.417	0.406
3.004	0.729	0.639	0.568	0.418	0.406
3.495	0.728	0.640	0.567	0.419	0.406
4.005	0.729	0.639	0.568	0.417	0.407
4.503	0.728	0.639	0.568	0.417	0.407
5.012	0.728	0.639	0.567	0.417	0.407
6.017	0.727	0.638	0.567	0.416	0.407
8.002	0.726	0.637	0.566	0.415	0.406
9.998	0.725	0.636	0.565	0.414	0.406

UL quadrant: $y/(w/2) = -0.491$

NPR	$p/p_{t,j}$ at x/L of— 0.068	0.236	0.345	0.402	0.440	0.490	0.540	0.592	0.681	0.770
2.001	0.960	0.833	0.661	0.540	0.461	0.346	0.472	0.522	0.440	0.496
2.501	0.959	0.832	0.659	0.541	0.461	0.348	0.323	0.446	0.393	0.376
3.004	0.960	0.832	0.659	0.541	0.462	0.347	0.323	0.333	0.396	0.291
3.495	0.959	0.832	0.659	0.541	0.462	0.348	0.323	0.327	0.394	0.269
4.005	0.958	0.832	0.659	0.541	0.462	0.347	0.324	0.325	0.394	0.267
4.503	0.958	0.831	0.658	0.540	0.462	0.347	0.324	0.323	0.393	0.268
5.012	0.958	0.831	0.657	0.540	0.462	0.347	0.324	0.322	0.395	0.270
6.017	0.957	0.830	0.657	0.540	0.462	0.346	0.324	0.320	0.397	0.273
8.002	0.956	0.829	0.655	0.539	0.461	0.346	0.324	0.318	0.401	0.278
9.998	0.956	0.829	0.654	0.538	0.461	0.345	0.324	0.317	0.397	0.281

Table 31. Continued

UL quadrant: $y/(w/2) = -0.708$

NPR	$p/p_{t,j}$ at x/L of— 0.385	0.442	0.480	0.540
2.001	0.594	0.397	0.311	0.427
2.501	0.592	0.397	0.312	0.331
3.004	0.592	0.398	0.312	0.249
3.495	0.591	0.398	0.313	0.241
4.005	0.591	0.398	0.312	0.232
4.503	0.590	0.398	0.312	0.227
5.012	0.590	0.397	0.312	0.221
6.017	0.589	0.397	0.312	0.215
8.002	0.587	0.396	0.311	0.214
9.998	0.587	0.396	0.311	0.214

UL quadrant: $y/(w/2) = -0.924$

NPR	$p/p_{t,j}$ at x/L of— 0.068	0.236	0.426	0.483	0.592	0.681	0.770	0.858	0.947
2.001	0.967	0.907	0.541	0.377	0.398	0.369	0.430	0.520	0.510
2.501	0.967	0.906	0.537	0.290	0.296	0.278	0.368	0.418	0.405
3.004	0.967	0.906	0.536	0.273	0.263	0.250	0.349	0.369	0.334
3.495	0.966	0.905	0.534	0.269	0.254	0.244	0.344	0.328	0.282
4.005	0.966	0.905	0.533	0.261	0.254	0.243	0.344	0.321	0.240
4.503	0.967	0.904	0.531	0.251	0.255	0.243	0.344	0.321	0.190
5.012	0.966	0.904	0.529	0.245	0.258	0.245	0.341	0.320	0.180
6.017	0.966	0.903	0.527	0.241	0.264	0.246	0.340	0.319	0.176
8.002	0.965	0.902	0.524	0.235	0.267	0.250	0.337	0.317	0.187
9.998	0.966	0.901	0.522	0.233	0.265	0.253	0.335	0.315	0.184

LL quadrant: $y/(w/2) = -0.058$

NPR	$p/p_{t,j}$ at x/L of— 0.068	0.230	0.281	0.319	0.357	0.417	0.481	0.592
2.001	0.948	0.811	0.758	0.698	0.630	0.515	0.485	0.533
2.501	0.948	0.810	0.756	0.698	0.630	0.514	0.484	0.393
3.004	0.946	0.810	0.755	0.698	0.630	0.514	0.484	0.386
3.495	0.947	0.810	0.755	0.698	0.629	0.514	0.484	0.385
4.005	0.947	0.810	0.755	0.697	0.629	0.514	0.484	0.384
4.503	0.947	0.808	0.754	0.697	0.628	0.513	0.483	0.384
5.012	0.946	0.808	0.753	0.696	0.628	0.513	0.483	0.384
6.017	0.946	0.807	0.752	0.696	0.627	0.512	0.483	0.383
8.002	0.945	0.806	0.751	0.694	0.625	0.511	0.482	0.383
9.998	0.945	0.805	0.749	0.693	0.623	0.510	0.481	0.383

LL quadrant: $y/(w/2) = -0.275$

NPR	$p/p_{t,j}$ at x/L of— 0.322	0.360	0.398	0.464	0.540
2.001	0.697	0.633	0.557	0.452	0.423
2.501	0.696	0.633	0.557	0.452	0.423
3.004	0.695	0.633	0.557	0.452	0.423
3.495	0.695	0.632	0.557	0.452	0.424
4.005	0.695	0.632	0.557	0.452	0.424
4.503	0.694	0.632	0.557	0.451	0.424
5.012	0.693	0.631	0.557	0.451	0.424
6.017	0.693	0.631	0.556	0.450	0.425
8.002	0.691	0.629	0.555	0.449	0.425
9.998	0.690	0.628	0.554	0.448	0.425

Table 31. Concluded

LL quadrant: $y/(w/2) = -0.491$

NPR	$p/p_{t,j}$ at x/L of— 0.068	0.236	0.362	0.400	0.438	0.488	0.540	0.592	0.681	0.770
2.001	0.960	0.832	0.610	0.541	0.456	0.373	0.452	0.531	0.434	0.496
2.501	0.961	0.831	0.608	0.542	0.455	0.374	0.358	0.411	0.388	0.378
3.004	0.961	0.830	0.608	0.542	0.456	0.374	0.358	0.308	0.397	0.286
3.495	0.959	0.830	0.608	0.542	0.457	0.374	0.358	0.308	0.395	0.267
4.005	0.960	0.830	0.608	0.542	0.456	0.375	0.359	0.308	0.396	0.264
4.503	0.959	0.830	0.608	0.542	0.456	0.375	0.360	0.307	0.395	0.265
5.012	0.959	0.829	0.607	0.541	0.456	0.375	0.359	0.306	0.397	0.267
6.017	0.959	0.828	0.606	0.541	0.455	0.376	0.360	0.306	0.400	0.270
8.002	0.958	0.827	0.604	0.540	0.455	0.376	0.360	0.306	0.405	0.274
9.998	0.958	0.826	0.603	0.539	0.454	0.376	0.361	0.306	0.405	0.277

LL quadrant: $y/(w/2) = -0.708$

NPR	$p/p_{t,j}$ at x/L of— 0.403	0.441	0.479	0.540
2.001	0.507	0.413	0.310	0.447
2.501	0.504	0.412	0.310	0.335
3.004	0.505	0.413	0.311	0.250
3.495	0.504	0.412	0.311	0.246
4.005	0.504	0.413	0.311	0.241
4.503	0.503	0.413	0.311	0.239
5.012	0.503	0.412	0.311	0.237
6.017	0.502	0.412	0.311	0.236
8.002	0.501	0.411	0.312	0.236
9.998	0.500	0.411	0.312	0.236

LL quadrant: $y/(w/2) = -0.924$

NPR	$p/p_{t,j}$ at x/L of— 0.068	0.236	0.444	0.482	0.592	0.681	0.770	0.858	0.947
2.001	0.969	0.903	0.436	0.339	0.395	0.368	0.427	0.520	0.510
2.501	0.968	0.903	0.438	0.273	0.296	0.279	0.367	0.419	0.406
3.004	0.968	0.902	0.437	0.269	0.261	0.251	0.350	0.372	0.337
3.495	0.968	0.901	0.438	0.269	0.253	0.245	0.345	0.330	0.287
4.005	0.969	0.902	0.437	0.265	0.254	0.244	0.344	0.324	0.247
4.503	0.968	0.901	0.436	0.262	0.253	0.244	0.344	0.325	0.199
5.012	0.968	0.900	0.435	0.261	0.256	0.246	0.342	0.323	0.190
6.017	0.967	0.900	0.433	0.257	0.262	0.248	0.340	0.322	0.185
8.002	0.966	0.898	0.432	0.253	0.269	0.251	0.338	0.320	0.199
9.998	0.966	0.897	0.431	0.253	0.267	0.254	0.335	0.317	0.195

Table 32. Nozzle Internal Static Pressure Ratios for Configuration 6

UL quadrant: $y/(w/2) = -0.058$

	$p/p_{t,j}$ at x/L of—								
NPR	0.068	0.233	0.297	0.361	0.399	0.439	0.490	0.540	0.592
2.009	0.957	0.879	0.844	0.886	0.527	0.599	0.600	0.617	0.554
2.504	0.956	0.877	0.843	0.884	0.582	0.578	0.485	0.554	0.503
2.986	0.957	0.877	0.843	0.884	0.567	0.575	0.482	0.479	0.461
4.008	0.957	0.877	0.843	0.883	0.532	0.573	0.482	0.477	0.436
4.496	0.957	0.877	0.842	0.883	0.514	0.574	0.480	0.478	0.437
5.014	0.957	0.877	0.842	0.882	0.504	0.574	0.478	0.480	0.438
6.047	0.956	0.876	0.841	0.881	0.500	0.577	0.478	0.478	0.434
7.034	0.956	0.876	0.841	0.880	0.518	0.579	0.478	0.479	0.438
8.003	0.955	0.875	0.840	0.880	0.547	0.578	0.483	0.479	0.440

UL quadrant: $y/(w/2) = -0.275$

	$p/p_{t,j}$ at x/L of—					
NPR	0.271	0.338	0.402	0.440	0.490	0.540
2.009	0.857	0.819	0.859	0.294	0.386	0.679
2.504	0.856	0.817	0.858	0.250	0.318	0.576
2.986	0.857	0.817	0.858	0.247	0.306	0.506
4.008	0.856	0.817	0.859	0.247	0.313	0.485
4.496	0.857	0.817	0.858	0.247	0.351	0.451
5.014	0.856	0.817	0.859	0.249	0.358	0.444
6.047	0.856	0.816	0.858	0.254	0.365	0.439
7.034	0.855	0.816	0.858	0.256	0.368	0.436
8.003	0.855	0.815	0.858	0.250	0.339	0.455

UL quadrant: $y/(w/2) = -0.491$

	$p/p_{t,j}$ at x/L of—								
NPR	0.068	0.210	0.379	0.442	0.480	0.540	0.592	0.681	0.770
2.009	0.966	0.902	0.787	0.850	0.368	0.363	0.393	0.498	0.504
2.504	0.967	0.900	0.784	0.848	0.277	0.287	0.264	0.383	0.418
2.986	0.967	0.901	0.784	0.848	0.184	0.235	0.247	0.377	0.344
4.008	0.966	0.902	0.783	0.848	0.182	0.207	0.265	0.368	0.276
4.496	0.966	0.901	0.783	0.848	0.179	0.208	0.274	0.364	0.269
5.014	0.967	0.901	0.783	0.849	0.178	0.213	0.280	0.352	0.270
6.047	0.966	0.900	0.782	0.848	0.176	0.215	0.283	0.356	0.266
7.034	0.966	0.900	0.782	0.848	0.174	0.218	0.287	0.353	0.266
8.003	0.966	0.899	0.781	0.848	0.179	0.215	0.285	0.353	0.268

Table 32. Continued

UL quadrant: $y/(w/2) = -0.708$

NPR	$p/p_{t,j}$ at x/L of— 0.419	0.483	0.521
2.009	0.785	0.831	0.397
2.504	0.781	0.824	0.297
2.986	0.781	0.824	0.245
4.008	0.781	0.825	0.203
4.496	0.781	0.825	0.199
5.014	0.781	0.824	0.198
6.047	0.780	0.824	0.195
7.034	0.779	0.823	0.194
8.003	0.779	0.823	0.194

UL quadrant: $y/(w/2) = -0.924$

NPR	$p/p_{t,j}$ at x/L of— 0.068	0.210	0.460	0.524	0.592	0.681	0.770	0.858	0.947
2.009	0.977	0.938	0.830	0.595	0.475	0.492	0.511	0.508	0.497
2.504	0.976	0.938	0.825	0.504	0.368	0.346	0.417	0.440	0.406
2.986	0.977	0.939	0.824	0.502	0.301	0.289	0.340	0.376	0.349
4.008	0.976	0.938	0.825	0.499	0.254	0.252	0.304	0.296	0.263
4.496	0.975	0.938	0.825	0.503	0.251	0.248	0.297	0.274	0.236
5.014	0.976	0.938	0.824	0.490	0.250	0.247	0.295	0.256	0.212
6.047	0.975	0.937	0.823	0.495	0.250	0.242	0.293	0.242	0.176
7.034	0.975	0.937	0.822	0.506	0.248	0.241	0.290	0.241	0.143
8.003	0.975	0.936	0.821	0.516	0.248	0.241	0.287	0.239	0.130

LL quadrant: $y/(w/2) = -0.058$

NPR	$p/p_{t,j}$ at x/L of— 0.068	0.263	0.320	0.358	0.415	0.477	0.540	0.592
2.009	0.958	0.866	0.886	0.425	0.663	0.593	0.603	0.524
2.504	0.958	0.864	0.886	0.423	0.655	0.519	0.483	0.485
2.986	0.958	0.864	0.886	0.425	0.655	0.516	0.466	0.377
4.008	0.958	0.864	0.887	0.433	0.655	0.514	0.467	0.375
4.496	0.958	0.863	0.887	0.436	0.654	0.514	0.468	0.373
5.014	0.957	0.864	0.887	0.434	0.653	0.516	0.470	0.373
6.047	0.957	0.863	0.887	0.435	0.653	0.515	0.470	0.377
7.034	0.956	0.863	0.886	0.435	0.654	0.513	0.470	0.377
8.003	0.956	0.862	0.886	0.437	0.651	0.513	0.468	0.379

LL quadrant: $y/(w/2) = -0.275$

NPR	$p/p_{t,j}$ at x/L of— 0.304	0.361	0.399	0.472	0.540
2.009	0.843	0.872	0.449	0.565	0.579
2.504	0.842	0.871	0.426	0.515	0.482
2.986	0.842	0.871	0.437	0.506	0.407
4.008	0.840	0.872	0.445	0.499	0.407
4.496	0.839	0.871	0.439	0.500	0.409
5.014	0.839	0.871	0.415	0.518	0.414
6.047	0.838	0.871	0.424	0.512	0.412
7.034	0.837	0.871	0.423	0.513	0.412
8.003	0.836	0.870	0.406	0.518	0.414

Table 32. Concluded

LL quadrant: $y/(w/2) = -0.491$

NPR	$p/p_{t,j}$ at x/L of—									
	0.068	0.236	0.345	0.402	0.440	0.490	0.540	0.592	0.681	0.770
2.009	0.967	0.889	0.818	0.868	0.435	0.480	0.500	0.483	0.495	0.500
2.504	0.967	0.886	0.816	0.867	0.384	0.448	0.405	0.424	0.387	0.402
2.986	0.968	0.886	0.814	0.867	0.364	0.457	0.313	0.301	0.300	0.336
4.008	0.967	0.886	0.814	0.868	0.357	0.454	0.316	0.241	0.303	0.223
4.496	0.968	0.885	0.814	0.867	0.357	0.447	0.314	0.234	0.304	0.217
5.014	0.967	0.886	0.813	0.868	0.386	0.465	0.320	0.247	0.303	0.214
6.047	0.967	0.884	0.813	0.867	0.367	0.457	0.320	0.241	0.308	0.214
7.034	0.967	0.884	0.812	0.867	0.341	0.452	0.319	0.238	0.310	0.214
8.003	0.966	0.883	0.811	0.866	0.341	0.451	0.319	0.232	0.314	0.212

LL quadrant: $y/(w/2) = -0.708$

NPR	$p/p_{t,j}$ at x/L of—			
	0.385	0.442	0.480	0.540
2.009	0.811	0.873	0.462	0.503
2.504	0.808	0.871	0.409	0.409
2.986	0.807	0.871	0.408	0.337
4.008	0.807	0.871	0.417	0.278
4.496	0.807	0.871	0.414	0.280
5.014	0.805	0.871	0.404	0.284
6.047	0.805	0.870	0.401	0.284
7.034	0.804	0.869	0.400	0.285
8.003	0.803	0.869	0.398	0.287

LL quadrant: $y/(w/2) = -0.924$

NPR	$p/p_{t,j}$ at x/L of—							
	0.236	0.426	0.483	0.592	0.681	0.770	0.858	0.947
2.009	0.928	0.826	0.875	0.475	0.492	0.503	0.509	0.493
2.504	0.928	0.822	0.874	0.361	0.345	0.407	0.437	0.401
2.986	0.929	0.821	0.875	0.300	0.288	0.333	0.371	0.342
4.008	0.928	0.822	0.876	0.255	0.254	0.299	0.292	0.255
4.496	0.927	0.822	0.876	0.252	0.251	0.293	0.270	0.229
5.014	0.927	0.821	0.876	0.251	0.249	0.290	0.253	0.204
6.047	0.927	0.820	0.875	0.252	0.245	0.289	0.240	0.167
7.034	0.927	0.818	0.874	0.252	0.243	0.288	0.239	0.136
8.003	0.926	0.817	0.873	0.251	0.243	0.286	0.237	0.123

Table 33. Nozzle Internal Static Pressure Ratios for Configuration 7

UL quadrant: $y/(w/2) = -0.058$

	$p/p_{t,j}$ at x/L of—								
NPR	0.068	0.230	0.281	0.319	0.357	0.417	0.481	0.540	0.592
2.031	0.929	0.763	0.698	0.634	0.561	0.451	0.420	0.427	0.479
2.489	0.928	0.763	0.698	0.633	0.560	0.451	0.420	0.426	0.421
2.991	0.928	0.762	0.698	0.632	0.560	0.451	0.419	0.426	0.413
3.491	0.927	0.762	0.698	0.632	0.559	0.451	0.419	0.425	0.413
3.986	0.927	0.762	0.697	0.631	0.558	0.451	0.419	0.425	0.413
4.530	0.927	0.762	0.698	0.630	0.558	0.452	0.418	0.424	0.413
4.989	0.926	0.762	0.697	0.630	0.557	0.452	0.418	0.424	0.413
6.014	0.926	0.762	0.697	0.629	0.556	0.452	0.418	0.424	0.413
6.945	0.925	0.761	0.697	0.628	0.556	0.451	0.418	0.423	0.413
7.989	0.925	0.760	0.696	0.627	0.554	0.451	0.417	0.422	0.414

UL quadrant: $y/(w/2) = -0.275$

	$p/p_{t,j}$ at x/L of—				
NPR	0.322	0.360	0.398	0.464	0.540
2.031	0.628	0.564	0.484	0.384	0.405
2.489	0.626	0.564	0.485	0.384	0.403
2.991	0.626	0.564	0.486	0.384	0.403
3.491	0.625	0.564	0.486	0.384	0.403
3.986	0.625	0.564	0.487	0.383	0.403
4.530	0.624	0.564	0.487	0.383	0.402
4.989	0.624	0.564	0.487	0.383	0.402
6.014	0.624	0.564	0.487	0.383	0.401
6.945	0.623	0.563	0.487	0.382	0.401
7.989	0.622	0.563	0.487	0.382	0.400

UL quadrant: $y/(w/2) = -0.491$

	$p/p_{t,j}$ at x/L of—									
NPR	0.068	0.236	0.362	0.400	0.438	0.488	0.540	0.592	0.681	0.770
2.031	0.941	0.780	0.536	0.465	0.390	0.318	0.368	0.502	0.481	0.494
2.489	0.941	0.779	0.536	0.465	0.390	0.318	0.340	0.382	0.402	0.385
2.991	0.940	0.780	0.536	0.465	0.390	0.319	0.340	0.381	0.383	0.342
3.491	0.941	0.779	0.536	0.465	0.390	0.319	0.340	0.381	0.366	0.292
3.986	0.940	0.780	0.535	0.465	0.390	0.319	0.339	0.382	0.357	0.289
4.530	0.940	0.779	0.535	0.465	0.389	0.319	0.339	0.381	0.350	0.290
4.989	0.940	0.779	0.535	0.465	0.389	0.319	0.339	0.381	0.348	0.291
6.014	0.939	0.778	0.534	0.465	0.388	0.319	0.338	0.381	0.342	0.292
6.945	0.939	0.778	0.534	0.465	0.388	0.319	0.338	0.381	0.339	0.293
7.989	0.939	0.777	0.533	0.465	0.388	0.319	0.337	0.380	0.336	0.293

Table 33. Continued

UL quadrant: $y/(w/2) = -0.708$

NPR	$p/p_{t,j}$ at x/L of— 0.403	0.441	0.479	0.540
2.031	0.418	0.338	0.273	0.395
2.489	0.419	0.338	0.273	0.229
2.991	0.417	0.337	0.273	0.230
3.491	0.417	0.337	0.274	0.230
3.986	0.417	0.337	0.274	0.230
4.530	0.417	0.337	0.274	0.231
4.989	0.417	0.337	0.274	0.231
6.014	0.417	0.336	0.275	0.231
6.945	0.416	0.336	0.275	0.231
7.989	0.416	0.336	0.275	0.232

UL quadrant: $y/(w/2) = -0.924$

NPR	$p/p_{t,j}$ at x/L of— 0.068	0.236	0.444	0.482	0.592	0.681	0.770	0.858	0.947
2.031	0.955	0.864	0.298	0.225	0.377	0.396	0.464	0.505	0.494
2.489	0.955	0.863	0.295	0.205	0.314	0.326	0.403	0.420	0.403
2.991	0.954	0.863	0.295	0.205	0.287	0.310	0.376	0.339	0.335
3.491	0.954	0.862	0.296	0.205	0.291	0.316	0.367	0.301	0.296
3.986	0.954	0.862	0.296	0.206	0.290	0.319	0.365	0.295	0.259
4.530	0.953	0.861	0.296	0.206	0.290	0.323	0.363	0.294	0.201
4.989	0.954	0.861	0.296	0.206	0.291	0.323	0.362	0.294	0.166
6.014	0.953	0.861	0.296	0.207	0.290	0.326	0.359	0.294	0.146
6.945	0.953	0.860	0.296	0.208	0.287	0.326	0.357	0.293	0.144
7.989	0.952	0.860	0.296	0.209	0.286	0.327	0.355	0.292	0.144

LL quadrant: $y/(w/2) = -0.058$

NPR	$p/p_{t,j}$ at x/L of— 0.014	0.177	0.227	0.266	0.304	0.364	0.427	0.487	0.538
2.031	0.924	0.826	0.770	0.713	0.647	0.542	0.524	0.485	0.477
2.489	0.923	0.825	0.769	0.713	0.647	0.542	0.524	0.485	0.424
2.991	0.923	0.825	0.769	0.713	0.647	0.542	0.524	0.485	0.417
3.491	0.923	0.825	0.769	0.713	0.647	0.541	0.524	0.484	0.416
3.986	0.922	0.824	0.767	0.712	0.647	0.541	0.524	0.485	0.416
4.530	0.922	0.824	0.767	0.712	0.646	0.541	0.524	0.484	0.416
4.989	0.922	0.823	0.767	0.712	0.646	0.541	0.524	0.485	0.416
6.014	0.921	0.823	0.766	0.711	0.646	0.540	0.524	0.484	0.416
6.945	0.920	0.822	0.766	0.710	0.645	0.539	0.524	0.484	0.416
7.989	0.920	0.821	0.765	0.710	0.644	0.539	0.524	0.484	0.415

LL quadrant: $y/(w/2) = -0.275$

NPR	$p/p_{t,j}$ at x/L of— 0.268	0.306	0.344	0.411	0.487
2.031	0.716	0.653	0.580	0.483	0.469
2.489	0.715	0.650	0.580	0.483	0.470
2.991	0.716	0.649	0.580	0.483	0.471
3.491	0.715	0.653	0.580	0.483	0.471
3.986	0.714	0.653	0.580	0.483	0.471
4.530	0.713	0.653	0.579	0.483	0.472
4.989	0.714	0.653	0.579	0.482	0.472
6.014	0.713	0.652	0.573	0.482	0.472
6.945	0.713	0.652	0.571	0.481	0.472
7.989	0.712	0.651	0.569	0.481	0.472

Table 33. Concluded

LL quadrant: $y/(w/2) = -0.491$

NPR	0.014	0.182	0.309	0.347	0.385	0.435	0.487	0.627	0.716
	$p/p_{t,j}$ at x/L of—								
2.031	0.942	0.846	0.644	0.577	0.492	0.418	0.406	0.500	0.501
2.489	0.942	0.846	0.643	0.577	0.491	0.419	0.406	0.339	0.431
2.991	0.941	0.845	0.642	0.577	0.492	0.419	0.406	0.307	0.392
3.491	0.940	0.845	0.642	0.577	0.492	0.420	0.407	0.308	0.328
3.986	0.940	0.845	0.642	0.577	0.491	0.420	0.407	0.308	0.315
4.530	0.939	0.843	0.641	0.577	0.492	0.420	0.407	0.309	0.312
4.989	0.939	0.843	0.641	0.577	0.491	0.420	0.408	0.309	0.313
6.014	0.938	0.842	0.640	0.576	0.491	0.420	0.407	0.310	0.313
6.945	0.938	0.842	0.640	0.575	0.491	0.420	0.408	0.310	0.312
7.989	0.937	0.841	0.639	0.573	0.491	0.420	0.408	0.311	0.307

LL quadrant: $y/(w/2) = -0.708$

NPR	0.349	0.388	0.426	0.487
	$p/p_{t,j}$ at x/L of—			
2.031	0.569	0.486	0.382	0.297
2.489	0.569	0.486	0.382	0.296
2.991	0.568	0.486	0.382	0.296
3.491	0.568	0.486	0.382	0.296
3.986	0.569	0.486	0.382	0.297
4.530	0.568	0.486	0.382	0.297
4.989	0.568	0.486	0.382	0.297
6.014	0.568	0.486	0.382	0.297
6.945	0.567	0.485	0.382	0.298
7.989	0.567	0.485	0.381	0.298

LL quadrant: $y/(w/2) = -0.924$

NPR	0.014	0.182	0.390	0.428	0.538	0.627	0.716	0.805	0.894
	$p/p_{t,j}$ at x/L of—								
2.031	0.939	0.901	0.508	0.390	0.376	0.450	0.491	0.499	0.494
2.489	0.940	0.899	0.506	0.389	0.306	0.401	0.442	0.411	0.403
2.991	0.941	0.898	0.506	0.389	0.262	0.379	0.398	0.339	0.340
3.491	0.942	0.898	0.505	0.390	0.259	0.376	0.390	0.309	0.305
3.986	0.942	0.899	0.506	0.390	0.256	0.374	0.389	0.304	0.241
4.530	0.943	0.898	0.505	0.390	0.255	0.374	0.389	0.304	0.177
4.989	0.943	0.898	0.505	0.391	0.257	0.374	0.390	0.304	0.163
6.014	0.944	0.898	0.505	0.391	0.254	0.372	0.389	0.304	0.159
6.945	0.944	0.897	0.504	0.391	0.253	0.368	0.388	0.305	0.159
7.989	0.943	0.896	0.503	0.392	0.263	0.353	0.386	0.306	0.160

Table 34. Nozzle Internal Static Pressure Ratios for Configuration 8

UL quadrant: $y/(w/2) = -0.058$

	$p/p_{t,j}$ at x/L of—								
NPR	0.068	0.230	0.281	0.319	0.357	0.417	0.481	0.540	0.592
2.005	0.908	0.724	0.660	0.597	0.525	0.429	0.425	0.473	0.497
2.498	0.909	0.724	0.659	0.597	0.525	0.429	0.424	0.472	0.428
2.977	0.909	0.724	0.660	0.596	0.524	0.429	0.424	0.472	0.422
3.523	0.909	0.725	0.660	0.596	0.523	0.429	0.424	0.472	0.422
3.980	0.908	0.725	0.661	0.596	0.523	0.430	0.424	0.472	0.422
4.521	0.908	0.725	0.660	0.595	0.522	0.430	0.424	0.472	0.423
4.987	0.908	0.725	0.660	0.595	0.522	0.430	0.424	0.472	0.423
5.972	0.908	0.725	0.660	0.594	0.521	0.430	0.423	0.471	0.424
6.984	0.907	0.724	0.660	0.593	0.520	0.430	0.423	0.470	0.425
7.539	0.907	0.724	0.659	0.593	0.519	0.429	0.422	0.469	0.425

UL quadrant: $y/(w/2) = -0.275$

	$p/p_{t,j}$ at x/L of—				
NPR	0.322	0.360	0.398	0.464	0.540
2.005	0.589	0.531	0.461	0.384	0.449
2.498	0.589	0.531	0.467	0.383	0.448
2.977	0.589	0.532	0.469	0.383	0.448
3.523	0.589	0.532	0.469	0.383	0.448
3.980	0.588	0.532	0.470	0.383	0.448
4.521	0.588	0.532	0.471	0.383	0.448
4.987	0.587	0.532	0.472	0.383	0.448
5.972	0.587	0.532	0.472	0.382	0.447
6.984	0.586	0.532	0.463	0.381	0.446
7.539	0.586	0.532	0.463	0.381	0.445

UL quadrant: $y/(w/2) = -0.491$

	$p/p_{t,j}$ at x/L of—									
NPR	0.068	0.236	0.362	0.400	0.438	0.488	0.540	0.592	0.681	0.770
2.005	0.923	0.736	0.499	0.439	0.376	0.347	0.416	0.518	0.510	0.499
2.498	0.925	0.736	0.499	0.439	0.376	0.346	0.416	0.417	0.319	0.409
2.977	0.924	0.737	0.499	0.440	0.376	0.345	0.416	0.418	0.315	0.379
3.523	0.923	0.737	0.499	0.440	0.376	0.345	0.417	0.418	0.314	0.313
3.980	0.923	0.737	0.499	0.440	0.376	0.345	0.417	0.419	0.315	0.299
4.521	0.924	0.737	0.500	0.440	0.376	0.345	0.417	0.419	0.315	0.297
4.987	0.924	0.738	0.500	0.440	0.376	0.345	0.417	0.419	0.316	0.297
5.972	0.923	0.737	0.500	0.440	0.375	0.344	0.417	0.420	0.316	0.298
6.984	0.922	0.736	0.499	0.440	0.374	0.344	0.417	0.420	0.316	0.299
7.539	0.922	0.736	0.499	0.440	0.374	0.343	0.417	0.420	0.316	0.299

Table 34. Continued

UL quadrant: $y/(w/2) = -0.708$

NPR	$p/p_{t,j}$ at x/L of— 0.403	0.441	0.479	0.540
2.005	0.395	0.328	0.284	0.336
2.498	0.395	0.327	0.285	0.330
2.977	0.394	0.327	0.286	0.331
3.523	0.393	0.327	0.286	0.332
3.980	0.393	0.327	0.286	0.332
4.521	0.393	0.327	0.286	0.333
4.987	0.393	0.327	0.287	0.333
5.972	0.393	0.327	0.286	0.334
6.984	0.392	0.326	0.287	0.334
7.539	0.392	0.326	0.286	0.335

UL quadrant: $y/(w/2) = -0.924$

NPR	$p/p_{t,j}$ at x/L of— 0.068	0.236	0.444	0.482	0.592	0.681	0.770	0.858	0.947
2.005	0.939	0.819	0.302	0.229	0.384	0.497	0.512	0.499	0.498
2.498	0.939	0.819	0.302	0.228	0.330	0.434	0.439	0.386	0.401
2.977	0.940	0.820	0.301	0.229	0.302	0.418	0.399	0.304	0.343
3.523	0.939	0.820	0.302	0.230	0.298	0.417	0.377	0.278	0.301
3.980	0.939	0.819	0.302	0.231	0.296	0.417	0.378	0.273	0.257
4.521	0.939	0.819	0.302	0.231	0.292	0.416	0.380	0.273	0.170
4.987	0.939	0.819	0.302	0.231	0.290	0.416	0.380	0.274	0.125
5.972	0.938	0.818	0.302	0.231	0.285	0.416	0.381	0.274	0.114
6.984	0.938	0.818	0.302	0.231	0.280	0.416	0.381	0.275	0.114
7.539	0.937	0.818	0.302	0.232	0.275	0.415	0.381	0.275	0.115

LL quadrant: $y/(w/2) = -0.058$

NPR	$p/p_{t,j}$ at x/L of— 0.137	0.188	0.226	0.264	0.324	0.387	0.447	0.498
2.005	0.831	0.780	0.728	0.667	0.575	0.570	0.532	0.502
2.498	0.831	0.779	0.728	0.667	0.575	0.570	0.532	0.432
2.977	0.831	0.779	0.728	0.667	0.575	0.571	0.533	0.427
3.523	0.830	0.779	0.728	0.667	0.575	0.571	0.533	0.427
3.980	0.830	0.778	0.728	0.667	0.575	0.571	0.533	0.428
4.521	0.829	0.779	0.727	0.667	0.575	0.571	0.533	0.429
4.987	0.829	0.778	0.727	0.667	0.574	0.571	0.533	0.429
5.972	0.829	0.777	0.727	0.666	0.574	0.571	0.533	0.429
6.984	0.828	0.776	0.726	0.665	0.573	0.571	0.533	0.430
7.539	0.827	0.776	0.726	0.665	0.573	0.570	0.532	0.430

LL quadrant: $y/(w/2) = -0.275$

NPR	$p/p_{t,j}$ at x/L of— 0.228	0.266	0.304	0.371	0.447
2.005	0.733	0.675	0.608	0.532	0.518
2.498	0.732	0.675	0.608	0.532	0.519
2.977	0.732	0.675	0.608	0.532	0.520
3.523	0.732	0.675	0.608	0.532	0.521
3.980	0.731	0.675	0.609	0.532	0.521
4.521	0.731	0.675	0.608	0.531	0.521
4.987	0.731	0.675	0.608	0.531	0.521
5.972	0.730	0.674	0.600	0.530	0.521
6.984	0.729	0.674	0.599	0.530	0.521
7.539	0.729	0.674	0.599	0.529	0.521

Table 34. Concluded

LL quadrant: $y/(w/2) = -0.491$

NPR	$p/p_{t,j}$ at x/L of— 0.142	0.269	0.307	0.345	0.395	0.447	0.498	0.587	0.676
2.005	0.847	0.670	0.611	0.534	0.482	0.472	0.503	0.516	0.503
2.498	0.848	0.668	0.611	0.534	0.482	0.473	0.410	0.316	0.417
2.977	0.848	0.668	0.611	0.535	0.482	0.474	0.411	0.313	0.383
3.523	0.847	0.669	0.612	0.535	0.483	0.474	0.413	0.313	0.324
3.980	0.847	0.668	0.612	0.535	0.483	0.475	0.414	0.314	0.306
4.521	0.847	0.668	0.612	0.534	0.482	0.475	0.415	0.314	0.303
4.987	0.847	0.667	0.612	0.534	0.483	0.475	0.415	0.315	0.303
5.972	0.847	0.667	0.611	0.534	0.483	0.475	0.415	0.315	0.304
6.984	0.846	0.667	0.610	0.533	0.482	0.475	0.415	0.315	0.305
7.539	0.845	0.666	0.609	0.533	0.482	0.475	0.415	0.315	0.306

LL quadrant: $y/(w/2) = -0.708$

NPR	$p/p_{t,j}$ at x/L of— 0.310	0.348	0.386	0.447
2.005	0.607	0.541	0.454	0.395
2.498	0.608	0.542	0.454	0.396
2.977	0.608	0.542	0.454	0.396
3.523	0.608	0.542	0.454	0.397
3.980	0.609	0.542	0.454	0.398
4.521	0.608	0.542	0.454	0.398
4.987	0.608	0.542	0.453	0.398
5.972	0.608	0.541	0.453	0.398
6.984	0.608	0.541	0.452	0.398
7.539	0.608	0.540	0.450	0.398

LL quadrant: $y/(w/2) = -0.924$

NPR	$p/p_{t,j}$ at x/L of— 0.142	0.350	0.388	0.498	0.587	0.676	0.765	0.854
2.005	0.897	0.548	0.481	0.405	0.514	0.519	0.504	0.500
2.498	0.896	0.548	0.482	0.326	0.452	0.450	0.383	0.402
2.977	0.894	0.548	0.482	0.302	0.426	0.404	0.314	0.352
3.523	0.893	0.548	0.483	0.299	0.426	0.385	0.287	0.307
3.980	0.894	0.548	0.483	0.296	0.426	0.385	0.281	0.244
4.521	0.893	0.547	0.484	0.292	0.426	0.385	0.281	0.150
4.987	0.893	0.547	0.484	0.290	0.427	0.386	0.281	0.123
5.972	0.892	0.547	0.484	0.282	0.428	0.387	0.281	0.120
6.984	0.891	0.546	0.484	0.276	0.429	0.387	0.281	0.121
7.539	0.891	0.546	0.483	0.272	0.430	0.387	0.282	0.122

Table 35. Nozzle Internal Static Pressure Ratios for Configuration 9

UL quadrant: $y/(w/2) = -0.058$

NPR	$p/p_{t,j}$ at x/L of— 0.068	0.230	0.281	0.319	0.357	0.417	0.481	0.540	0.592	0.681	0.770	0.897
2.016	0.927	0.764	0.699	0.634	0.560	0.452	0.418	0.600	0.596	0.549	0.506	0.499
2.497	0.927	0.763	0.700	0.633	0.560	0.452	0.419	0.430	0.442	0.409	0.468	0.395
3.001	0.927	0.763	0.699	0.633	0.559	0.452	0.418	0.430	0.441	0.368	0.327	0.334
3.503	0.927	0.763	0.699	0.633	0.559	0.452	0.418	0.430	0.441	0.368	0.279	0.331
4.002	0.927	0.762	0.698	0.632	0.559	0.452	0.418	0.429	0.441	0.368	0.278	0.342
4.499	0.928	0.763	0.699	0.632	0.558	0.453	0.418	0.430	0.441	0.368	0.278	0.354
5.014	0.927	0.763	0.698	0.631	0.558	0.453	0.419	0.430	0.442	0.369	0.278	0.341
6.000	0.927	0.762	0.698	0.630	0.556	0.452	0.418	0.429	0.441	0.369	0.278	0.317
6.981	0.927	0.761	0.698	0.629	0.556	0.452	0.418	0.429	0.441	0.370	0.278	0.300
8.028	0.926	0.761	0.697	0.628	0.554	0.452	0.418	0.428	0.441	0.370	0.278	0.289
8.921	0.926	0.760	0.696	0.628	0.554	0.451	0.417	0.428	0.441	0.370	0.278	0.283

UL quadrant: $y/(w/2) = -0.275$

NPR	$p/p_{t,j}$ at x/L of— 0.322	0.360	0.398	0.464	0.540
2.016	0.629	0.564	0.487	0.383	0.589
2.497	0.627	0.565	0.487	0.384	0.403
3.001	0.627	0.565	0.488	0.383	0.403
3.503	0.626	0.564	0.488	0.383	0.402
4.002	0.626	0.564	0.488	0.383	0.402
4.499	0.625	0.564	0.488	0.383	0.402
5.014	0.625	0.564	0.489	0.383	0.402
6.000	0.624	0.564	0.489	0.383	0.401
6.981	0.623	0.564	0.488	0.382	0.400
8.028	0.623	0.563	0.488	0.382	0.399
8.921	0.622	0.563	0.488	0.381	0.399

UL quadrant: $y/(w/2) = -0.491$

NPR	$p/p_{t,j}$ at x/L of— 0.068	0.236	0.362	0.400	0.438	0.488	0.540	0.592	0.681	0.770
2.016	0.940	0.778	0.535	0.465	0.389	0.318	0.536	0.580	0.533	0.496
2.497	0.942	0.778	0.536	0.465	0.389	0.318	0.342	0.460	0.428	0.440
3.001	0.941	0.779	0.535	0.465	0.389	0.318	0.341	0.393	0.402	0.322
3.503	0.941	0.779	0.536	0.465	0.389	0.319	0.340	0.388	0.366	0.308
4.002	0.941	0.779	0.536	0.465	0.388	0.319	0.340	0.387	0.329	0.306
4.499	0.941	0.779	0.536	0.465	0.388	0.319	0.339	0.386	0.313	0.310
5.014	0.941	0.779	0.535	0.465	0.388	0.319	0.340	0.387	0.311	0.319
6.000	0.940	0.778	0.534	0.465	0.387	0.319	0.339	0.387	0.310	0.325
6.981	0.940	0.778	0.534	0.465	0.387	0.319	0.338	0.386	0.310	0.321
8.028	0.940	0.778	0.534	0.465	0.386	0.319	0.337	0.385	0.310	0.321
8.921	0.939	0.778	0.533	0.464	0.386	0.319	0.337	0.385	0.309	0.319

Table 35. Continued

UL quadrant: $y/(w/2) = -0.708$

NPR	$p/p_{t,j}$ at x/L of— 0.403	0.441	0.479	0.540
2.016	0.418	0.335	0.342	0.457
2.497	0.418	0.335	0.272	0.365
3.001	0.417	0.334	0.272	0.227
3.503	0.417	0.334	0.273	0.228
4.002	0.416	0.334	0.273	0.228
4.499	0.416	0.334	0.272	0.228
5.014	0.416	0.334	0.274	0.228
6.000	0.415	0.333	0.274	0.229
6.981	0.414	0.332	0.273	0.229
8.028	0.414	0.332	0.273	0.229
8.921	0.413	0.331	0.273	0.229

UL quadrant: $y/(w/2) = -0.924$

NPR	$p/p_{t,j}$ at x/L of— 0.068	0.236	0.444	0.482	0.592
2.016	0.953	0.862	0.288	0.384	0.492
2.497	0.952	0.861	0.288	0.204	0.403
3.001	0.954	0.861	0.287	0.204	0.349
3.503	0.953	0.862	0.289	0.203	0.301
4.002	0.954	0.861	0.288	0.202	0.269
4.499	0.954	0.861	0.277	0.204	0.246
5.014	0.954	0.861	0.286	0.203	0.227
6.000	0.953	0.860	0.285	0.203	0.195
6.981	0.953	0.859	0.283	0.199	0.163
8.028	0.953	0.859	0.282	0.201	0.144
8.921	0.953	0.858	0.284	0.201	0.140

LL quadrant: $y/(w/2) = -0.058$

NPR	$p/p_{t,j}$ at x/L of— 0.014	0.177	0.227	0.266	0.304	0.364	0.427	0.487	0.538	0.627	0.716	0.843
2.016	0.942	0.826	0.771	0.713	0.649	0.541	0.526	0.486	0.555	0.570	0.530	0.497
2.497	0.942	0.825	0.770	0.713	0.649	0.541	0.526	0.489	0.435	0.325	0.496	0.422
3.001	0.943	0.825	0.769	0.713	0.649	0.541	0.526	0.490	0.435	0.321	0.430	0.347
3.503	0.942	0.824	0.769	0.713	0.649	0.541	0.526	0.490	0.435	0.320	0.365	0.331
4.002	0.943	0.824	0.768	0.713	0.649	0.540	0.527	0.491	0.435	0.319	0.361	0.324
4.499	0.942	0.824	0.768	0.713	0.649	0.540	0.527	0.491	0.435	0.319	0.359	0.315
5.014	0.942	0.824	0.768	0.713	0.648	0.540	0.527	0.491	0.435	0.319	0.359	0.305
6.000	0.941	0.823	0.767	0.712	0.648	0.539	0.527	0.491	0.435	0.319	0.358	0.305
6.981	0.941	0.822	0.766	0.712	0.648	0.539	0.527	0.491	0.435	0.318	0.357	0.306
8.028	0.940	0.822	0.765	0.711	0.647	0.538	0.526	0.491	0.435	0.318	0.357	0.307
8.921	0.940	0.821	0.765	0.710	0.646	0.538	0.526	0.492	0.434	0.317	0.356	0.308

LL quadrant: $y/(w/2) = -0.275$

NPR	$p/p_{t,j}$ at x/L of— 0.268	0.306	0.344	0.411	0.487
2.016	0.718	0.652	0.580	0.482	0.470
2.497	0.717	0.653	0.580	0.482	0.471
3.001	0.716	0.653	0.579	0.482	0.471
3.503	0.715	0.653	0.580	0.482	0.472
4.002	0.714	0.653	0.579	0.481	0.472
4.499	0.714	0.653	0.579	0.481	0.472
5.014	0.714	0.653	0.580	0.481	0.472
6.000	0.714	0.652	0.572	0.480	0.472
6.981	0.713	0.652	0.571	0.479	0.473
8.028	0.712	0.651	0.570	0.478	0.473
8.921	0.712	0.651	0.568	0.477	0.473

Table 35. Concluded

LL quadrant: $y/(w/2) = -0.491$

NPR	$p/p_{t,j}$ at x/L of— 0.014	0.182	0.309	0.385	0.435	0.487	0.538	0.627	0.716
2.016	0.956	0.845	0.644	0.490	0.418	0.405	0.553	0.552	0.511
2.497	0.957	0.846	0.643	0.490	0.419	0.406	0.362	0.470	0.420
3.001	0.957	0.845	0.642	0.490	0.419	0.406	0.362	0.410	0.375
3.503	0.957	0.845	0.641	0.490	0.420	0.407	0.363	0.277	0.363
4.002	0.957	0.844	0.641	0.490	0.419	0.407	0.363	0.276	0.362
4.499	0.957	0.845	0.640	0.490	0.420	0.407	0.363	0.275	0.362
5.014	0.956	0.844	0.640	0.490	0.420	0.407	0.363	0.275	0.359
6.000	0.957	0.844	0.639	0.489	0.419	0.407	0.363	0.275	0.349
6.981	0.956	0.843	0.639	0.489	0.420	0.407	0.363	0.274	0.348
8.028	0.956	0.843	0.638	0.488	0.423	0.407	0.363	0.273	0.346
8.921	0.956	0.842	0.637	0.488	0.420	0.407	0.363	0.272	0.344

LL quadrant: $y/(w/2) = -0.708$

NPR	$p/p_{t,j}$ at x/L of— 0.349	0.388	0.426	0.487
2.016	0.567	0.484	0.381	0.301
2.497	0.566	0.485	0.381	0.294
3.001	0.566	0.484	0.381	0.294
3.503	0.566	0.484	0.381	0.295
4.002	0.566	0.482	0.381	0.295
4.499	0.566	0.483	0.381	0.294
5.014	0.565	0.483	0.381	0.295
6.000	0.565	0.482	0.380	0.294
6.981	0.564	0.482	0.380	0.294
8.028	0.564	0.481	0.379	0.295
8.921	0.563	0.481	0.377	0.295

LL quadrant: $y/(w/2) = -0.924$

NPR	$p/p_{t,j}$ at x/L of— 0.014	0.182	0.390	0.428	0.538
2.016	0.967	0.902	0.498	0.381	0.468
2.497	0.966	0.901	0.497	0.381	0.379
3.001	0.966	0.900	0.498	0.381	0.268
3.503	0.964	0.899	0.498	0.383	0.229
4.002	0.962	0.899	0.494	0.382	0.186
4.499	0.962	0.899	0.496	0.379	0.167
5.014	0.962	0.898	0.495	0.381	0.162
6.000	0.961	0.897	0.495	0.378	0.160
6.981	0.960	0.895	0.494	0.376	0.152
8.028	0.959	0.895	0.493	0.375	0.154
8.921	0.959	0.894	0.495	0.376	0.154

Table 36. Nozzle Internal Static Pressure Ratios for Configuration 10

UL quadrant: $y/(w/2) = -0.058$

	$p/p_{t,j}$ at x/L of—											
NPR	0.068	0.230	0.281	0.319	0.357	0.417	0.481	0.540	0.592	0.681	0.770	0.897
2.000	0.909	0.726	0.663	0.597	0.528	0.429	0.443	0.604	0.591	0.540	0.502	0.500
2.488	0.908	0.726	0.662	0.596	0.527	0.429	0.424	0.481	0.483	0.415	0.446	0.374
3.010	0.909	0.726	0.661	0.596	0.526	0.429	0.424	0.481	0.482	0.369	0.323	0.312
3.500	0.909	0.725	0.661	0.596	0.526	0.429	0.424	0.480	0.482	0.367	0.284	0.304
4.018	0.909	0.725	0.662	0.595	0.525	0.429	0.424	0.479	0.483	0.368	0.281	0.317
4.504	0.908	0.725	0.661	0.594	0.524	0.429	0.424	0.478	0.484	0.368	0.281	0.317
4.988	0.908	0.724	0.660	0.594	0.523	0.429	0.424	0.478	0.484	0.368	0.281	0.310
5.983	0.908	0.724	0.660	0.593	0.522	0.429	0.423	0.477	0.485	0.368	0.281	0.309
6.986	0.907	0.724	0.660	0.592	0.521	0.428	0.423	0.476	0.486	0.368	0.281	0.311
7.365	0.907	0.724	0.659	0.591	0.520	0.428	0.422	0.476	0.486	0.368	0.281	0.311

UL quadrant: $y/(w/2) = -0.275$

	$p/p_{t,j}$ at x/L of—				
NPR	0.322	0.360	0.398	0.464	0.540
2.000	0.589	0.531	0.459	0.383	0.597
2.488	0.590	0.531	0.459	0.383	0.455
3.010	0.588	0.531	0.460	0.382	0.453
3.500	0.589	0.531	0.461	0.382	0.452
4.018	0.588	0.531	0.461	0.382	0.451
4.504	0.587	0.531	0.461	0.382	0.451
4.988	0.587	0.531	0.461	0.381	0.450
5.983	0.586	0.531	0.461	0.381	0.449
6.986	0.585	0.530	0.461	0.380	0.448
7.365	0.585	0.530	0.461	0.380	0.448

UL quadrant: $y/(w/2) = -0.491$

	$p/p_{t,j}$ at x/L of—									
NPR	0.068	0.236	0.362	0.400	0.438	0.488	0.540	0.592	0.681	0.770
2.000	0.924	0.737	0.502	0.439	0.376	0.405	0.569	0.578	0.526	0.499
2.488	0.925	0.737	0.500	0.439	0.376	0.345	0.426	0.477	0.418	0.430
3.010	0.924	0.737	0.499	0.439	0.375	0.345	0.419	0.429	0.385	0.315
3.500	0.924	0.737	0.500	0.439	0.375	0.345	0.419	0.419	0.350	0.291
4.018	0.923	0.738	0.499	0.439	0.375	0.344	0.419	0.419	0.338	0.299
4.504	0.924	0.737	0.499	0.439	0.374	0.344	0.419	0.418	0.322	0.303
4.988	0.924	0.737	0.499	0.439	0.374	0.344	0.419	0.419	0.321	0.298
5.983	0.923	0.736	0.499	0.438	0.373	0.343	0.419	0.418	0.320	0.292
6.986	0.923	0.736	0.498	0.438	0.372	0.342	0.419	0.418	0.320	0.292
7.365	0.922	0.736	0.497	0.438	0.372	0.342	0.418	0.418	0.320	0.292

Table 36. Continued

UL quadrant: $y/(w/2) = -0.708$

NPR	$p/p_{t,j}$ at x/L of— 0.403	0.441	0.479	0.540
2.000	0.395	0.327	0.406	0.504
2.488	0.395	0.326	0.284	0.440
3.010	0.394	0.326	0.285	0.334
3.500	0.392	0.325	0.284	0.332
4.018	0.393	0.325	0.284	0.333
4.504	0.392	0.324	0.284	0.333
4.988	0.391	0.324	0.284	0.333
5.983	0.391	0.323	0.283	0.333
6.986	0.390	0.322	0.283	0.333
7.365	0.390	0.322	0.283	0.333

UL quadrant: $y/(w/2) = -0.924$

NPR	$p/p_{t,j}$ at x/L of— 0.068	0.236	0.444	0.482	0.592
2.000	0.938	0.821	0.305	0.415	0.497
2.488	0.939	0.820	0.302	0.228	0.398
3.010	0.940	0.819	0.301	0.227	0.337
3.500	0.939	0.819	0.305	0.222	0.301
4.018	0.939	0.819	0.302	0.230	0.285
4.504	0.939	0.818	0.303	0.230	0.270
4.988	0.939	0.818	0.297	0.229	0.251
5.983	0.938	0.817	0.302	0.227	0.214
6.986	0.938	0.816	0.300	0.231	0.181
7.365	0.938	0.816	0.299	0.227	0.174

LL quadrant: $y/(w/2) = -0.058$

NPR	$p/p_{t,j}$ at x/L of— 0.137	0.188	0.226	0.264	0.324	0.387	0.447	0.498	0.587	0.676	0.803
2.000	0.832	0.780	0.728	0.668	0.575	0.572	0.536	0.485	0.575	0.540	0.502
2.488	0.831	0.779	0.728	0.668	0.575	0.571	0.536	0.482	0.354	0.506	0.406
3.010	0.831	0.779	0.728	0.668	0.574	0.572	0.537	0.482	0.351	0.430	0.357
3.500	0.830	0.779	0.727	0.668	0.574	0.572	0.537	0.482	0.351	0.401	0.350
4.018	0.830	0.778	0.727	0.668	0.573	0.572	0.537	0.482	0.351	0.395	0.332
4.504	0.829	0.778	0.727	0.668	0.573	0.572	0.537	0.482	0.351	0.390	0.329
4.988	0.829	0.777	0.727	0.667	0.572	0.572	0.537	0.482	0.351	0.386	0.329
5.983	0.828	0.776	0.726	0.667	0.571	0.572	0.538	0.482	0.350	0.381	0.329
6.986	0.828	0.776	0.725	0.666	0.570	0.572	0.538	0.481	0.350	0.377	0.330
7.365	0.827	0.775	0.725	0.666	0.570	0.572	0.538	0.481	0.350	0.377	0.330

LL quadrant: $y/(w/2) = -0.275$

NPR	$p/p_{t,j}$ at x/L of— 0.228	0.266	0.304	0.371	0.447
2.000	0.733	0.674	0.608	0.531	0.519
2.488	0.732	0.674	0.608	0.531	0.521
3.010	0.731	0.674	0.608	0.531	0.522
3.500	0.731	0.674	0.608	0.531	0.522
4.018	0.730	0.674	0.608	0.530	0.522
4.504	0.730	0.674	0.607	0.530	0.523
4.988	0.730	0.674	0.605	0.529	0.523
5.983	0.729	0.673	0.599	0.528	0.523
6.986	0.729	0.673	0.598	0.527	0.522
7.365	0.728	0.672	0.597	0.527	0.523

Table 36. Concluded

LL quadrant: $y/(w/2) = -0.491$

NPR	$p/p_{t,j}$ at x/L of— 0.142	0.269	0.345	0.395	0.447	0.498	0.587	0.676
2.000	0.848	0.670	0.533	0.482	0.472	0.422	0.561	0.519
2.488	0.848	0.667	0.533	0.483	0.474	0.422	0.385	0.428
3.010	0.848	0.668	0.533	0.483	0.474	0.423	0.304	0.399
3.500	0.848	0.668	0.533	0.482	0.474	0.423	0.304	0.400
4.018	0.847	0.667	0.533	0.483	0.474	0.423	0.304	0.389
4.504	0.847	0.667	0.533	0.482	0.474	0.423	0.304	0.381
4.988	0.846	0.666	0.532	0.482	0.474	0.423	0.304	0.381
5.983	0.846	0.665	0.531	0.482	0.474	0.423	0.304	0.381
6.986	0.845	0.665	0.530	0.481	0.474	0.423	0.303	0.382
7.365	0.845	0.664	0.530	0.481	0.474	0.423	0.303	0.382

LL quadrant: $y/(w/2) = -0.708$

NPR	$p/p_{t,j}$ at x/L of— 0.310	0.348	0.386	0.447
2.000	0.607	0.539	0.452	0.395
2.488	0.607	0.539	0.452	0.396
3.010	0.606	0.539	0.452	0.396
3.500	0.606	0.539	0.452	0.396
4.018	0.606	0.539	0.452	0.396
4.504	0.605	0.538	0.451	0.396
4.988	0.605	0.538	0.451	0.396
5.983	0.604	0.537	0.450	0.395
6.986	0.604	0.536	0.450	0.395
7.365	0.603	0.535	0.447	0.395

LL quadrant: $y/(w/2) = -0.924$

NPR	$p/p_{t,j}$ at x/L of— 0.142	0.350	0.388	0.498
2.000	0.896	0.543	0.475	0.465
2.488	0.895	0.541	0.475	0.329
3.010	0.893	0.541	0.475	0.239
3.500	0.893	0.541	0.475	0.229
4.018	0.892	0.541	0.475	0.227
4.504	0.891	0.540	0.474	0.228
4.988	0.891	0.539	0.474	0.229
5.983	0.890	0.538	0.473	0.230
6.986	0.889	0.537	0.473	0.227
7.365	0.889	0.537	0.473	0.228

Table 37. Nozzle Internal Static Pressure Ratios for Configuration 11

UL quadrant: $y/(w/2) = -0.058$

	$p/p_{t,j}$ at x/L of—								
NPR	0.068	0.212	0.250	0.314	0.377	0.439	0.490	0.540	0.592
2.024	0.964	0.689	0.537	0.542	0.532	0.516	0.513	0.504	0.500
2.499	0.961	0.687	0.529	0.510	0.473	0.484	0.472	0.455	0.414
2.997	0.964	0.688	0.530	0.507	0.443	0.465	0.465	0.448	0.390
3.497	0.963	0.687	0.529	0.505	0.444	0.440	0.455	0.442	0.383
4.007	0.964	0.686	0.529	0.503	0.441	0.434	0.448	0.439	0.379
5.028	0.963	0.686	0.529	0.503	0.442	0.434	0.431	0.432	0.379
5.994	0.963	0.685	0.527	0.502	0.447	0.430	0.438	0.435	0.384
8.011	0.963	0.683	0.525	0.499	0.445	0.427	0.433	0.435	0.388
9.985	0.962	0.681	0.524	0.498	0.444	0.420	0.437	0.435	0.387

UL quadrant: $y/(w/2) = -0.275$

	$p/p_{t,j}$ at x/L of—					
NPR	0.253	0.291	0.355	0.418	0.477	0.540
2.024	0.583	0.331	0.336	0.533	0.552	0.533
2.499	0.582	0.331	0.273	0.604	0.522	0.476
2.997	0.578	0.334	0.250	0.578	0.523	0.462
3.497	0.575	0.334	0.244	0.548	0.516	0.456
4.007	0.575	0.335	0.241	0.543	0.510	0.451
5.028	0.573	0.335	0.236	0.519	0.485	0.440
5.994	0.572	0.334	0.232	0.533	0.496	0.445
8.011	0.570	0.331	0.227	0.529	0.486	0.449
9.985	0.568	0.331	0.223	0.538	0.494	0.452

UL quadrant: $y/(w/2) = -0.491$

	$p/p_{t,j}$ at x/L of—									
NPR	0.068	0.210	0.294	0.332	0.395	0.464	0.540	0.592	0.681	0.770
2.024	0.980	0.930	0.599	0.301	0.379	0.434	0.411	0.420	0.476	0.498
2.499	0.978	0.930	0.595	0.301	0.245	0.306	0.370	0.379	0.389	0.404
2.997	0.980	0.931	0.591	0.302	0.210	0.249	0.378	0.350	0.338	0.337
3.497	0.979	0.930	0.590	0.301	0.183	0.229	0.354	0.329	0.309	0.292
4.007	0.980	0.930	0.588	0.303	0.196	0.221	0.338	0.324	0.303	0.263
5.028	0.978	0.930	0.585	0.301	0.230	0.247	0.329	0.320	0.317	0.234
5.994	0.979	0.930	0.583	0.300	0.211	0.223	0.322	0.319	0.308	0.234
8.011	0.978	0.929	0.580	0.300	0.219	0.217	0.305	0.319	0.316	0.234
9.985	0.978	0.928	0.579	0.299	0.204	0.202	0.306	0.316	0.307	0.234

Table 37. Continued

UL quadrant: $y/(w/2) = -0.708$

NPR	$p/p_{t,j}$ at x/L of— 0.334	0.372	0.436	0.540
2.024	0.665	0.283	0.389	0.394
2.499	0.663	0.285	0.352	0.333
2.997	0.664	0.286	0.286	0.315
3.497	0.663	0.285	0.241	0.290
4.007	0.662	0.284	0.245	0.283
5.028	0.662	0.284	0.192	0.276
5.994	0.660	0.283	0.226	0.282
8.011	0.659	0.282	0.215	0.280
9.985	0.657	0.282	0.226	0.281

UL quadrant: $y/(w/2) = -0.924$

NPR	$p/p_{t,j}$ at x/L of— 0.068	0.210	0.375	0.413	0.540	0.592	0.681	0.770	0.858	0.947
2.024	0.986	0.973	0.787	0.371	0.429	0.454	0.513	0.516	0.506	0.494
2.499	0.988	0.973	0.784	0.218	0.354	0.384	0.398	0.402	0.410	0.401
2.997	0.989	0.973	0.783	0.176	0.326	0.336	0.344	0.348	0.348	0.337
3.497	0.987	0.973	0.782	0.164	0.319	0.320	0.323	0.324	0.310	0.289
4.007	0.987	0.973	0.782	0.163	0.312	0.312	0.313	0.303	0.275	0.252
5.028	0.986	0.973	0.780	0.153	0.304	0.305	0.307	0.299	0.246	0.206
5.994	0.986	0.972	0.778	0.164	0.307	0.308	0.308	0.289	0.219	0.169
8.011	0.986	0.971	0.773	0.150	0.304	0.305	0.307	0.292	0.223	0.119
9.985	0.985	0.970	0.769	0.152	0.307	0.307	0.307	0.285	0.215	0.112

UR quadrant: $y/(w/2) = 0.058$

NPR	$p/p_{t,j}$ at x/L of— 0.068	0.233	0.297	0.361	0.399	0.439	0.490	0.540	0.592
2.024	0.955	0.752	0.644	0.578	0.543	0.506	0.505	0.507	0.513
2.499	0.957	0.748	0.633	0.525	0.506	0.476	0.465	0.461	0.409
2.997	0.959	0.748	0.633	0.524	0.466	0.431	0.452	0.449	0.381
3.497	0.955	0.748	0.633	0.524	0.466	0.413	0.439	0.441	0.373
4.007	0.956	0.748	0.633	0.524	0.466	0.411	0.432	0.438	0.371
5.028	0.956	0.748	0.633	0.524	0.465	0.410	0.421	0.430	0.369
5.994	0.955	0.748	0.633	0.524	0.466	0.408	0.428	0.434	0.371
8.011	0.955	0.747	0.632	0.523	0.465	0.407	0.425	0.431	0.374
9.985	0.954	0.746	0.631	0.523	0.464	0.406	0.428	0.433	0.376

UR quadrant: $y/(w/2) = 0.275$

NPR	$p/p_{t,j}$ at x/L of— 0.271	0.338	0.402	0.440	0.490	0.540
2.024	0.725	0.619	0.543	0.489	0.417	0.445
2.499	0.721	0.603	0.502	0.459	0.386	0.395
2.997	0.720	0.603	0.501	0.434	0.341	0.383
3.497	0.720	0.603	0.503	0.434	0.340	0.365
4.007	0.720	0.603	0.503	0.435	0.340	0.355
5.028	0.720	0.603	0.503	0.435	0.341	0.351
5.994	0.719	0.603	0.503	0.435	0.341	0.346
8.011	0.718	0.602	0.503	0.435	0.341	0.338
9.985	0.717	0.601	0.502	0.434	0.341	0.332

Table 37. Concluded

UR quadrant: $y/(w/2) = 0.491$

NPR	$p/p_{t,j}$ at x/L of— 0.068	0.210	0.379	0.442	0.480	0.540	0.592	0.681	0.770
2.024	0.958	0.849	0.582	0.477	0.412	0.324	0.506	0.457	0.491
2.499	0.957	0.847	0.569	0.450	0.382	0.300	0.277	0.423	0.367
2.997	0.958	0.847	0.569	0.449	0.378	0.280	0.248	0.377	0.285
3.497	0.958	0.846	0.568	0.448	0.378	0.281	0.240	0.270	0.311
4.007	0.958	0.846	0.569	0.449	0.379	0.282	0.240	0.246	0.318
5.028	0.958	0.846	0.568	0.449	0.381	0.283	0.241	0.237	0.253
5.994	0.957	0.845	0.568	0.449	0.381	0.284	0.241	0.235	0.253
8.011	0.956	0.845	0.567	0.448	0.382	0.286	0.242	0.232	0.254
9.985	0.957	0.844	0.566	0.448	0.382	0.287	0.242	0.229	0.256

UR quadrant: $y/(w/2) = 0.708$

NPR	$p/p_{t,j}$ at x/L of— 0.419	0.483	0.521
2.024	0.528	0.378	0.287
2.499	0.519	0.362	0.269
2.997	0.518	0.363	0.270
3.497	0.519	0.364	0.271
4.007	0.519	0.365	0.271
5.028	0.519	0.366	0.273
5.994	0.519	0.367	0.274
8.011	0.518	0.368	0.275
9.985	0.518	0.370	0.275

UR quadrant: $y/(w/2) = 0.924$

NPR	$p/p_{t,j}$ at x/L of— 0.068	0.210	0.460	0.524	0.592	0.681	0.770	0.858	0.947
2.024	0.966	0.901	0.502	0.309	0.392	0.358	0.405	0.510	0.508
2.499	0.963	0.901	0.497	0.242	0.312	0.289	0.287	0.399	0.422
2.997	0.966	0.901	0.496	0.238	0.250	0.234	0.229	0.324	0.355
3.497	0.966	0.901	0.497	0.239	0.213	0.196	0.188	0.288	0.303
4.007	0.966	0.901	0.497	0.239	0.188	0.176	0.166	0.270	0.260
5.028	0.966	0.901	0.498	0.240	0.155	0.163	0.151	0.247	0.210
5.994	0.966	0.901	0.498	0.241	0.148	0.166	0.149	0.247	0.178
8.011	0.964	0.900	0.498	0.244	0.162	0.160	0.145	0.239	0.157
9.985	0.963	0.899	0.497	0.247	0.153	0.164	0.141	0.238	0.159

Table 38. Nozzle Internal Static Pressure Ratios for Configuration 11-I

UL quadrant: $y/(w/2) = -0.058$

	$p/p_{t,j}$ at x/L of—								
NPR	0.068	0.212	0.250	0.314	0.377	0.439	0.490	0.540	0.592
2.014	0.960	0.690	0.537	0.553	0.563	0.524	0.516	0.495	0.473
2.532	0.963	0.687	0.526	0.508	0.504	0.469	0.460	0.453	0.403
3.014	0.963	0.687	0.526	0.505	0.476	0.467	0.461	0.447	0.390
3.504	0.964	0.686	0.527	0.502	0.474	0.439	0.453	0.442	0.384
3.991	0.963	0.686	0.526	0.501	0.472	0.435	0.444	0.438	0.381
4.485	0.963	0.686	0.526	0.499	0.470	0.436	0.433	0.433	0.377
5.015	0.963	0.685	0.526	0.497	0.469	0.429	0.440	0.435	0.379
6.011	0.962	0.684	0.526	0.495	0.449	0.428	0.435	0.432	0.377
7.993	0.962	0.683	0.525	0.493	0.449	0.422	0.438	0.434	0.380
9.984	0.962	0.681	0.523	0.493	0.448	0.415	0.439	0.432	0.380

UL quadrant: $y/(w/2) = -0.275$

	$p/p_{t,j}$ at x/L of—					
NPR	0.253	0.291	0.355	0.418	0.477	0.540
2.014	0.582	0.330	0.335	0.568	0.551	0.490
2.532	0.578	0.331	0.265	0.540	0.515	0.472
3.014	0.576	0.335	0.251	0.576	0.508	0.453
3.504	0.574	0.335	0.243	0.544	0.503	0.445
3.991	0.574	0.335	0.239	0.538	0.497	0.446
4.485	0.573	0.334	0.235	0.519	0.478	0.434
5.015	0.572	0.334	0.232	0.535	0.493	0.443
6.011	0.570	0.333	0.228	0.527	0.485	0.440
7.993	0.569	0.333	0.222	0.532	0.490	0.443
9.984	0.568	0.333	0.219	0.534	0.491	0.442

UL quadrant: $y/(w/2) = -0.491$

	$p/p_{t,j}$ at x/L of—									
NPR	0.068	0.210	0.294	0.332	0.395	0.464	0.540	0.592	0.681	0.770
2.014	0.976	0.929	0.590	0.304	0.386	0.487	0.430	0.388	0.432	0.501
2.532	0.978	0.930	0.587	0.302	0.267	0.288	0.333	0.363	0.388	0.400
3.014	0.979	0.930	0.585	0.302	0.197	0.250	0.378	0.353	0.332	0.335
3.504	0.979	0.929	0.584	0.302	0.139	0.236	0.355	0.331	0.307	0.292
3.991	0.979	0.930	0.584	0.302	0.158	0.225	0.348	0.328	0.297	0.264
4.485	0.979	0.929	0.582	0.302	0.216	0.237	0.319	0.331	0.307	0.238
5.015	0.979	0.929	0.582	0.301	0.179	0.216	0.335	0.326	0.295	0.233
6.011	0.978	0.929	0.581	0.301	0.200	0.220	0.321	0.329	0.300	0.232
7.993	0.978	0.929	0.580	0.300	0.179	0.210	0.329	0.328	0.295	0.232
9.984	0.978	0.928	0.578	0.299	0.174	0.208	0.329	0.330	0.293	0.232

Table 38. Continued

UL quadrant: $y/(w/2) = -0.708$

NPR	$p/p_{t,j}$ at x/L of— 0.334	0.372	0.436	0.540
2.014	0.664	0.283	0.328	0.395
2.532	0.663	0.285	0.295	0.317
3.014	0.662	0.285	0.280	0.310
3.504	0.663	0.284	0.236	0.293
3.991	0.662	0.284	0.235	0.280
4.485	0.661	0.283	0.221	0.282
5.015	0.661	0.283	0.235	0.281
6.011	0.660	0.283	0.228	0.281
7.993	0.658	0.282	0.228	0.279
9.984	0.656	0.282	0.228	0.278

UL quadrant: $y/(w/2) = -0.924$

NPR	$p/p_{t,j}$ at x/L of— 0.068	0.210	0.375	0.413	0.540	0.592	0.681	0.770	0.858	0.947
2.014	0.986	0.972	0.784	0.294	0.431	0.403	0.453	0.562	0.549	0.503
2.532	0.986	0.972	0.781	0.213	0.352	0.394	0.409	0.409	0.406	0.396
3.014	0.986	0.972	0.782	0.170	0.315	0.332	0.344	0.346	0.346	0.335
3.504	0.986	0.972	0.781	0.147	0.316	0.319	0.323	0.323	0.308	0.288
3.991	0.985	0.973	0.780	0.149	0.309	0.310	0.313	0.306	0.279	0.254
4.485	0.986	0.972	0.778	0.147	0.301	0.309	0.311	0.301	0.261	0.229
5.015	0.986	0.972	0.778	0.156	0.307	0.308	0.309	0.288	0.230	0.202
6.011	0.986	0.972	0.776	0.154	0.306	0.308	0.309	0.289	0.219	0.168
7.993	0.985	0.971	0.770	0.152	0.307	0.307	0.308	0.285	0.214	0.112
9.984	0.985	0.970	0.766	0.153	0.308	0.308	0.306	0.283	0.212	0.109

UR quadrant: $y/(w/2) = 0.058$

NPR	$p/p_{t,j}$ at x/L of— 0.068	0.233	0.297	0.361	0.399	0.439	0.490	0.540	0.592
2.014	0.953	0.753	0.649	0.588	0.553	0.516	0.509	0.502	0.500
2.532	0.955	0.747	0.632	0.525	0.506	0.467	0.449	0.455	0.405
3.014	0.955	0.748	0.632	0.524	0.466	0.430	0.449	0.447	0.383
3.504	0.955	0.748	0.632	0.524	0.466	0.408	0.439	0.441	0.377
3.991	0.955	0.748	0.632	0.524	0.466	0.408	0.434	0.437	0.374
4.485	0.955	0.748	0.632	0.524	0.466	0.409	0.425	0.430	0.372
5.015	0.955	0.748	0.632	0.524	0.465	0.407	0.432	0.434	0.374
6.011	0.955	0.747	0.631	0.523	0.465	0.407	0.429	0.431	0.374
7.993	0.955	0.746	0.631	0.523	0.464	0.406	0.432	0.432	0.375
9.984	0.954	0.745	0.630	0.522	0.464	0.406	0.430	0.432	0.376

UR quadrant: $y/(w/2) = 0.275$

NPR	$p/p_{t,j}$ at x/L of— 0.271	0.338	0.402	0.440	0.490	0.540
2.014	0.727	0.624	0.551	0.495	0.423	0.448
2.532	0.719	0.602	0.505	0.458	0.379	0.384
3.014	0.720	0.602	0.502	0.434	0.339	0.381
3.504	0.719	0.603	0.502	0.434	0.339	0.363
3.991	0.719	0.602	0.502	0.434	0.340	0.352
4.485	0.719	0.602	0.502	0.434	0.340	0.350
5.015	0.718	0.602	0.502	0.435	0.340	0.342
6.011	0.718	0.602	0.502	0.434	0.341	0.342
7.993	0.717	0.602	0.502	0.434	0.341	0.335
9.984	0.716	0.601	0.501	0.434	0.341	0.330

Table 38. Concluded

UR quadrant: $y/(w/2) = 0.491$

NPR	$p/p_{t,j}$ at x/L of— 0.068	0.210	0.379	0.442	0.480	0.540	0.592	0.681	0.770
2.014	0.958	0.851	0.585	0.483	0.416	0.330	0.505	0.458	0.490
2.532	0.957	0.846	0.567	0.449	0.384	0.298	0.271	0.425	0.364
3.014	0.956	0.847	0.567	0.448	0.377	0.280	0.248	0.374	0.285
3.504	0.956	0.846	0.568	0.448	0.378	0.281	0.240	0.271	0.311
3.991	0.957	0.846	0.568	0.448	0.379	0.281	0.240	0.242	0.317
4.485	0.957	0.845	0.568	0.448	0.379	0.282	0.241	0.236	0.267
5.015	0.957	0.845	0.567	0.448	0.380	0.283	0.241	0.233	0.259
6.011	0.957	0.845	0.567	0.448	0.381	0.284	0.241	0.231	0.255
7.993	0.957	0.844	0.567	0.448	0.381	0.286	0.242	0.227	0.255
9.984	0.956	0.844	0.566	0.448	0.382	0.287	0.242	0.224	0.256

UR quadrant: $y/(w/2) = 0.708$

NPR	$p/p_{t,j}$ at x/L of— 0.419	0.483	0.521
2.014	0.531	0.382	0.291
2.532	0.519	0.363	0.269
3.014	0.518	0.363	0.270
3.504	0.519	0.364	0.271
3.991	0.519	0.365	0.271
4.485	0.519	0.365	0.272
5.015	0.519	0.366	0.272
6.011	0.519	0.367	0.273
7.993	0.518	0.368	0.274
9.984	0.517	0.369	0.275

UR quadrant: $y/(w/2) = 0.924$

NPR	$p/p_{t,j}$ at x/L of— 0.068	0.210	0.460	0.524	0.592	0.681	0.770	0.858	0.947
2.014	0.965	0.901	0.505	0.315	0.395	0.364	0.403	0.510	0.510
2.532	0.965	0.900	0.497	0.242	0.311	0.290	0.280	0.387	0.420
3.014	0.966	0.900	0.497	0.238	0.250	0.233	0.225	0.322	0.354
3.504	0.966	0.901	0.497	0.238	0.214	0.197	0.186	0.285	0.303
3.991	0.965	0.900	0.497	0.238	0.190	0.178	0.163	0.267	0.262
4.485	0.965	0.900	0.497	0.239	0.168	0.169	0.152	0.254	0.233
5.015	0.965	0.901	0.497	0.239	0.158	0.168	0.150	0.250	0.210
6.011	0.966	0.900	0.497	0.240	0.152	0.164	0.147	0.242	0.179
7.993	0.965	0.900	0.497	0.243	0.147	0.165	0.144	0.239	0.157
9.984	0.964	0.899	0.497	0.247	0.153	0.163	0.139	0.237	0.159

Table 39. Nozzle Internal Static Pressure Ratios for Configuration 12

UL quadrant: $y/(w/2) = -0.058$

	$p/p_{t,j}$ at x/L of—								
NPR	0.068	0.212	0.250	0.314	0.377	0.439	0.490	0.540	0.592
2.010	0.970	0.753	0.652	0.652	0.487	0.589	0.615	0.597	0.532
2.507	0.971	0.749	0.644	0.638	0.460	0.517	0.552	0.557	0.480
3.011	0.970	0.749	0.643	0.638	0.450	0.496	0.476	0.543	0.474
3.506	0.970	0.749	0.642	0.642	0.446	0.487	0.452	0.451	0.470
4.005	0.970	0.749	0.641	0.649	0.443	0.479	0.441	0.442	0.386
4.503	0.970	0.750	0.639	0.655	0.438	0.472	0.437	0.434	0.383
4.999	0.970	0.749	0.639	0.656	0.437	0.471	0.437	0.427	0.385
6.002	0.971	0.749	0.639	0.656	0.436	0.470	0.437	0.429	0.384

UL quadrant: $y/(w/2) = -0.275$

	$p/p_{t,j}$ at x/L of—					
NPR	0.253	0.291	0.355	0.418	0.477	0.540
2.010	0.622	0.374	0.613	0.607	0.608	0.570
2.507	0.618	0.369	0.547	0.551	0.560	0.528
3.011	0.616	0.370	0.534	0.528	0.527	0.529
3.506	0.613	0.370	0.536	0.508	0.503	0.458
4.005	0.612	0.371	0.536	0.502	0.482	0.447
4.503	0.611	0.371	0.536	0.497	0.469	0.445
4.999	0.611	0.371	0.536	0.495	0.462	0.446
6.002	0.609	0.371	0.538	0.495	0.461	0.445

UL quadrant: $y/(w/2) = -0.491$

	$p/p_{t,j}$ at x/L of—									
NPR	0.068	0.210	0.294	0.332	0.395	0.464	0.540	0.592	0.681	0.770
2.010	0.984	0.937	0.603	0.312	0.407	0.472	0.450	0.448	0.513	0.514
2.507	0.982	0.936	0.599	0.309	0.305	0.380	0.421	0.416	0.419	0.416
3.011	0.984	0.936	0.596	0.309	0.279	0.403	0.459	0.413	0.374	0.342
3.506	0.983	0.935	0.593	0.309	0.281	0.314	0.408	0.393	0.359	0.299
4.005	0.982	0.935	0.591	0.309	0.271	0.301	0.407	0.387	0.400	0.272
4.503	0.982	0.935	0.590	0.309	0.262	0.293	0.406	0.385	0.336	0.278
4.999	0.982	0.935	0.590	0.309	0.257	0.289	0.409	0.386	0.335	0.258
6.002	0.981	0.934	0.589	0.308	0.258	0.291	0.407	0.387	0.335	0.259

Table 39. Continued

UL quadrant: $y/(w/2) = -0.708$

NPR	$p/p_{t,j}$ at x/L of— 0.334	0.372	0.436	0.540
2.010	0.669	0.287	0.454	0.391
2.507	0.668	0.288	0.370	0.341
3.011	0.667	0.288	0.345	0.352
3.506	0.667	0.287	0.339	0.313
4.005	0.666	0.286	0.292	0.317
4.503	0.666	0.286	0.278	0.320
4.999	0.665	0.285	0.275	0.323
6.002	0.664	0.285	0.278	0.321

UL quadrant: $y/(w/2) = -0.924$

NPR	$p/p_{t,j}$ at x/L of— 0.068	0.210	0.375	0.413	0.540	0.592	0.681	0.770	0.858	0.947
2.010	0.990	0.977	0.787	0.375	0.435	0.470	0.591	0.563	0.526	0.501
2.507	0.986	0.975	0.784	0.239	0.370	0.408	0.490	0.461	0.425	0.401
3.011	0.989	0.975	0.784	0.217	0.362	0.396	0.400	0.388	0.361	0.336
3.506	0.989	0.975	0.782	0.203	0.329	0.379	0.400	0.367	0.315	0.290
4.005	0.989	0.975	0.781	0.179	0.319	0.350	0.369	0.356	0.289	0.255
4.503	0.989	0.974	0.780	0.167	0.321	0.342	0.354	0.343	0.267	0.226
4.999	0.989	0.974	0.780	0.165	0.328	0.341	0.351	0.336	0.257	0.206
6.002	0.990	0.974	0.777	0.153	0.331	0.343	0.349	0.334	0.257	0.145

UR quadrant: $y/(w/2) = 0.058$

NPR	$p/p_{t,j}$ at x/L of— 0.068	0.233	0.297	0.361	0.399	0.439	0.490	0.540	0.592
2.010	0.966	0.819	0.763	0.835	0.229	0.619	0.630	0.611	0.541
2.507	0.966	0.813	0.755	0.831	0.130	0.559	0.545	0.566	0.479
3.011	0.964	0.812	0.758	0.831	0.113	0.545	0.469	0.544	0.459
3.506	0.965	0.813	0.758	0.831	0.105	0.541	0.451	0.431	0.456
4.005	0.965	0.813	0.758	0.832	0.110	0.540	0.446	0.397	0.372
4.503	0.964	0.812	0.758	0.832	0.127	0.548	0.442	0.384	0.363
4.999	0.964	0.812	0.758	0.832	0.117	0.542	0.442	0.381	0.365
6.002	0.965	0.812	0.757	0.832	0.129	0.550	0.442	0.383	0.364

UR quadrant: $y/(w/2) = 0.275$

NPR	$p/p_{t,j}$ at x/L of— 0.271	0.338	0.402	0.440	0.490	0.540
2.010	0.811	0.778	0.854	0.377	0.387	0.433
2.507	0.806	0.773	0.852	0.292	0.322	0.376
3.011	0.806	0.772	0.853	0.258	0.349	0.403
3.506	0.806	0.772	0.853	0.235	0.303	0.290
4.005	0.806	0.772	0.853	0.233	0.307	0.277
4.503	0.805	0.772	0.853	0.233	0.312	0.284
4.999	0.805	0.772	0.854	0.230	0.313	0.285
6.002	0.805	0.772	0.854	0.240	0.312	0.292

Table 39. Concluded

UR quadrant: $y/(w/2) = 0.491$

NPR	$p/p_{t,j}$ at x/L of— 0.068	0.210	0.379	0.442	0.480	0.540	0.592	0.681	0.770
2.010	0.971	0.889	0.791	0.865	0.421	0.445	0.479	0.461	0.479
2.507	0.970	0.886	0.787	0.863	0.328	0.347	0.392	0.365	0.379
3.011	0.969	0.886	0.787	0.863	0.229	0.294	0.331	0.314	0.309
3.506	0.969	0.887	0.787	0.864	0.163	0.237	0.302	0.283	0.261
4.005	0.969	0.887	0.787	0.864	0.158	0.228	0.269	0.245	0.243
4.503	0.968	0.886	0.787	0.864	0.158	0.228	0.146	0.221	0.216
4.999	0.968	0.886	0.787	0.864	0.159	0.229	0.125	0.229	0.186
6.002	0.967	0.886	0.787	0.865	0.160	0.231	0.124	0.213	0.127

UR quadrant: $y/(w/2) = 0.708$

NPR	$p/p_{t,j}$ at x/L of— 0.419	0.483	0.521
2.010	0.813	0.889	0.412
2.507	0.810	0.888	0.303
3.011	0.810	0.889	0.219
3.506	0.809	0.890	0.194
4.005	0.809	0.890	0.148
4.503	0.810	0.890	0.120
4.999	0.809	0.890	0.118
6.002	0.809	0.890	0.119

UR quadrant: $y/(w/2) = 0.924$

NPR	$p/p_{t,j}$ at x/L of— 0.068	0.210	0.460	0.524	0.592	0.681	0.770	0.858	0.947
2.010	0.976	0.932	0.858	0.917	0.485	0.452	0.502	0.512	0.498
2.507	0.974	0.930	0.856	0.918	0.386	0.342	0.395	0.431	0.401
3.011	0.975	0.930	0.856	0.920	0.316	0.282	0.304	0.369	0.336
3.506	0.975	0.929	0.855	0.920	0.268	0.248	0.256	0.302	0.289
4.005	0.974	0.930	0.854	0.921	0.225	0.213	0.214	0.281	0.257
4.503	0.974	0.930	0.854	0.920	0.197	0.182	0.183	0.263	0.235
4.999	0.974	0.930	0.854	0.920	0.177	0.160	0.159	0.237	0.215
6.002	0.976	0.929	0.853	0.920	0.145	0.130	0.129	0.201	0.181

Table 40. Nozzle Internal Static Pressure Ratios for Configuration 12-I

UL quadrant: $y/(w/2) = -0.058$

	$p/p_{t,j}$ at x/L of—								
NPR	0.068	0.212	0.250	0.314	0.377	0.439	0.490	0.540	0.592
1.994	0.972	0.754	0.653	0.652	0.490	0.594	0.615	0.595	0.532
2.498	0.971	0.751	0.645	0.638	0.461	0.517	0.549	0.557	0.481
3.003	0.971	0.750	0.644	0.636	0.451	0.495	0.471	0.543	0.477
3.507	0.970	0.751	0.642	0.642	0.447	0.487	0.450	0.448	0.468
3.995	0.970	0.750	0.641	0.649	0.443	0.479	0.440	0.440	0.387
4.508	0.970	0.750	0.640	0.653	0.440	0.473	0.438	0.432	0.383
5.006	0.970	0.750	0.639	0.656	0.437	0.469	0.436	0.427	0.382
5.992	0.969	0.749	0.639	0.656	0.436	0.469	0.436	0.425	0.382
6.993	0.969	0.748	0.638	0.653	0.437	0.469	0.437	0.421	0.384
8.010	0.969	0.747	0.638	0.650	0.437	0.466	0.438	0.418	0.388

UL quadrant: $y/(w/2) = -0.275$

	$p/p_{t,j}$ at x/L of—					
NPR	0.253	0.291	0.355	0.418	0.477	0.540
1.994	0.626	0.411	0.621	0.615	0.615	0.572
2.498	0.621	0.400	0.559	0.544	0.552	0.531
3.003	0.620	0.397	0.534	0.527	0.524	0.528
3.507	0.616	0.394	0.540	0.508	0.498	0.457
3.995	0.614	0.392	0.539	0.502	0.480	0.447
4.508	0.613	0.390	0.538	0.497	0.467	0.443
5.006	0.612	0.388	0.538	0.495	0.462	0.443
5.992	0.610	0.386	0.539	0.497	0.463	0.441
6.993	0.610	0.384	0.539	0.496	0.460	0.444
8.010	0.608	0.382	0.540	0.488	0.454	0.452

UL quadrant: $y/(w/2) = -0.491$

	$p/p_{t,j}$ at x/L of—									
NPR	0.068	0.210	0.294	0.332	0.395	0.464	0.540	0.592	0.681	0.770
1.994	0.986	0.938	0.609	0.312	0.406	0.442	0.453	0.451	0.515	0.517
2.498	0.984	0.936	0.603	0.310	0.307	0.357	0.416	0.420	0.423	0.418
3.003	0.984	0.937	0.600	0.309	0.275	0.406	0.463	0.414	0.373	0.343
3.507	0.983	0.937	0.596	0.310	0.282	0.315	0.413	0.392	0.359	0.299
3.995	0.983	0.937	0.594	0.309	0.271	0.301	0.409	0.387	0.391	0.273
4.508	0.983	0.936	0.593	0.309	0.261	0.294	0.407	0.385	0.335	0.278
5.006	0.983	0.935	0.592	0.309	0.258	0.293	0.409	0.386	0.334	0.257
5.992	0.982	0.935	0.591	0.308	0.261	0.292	0.403	0.385	0.335	0.259
6.993	0.982	0.935	0.590	0.308	0.260	0.291	0.403	0.385	0.335	0.259
8.010	0.981	0.935	0.589	0.307	0.249	0.289	0.413	0.390	0.334	0.258

Table 40. Continued

UL quadrant: $y/(w/2) = -0.708$

NPR	$p/p_{t,j}$ at x/L of— 0.334	0.372	0.436	0.540
1.994	0.673	0.287	0.442	0.404
2.498	0.670	0.288	0.371	0.338
3.003	0.668	0.288	0.336	0.355
3.507	0.668	0.287	0.321	0.312
3.995	0.667	0.287	0.290	0.317
4.508	0.666	0.286	0.277	0.320
5.006	0.666	0.286	0.276	0.321
5.992	0.665	0.285	0.277	0.318
6.993	0.664	0.285	0.275	0.320
8.010	0.663	0.285	0.275	0.325

UL quadrant: $y/(w/2) = -0.924$

NPR	$p/p_{t,j}$ at x/L of— 0.068	0.210	0.375	0.413	0.540	0.592	0.681	0.770	0.858	0.947
1.994	0.994	0.976	0.790	0.314	0.444	0.460	0.590	0.572	0.529	0.506
2.498	0.993	0.975	0.787	0.239	0.366	0.415	0.500	0.465	0.427	0.404
3.003	0.991	0.975	0.785	0.200	0.366	0.395	0.398	0.388	0.361	0.337
3.507	0.992	0.975	0.783	0.173	0.329	0.373	0.402	0.366	0.313	0.288
3.995	0.991	0.975	0.782	0.155	0.319	0.348	0.372	0.356	0.288	0.254
4.508	0.991	0.974	0.781	0.152	0.321	0.343	0.353	0.342	0.266	0.225
5.006	0.989	0.974	0.780	0.154	0.329	0.341	0.349	0.336	0.257	0.206
5.992	0.990	0.974	0.778	0.152	0.325	0.343	0.347	0.333	0.258	0.146
6.993	0.989	0.973	0.776	0.150	0.325	0.344	0.347	0.332	0.258	0.143
8.010	0.989	0.973	0.773	0.153	0.339	0.344	0.348	0.329	0.253	0.142

UR quadrant: $y/(w/2) = 0.058$

NPR	$p/p_{t,j}$ at x/L of— 0.068	0.233	0.297	0.361	0.399	0.439	0.490	0.540	0.592
1.994	0.966	0.817	0.767	0.836	0.249	0.612	0.629	0.607	0.542
2.498	0.964	0.814	0.761	0.833	0.132	0.558	0.544	0.565	0.479
3.003	0.964	0.812	0.759	0.832	0.106	0.545	0.464	0.546	0.465
3.507	0.965	0.813	0.758	0.832	0.104	0.541	0.450	0.424	0.458
3.995	0.965	0.813	0.758	0.832	0.105	0.539	0.446	0.395	0.370
4.508	0.964	0.813	0.758	0.832	0.109	0.540	0.443	0.385	0.362
5.006	0.964	0.813	0.758	0.832	0.123	0.548	0.441	0.382	0.363
5.992	0.964	0.812	0.757	0.832	0.143	0.559	0.442	0.382	0.366
6.993	0.963	0.812	0.757	0.832	0.144	0.557	0.442	0.381	0.368
8.010	0.963	0.811	0.757	0.832	0.143	0.553	0.440	0.381	0.371

UR quadrant: $y/(w/2) = 0.275$

NPR	$p/p_{t,j}$ at x/L of— 0.271	0.338	0.402	0.440	0.490	0.540
1.994	0.813	0.779	0.854	0.401	0.409	0.438
2.498	0.807	0.774	0.853	0.291	0.322	0.377
3.003	0.807	0.773	0.852	0.240	0.312	0.390
3.507	0.807	0.773	0.853	0.233	0.305	0.290
3.995	0.806	0.772	0.853	0.231	0.306	0.284
4.508	0.806	0.772	0.853	0.230	0.306	0.284
5.006	0.805	0.772	0.853	0.231	0.305	0.284
5.992	0.805	0.772	0.854	0.232	0.303	0.288
6.993	0.804	0.772	0.854	0.232	0.307	0.288
8.010	0.804	0.772	0.854	0.231	0.307	0.288

Table 40. Concluded

UR quadrant: $y/(w/2) = 0.491$

NPR	$p/p_{t,j}$ at x/L of— 0.068	0.210	0.379	0.442	0.480	0.540	0.592	0.681	0.770
1.994	0.967	0.891	0.791	0.866	0.436	0.448	0.469	0.458	0.486
2.498	0.968	0.888	0.788	0.863	0.326	0.348	0.389	0.367	0.378
3.003	0.969	0.887	0.787	0.864	0.234	0.294	0.330	0.318	0.311
3.507	0.968	0.888	0.787	0.864	0.174	0.237	0.303	0.277	0.263
3.995	0.968	0.887	0.787	0.864	0.171	0.229	0.271	0.238	0.242
4.508	0.967	0.887	0.787	0.864	0.170	0.229	0.136	0.221	0.215
5.006	0.967	0.887	0.787	0.864	0.168	0.230	0.124	0.227	0.184
5.992	0.967	0.887	0.787	0.864	0.168	0.231	0.124	0.210	0.133
6.993	0.967	0.886	0.787	0.864	0.169	0.232	0.125	0.199	0.103
8.010	0.967	0.886	0.786	0.864	0.169	0.233	0.126	0.173	0.113

UR quadrant: $y/(w/2) = 0.708$

NPR	$p/p_{t,j}$ at x/L of— 0.419	0.483	0.521
1.994	0.813	0.890	0.434
2.498	0.810	0.889	0.300
3.003	0.810	0.890	0.223
3.507	0.809	0.890	0.193
3.995	0.809	0.890	0.141
4.508	0.809	0.890	0.123
5.006	0.809	0.890	0.123
5.992	0.809	0.891	0.123
6.993	0.809	0.891	0.123
8.010	0.808	0.891	0.122

UR quadrant: $y/(w/2) = 0.924$

NPR	$p/p_{t,j}$ at x/L of— 0.068	0.210	0.460	0.524	0.592	0.681	0.770	0.858	0.947
1.994	0.977	0.932	0.858	0.917	0.485	0.458	0.507	0.514	0.500
2.498	0.974	0.931	0.857	0.917	0.388	0.347	0.397	0.428	0.401
3.003	0.975	0.931	0.855	0.919	0.318	0.287	0.307	0.366	0.337
3.507	0.974	0.931	0.855	0.920	0.269	0.245	0.255	0.310	0.289
3.995	0.974	0.930	0.854	0.920	0.221	0.213	0.215	0.282	0.258
4.508	0.974	0.930	0.854	0.920	0.195	0.183	0.184	0.259	0.234
5.006	0.974	0.930	0.854	0.920	0.174	0.160	0.158	0.236	0.214
5.992	0.974	0.930	0.853	0.920	0.147	0.134	0.128	0.201	0.181
6.993	0.974	0.930	0.852	0.918	0.132	0.116	0.115	0.177	0.154
8.010	0.973	0.929	0.850	0.917	0.112	0.102	0.103	0.169	0.133

Table 41. Nozzle Internal Static Pressure Ratios for Configuration 13

UL quadrant: $y/(w/2) = -0.058$

	$p/p_{t,j}$ at x/L of—							
NPR	0.068	0.244	0.282	0.333	0.402	0.472	0.540	0.592
2.025	0.919	0.827	0.787	0.656	0.514	0.611	0.615	0.558
2.496	0.746	0.825	0.784	0.652	0.496	0.405	0.577	0.512
3.010	0.618	0.824	0.784	0.651	0.495	0.395	0.426	0.503
3.500	0.532	0.824	0.784	0.651	0.494	0.395	0.344	0.386
3.998	0.466	0.824	0.784	0.650	0.495	0.394	0.344	0.332
5.002	0.455	0.823	0.783	0.646	0.495	0.393	0.344	0.332
5.996	0.940	0.822	0.782	0.645	0.495	0.392	0.345	0.333
6.992	0.852	0.822	0.782	0.644	0.494	0.392	0.346	0.334
7.979	0.848	0.822	0.781	0.644	0.494	0.393	0.346	0.334

UL quadrant: $y/(w/2) = -0.275$

	$p/p_{t,j}$ at x/L of—				
NPR	0.285	0.323	0.374	0.440	0.540
2.025	0.739	0.665	0.527	0.433	0.629
2.496	0.737	0.663	0.523	0.380	0.595
3.010	0.737	0.662	0.523	0.378	0.473
3.500	0.738	0.662	0.523	0.379	0.358
3.998	0.738	0.662	0.523	0.379	0.358
5.002	0.737	0.661	0.523	0.380	0.358
5.996	0.737	0.661	0.523	0.380	0.359
6.992	0.737	0.660	0.523	0.380	0.359
7.979	0.737	0.660	0.523	0.379	0.360

UL quadrant: $y/(w/2) = -0.491$

	$p/p_{t,j}$ at x/L of—									
NPR	0.068	0.236	0.325	0.363	0.414	0.477	0.540	0.592	0.681	0.770
2.025	0.974	0.880	0.640	0.529	0.377	0.506	0.575	0.513	0.444	0.502
2.496	0.974	0.878	0.637	0.526	0.375	0.391	0.465	0.481	0.357	0.464
3.010	0.974	0.878	0.638	0.526	0.375	0.250	0.398	0.457	0.343	0.332
3.500	0.973	0.879	0.637	0.528	0.375	0.250	0.342	0.410	0.342	0.259
3.998	0.973	0.879	0.637	0.528	0.375	0.251	0.309	0.420	0.308	0.238
5.002	0.973	0.879	0.636	0.528	0.376	0.251	0.269	0.423	0.305	0.209
5.996	0.973	0.879	0.635	0.528	0.376	0.251	0.268	0.424	0.306	0.207
6.992	0.973	0.878	0.634	0.527	0.375	0.251	0.266	0.427	0.306	0.207
7.979	0.972	0.878	0.634	0.527	0.375	0.251	0.265	0.428	0.308	0.208

Table 41. Continued

UL quadrant: $y/(w/2) = -0.708$

NPR	$p/p_{t,j}$ at x/L of— 0.366	0.404	0.455	0.540
2.025	0.565	0.346	0.404	0.417
2.496	0.565	0.348	0.200	0.331
3.010	0.565	0.348	0.181	0.287
3.500	0.564	0.348	0.182	0.262
3.998	0.564	0.349	0.182	0.241
5.002	0.562	0.349	0.182	0.223
5.996	0.562	0.349	0.183	0.227
6.992	0.561	0.349	0.183	0.230
7.979	0.560	0.349	0.183	0.229

UL quadrant: $y/(w/2) = -0.924$

NPR	$p/p_{t,j}$ at x/L of— 0.068	0.236	0.407	0.445	0.540	0.592	0.681	0.770	0.858	0.947
2.025	0.982	0.943	0.574	0.267	0.425	0.386	0.473	0.554	0.531	0.494
2.496	0.980	0.942	0.572	0.221	0.330	0.288	0.405	0.498	0.448	0.401
3.010	0.981	0.943	0.572	0.185	0.275	0.241	0.344	0.444	0.394	0.333
3.500	0.981	0.942	0.572	0.160	0.243	0.219	0.280	0.398	0.359	0.286
3.998	0.981	0.942	0.572	0.159	0.222	0.204	0.251	0.360	0.330	0.251
5.002	0.980	0.942	0.571	0.161	0.204	0.188	0.244	0.347	0.312	0.181
5.996	0.980	0.941	0.570	0.163	0.204	0.189	0.241	0.348	0.309	0.175
6.992	0.980	0.941	0.570	0.164	0.203	0.193	0.240	0.348	0.310	0.175
7.979	0.979	0.940	0.569	0.165	0.203	0.199	0.240	0.345	0.308	0.174

UR quadrant: $y/(w/2) = 0.058$

NPR	$p/p_{t,j}$ at x/L of— 0.068	0.263	0.320	0.358	0.415	0.477	0.540	0.592
2.025	0.965	0.837	0.868	0.302	0.554	0.596	0.617	0.537
2.496	0.963	0.836	0.867	0.263	0.529	0.402	0.569	0.480
3.010	0.963	0.836	0.867	0.316	0.525	0.380	0.487	0.468
3.500	0.964	0.835	0.868	0.332	0.519	0.383	0.376	0.408
3.998	0.964	0.836	0.868	0.335	0.519	0.383	0.376	0.339
5.002	0.963	0.836	0.868	0.341	0.521	0.382	0.376	0.315
5.996	0.963	0.835	0.868	0.346	0.521	0.382	0.377	0.316
6.992	0.962	0.835	0.868	0.344	0.518	0.383	0.378	0.316
7.979	0.962	0.834	0.867	0.339	0.515	0.384	0.379	0.315

UR quadrant: $y/(w/2) = 0.275$

NPR	$p/p_{t,j}$ at x/L of— 0.304	0.361	0.399	0.472	0.540
2.025	0.829	0.872	0.391	0.485	0.530
2.496	0.825	0.870	0.328	0.382	0.491
3.010	0.825	0.870	0.299	0.327	0.452
3.500	0.825	0.870	0.283	0.317	0.398
3.998	0.825	0.871	0.271	0.321	0.268
5.002	0.824	0.870	0.263	0.322	0.272
5.996	0.823	0.870	0.259	0.322	0.274
6.992	0.823	0.870	0.258	0.323	0.275
7.979	0.823	0.870	0.253	0.328	0.278

Table 41. Concluded

UR quadrant: $y/(w/2) = 0.491$

NPR	$p/p_{t,j}$ at x/L of— 0.068	0.236	0.345	0.402	0.440	0.490	0.540	0.592	0.681	0.770
2.025	0.970	0.891	0.823	0.877	0.416	0.448	0.475	0.494	0.454	0.464
2.496	0.971	0.889	0.821	0.876	0.313	0.354	0.366	0.409	0.350	0.363
3.010	0.972	0.888	0.820	0.876	0.195	0.277	0.336	0.339	0.248	0.303
3.500	0.972	0.888	0.820	0.876	0.194	0.240	0.325	0.311	0.207	0.256
3.998	0.971	0.888	0.820	0.876	0.195	0.240	0.222	0.290	0.163	0.235
5.002	0.971	0.888	0.819	0.876	0.190	0.239	0.144	0.284	0.142	0.174
5.996	0.971	0.887	0.819	0.876	0.191	0.238	0.149	0.265	0.133	0.153
6.992	0.970	0.887	0.818	0.876	0.195	0.235	0.152	0.236	0.140	0.131
7.979	0.970	0.886	0.818	0.875	0.199	0.235	0.153	0.222	0.142	0.119

UR quadrant: $y/(w/2) = 0.708$

NPR	$p/p_{t,j}$ at x/L of— 0.385	0.442	0.480	0.540
2.025	0.847	0.902	0.347	0.461
2.496	0.845	0.901	0.282	0.364
3.010	0.845	0.902	0.249	0.324
3.500	0.844	0.902	0.201	0.269
3.998	0.844	0.902	0.140	0.210
5.002	0.844	0.902	0.135	0.173
5.996	0.843	0.902	0.132	0.150
6.992	0.842	0.902	0.128	0.137
7.979	0.842	0.901	0.128	0.129

UR quadrant: $y/(w/2) = 0.924$

NPR	$p/p_{t,j}$ at x/L of— 0.236	0.426	0.483	0.592	0.681	0.770	0.858	0.947
2.025	0.938	0.904	0.954	0.468	0.462	0.480	0.505	0.491
2.496	0.938	0.901	0.955	0.365	0.355	0.384	0.433	0.403
3.010	0.937	0.901	0.956	0.297	0.250	0.321	0.417	0.342
3.500	0.937	0.901	0.956	0.257	0.211	0.247	0.353	0.303
3.998	0.937	0.901	0.956	0.216	0.173	0.214	0.310	0.266
5.002	0.936	0.900	0.956	0.171	0.139	0.181	0.252	0.210
5.996	0.936	0.899	0.956	0.151	0.126	0.167	0.217	0.175
6.992	0.936	0.898	0.956	0.138	0.117	0.162	0.199	0.148
7.979	0.936	0.898	0.956	0.132	0.113	0.161	0.188	0.128

Table 42. Nozzle Internal Static Pressure Ratios for Configuration 14

UL quadrant: $y/(w/2) = -0.058$

	$p/p_{t,j}$ at x/L of—							
NPR	0.068	0.244	0.282	0.333	0.402	0.472	0.540	0.592
1.995	0.802	0.827	0.788	0.732	0.494	0.597	0.614	0.552
2.509	0.814	0.825	0.786	0.730	0.444	0.458	0.589	0.509
3.029	0.889	0.824	0.785	0.730	0.442	0.449	0.404	0.521
3.493	0.906	0.824	0.785	0.729	0.443	0.448	0.401	0.366
4.019	0.891	0.823	0.784	0.729	0.443	0.448	0.399	0.365
4.532	0.904	0.823	0.783	0.728	0.444	0.447	0.398	0.365
4.999	0.915	0.823	0.783	0.728	0.445	0.447	0.398	0.365
5.991	0.926	0.822	0.782	0.728	0.446	0.446	0.398	0.366
7.018	0.949	0.821	0.781	0.727	0.446	0.445	0.398	0.366
8.003	0.947	0.821	0.780	0.726	0.446	0.445	0.398	0.367

UL quadrant: $y/(w/2) = -0.275$

	$p/p_{t,j}$ at x/L of—				
NPR	0.285	0.323	0.374	0.440	0.540
1.995	0.746	0.687	0.576	0.444	0.628
2.509	0.744	0.686	0.573	0.407	0.603
3.029	0.744	0.685	0.574	0.406	0.506
3.493	0.744	0.685	0.574	0.407	0.396
4.019	0.745	0.685	0.574	0.407	0.395
4.532	0.743	0.684	0.574	0.408	0.396
4.999	0.744	0.684	0.574	0.408	0.396
5.991	0.743	0.683	0.574	0.408	0.397
7.018	0.743	0.683	0.574	0.408	0.398
8.003	0.742	0.682	0.573	0.408	0.398

UL quadrant: $y/(w/2) = -0.491$

	$p/p_{t,j}$ at x/L of—									
NPR	0.068	0.236	0.325	0.363	0.414	0.477	0.540	0.592	0.681	0.770
1.995	0.974	0.879	0.647	0.545	0.409	0.547	0.589	0.524	0.474	0.512
2.509	0.973	0.877	0.644	0.544	0.407	0.356	0.527	0.497	0.377	0.439
3.029	0.974	0.876	0.644	0.543	0.407	0.292	0.472	0.485	0.363	0.339
3.493	0.973	0.878	0.643	0.543	0.407	0.292	0.443	0.446	0.354	0.307
4.019	0.972	0.877	0.643	0.543	0.408	0.292	0.404	0.455	0.328	0.263
4.532	0.972	0.877	0.642	0.543	0.408	0.293	0.399	0.457	0.328	0.243
4.999	0.973	0.877	0.642	0.543	0.408	0.292	0.398	0.458	0.328	0.242
5.991	0.972	0.877	0.641	0.542	0.408	0.293	0.397	0.460	0.328	0.240
7.018	0.972	0.876	0.641	0.542	0.408	0.293	0.391	0.461	0.331	0.244
8.003	0.972	0.876	0.639	0.541	0.408	0.293	0.386	0.462	0.331	0.244

Table 42. Continued

UL quadrant: $y/(w/2) = -0.708$

NPR	$p/p_{t,j}$ at x/L of— 0.366	0.404	0.455	0.540
1.995	0.568	0.348	0.427	0.434
2.509	0.566	0.352	0.292	0.358
3.029	0.566	0.352	0.192	0.325
3.493	0.565	0.352	0.193	0.312
4.019	0.565	0.352	0.193	0.297
4.532	0.564	0.352	0.193	0.299
4.999	0.564	0.351	0.193	0.299
5.991	0.563	0.351	0.193	0.305
7.018	0.562	0.351	0.193	0.300
8.003	0.561	0.350	0.193	0.300

UL quadrant: $y/(w/2) = -0.924$

NPR	$p/p_{t,j}$ at x/L of— 0.068	0.236	0.407	0.445	0.540	0.592	0.681	0.770	0.858	0.947
1.995	0.981	0.943	0.572	0.270	0.433	0.399	0.502	0.569	0.535	0.503
2.509	0.980	0.942	0.570	0.224	0.340	0.305	0.448	0.497	0.438	0.400
3.029	0.980	0.941	0.569	0.190	0.295	0.266	0.393	0.449	0.382	0.331
3.493	0.980	0.941	0.568	0.165	0.268	0.247	0.337	0.420	0.348	0.287
4.019	0.980	0.941	0.568	0.164	0.248	0.232	0.331	0.400	0.330	0.253
4.532	0.980	0.941	0.567	0.165	0.246	0.232	0.329	0.395	0.320	0.190
4.999	0.980	0.941	0.567	0.166	0.246	0.235	0.327	0.395	0.319	0.185
5.991	0.979	0.940	0.565	0.167	0.246	0.238	0.326	0.394	0.320	0.184
7.018	0.980	0.940	0.564	0.168	0.246	0.241	0.325	0.392	0.319	0.183
8.003	0.979	0.939	0.563	0.168	0.247	0.241	0.324	0.390	0.318	0.183

UR quadrant: $y/(w/2) = 0.058$

NPR	$p/p_{t,j}$ at x/L of— 0.068	0.233	0.297	0.361	0.399	0.439	0.490	0.540	0.592
1.995	0.962	0.857	0.814	0.862	0.337	0.517	0.596	0.617	0.554
2.509	0.962	0.855	0.813	0.860	0.198	0.581	0.463	0.586	0.505
3.029	0.960	0.857	0.812	0.860	0.180	0.572	0.446	0.399	0.517
3.493	0.962	0.856	0.812	0.861	0.189	0.572	0.445	0.396	0.349
4.019	0.961	0.856	0.812	0.861	0.206	0.571	0.445	0.396	0.348
4.532	0.961	0.856	0.812	0.861	0.218	0.570	0.445	0.397	0.349
4.999	0.961	0.856	0.812	0.861	0.226	0.569	0.446	0.397	0.349
5.991	0.960	0.856	0.811	0.861	0.240	0.566	0.446	0.399	0.349
7.018	0.960	0.855	0.811	0.861	0.241	0.566	0.446	0.400	0.349
8.003	0.959	0.855	0.810	0.861	0.245	0.565	0.446	0.401	0.349

UR quadrant: $y/(w/2) = 0.275$

NPR	$p/p_{t,j}$ at x/L of— 0.271	0.338	0.402	0.440	0.490	0.540
1.995	0.847	0.806	0.864	0.430	0.451	0.484
2.509	0.845	0.804	0.862	0.292	0.325	0.407
3.029	0.843	0.804	0.863	0.254	0.316	0.336
3.493	0.845	0.804	0.863	0.252	0.318	0.306
4.019	0.844	0.804	0.863	0.252	0.321	0.307
4.532	0.843	0.804	0.863	0.251	0.324	0.309
4.999	0.843	0.804	0.863	0.252	0.326	0.309
5.991	0.842	0.804	0.863	0.256	0.329	0.310
7.018	0.842	0.803	0.864	0.257	0.328	0.310
8.003	0.841	0.803	0.864	0.259	0.332	0.312

Table 42. Concluded

UR quadrant: $y/(w/2) = 0.491$

NPR	$p/p_{t,j}$ at x/L of— 0.068	0.210	0.379	0.442	0.480	0.540	0.592	0.681	0.770
1.995	0.967	0.902	0.807	0.871	0.449	0.456	0.462	0.444	0.484
2.509	0.969	0.900	0.805	0.870	0.314	0.351	0.389	0.368	0.375
3.029	0.967	0.900	0.804	0.870	0.204	0.270	0.331	0.316	0.310
3.493	0.968	0.901	0.805	0.870	0.195	0.239	0.328	0.249	0.271
4.019	0.968	0.900	0.805	0.871	0.193	0.236	0.257	0.220	0.245
4.532	0.967	0.900	0.805	0.871	0.192	0.237	0.137	0.202	0.213
4.999	0.967	0.900	0.805	0.871	0.190	0.239	0.137	0.219	0.179
5.991	0.967	0.899	0.804	0.871	0.188	0.241	0.137	0.249	0.134
7.018	0.967	0.899	0.804	0.871	0.186	0.243	0.138	0.242	0.110
8.003	0.966	0.898	0.803	0.871	0.186	0.243	0.139	0.245	0.121

UR quadrant: $y/(w/2) = 0.708$

NPR	$p/p_{t,j}$ at x/L of— 0.419	0.483	0.521
1.995	0.823	0.894	0.462
2.509	0.821	0.893	0.298
3.029	0.821	0.894	0.232
3.493	0.821	0.894	0.193
4.019	0.821	0.894	0.135
4.532	0.820	0.894	0.133
4.999	0.820	0.895	0.132
5.991	0.820	0.895	0.130
7.018	0.820	0.895	0.128
8.003	0.819	0.895	0.127

UR quadrant: $y/(w/2) = 0.924$

NPR	$p/p_{t,j}$ at x/L of— 0.068	0.210	0.460	0.524	0.592	0.681	0.770	0.858	0.947
1.995	0.976	0.936	0.864	0.929	0.474	0.466	0.497	0.502	0.499
2.509	0.976	0.936	0.863	0.928	0.369	0.347	0.381	0.432	0.400
3.029	0.975	0.935	0.862	0.928	0.300	0.283	0.301	0.365	0.334
3.493	0.975	0.935	0.862	0.928	0.257	0.241	0.247	0.334	0.293
4.019	0.975	0.935	0.861	0.927	0.221	0.214	0.206	0.284	0.259
4.532	0.974	0.935	0.861	0.927	0.194	0.187	0.182	0.242	0.233
4.999	0.974	0.935	0.860	0.928	0.167	0.169	0.165	0.217	0.214
5.991	0.974	0.935	0.860	0.929	0.138	0.140	0.128	0.179	0.182
7.018	0.974	0.934	0.860	0.930	0.107	0.119	0.113	0.173	0.153
8.003	0.973	0.934	0.860	0.931	0.105	0.110	0.108	0.160	0.133

Table 43. Nozzle Internal Static Pressure Ratios for Configuration 15

UL quadrant: $y/(w/2) = -0.058$

NPR	$p/p_{t,j}$ at x/L of— 0.068	0.244	0.282	0.333	0.402	0.472	0.540	0.592	0.681	0.770	0.897
2.003	0.965	0.823	0.787	0.727	0.468	0.611	0.647	0.625	0.573	0.527	0.501
2.479	0.964	0.823	0.786	0.726	0.438	0.456	0.604	0.581	0.496	0.429	0.392
3.009	0.964	0.822	0.786	0.725	0.437	0.447	0.405	0.576	0.473	0.373	0.317
3.494	0.964	0.822	0.785	0.725	0.437	0.446	0.400	0.493	0.478	0.360	0.275
4.005	0.963	0.821	0.785	0.725	0.437	0.446	0.396	0.375	0.490	0.367	0.267
4.491	0.963	0.821	0.784	0.724	0.438	0.446	0.396	0.373	0.432	0.372	0.249
4.992	0.964	0.821	0.784	0.724	0.438	0.446	0.396	0.373	0.322	0.357	0.242
5.998	0.963	0.819	0.783	0.723	0.437	0.446	0.396	0.374	0.315	0.342	0.243
6.994	0.962	0.819	0.782	0.722	0.437	0.444	0.396	0.373	0.314	0.267	0.243
8.029	0.962	0.818	0.782	0.722	0.439	0.443	0.395	0.372	0.314	0.261	0.259

UL quadrant: $y/(w/2) = -0.275$

NPR	$p/p_{t,j}$ at x/L of— 0.285	0.323	0.374	0.440	0.540
2.003	0.740	0.684	0.573	0.448	0.652
2.479	0.739	0.682	0.572	0.406	0.615
3.009	0.740	0.682	0.572	0.406	0.502
3.494	0.740	0.682	0.572	0.406	0.392
4.005	0.741	0.682	0.572	0.406	0.391
4.491	0.740	0.681	0.572	0.406	0.392
4.992	0.740	0.681	0.572	0.407	0.392
5.998	0.740	0.680	0.571	0.407	0.392
6.994	0.739	0.679	0.571	0.406	0.393
8.029	0.738	0.678	0.570	0.407	0.394

UL quadrant: $y/(w/2) = -0.491$

NPR	$p/p_{t,j}$ at x/L of— 0.068	0.236	0.325	0.363	0.414	0.477	0.540	0.592	0.681	0.770
2.003	0.972	0.876	0.639	0.543	0.405	0.553	0.613	0.564	0.532	0.502
2.479	0.972	0.875	0.638	0.542	0.405	0.327	0.561	0.524	0.442	0.416
3.009	0.972	0.875	0.640	0.542	0.405	0.290	0.474	0.522	0.403	0.372
3.494	0.972	0.876	0.639	0.542	0.406	0.290	0.362	0.504	0.418	0.353
4.005	0.971	0.876	0.639	0.541	0.406	0.290	0.285	0.464	0.359	0.352
4.491	0.971	0.876	0.638	0.541	0.406	0.290	0.285	0.437	0.356	0.340
4.992	0.971	0.876	0.638	0.541	0.406	0.290	0.284	0.380	0.362	0.274
5.998	0.971	0.876	0.637	0.540	0.406	0.290	0.283	0.302	0.372	0.271
6.994	0.971	0.875	0.636	0.539	0.405	0.290	0.282	0.302	0.383	0.280
8.029	0.971	0.875	0.635	0.538	0.405	0.290	0.280	0.301	0.377	0.290

Table 43. Continued

UL quadrant: $y/(w/2) = -0.708$

NPR	$p/p_{t,j}$ at x/L of— 0.366	0.404	0.455	0.540
2.003	0.561	0.344	0.416	0.471
2.479	0.562	0.347	0.229	0.412
3.009	0.561	0.348	0.191	0.373
3.494	0.560	0.348	0.191	0.331
4.005	0.559	0.348	0.191	0.272
4.491	0.559	0.348	0.191	0.250
4.992	0.558	0.348	0.191	0.224
5.998	0.557	0.348	0.192	0.176
6.994	0.556	0.348	0.192	0.119
8.029	0.556	0.332	0.192	0.120

UL quadrant: $y/(w/2) = -0.924$

NPR	$p/p_{t,j}$ at x/L of— 0.068	0.236	0.407	0.445	0.540	0.592
2.003	0.977	0.943	0.567	0.265	0.444	0.448
2.479	0.977	0.941	0.565	0.204	0.342	0.347
3.009	0.977	0.942	0.564	0.158	0.268	0.275
3.494	0.977	0.941	0.564	0.156	0.233	0.236
4.005	0.977	0.941	0.564	0.157	0.200	0.203
4.491	0.977	0.941	0.563	0.158	0.177	0.180
4.992	0.977	0.941	0.563	0.159	0.162	0.164
5.998	0.977	0.940	0.561	0.161	0.136	0.139
6.994	0.977	0.939	0.560	0.162	0.116	0.122
8.029	0.977	0.939	0.559	0.162	0.102	0.107

UR quadrant: $y/(w/2) = 0.058$

NPR	$p/p_{t,j}$ at x/L of— 0.068	0.233	0.297	0.361	0.399	0.439	0.490	0.540	0.592	0.681	0.770	0.897
2.003	0.957	0.856	0.812	0.861	0.197	0.606	0.626	0.651	0.627	0.576	0.531	0.504
2.479	0.957	0.856	0.811	0.860	0.161	0.570	0.466	0.599	0.574	0.500	0.438	0.402
3.009	0.957	0.856	0.811	0.860	0.155	0.564	0.446	0.409	0.564	0.470	0.382	0.321
3.494	0.958	0.856	0.810	0.861	0.154	0.564	0.444	0.404	0.502	0.472	0.361	0.278
4.005	0.958	0.856	0.810	0.861	0.154	0.564	0.445	0.401	0.353	0.470	0.368	0.258
4.491	0.958	0.855	0.810	0.860	0.157	0.564	0.445	0.402	0.351	0.390	0.375	0.253
4.992	0.957	0.855	0.809	0.860	0.158	0.567	0.446	0.402	0.351	0.392	0.347	0.245
5.998	0.956	0.854	0.809	0.861	0.164	0.566	0.445	0.402	0.352	0.307	0.314	0.244
6.994	0.957	0.854	0.808	0.861	0.170	0.569	0.449	0.403	0.351	0.305	0.320	0.244
8.029	0.956	0.853	0.807	0.862	0.197	0.569	0.447	0.401	0.350	0.305	0.263	0.248

UR quadrant: $y/(w/2) = 0.275$

NPR	$p/p_{t,j}$ at x/L of— 0.271	0.338	0.402	0.440	0.490	0.540
2.003	0.845	0.804	0.862	0.399	0.406	0.455
2.479	0.843	0.803	0.862	0.285	0.345	0.423
3.009	0.843	0.803	0.862	0.254	0.337	0.373
3.494	0.842	0.803	0.862	0.252	0.337	0.311
4.005	0.842	0.803	0.862	0.250	0.339	0.312
4.491	0.841	0.803	0.862	0.249	0.340	0.313
4.992	0.841	0.803	0.862	0.248	0.341	0.313
5.998	0.840	0.802	0.862	0.246	0.341	0.313
6.994	0.840	0.801	0.862	0.245	0.342	0.313
8.029	0.839	0.801	0.862	0.240	0.341	0.314

Table 43. Concluded

UR quadrant: $y/(w/2) = 0.491$

NPR	$p/p_{t,j}$ at x/L of— 0.068	0.210	0.379	0.442	0.480	0.540	0.592	0.681	0.770
2.003	0.965	0.900	0.805	0.870	0.423	0.441	0.475	0.485	0.488
2.479	0.964	0.899	0.804	0.869	0.318	0.351	0.398	0.403	0.392
3.009	0.965	0.899	0.804	0.870	0.200	0.281	0.344	0.354	0.329
3.494	0.966	0.899	0.804	0.870	0.188	0.243	0.372	0.309	0.290
4.005	0.965	0.898	0.804	0.870	0.189	0.242	0.289	0.263	0.262
4.491	0.965	0.898	0.803	0.870	0.189	0.243	0.151	0.243	0.238
4.992	0.965	0.898	0.803	0.870	0.188	0.245	0.143	0.232	0.214
5.998	0.965	0.897	0.802	0.870	0.185	0.247	0.145	0.262	0.187
6.994	0.965	0.897	0.802	0.870	0.184	0.248	0.146	0.276	0.150
8.029	0.964	0.896	0.801	0.869	0.183	0.248	0.148	0.257	0.152

UR quadrant: $y/(w/2) = 0.708$

NPR	$p/p_{t,j}$ at x/L of— 0.419	0.483	0.521
2.003	0.822	0.893	0.453
2.479	0.821	0.893	0.339
3.009	0.820	0.894	0.247
3.494	0.820	0.894	0.171
4.005	0.820	0.894	0.138
4.491	0.820	0.894	0.138
4.992	0.819	0.894	0.138
5.998	0.818	0.894	0.140
6.994	0.817	0.894	0.141
8.029	0.817	0.894	0.134

UR quadrant: $y/(w/2) = 0.924$

NPR	$p/p_{t,j}$ at x/L of— 0.068	0.210	0.460	0.524	0.592
2.003	0.971	0.934	0.868	0.935	0.471
2.479	0.971	0.934	0.866	0.936	0.371
3.009	0.971	0.934	0.866	0.936	0.275
3.494	0.971	0.934	0.865	0.936	0.235
4.005	0.971	0.934	0.865	0.937	0.200
4.491	0.971	0.934	0.864	0.936	0.174
4.992	0.971	0.934	0.863	0.936	0.144
5.998	0.971	0.933	0.861	0.935	0.116
6.994	0.970	0.933	0.860	0.935	0.094
8.029	0.970	0.932	0.858	0.935	0.079

Table 44. Nozzle Internal Static Pressure Ratios for Configuration 15-I

UL quadrant: $y/(w/2) = -0.058$

NPR	$p/p_{t,j}$ at x/L of— 0.068	0.244	0.282	0.333	0.402	0.472	0.540	0.592	0.681	0.770	0.897
2.004	0.965	0.826	0.787	0.728	0.447	0.610	0.645	0.626	0.571	0.525	0.502
2.502	0.965	0.824	0.786	0.727	0.437	0.455	0.603	0.580	0.489	0.418	0.392
3.004	0.965	0.823	0.786	0.727	0.438	0.441	0.410	0.575	0.470	0.375	0.320
3.502	0.965	0.823	0.786	0.726	0.438	0.439	0.401	0.523	0.474	0.359	0.276
3.993	0.965	0.823	0.785	0.726	0.438	0.440	0.397	0.372	0.492	0.362	0.263
4.492	0.964	0.823	0.785	0.725	0.438	0.439	0.397	0.370	0.463	0.368	0.252
4.993	0.964	0.822	0.785	0.725	0.438	0.439	0.397	0.370	0.357	0.359	0.243
6.996	0.963	0.821	0.783	0.723	0.437	0.438	0.397	0.368	0.318	0.300	0.242
7.982	0.962	0.819	0.782	0.722	0.436	0.436	0.397	0.367	0.317	0.258	0.254
9.999	0.962	0.818	0.781	0.721	0.435	0.437	0.397	0.366	0.315	0.258	0.256

UL quadrant: $y/(w/2) = -0.275$

NPR	$p/p_{t,j}$ at x/L of— 0.285	0.323	0.374	0.440	0.540
2.004	0.743	0.685	0.573	0.460	0.651
2.502	0.744	0.684	0.573	0.407	0.615
3.004	0.743	0.684	0.573	0.407	0.511
3.502	0.744	0.684	0.573	0.407	0.392
3.993	0.744	0.683	0.573	0.407	0.392
4.492	0.743	0.683	0.573	0.407	0.392
4.993	0.743	0.683	0.573	0.407	0.392
6.996	0.741	0.680	0.572	0.407	0.393
7.982	0.740	0.679	0.571	0.406	0.393
9.999	0.739	0.677	0.570	0.406	0.394

UL quadrant: $y/(w/2) = -0.491$

NPR	$p/p_{t,j}$ at x/L of— 0.068	0.236	0.325	0.363	0.414	0.477	0.540	0.592	0.681	0.770
2.004	0.972	0.878	0.645	0.544	0.406	0.555	0.612	0.562	0.531	0.504
2.502	0.973	0.877	0.643	0.544	0.406	0.323	0.558	0.523	0.440	0.418
3.004	0.973	0.877	0.644	0.544	0.406	0.291	0.475	0.522	0.403	0.376
3.502	0.972	0.878	0.643	0.543	0.406	0.291	0.376	0.508	0.416	0.356
3.993	0.973	0.878	0.643	0.543	0.407	0.291	0.287	0.477	0.382	0.358
4.492	0.973	0.878	0.641	0.543	0.407	0.291	0.286	0.443	0.347	0.338
4.993	0.972	0.877	0.641	0.543	0.407	0.291	0.286	0.380	0.364	0.304
6.996	0.971	0.876	0.638	0.541	0.406	0.291	0.282	0.302	0.380	0.281
7.982	0.971	0.875	0.637	0.540	0.405	0.291	0.281	0.302	0.387	0.290
9.999	0.971	0.874	0.635	0.538	0.404	0.290	0.279	0.302	0.327	0.299

Table 44. Continued

UL quadrant: $y/(w/2) = -0.708$

NPR	$p/p_{t,j}$ at x/L of— 0.366	0.404	0.455	0.540
2.004	0.564	0.345	0.421	0.466
2.502	0.564	0.349	0.215	0.407
3.004	0.563	0.349	0.191	0.371
3.502	0.563	0.349	0.192	0.336
3.993	0.562	0.349	0.192	0.280
4.492	0.562	0.349	0.193	0.252
4.993	0.561	0.349	0.192	0.230
6.996	0.558	0.348	0.193	0.120
7.982	0.557	0.348	0.193	0.120
9.999	0.555	0.348	0.193	0.121

UL quadrant: $y/(w/2) = -0.924$

NPR	$p/p_{t,j}$ at x/L of— 0.068	0.236	0.407	0.445	0.540	0.592
2.004	0.980	0.943	0.571	0.285	0.443	0.446
2.502	0.980	0.942	0.570	0.211	0.337	0.340
3.004	0.979	0.943	0.568	0.162	0.262	0.268
3.502	0.980	0.942	0.569	0.158	0.233	0.236
3.993	0.980	0.942	0.569	0.160	0.205	0.207
4.492	0.980	0.942	0.568	0.161	0.179	0.180
4.993	0.980	0.941	0.567	0.161	0.157	0.159
6.996	0.979	0.940	0.564	0.163	0.117	0.120
7.982	0.978	0.939	0.562	0.164	0.103	0.107
9.999	0.978	0.938	0.560	0.165	0.084	0.084

UR quadrant: $y/(w/2) = 0.058$

NPR	$p/p_{t,j}$ at x/L of— 0.068	0.233	0.297	0.361	0.399	0.439	0.490	0.540	0.592	0.681	0.770	0.897
2.004	0.957	0.857	0.812	0.862	0.209	0.612	0.626	0.651	0.627	0.574	0.530	0.503
2.502	0.958	0.856	0.811	0.861	0.121	0.537	0.467	0.598	0.573	0.492	0.427	0.399
3.004	0.957	0.857	0.811	0.862	0.124	0.546	0.446	0.411	0.561	0.468	0.383	0.319
3.502	0.958	0.856	0.811	0.862	0.128	0.551	0.442	0.404	0.517	0.468	0.360	0.276
3.993	0.958	0.857	0.811	0.862	0.128	0.554	0.442	0.401	0.352	0.479	0.364	0.253
4.492	0.958	0.856	0.810	0.862	0.128	0.556	0.441	0.401	0.349	0.411	0.370	0.259
4.993	0.958	0.856	0.810	0.862	0.128	0.556	0.440	0.402	0.349	0.393	0.347	0.243
6.996	0.957	0.855	0.809	0.862	0.135	0.544	0.440	0.403	0.348	0.307	0.309	0.242
7.982	0.956	0.854	0.808	0.862	0.136	0.539	0.440	0.404	0.348	0.306	0.267	0.248
9.999	0.956	0.853	0.807	0.862	0.139	0.537	0.441	0.404	0.346	0.304	0.262	0.229

UR quadrant: $y/(w/2) = 0.275$

NPR	$p/p_{t,j}$ at x/L of— 0.271	0.338	0.402	0.440	0.490	0.540
2.004	0.846	0.805	0.862	0.400	0.416	0.464
2.502	0.844	0.804	0.862	0.275	0.353	0.439
3.004	0.844	0.804	0.862	0.253	0.341	0.382
3.502	0.844	0.804	0.863	0.250	0.341	0.309
3.993	0.843	0.804	0.863	0.247	0.345	0.310
4.492	0.843	0.803	0.863	0.245	0.347	0.311
4.993	0.843	0.804	0.863	0.244	0.348	0.311
6.996	0.841	0.802	0.862	0.238	0.342	0.310
7.982	0.840	0.801	0.862	0.238	0.338	0.309
9.999	0.839	0.801	0.862	0.227	0.340	0.312

Table 44. Concluded

UR quadrant: $y/(w/2) = 0.491$

NPR	$p/p_{t,j}$ at x/L of— 0.068	0.210	0.379	0.442	0.480	0.540	0.592	0.681	0.770
2.004	0.966	0.901	0.806	0.871	0.424	0.440	0.473	0.484	0.487
2.502	0.967	0.900	0.805	0.870	0.308	0.348	0.399	0.404	0.388
3.004	0.967	0.900	0.805	0.870	0.201	0.279	0.341	0.359	0.328
3.502	0.968	0.900	0.805	0.871	0.181	0.246	0.354	0.321	0.292
3.993	0.967	0.899	0.805	0.871	0.178	0.238	0.293	0.279	0.261
4.492	0.967	0.899	0.804	0.871	0.176	0.244	0.165	0.246	0.239
4.993	0.966	0.900	0.804	0.871	0.175	0.245	0.138	0.220	0.209
6.996	0.966	0.898	0.803	0.870	0.170	0.248	0.141	0.273	0.159
7.982	0.965	0.897	0.802	0.870	0.171	0.248	0.143	0.262	0.143
9.999	0.965	0.896	0.801	0.870	0.178	0.247	0.145	0.243	0.195

UR quadrant: $y/(w/2) = 0.708$

NPR	$p/p_{t,j}$ at x/L of— 0.419	0.483	0.521
2.004	0.823	0.894	0.454
2.502	0.822	0.894	0.327
3.004	0.822	0.894	0.253
3.502	0.822	0.895	0.199
3.993	0.822	0.895	0.154
4.492	0.821	0.895	0.147
4.993	0.821	0.895	0.147
6.996	0.819	0.895	0.132
7.982	0.818	0.895	0.131
9.999	0.816	0.881	0.130

UR quadrant: $y/(w/2) = 0.924$

NPR	$p/p_{t,j}$ at x/L of— 0.068	0.210	0.460	0.524	0.592
2.004	0.972	0.935	0.868	0.935	0.469
2.502	0.972	0.936	0.867	0.936	0.363
3.004	0.971	0.935	0.868	0.937	0.288
3.502	0.972	0.935	0.867	0.937	0.238
3.993	0.972	0.936	0.867	0.938	0.205
4.492	0.972	0.935	0.867	0.938	0.182
4.993	0.972	0.935	0.866	0.938	0.166
6.996	0.971	0.934	0.862	0.937	0.094
7.982	0.971	0.933	0.860	0.936	0.079
9.999	0.970	0.932	0.857	0.879	0.059

Table 45. Nozzle Internal Static Pressure Ratios for Configuration 16

UL quadrant: $y/(w/2) = -0.058$

	$p/p_{t,j}$ at x/L of—											
NPR	0.068	0.212	0.250	0.314	0.377	0.439	0.490	0.540	0.592	0.681	0.770	0.897
1.990	0.971	0.751	0.649	0.663	0.475	0.583	0.614	0.610	0.585	0.554	0.530	0.510
2.510	0.971	0.747	0.642	0.654	0.450	0.499	0.540	0.560	0.519	0.448	0.407	0.418
3.007	0.970	0.748	0.641	0.655	0.443	0.479	0.446	0.543	0.516	0.415	0.326	0.332
3.501	0.970	0.748	0.640	0.656	0.440	0.469	0.435	0.423	0.516	0.420	0.316	0.265
4.003	0.970	0.746	0.640	0.657	0.438	0.467	0.428	0.372	0.389	0.422	0.325	0.243
4.497	0.970	0.746	0.640	0.658	0.435	0.465	0.423	0.368	0.373	0.438	0.299	0.228
4.979	0.970	0.746	0.639	0.658	0.433	0.465	0.419	0.367	0.367	0.424	0.308	0.227
6.005	0.969	0.745	0.637	0.659	0.429	0.462	0.414	0.364	0.355	0.315	0.311	0.205
7.007	0.969	0.744	0.635	0.659	0.427	0.459	0.412	0.363	0.354	0.316	0.325	0.204
7.973	0.969	0.743	0.633	0.659	0.426	0.458	0.411	0.363	0.353	0.317	0.251	0.214
10.056	0.968	0.742	0.630	0.656	0.426	0.458	0.414	0.360	0.354	0.318	0.251	0.241

UL quadrant: $y/(w/2) = -0.275$

	$p/p_{t,j}$ at x/L of—					
NPR	0.253	0.291	0.355	0.418	0.477	0.540
1.990	0.621	0.375	0.600	0.598	0.609	0.587
2.510	0.618	0.372	0.541	0.522	0.546	0.537
3.007	0.616	0.373	0.541	0.501	0.495	0.516
3.501	0.614	0.372	0.543	0.492	0.475	0.460
4.003	0.612	0.371	0.542	0.464	0.451	0.452
4.497	0.611	0.371	0.542	0.458	0.448	0.441
4.979	0.609	0.370	0.543	0.458	0.449	0.435
6.005	0.608	0.369	0.544	0.457	0.449	0.420
7.007	0.606	0.368	0.545	0.457	0.451	0.416
7.973	0.605	0.368	0.545	0.457	0.452	0.418
10.056	0.604	0.367	0.547	0.457	0.451	0.390

UL quadrant: $y/(w/2) = -0.491$

	$p/p_{t,j}$ at x/L of—									
NPR	0.068	0.210	0.294	0.332	0.395	0.464	0.540	0.592	0.681	0.770
1.990	0.983	0.936	0.605	0.309	0.364	0.406	0.471	0.487	0.513	0.509
2.510	0.981	0.936	0.603	0.309	0.254	0.345	0.441	0.420	0.415	0.414
3.007	0.981	0.936	0.600	0.311	0.254	0.350	0.428	0.383	0.364	0.349
3.501	0.981	0.936	0.599	0.311	0.252	0.308	0.412	0.354	0.344	0.317
4.003	0.981	0.936	0.597	0.310	0.241	0.265	0.430	0.344	0.382	0.305
4.497	0.981	0.935	0.597	0.310	0.236	0.236	0.429	0.339	0.297	0.335
4.979	0.980	0.935	0.596	0.310	0.232	0.227	0.423	0.341	0.292	0.308
6.005	0.981	0.934	0.595	0.310	0.232	0.214	0.426	0.340	0.293	0.240
7.007	0.980	0.934	0.594	0.309	0.230	0.212	0.431	0.342	0.291	0.238
7.973	0.980	0.934	0.593	0.309	0.228	0.204	0.441	0.343	0.292	0.237
10.056	0.980	0.933	0.591	0.308	0.225	0.196	0.446	0.347	0.290	0.236

Table 45. Continued

UL quadrant: $y/(w/2) = -0.708$

NPR	$p/p_{t,j}$ at x/L of— 0.334	0.372	0.436	0.540
1.990	0.667	0.300	0.403	0.407
2.510	0.665	0.286	0.319	0.337
3.007	0.663	0.287	0.297	0.332
3.501	0.663	0.290	0.287	0.321
4.003	0.660	0.289	0.236	0.286
4.497	0.660	0.289	0.220	0.272
4.979	0.659	0.290	0.220	0.277
6.005	0.658	0.289	0.214	0.289
7.007	0.656	0.288	0.209	0.286
7.973	0.655	0.288	0.209	0.286
10.056	0.653	0.288	0.207	0.284

UL quadrant: $y/(w/2) = -0.924$

NPR	$p/p_{t,j}$ at x/L of— 0.068	0.210	0.375	0.413	0.540	0.592
1.990	0.988	0.975	0.784	0.261	0.445	0.506
2.510	0.988	0.975	0.781	0.201	0.364	0.422
3.007	0.988	0.975	0.779	0.174	0.334	0.368
3.501	0.987	0.974	0.777	0.148	0.346	0.345
4.003	0.987	0.974	0.775	0.145	0.306	0.320
4.497	0.987	0.973	0.774	0.146	0.292	0.308
4.979	0.987	0.973	0.772	0.147	0.306	0.295
6.005	0.987	0.973	0.768	0.151	0.295	0.289
7.007	0.987	0.972	0.765	0.155	0.295	0.289
7.973	0.986	0.972	0.762	0.156	0.297	0.283
10.056	0.986	0.970	0.756	0.158	0.299	0.282

UR quadrant: $y/(w/2) = 0.058$

NPR	$p/p_{t,j}$ at x/L of— 0.068	0.233	0.297	0.361	0.399	0.439	0.490	0.540	0.592	0.681	0.770	0.897
1.990	0.961	0.816	0.764	0.835	0.274	0.579	0.627	0.620	0.595	0.561	0.537	0.511
2.510	0.960	0.812	0.758	0.832	0.161	0.559	0.528	0.570	0.529	0.456	0.417	0.424
3.007	0.961	0.812	0.758	0.832	0.124	0.554	0.449	0.553	0.521	0.424	0.339	0.338
3.501	0.961	0.811	0.757	0.832	0.116	0.553	0.438	0.381	0.523	0.415	0.324	0.261
4.003	0.962	0.811	0.757	0.832	0.111	0.553	0.433	0.373	0.385	0.423	0.322	0.255
4.497	0.961	0.812	0.757	0.832	0.111	0.553	0.431	0.371	0.343	0.443	0.303	0.227
4.979	0.961	0.810	0.756	0.832	0.110	0.552	0.431	0.368	0.342	0.420	0.305	0.222
6.005	0.961	0.810	0.756	0.832	0.109	0.550	0.430	0.366	0.339	0.336	0.313	0.210
7.007	0.961	0.809	0.754	0.832	0.108	0.548	0.430	0.366	0.341	0.327	0.322	0.201
7.973	0.961	0.809	0.754	0.832	0.112	0.545	0.430	0.364	0.341	0.328	0.293	0.208
10.056	0.960	0.808	0.753	0.832	0.134	0.540	0.433	0.363	0.348	0.330	0.253	0.223

UR quadrant: $y/(w/2) = 0.275$

NPR	$p/p_{t,j}$ at x/L of— 0.271	0.338	0.402	0.440	0.490	0.540
1.990	0.811	0.776	0.854	0.414	0.424	0.452
2.510	0.806	0.772	0.852	0.302	0.335	0.404
3.007	0.807	0.772	0.852	0.244	0.309	0.383
3.501	0.805	0.771	0.852	0.236	0.301	0.290
4.003	0.805	0.771	0.852	0.237	0.295	0.278
4.497	0.804	0.771	0.852	0.238	0.291	0.278
4.979	0.804	0.771	0.852	0.239	0.294	0.281
6.005	0.803	0.771	0.852	0.234	0.306	0.277
7.007	0.802	0.770	0.852	0.232	0.305	0.282
7.973	0.801	0.769	0.852	0.228	0.302	0.284
10.056	0.800	0.768	0.852	0.230	0.300	0.282

Table 45. Concluded

UR quadrant: $y/(w/2) = 0.491$

NPR	$p/p_{t,j}$ at x/L of— 0.068	0.210	0.379	0.442	0.480	0.540	0.592	0.681	0.770
1.990	0.967	0.889	0.790	0.865	0.426	0.452	0.487	0.496	0.491
2.510	0.966	0.886	0.787	0.864	0.299	0.347	0.406	0.397	0.387
3.007	0.968	0.886	0.787	0.864	0.224	0.295	0.337	0.342	0.322
3.501	0.967	0.886	0.787	0.864	0.153	0.241	0.299	0.312	0.283
4.003	0.966	0.885	0.787	0.864	0.158	0.231	0.263	0.280	0.253
4.497	0.966	0.886	0.786	0.864	0.154	0.231	0.146	0.257	0.228
4.979	0.965	0.885	0.786	0.864	0.149	0.233	0.127	0.246	0.206
6.005	0.966	0.885	0.786	0.864	0.152	0.237	0.127	0.248	0.173
7.007	0.965	0.884	0.785	0.864	0.162	0.237	0.128	0.244	0.128
7.973	0.965	0.883	0.784	0.864	0.164	0.237	0.128	0.211	0.133
10.056	0.964	0.882	0.783	0.864	0.161	0.239	0.131	0.132	0.202

UR quadrant: $y/(w/2) = 0.708$

NPR	$p/p_{t,j}$ at x/L of— 0.419	0.483	0.521
1.990	0.814	0.890	0.450
2.510	0.811	0.890	0.309
3.007	0.811	0.890	0.237
3.501	0.810	0.890	0.201
4.003	0.810	0.890	0.157
4.497	0.810	0.891	0.124
4.979	0.809	0.890	0.122
6.005	0.809	0.891	0.123
7.007	0.808	0.890	0.124
7.973	0.807	0.890	0.124
10.056	0.805	0.877	0.122

UR quadrant: $y/(w/2) = 0.924$

NPR	$p/p_{t,j}$ at x/L of— 0.068	0.210	0.460	0.524	0.592
1.990	0.972	0.932	0.862	0.933	0.468
2.510	0.971	0.931	0.860	0.934	0.353
3.007	0.972	0.930	0.860	0.934	0.281
3.501	0.971	0.929	0.860	0.935	0.231
4.003	0.971	0.929	0.859	0.935	0.203
4.497	0.971	0.929	0.859	0.935	0.180
4.979	0.971	0.928	0.858	0.934	0.159
6.005	0.971	0.928	0.857	0.934	0.108
7.007	0.971	0.927	0.855	0.933	0.093
7.973	0.971	0.927	0.853	0.932	0.074
10.056	0.970	0.926	0.850	0.875	0.061

Table 46. Nozzle Internal Static Pressure Ratios for Configuration 16-I

UL quadrant: $y/(w/2) = -0.058$

	$p/p_{t,j}$ at x/L of—											
NPR	0.068	0.212	0.250	0.314	0.377	0.439	0.490	0.540	0.592	0.681	0.770	0.897
2.003	0.971	0.751	0.647	0.662	0.474	0.578	0.610	0.607	0.582	0.550	0.532	0.507
2.518	0.971	0.748	0.641	0.656	0.450	0.496	0.532	0.561	0.518	0.447	0.408	0.413
3.012	0.971	0.748	0.640	0.656	0.443	0.481	0.445	0.532	0.520	0.413	0.328	0.334
3.500	0.971	0.748	0.639	0.656	0.440	0.468	0.434	0.423	0.515	0.416	0.319	0.267
4.007	0.970	0.747	0.639	0.657	0.438	0.466	0.429	0.371	0.387	0.421	0.322	0.244
4.514	0.970	0.747	0.639	0.658	0.435	0.464	0.422	0.371	0.369	0.438	0.301	0.229
5.009	0.970	0.746	0.638	0.658	0.433	0.463	0.420	0.370	0.364	0.420	0.311	0.224
6.060	0.970	0.746	0.636	0.658	0.430	0.461	0.417	0.369	0.359	0.313	0.312	0.205
7.000	0.970	0.744	0.635	0.658	0.428	0.459	0.416	0.369	0.357	0.313	0.327	0.204
7.985	0.969	0.743	0.633	0.658	0.427	0.457	0.414	0.368	0.355	0.314	0.247	0.213
9.981	0.969	0.742	0.631	0.657	0.425	0.456	0.414	0.368	0.354	0.315	0.248	0.240

UL quadrant: $y/(w/2) = -0.275$

	$p/p_{t,j}$ at x/L of—					
NPR	0.253	0.291	0.355	0.418	0.477	0.540
2.003	0.620	0.373	0.600	0.595	0.606	0.581
2.518	0.618	0.370	0.543	0.519	0.540	0.536
3.012	0.616	0.371	0.538	0.503	0.488	0.490
3.500	0.614	0.371	0.542	0.488	0.476	0.457
4.007	0.612	0.370	0.542	0.467	0.447	0.454
4.514	0.610	0.370	0.542	0.459	0.449	0.444
5.009	0.610	0.370	0.543	0.458	0.449	0.443
6.060	0.608	0.369	0.544	0.458	0.450	0.439
7.000	0.607	0.368	0.544	0.458	0.451	0.433
7.985	0.606	0.368	0.545	0.458	0.451	0.423
9.981	0.604	0.367	0.547	0.458	0.452	0.402

UL quadrant: $y/(w/2) = -0.491$

	$p/p_{t,j}$ at x/L of—									
NPR	0.068	0.210	0.294	0.332	0.395	0.464	0.540	0.592	0.681	0.770
2.003	0.983	0.935	0.606	0.311	0.349	0.405	0.466	0.485	0.509	0.504
2.518	0.982	0.934	0.604	0.311	0.257	0.345	0.437	0.414	0.416	0.410
3.012	0.982	0.936	0.601	0.311	0.250	0.352	0.422	0.390	0.367	0.346
3.500	0.982	0.935	0.600	0.312	0.251	0.309	0.414	0.355	0.349	0.317
4.007	0.982	0.935	0.599	0.312	0.244	0.257	0.418	0.347	0.397	0.307
4.514	0.982	0.935	0.598	0.311	0.237	0.228	0.424	0.339	0.300	0.337
5.009	0.981	0.935	0.597	0.311	0.235	0.221	0.425	0.338	0.299	0.305
6.060	0.982	0.935	0.595	0.310	0.233	0.217	0.428	0.341	0.297	0.237
7.000	0.981	0.934	0.594	0.310	0.231	0.216	0.429	0.344	0.295	0.236
7.985	0.980	0.933	0.593	0.309	0.230	0.214	0.432	0.344	0.295	0.236
9.981	0.980	0.933	0.592	0.308	0.226	0.208	0.437	0.345	0.294	0.234

Table 46. Continued

UL quadrant: $y/(w/2) = -0.708$

NPR	$p/p_{t,j}$ at x/L of— 0.334	0.372	0.436	0.540
2.003	0.666	0.296	0.399	0.389
2.518	0.665	0.286	0.312	0.318
3.012	0.663	0.287	0.292	0.301
3.500	0.662	0.289	0.281	0.312
4.007	0.660	0.289	0.237	0.295
4.514	0.659	0.289	0.218	0.274
5.009	0.659	0.289	0.214	0.275
6.060	0.657	0.289	0.207	0.279
7.000	0.656	0.288	0.205	0.278
7.985	0.654	0.288	0.206	0.283
9.981	0.653	0.288	0.207	0.285

UL quadrant: $y/(w/2) = -0.924$

NPR	$p/p_{t,j}$ at x/L of— 0.068	0.210	0.375	0.413	0.540	0.592
2.003	0.989	0.974	0.784	0.260	0.438	0.504
2.518	0.989	0.975	0.781	0.200	0.356	0.420
3.012	0.989	0.974	0.780	0.168	0.318	0.361
3.500	0.989	0.974	0.778	0.150	0.334	0.338
4.007	0.989	0.974	0.775	0.147	0.306	0.323
4.514	0.989	0.974	0.773	0.148	0.291	0.305
5.009	0.989	0.973	0.772	0.149	0.291	0.301
6.060	0.988	0.973	0.768	0.153	0.288	0.294
7.000	0.988	0.972	0.765	0.155	0.291	0.291
7.985	0.987	0.972	0.762	0.156	0.292	0.290
9.981	0.987	0.971	0.758	0.158	0.292	0.289

UR quadrant: $y/(w/2) = 0.058$

NPR	$p/p_{t,j}$ at x/L of— 0.068	0.233	0.297	0.361	0.399	0.439	0.490	0.540	0.592	0.681	0.770	0.897
2.003	0.962	0.814	0.763	0.835	0.269	0.575	0.623	0.618	0.592	0.558	0.536	0.508
2.518	0.963	0.813	0.759	0.833	0.158	0.564	0.517	0.571	0.529	0.457	0.416	0.419
3.012	0.962	0.812	0.758	0.833	0.113	0.559	0.447	0.546	0.524	0.426	0.340	0.342
3.500	0.962	0.811	0.757	0.833	0.108	0.557	0.436	0.381	0.523	0.414	0.327	0.262
4.007	0.963	0.811	0.757	0.833	0.108	0.555	0.432	0.374	0.381	0.424	0.323	0.257
4.514	0.963	0.811	0.757	0.833	0.108	0.555	0.430	0.371	0.341	0.443	0.304	0.227
5.009	0.963	0.811	0.756	0.833	0.110	0.553	0.430	0.370	0.340	0.422	0.307	0.217
6.060	0.963	0.810	0.756	0.833	0.114	0.550	0.430	0.368	0.341	0.319	0.312	0.211
7.000	0.963	0.809	0.755	0.833	0.116	0.548	0.430	0.368	0.342	0.316	0.319	0.203
7.985	0.962	0.809	0.754	0.832	0.119	0.545	0.431	0.366	0.342	0.317	0.290	0.207
9.981	0.962	0.808	0.753	0.833	0.130	0.541	0.433	0.366	0.346	0.317	0.252	0.224

UR quadrant: $y/(w/2) = 0.275$

NPR	$p/p_{t,j}$ at x/L of— 0.271	0.338	0.402	0.440	0.490	0.540
2.003	0.809	0.776	0.853	0.408	0.417	0.446
2.518	0.806	0.772	0.852	0.295	0.331	0.403
3.012	0.806	0.772	0.852	0.240	0.307	0.383
3.500	0.805	0.771	0.852	0.235	0.299	0.289
4.007	0.805	0.771	0.852	0.235	0.299	0.275
4.514	0.804	0.771	0.852	0.235	0.299	0.275
5.009	0.803	0.771	0.852	0.235	0.299	0.275
6.060	0.803	0.771	0.852	0.235	0.300	0.276
7.000	0.802	0.770	0.852	0.234	0.302	0.279
7.985	0.801	0.769	0.852	0.234	0.302	0.280
9.981	0.800	0.768	0.852	0.234	0.301	0.282

Table 46. Concluded

UR quadrant: $y/(w/2) = 0.491$

NPR	$p/p_{t,j}$ at x/L of— 0.068	0.210	0.379	0.442	0.480	0.540	0.592	0.681	0.770
2.003	0.965	0.890	0.790	0.865	0.428	0.444	0.476	0.489	0.487
2.518	0.966	0.887	0.787	0.864	0.302	0.347	0.403	0.398	0.386
3.012	0.967	0.886	0.787	0.864	0.224	0.293	0.334	0.343	0.323
3.500	0.967	0.886	0.787	0.864	0.167	0.237	0.304	0.312	0.282
4.007	0.967	0.886	0.787	0.864	0.164	0.230	0.268	0.280	0.252
4.514	0.967	0.886	0.786	0.864	0.162	0.230	0.136	0.254	0.226
5.009	0.967	0.886	0.786	0.864	0.160	0.231	0.126	0.248	0.208
6.060	0.966	0.885	0.786	0.864	0.160	0.233	0.127	0.249	0.175
7.000	0.966	0.884	0.785	0.864	0.161	0.234	0.128	0.246	0.128
7.985	0.965	0.883	0.784	0.864	0.160	0.234	0.129	0.213	0.131
9.981	0.965	0.883	0.783	0.864	0.161	0.236	0.131	0.135	0.191

UR quadrant: $y/(w/2) = 0.708$

NPR	$p/p_{t,j}$ at x/L of— 0.419	0.483	0.521
2.003	0.812	0.890	0.449
2.518	0.811	0.889	0.310
3.012	0.810	0.890	0.239
3.500	0.810	0.890	0.196
4.007	0.810	0.890	0.150
4.514	0.810	0.890	0.123
5.009	0.809	0.891	0.122
6.060	0.809	0.891	0.122
7.000	0.808	0.890	0.122
7.985	0.807	0.890	0.121
9.981	0.805	0.883	0.120

UR quadrant: $y/(w/2) = 0.924$

NPR	$p/p_{t,j}$ at x/L of— 0.068	0.210	0.460	0.524	0.592
2.003	0.971	0.929	0.861	0.932	0.463
2.518	0.972	0.929	0.860	0.933	0.350
3.012	0.973	0.929	0.860	0.934	0.274
3.500	0.972	0.929	0.860	0.934	0.229
4.007	0.972	0.930	0.859	0.934	0.208
4.514	0.973	0.929	0.859	0.935	0.179
5.009	0.973	0.929	0.858	0.935	0.156
6.060	0.973	0.928	0.856	0.934	0.106
7.000	0.972	0.928	0.855	0.933	0.093
7.985	0.972	0.927	0.853	0.932	0.074
9.981	0.971	0.926	0.850	0.881	0.062

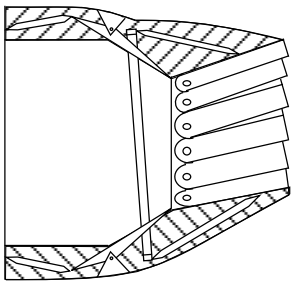

Axisymmetric vectoring nozzle
with internal synchronization ring
(sketch from ref. 1)

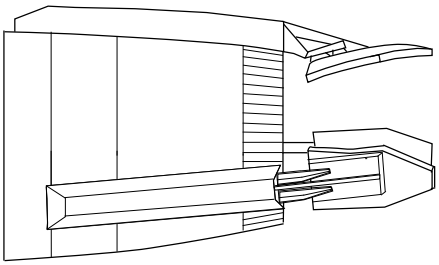

Axisymmetric vectoring nozzle
with postexit vanes
(sketch from ref. 6)

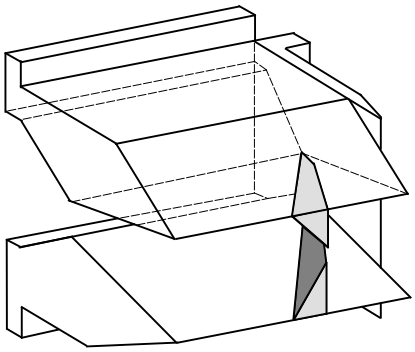

Nonaxisymmetric vectoring nozzle
with deployable deflectors
(sketch from ref. 7)

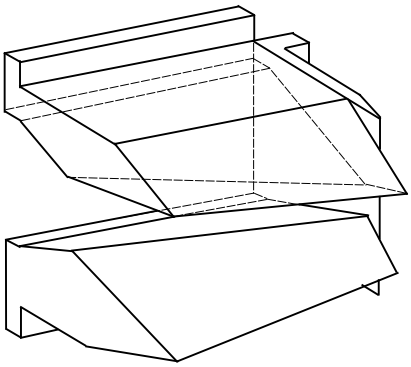

Nonaxisymmetric vectoring nozzle
with skewed throat-hinge line
(concept from ref. 8)

Figure 1. Examples of previously studied thrust-vectoring concepts.

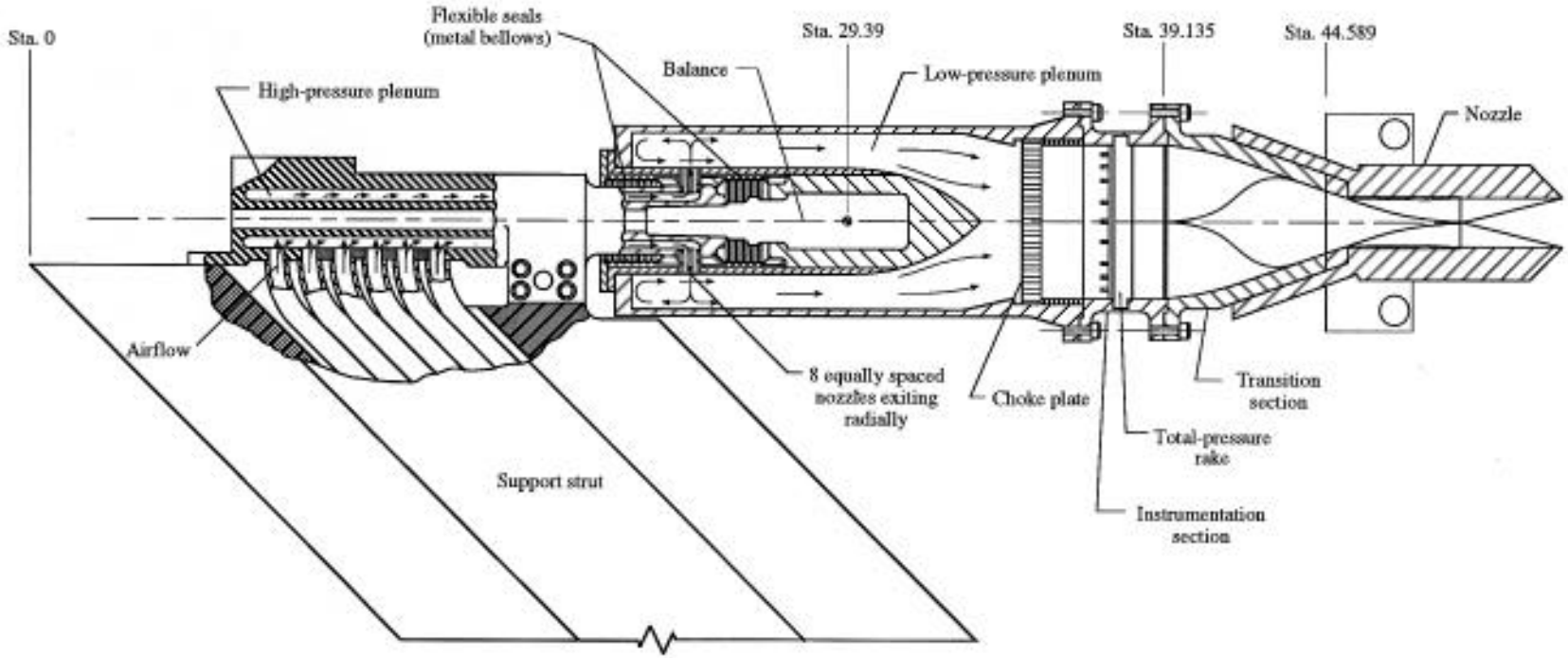

Figure 2. Propulsion simulation system with typical nozzle configuration installed. Station numbers are in inches.

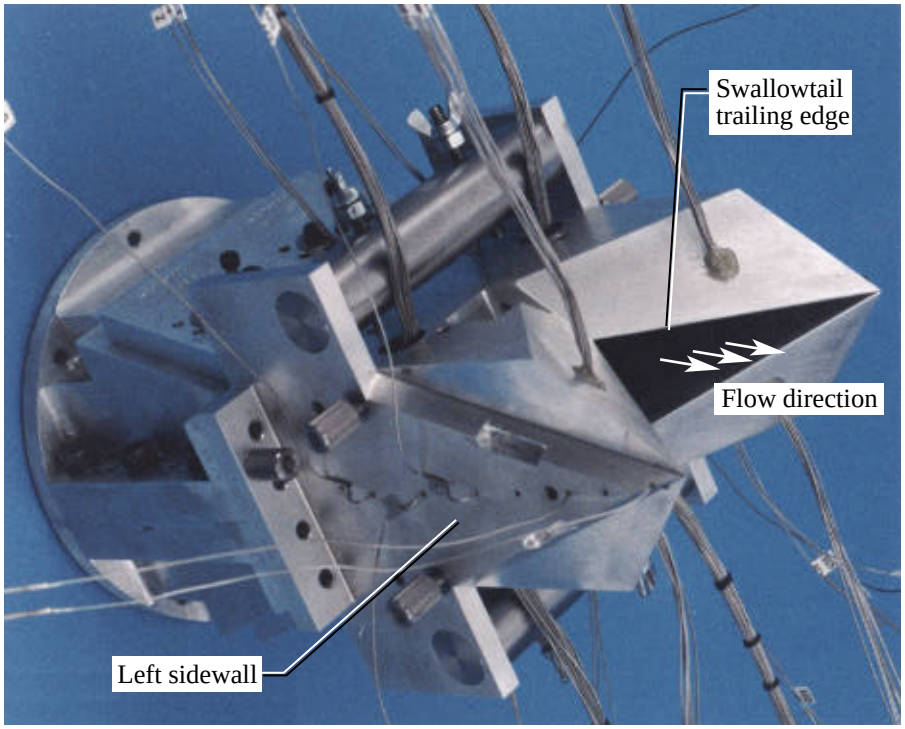

(a) Dry power configuration; full assembly.

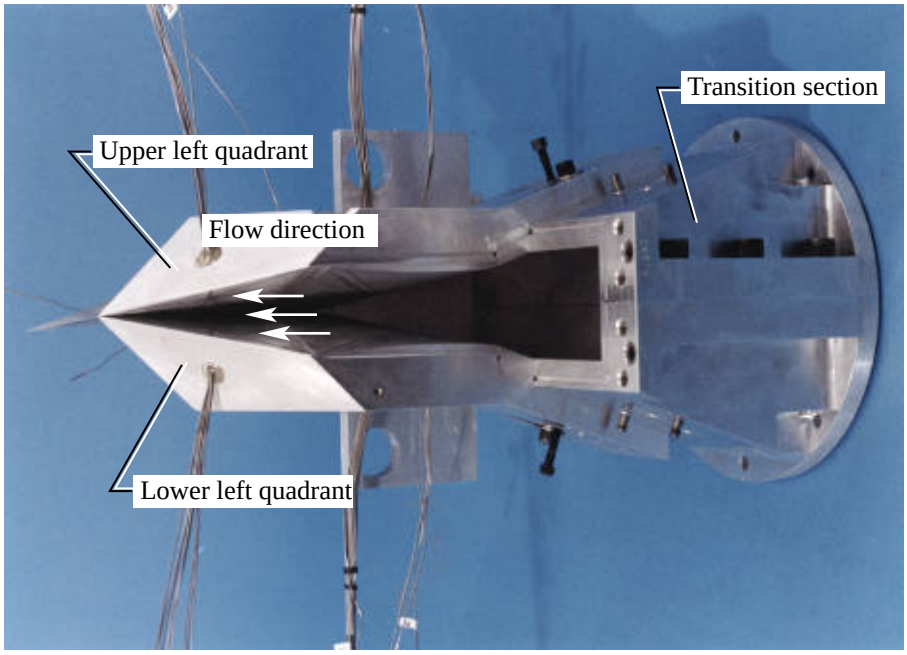

(b) Dry power configuration with interfairing; right-side quadrants removed.

Figure 3. Swallowtail VIC nozzle.

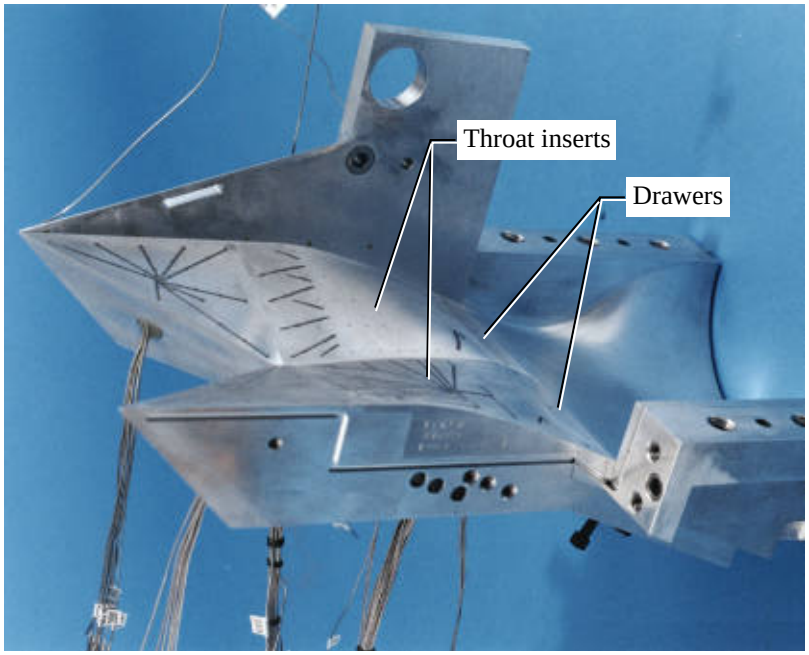

(c) Dry power configuration; lower quadrants, transition section, and left sidewall only.

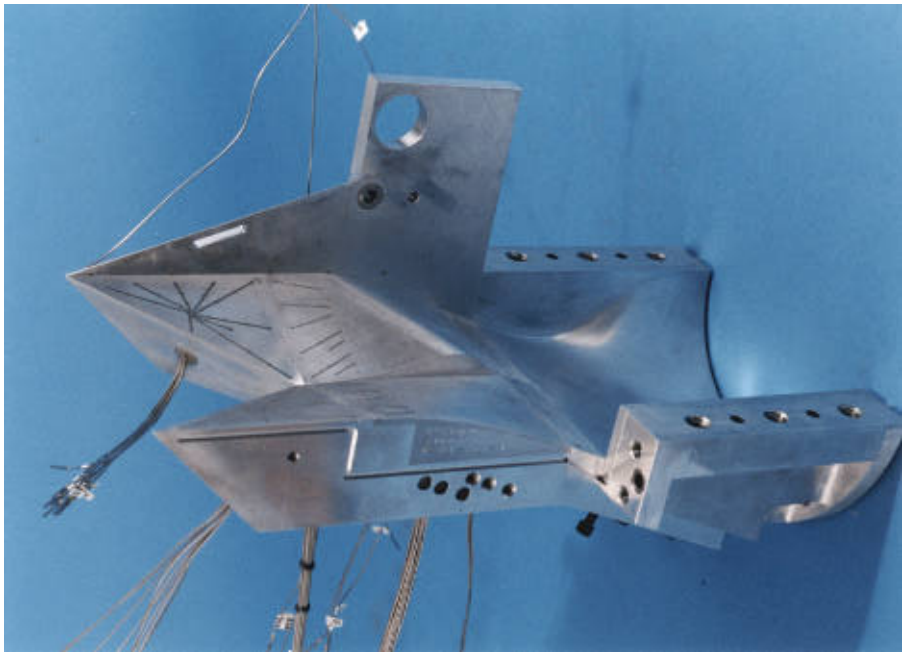

(d) Dry power yaw thrust-vectoring configuration; lower quadrants, transition section, and left sidewall only.

Figure 3. Continued.

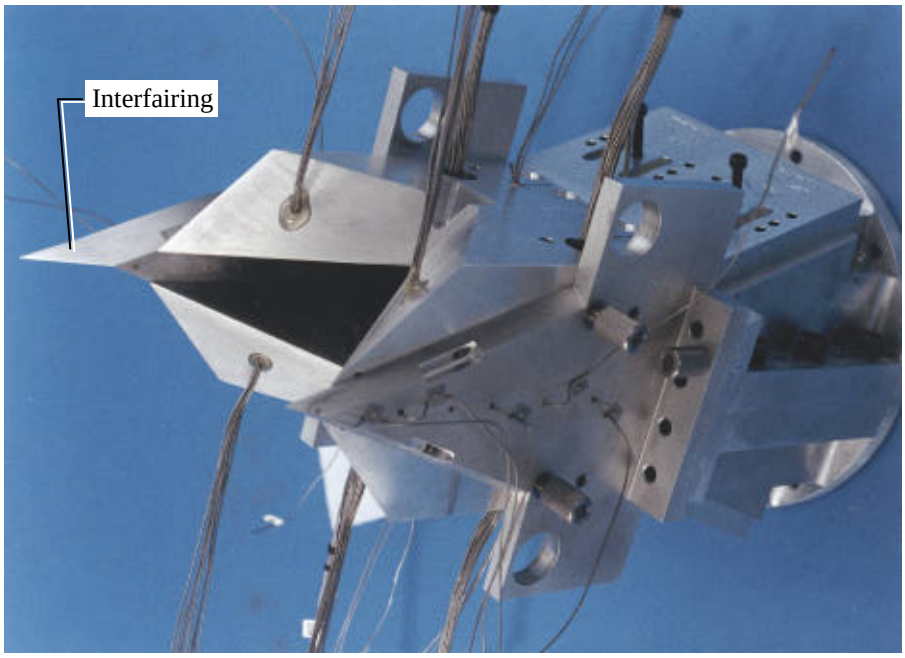

(e) Afterburning power configuration with interfairing; full assembly.

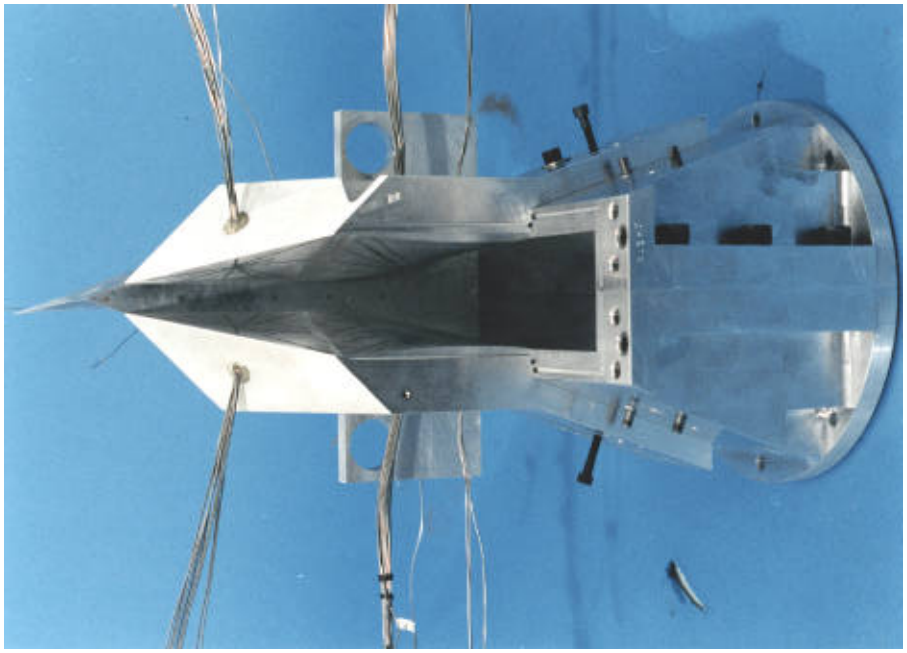

(f) Afterburning power configuration with interfairing; right-side quadrants removed.

Figure 3. Concluded.

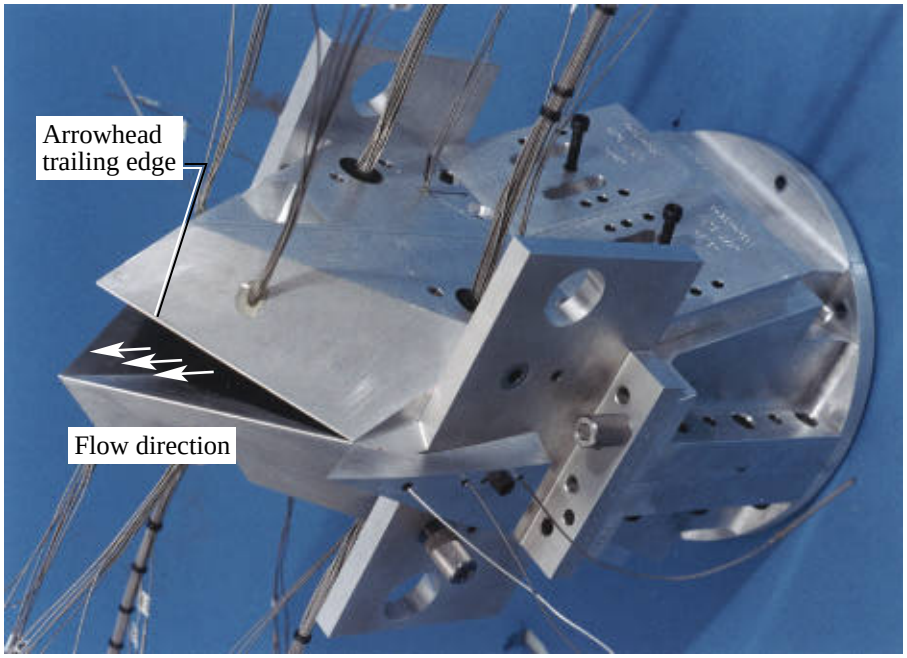

(a) Dry power configuration with interfairing; full assembly.

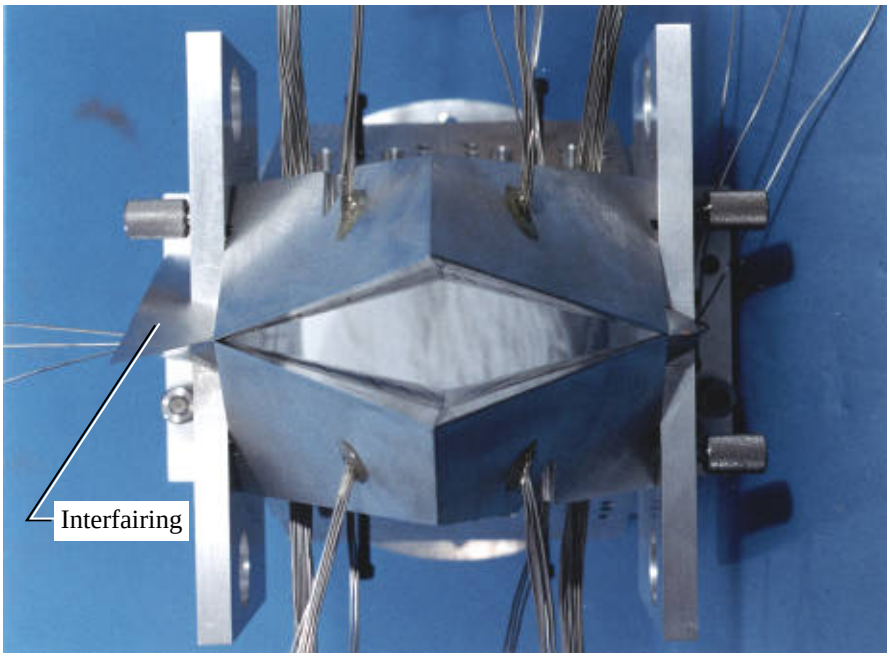

(b) Dry power unvectored configuration with interfairing; end view.

Figure 4. Arrowhead VIC nozzle.

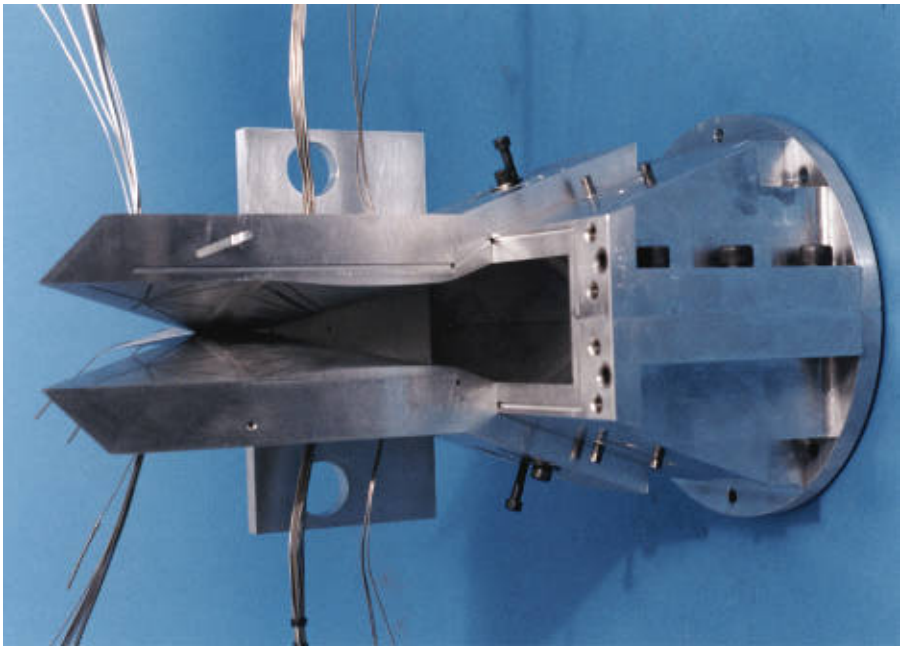

(c) Dry power configuration with interfairing; right-side quadrants removed.

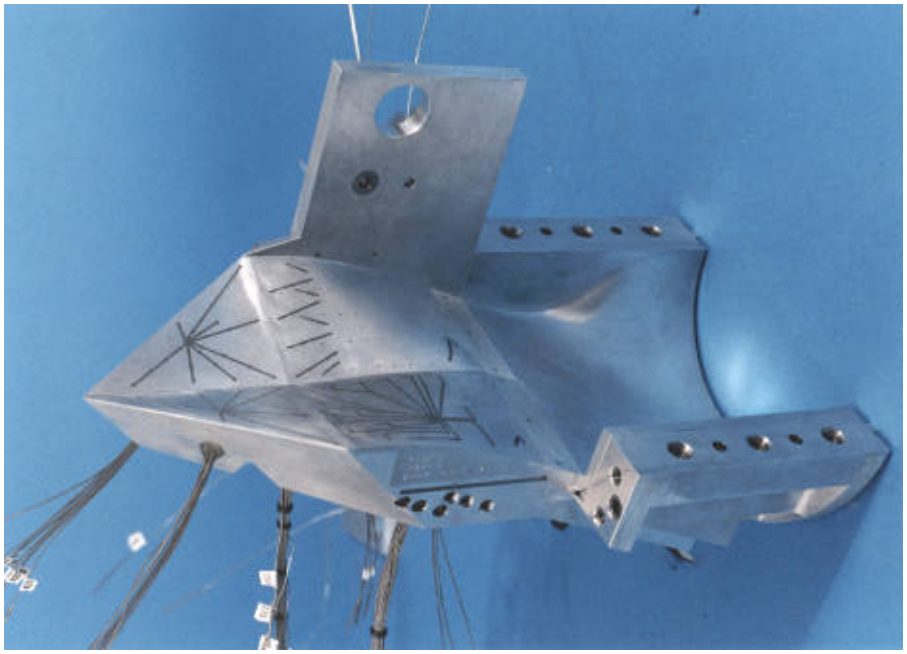

(d) Dry power configuration; lower quadrants, transition section, and left sidewall only.

Figure 4. Continued.

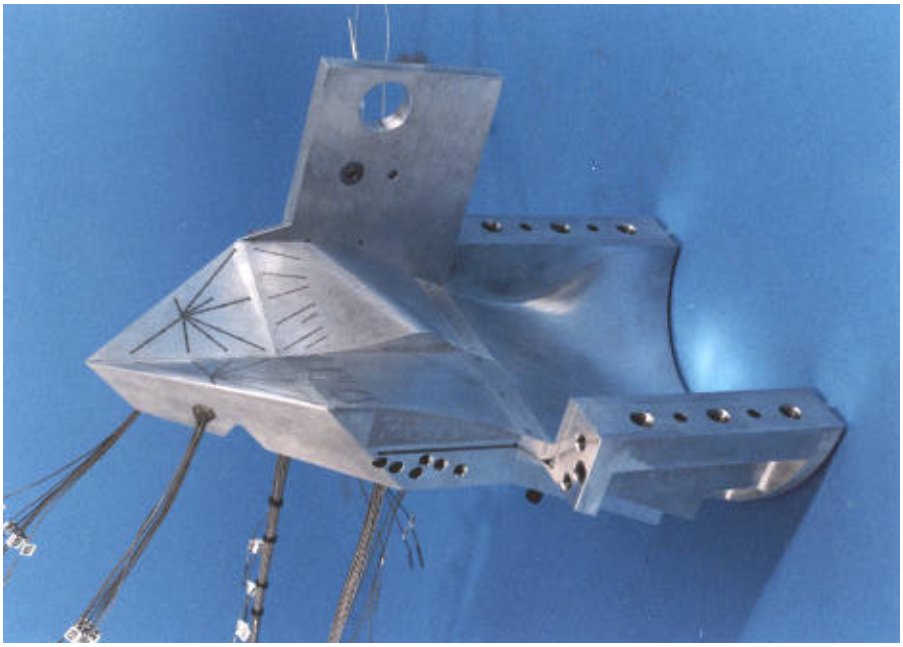

(e) Dry power yaw thrust-vectoring configuration; lower quadrants, transition section, and left sidewall only.

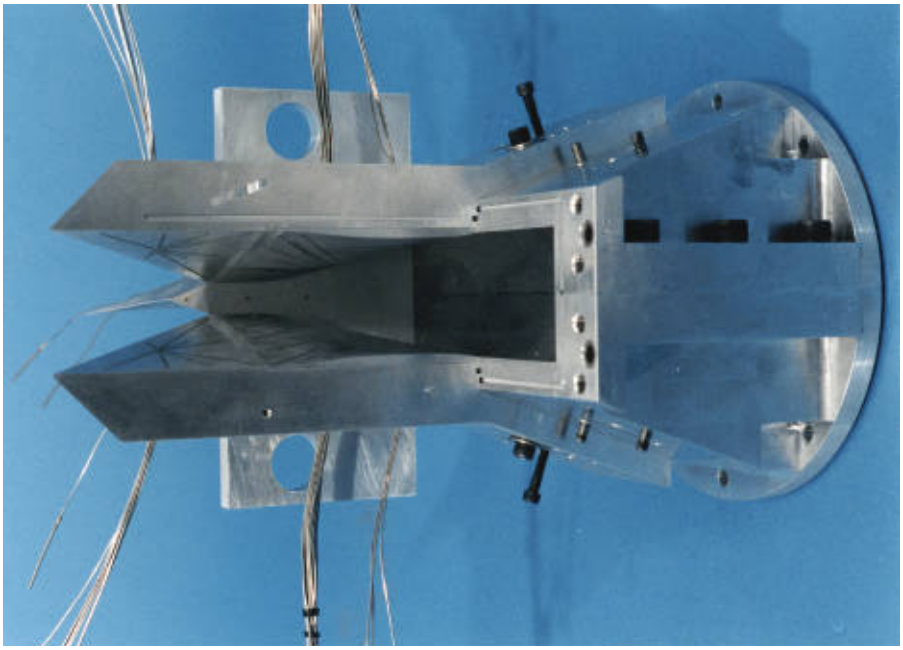

(f) Afterburning power configuration with interfairing; right-side quadrants removed.

Figure 4. Concluded.

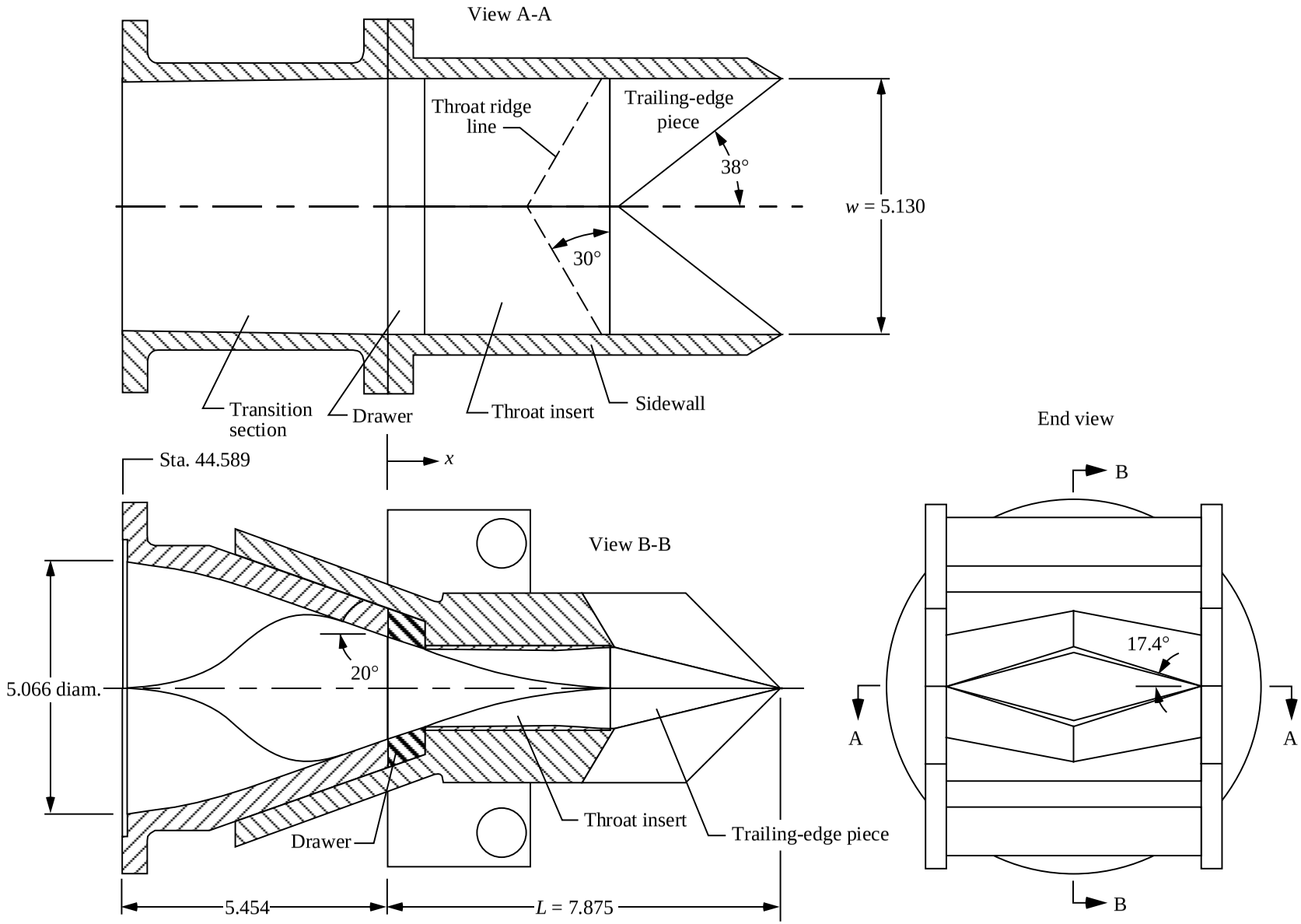

(a) Swallowtail configuration with throat insert 1 (smallest ridge) and no drawer retraction.

Figure 5. Sketches of VIC nozzle. Linear dimensions are in inches.

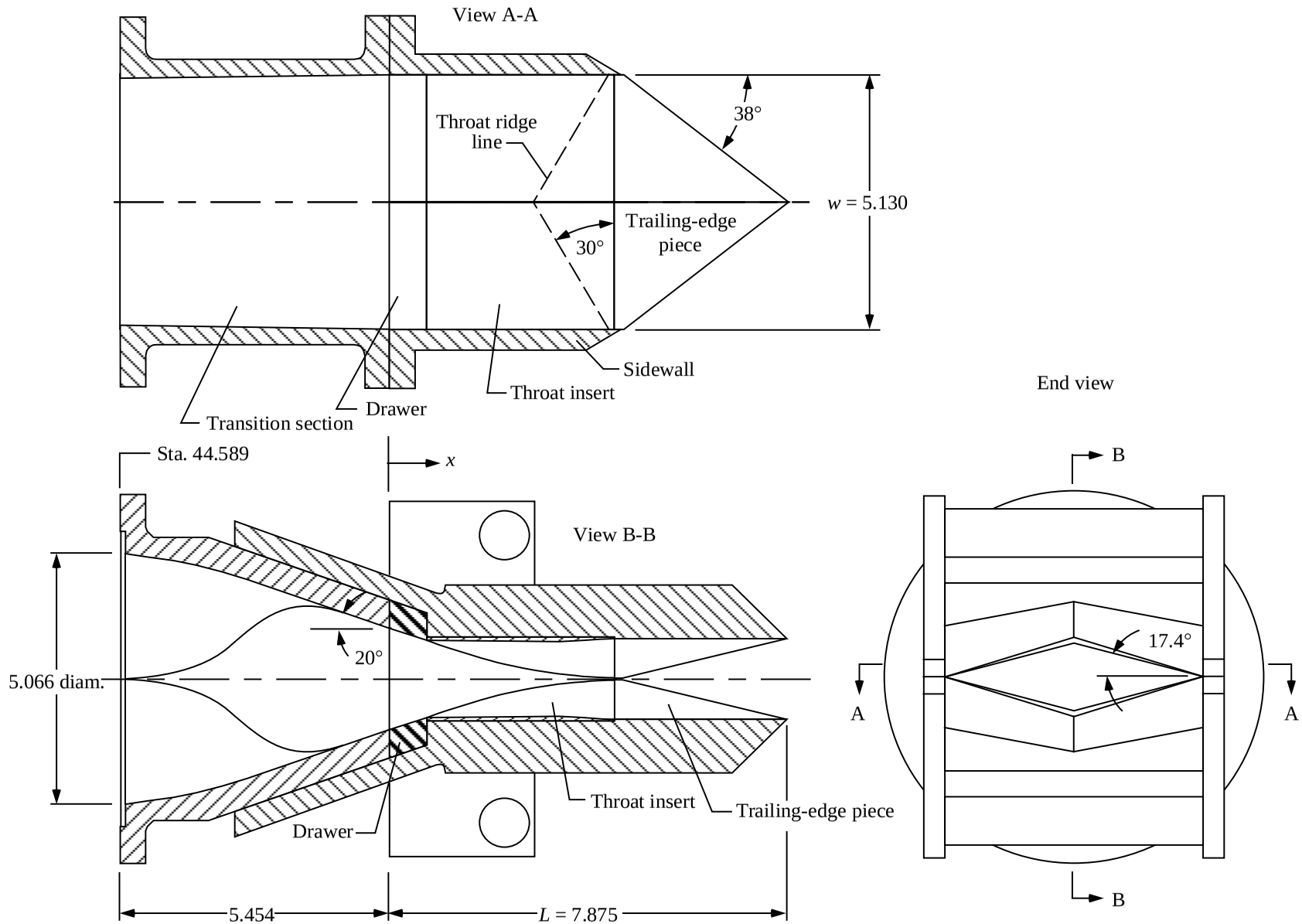

(b) Arrowhead configuration with throat insert 1 (smallest ridge) and no drawer retraction.

Figure 5. Concluded.

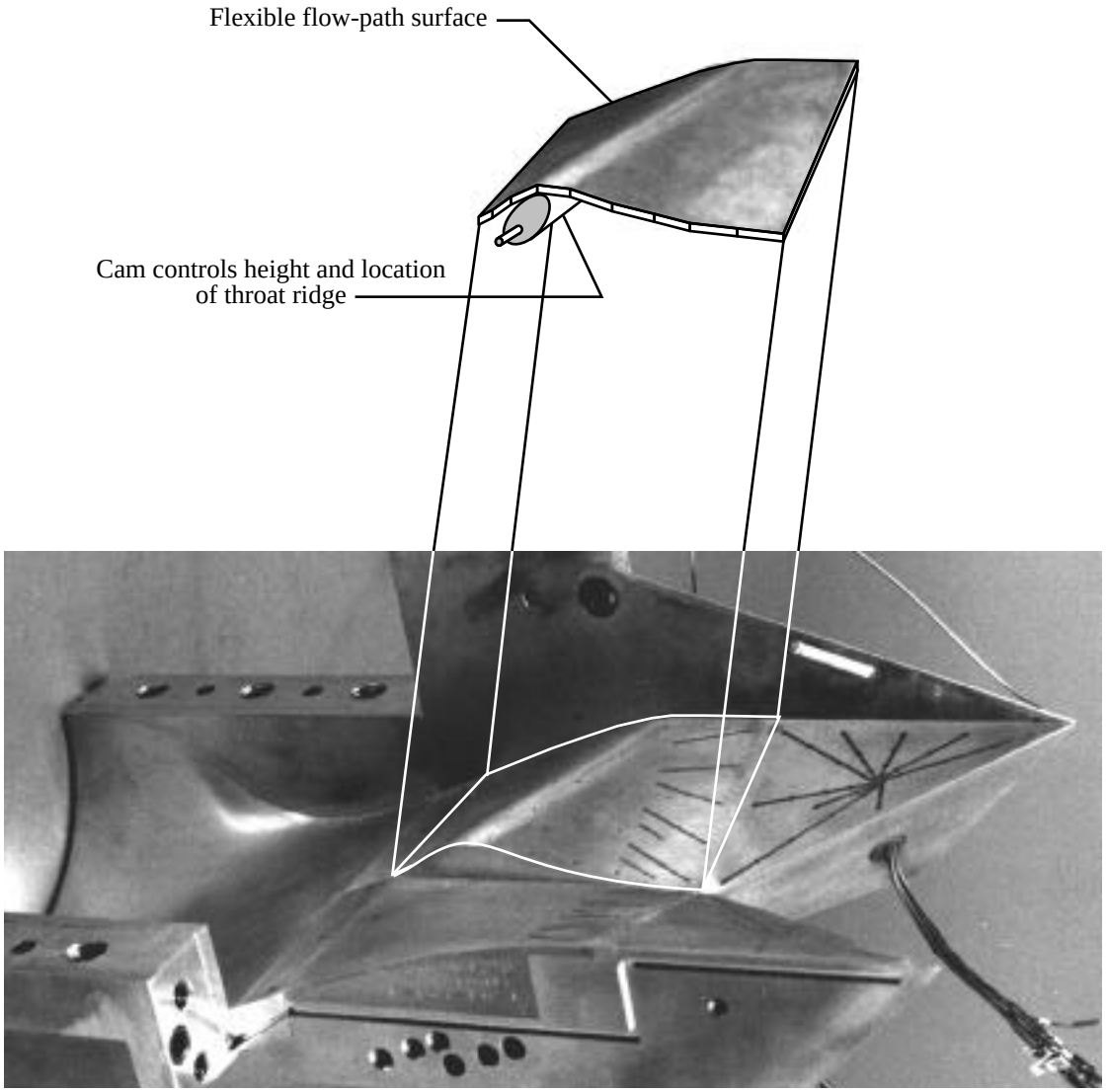

(a) Solid throat block insert in test hardware simulating cam-actuated flexible flow-path surface in nozzle concept.

Figure 6. Concept and geometry definitions of variable internal contour capability.

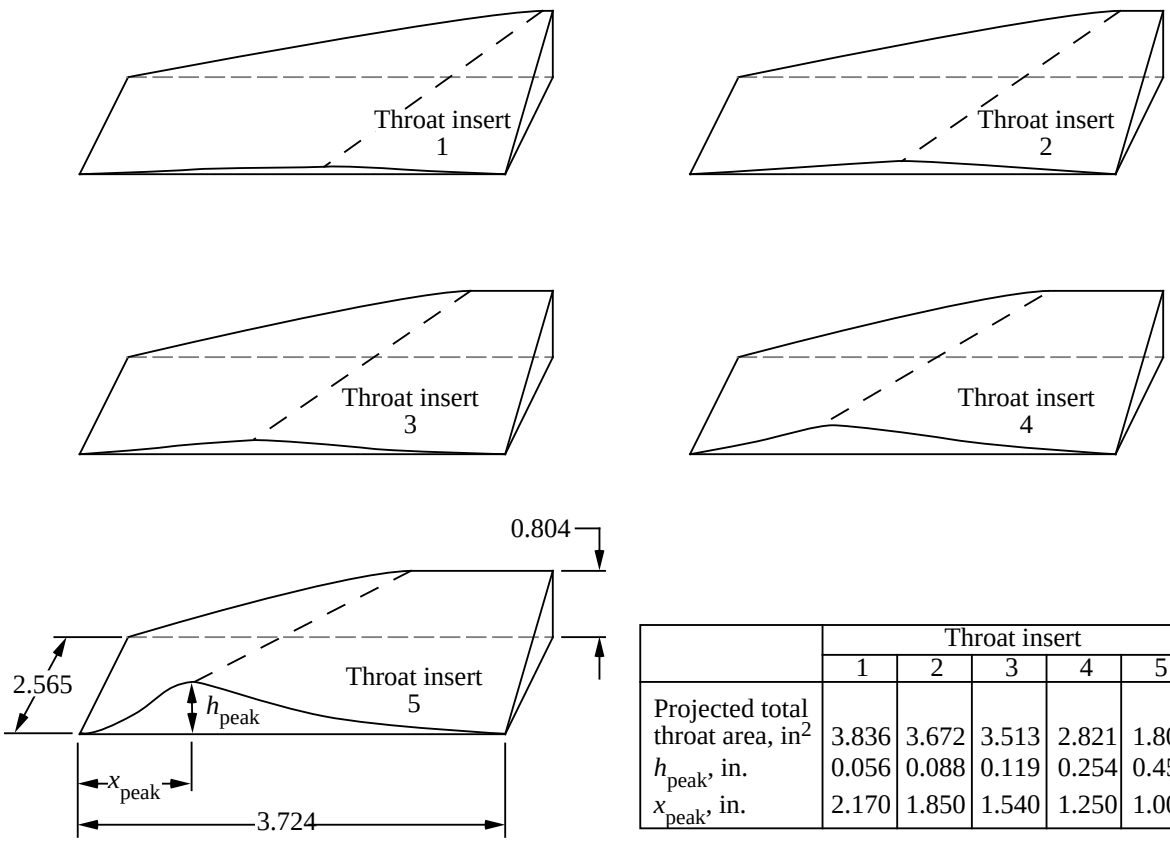

	Throat insert				
	1	2	3	4	5
Projected total throat area, in^2	3.836	3.672	3.513	2.821	1.800
h_{peak}, in.	0.056	0.088	0.119	0.254	0.453
x_{peak}, in.	2.170	1.850	1.540	1.250	1.000

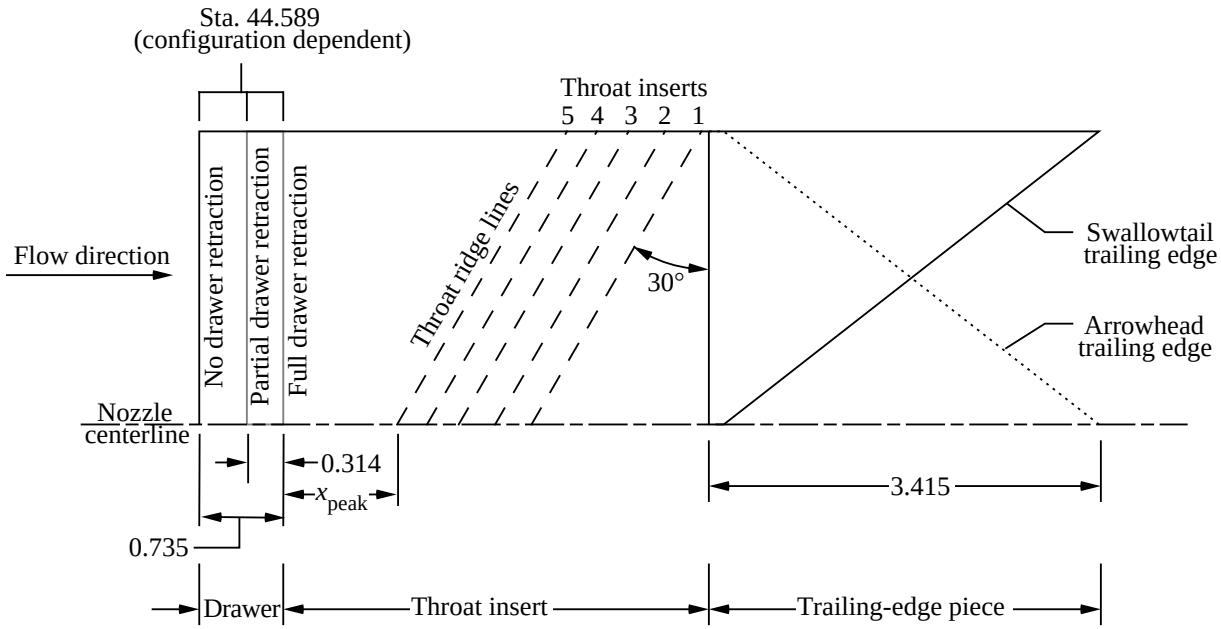

(b) Geometric details of throat inserts and layout of nozzle flow-path components as illustrated in top view lower right-hand quadrant of nozzle. Linear dimensions are in inches.

Figure 6. Concluded.

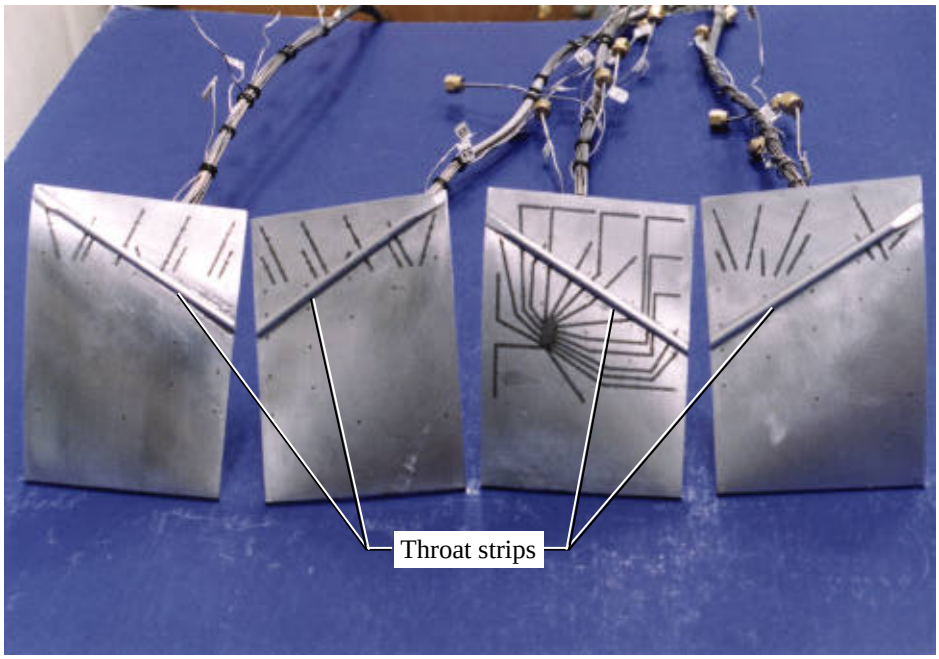

Figure 7. Throat inserts with throat strips installed along contour peaks.

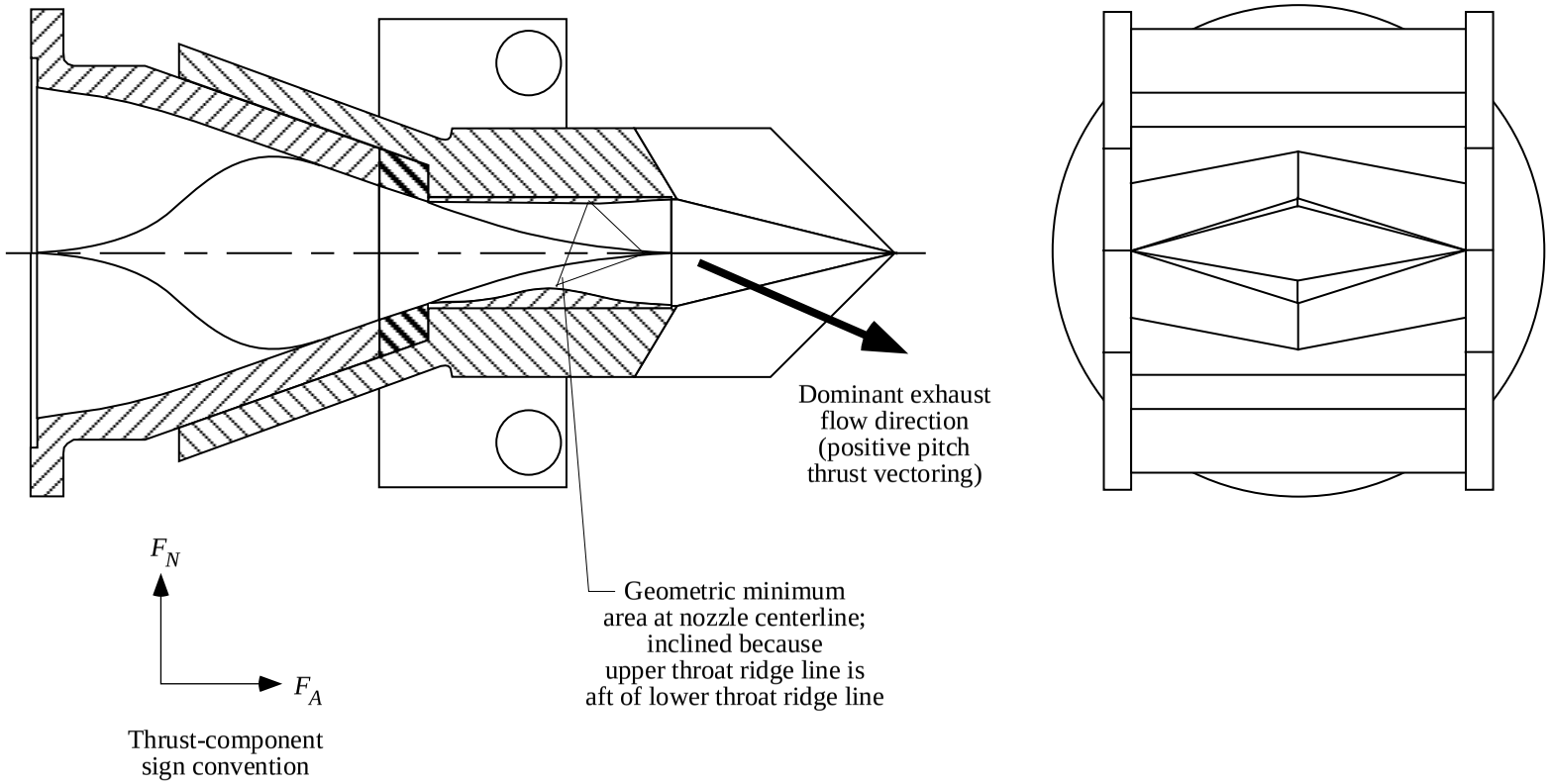

(a) Variable internal contour technique.

Figure 8. Pitch thrust-vectoring techniques as shown on swallowtail configuration.

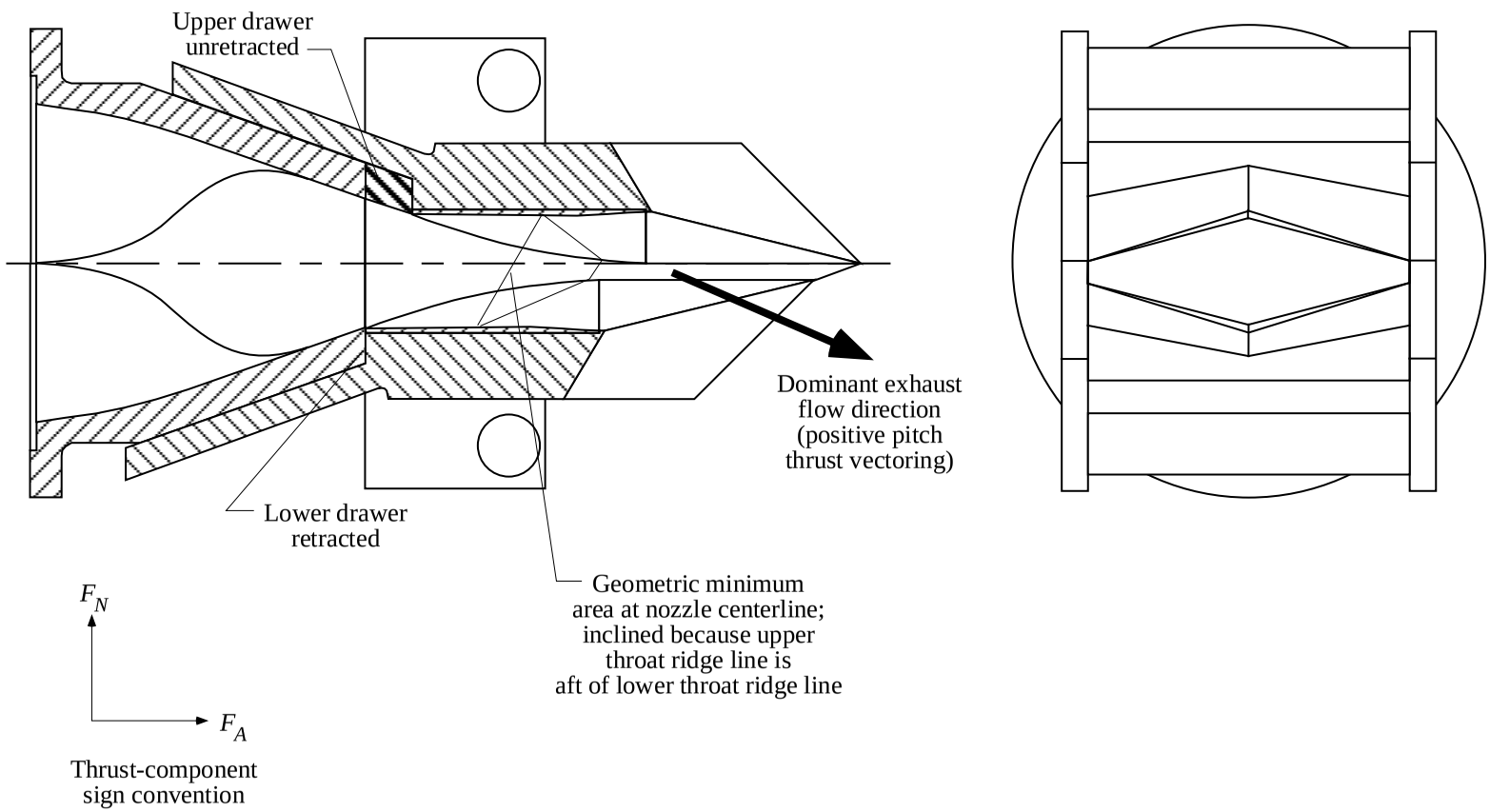

(b) Translation of quadrants along inclined plane.

Figure 8. Concluded.

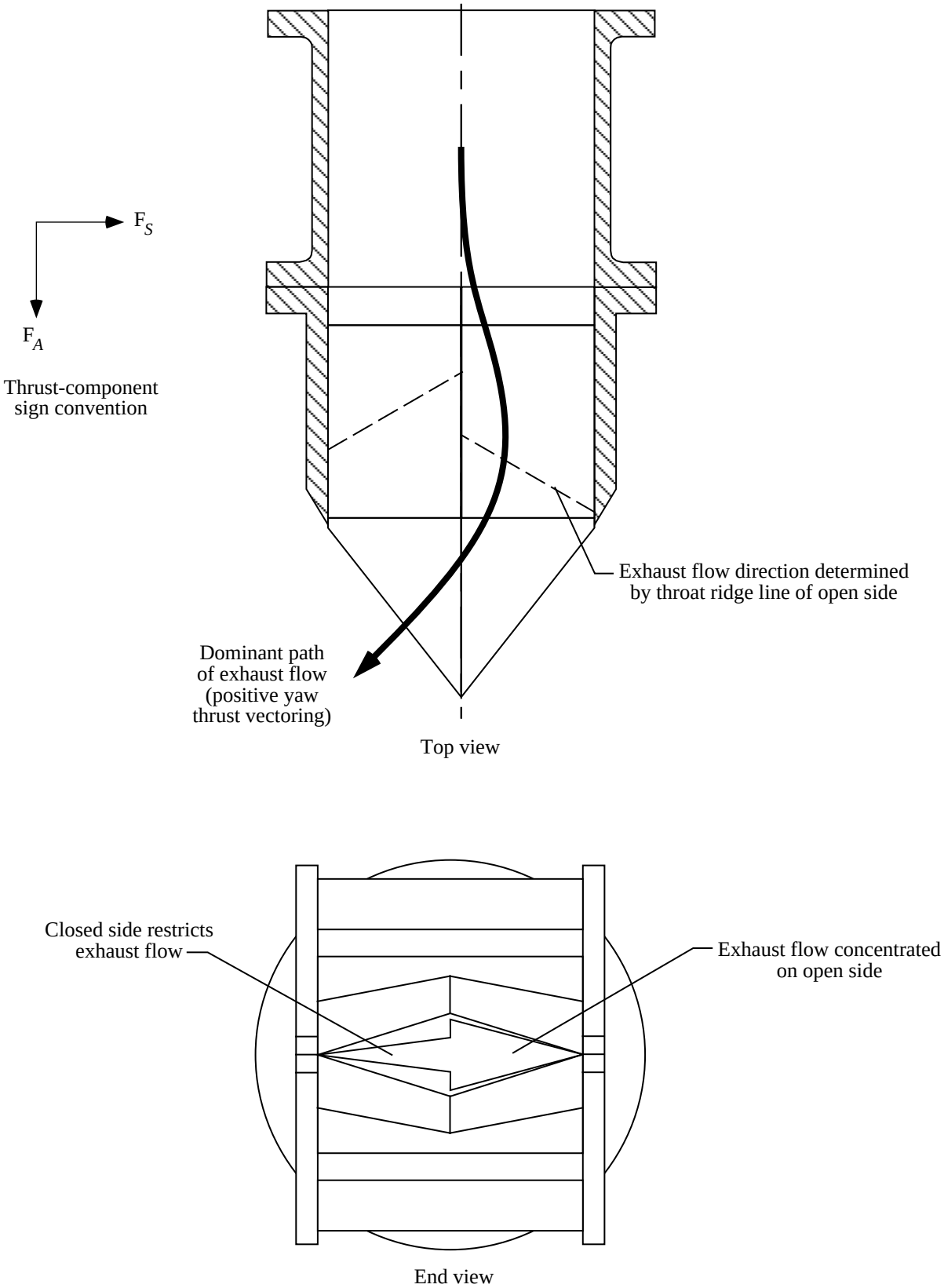

Figure 9. Yaw thrust vectoring using variable internal contour technique. Shown for arrowhead configuration.

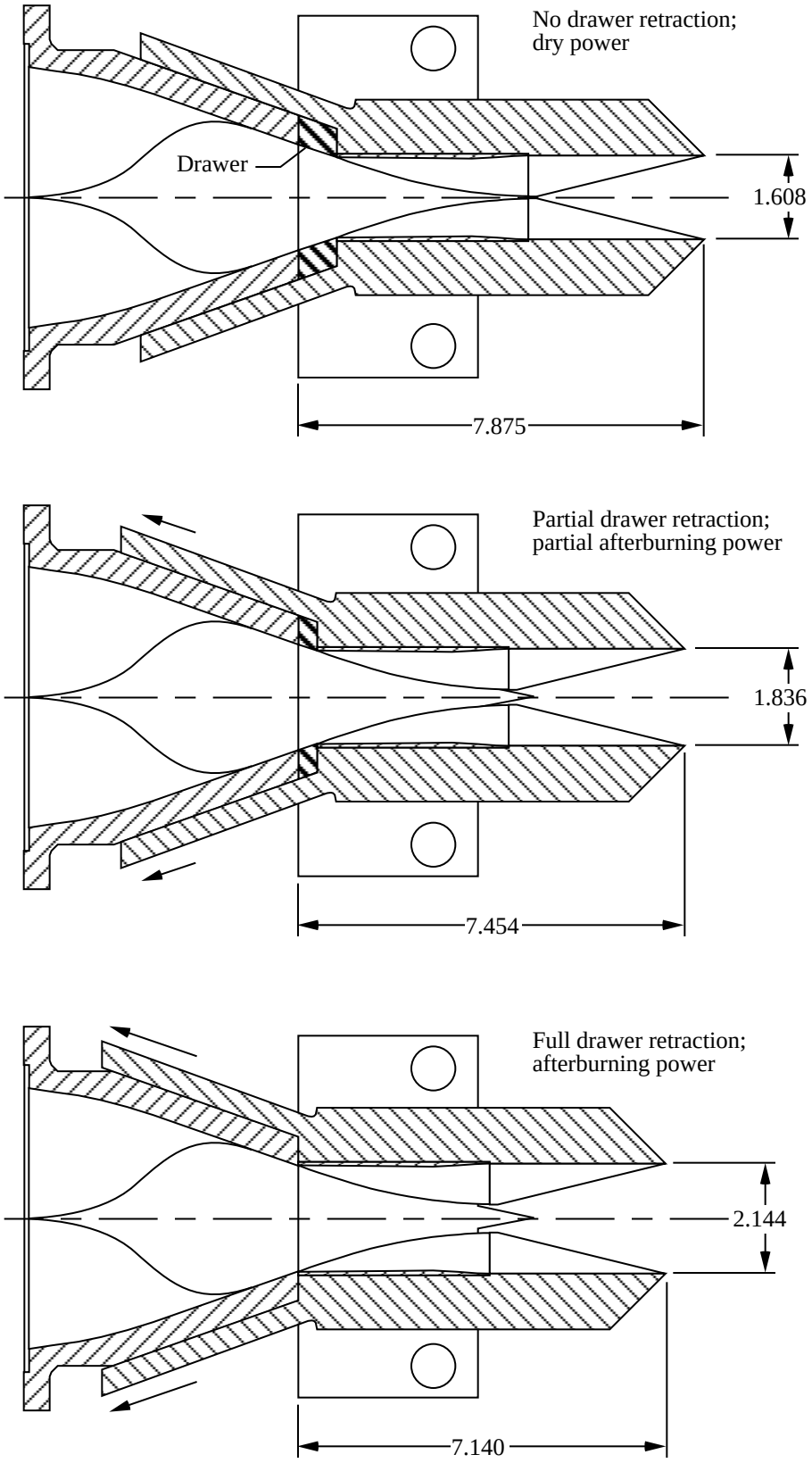

Figure 10. Sketches showing variation of power setting with drawer retraction. Linear dimensions are in inches.

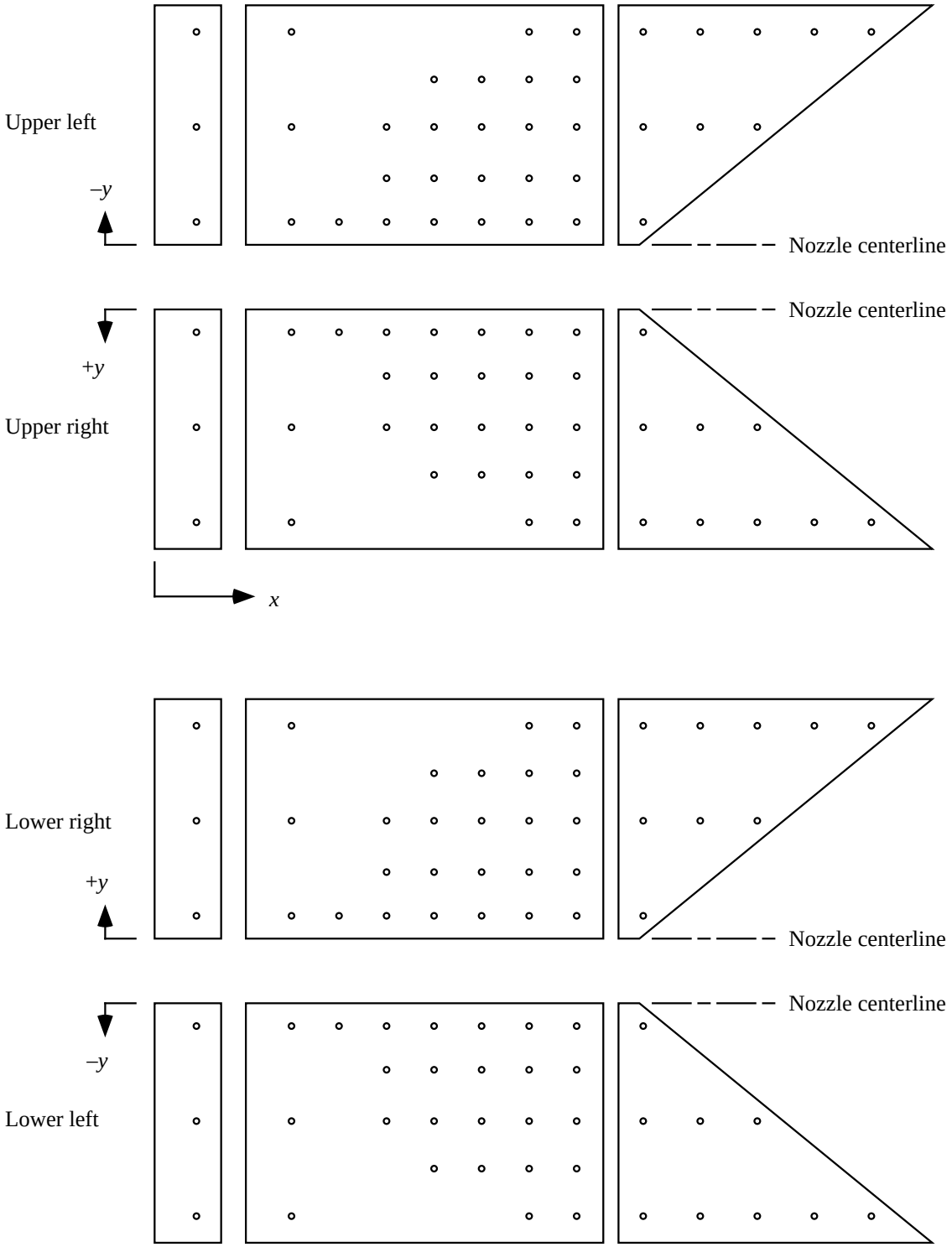

(a) Swallowtail configuration.

Figure 11. Typical pressure orifice distribution on drawers, throat inserts, and trailing-edge pieces. Orifice locations not to scale.

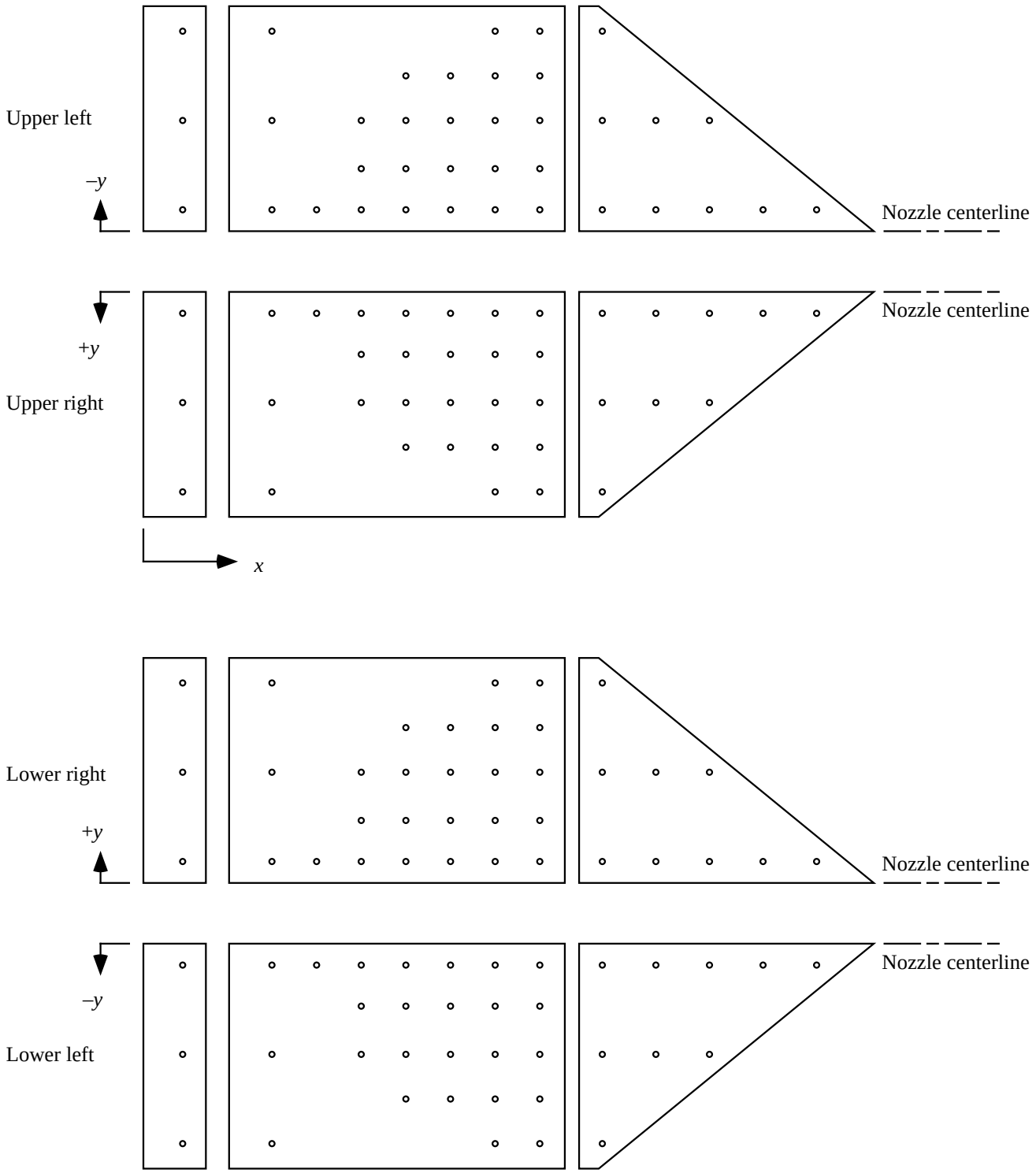

(b) Arrowhead configuration.

Figure 11. Concluded.

	Configuration	I_{ul}	I_{ur}	I_{ll}	I_{lr}	D_u	D_l	T.E.	T.S.	I-F
○	1	3	3	3	3	Ext.	Ext.	s.t.	No	No
□	2	3	3	3	3	Ret.	Ret.	s.t.	No	No
◇	1-I	3	3	3	3	Ext.	Ext.	s.t.	No	Yes

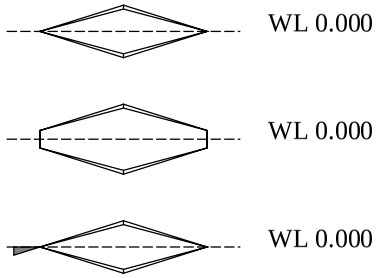

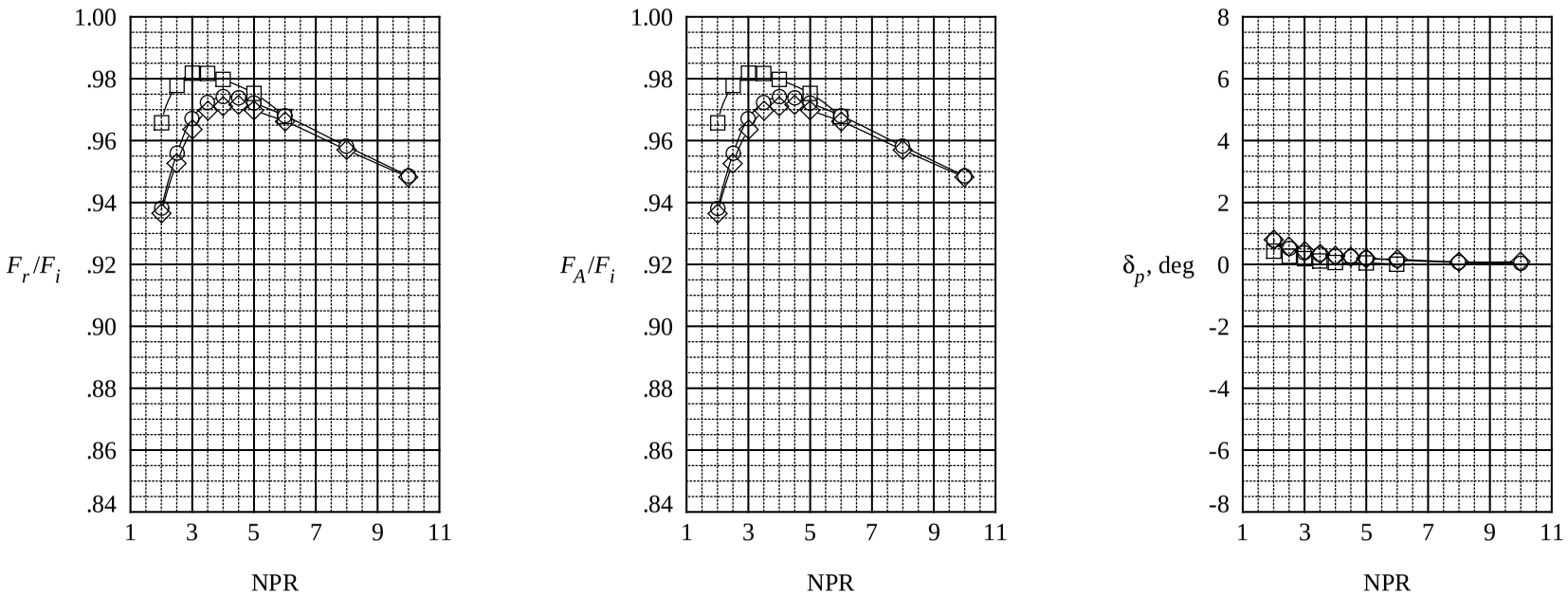

Figure 12. Effect of symmetric drawer retraction on internal performance of unvectored swallowtail configurations and effect of interfairing on internal performance.

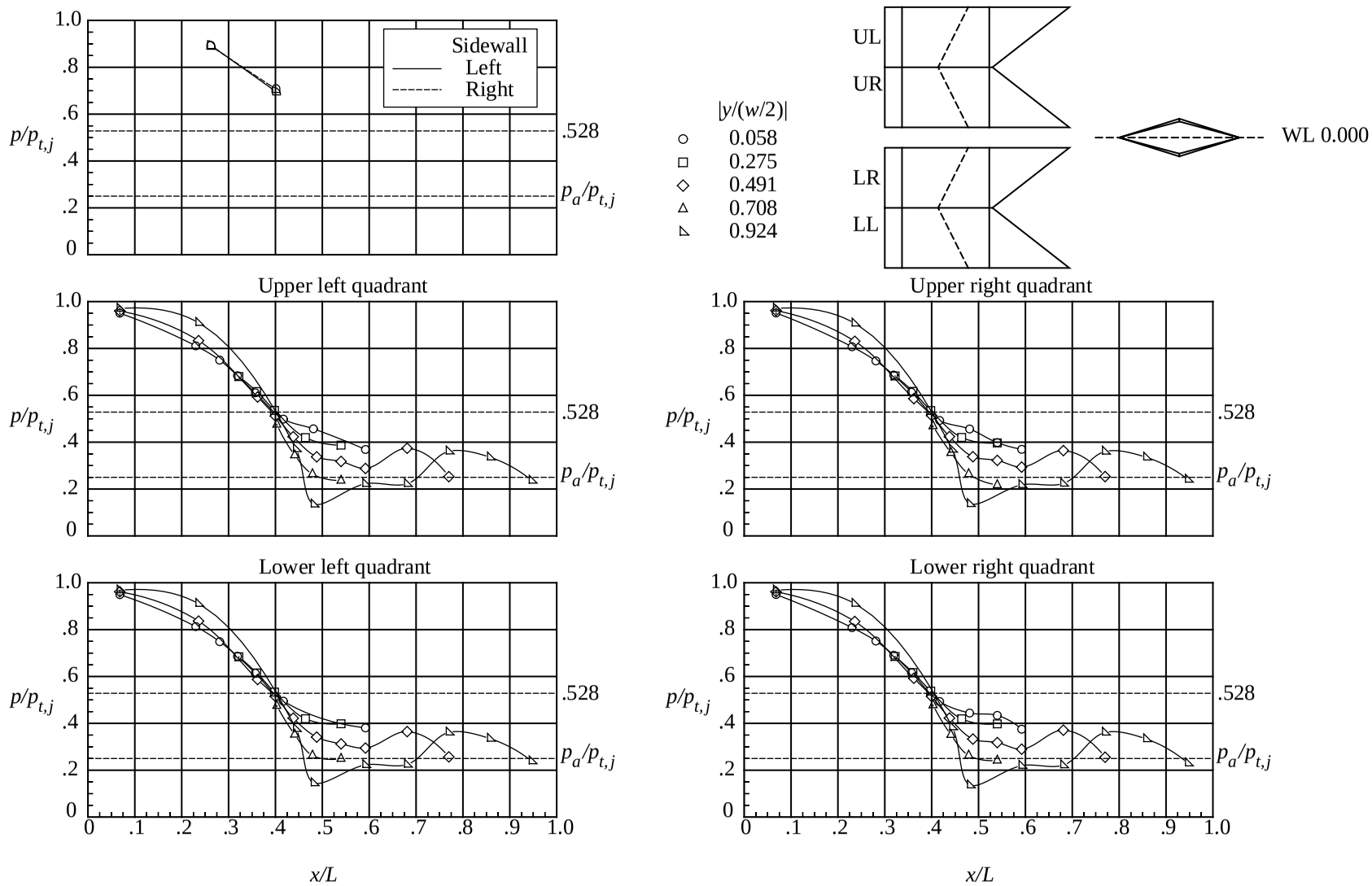

Figure 13. Internal static pressure distributions for configuration 1 at NPR = 4.00. L = 7.875 in.; w = 5.130 in.

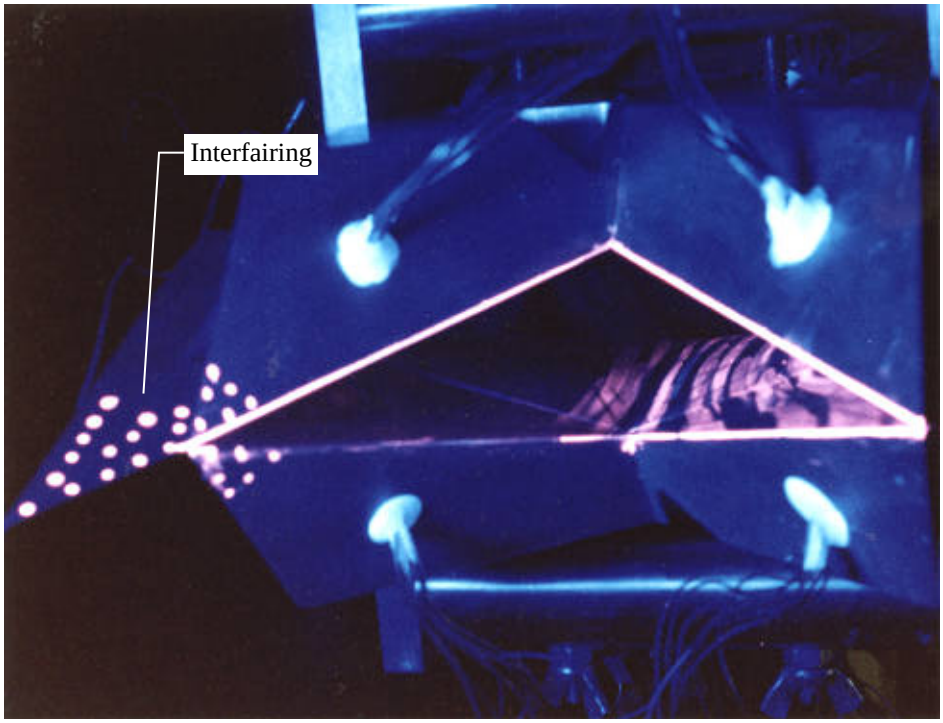

(a) End view.

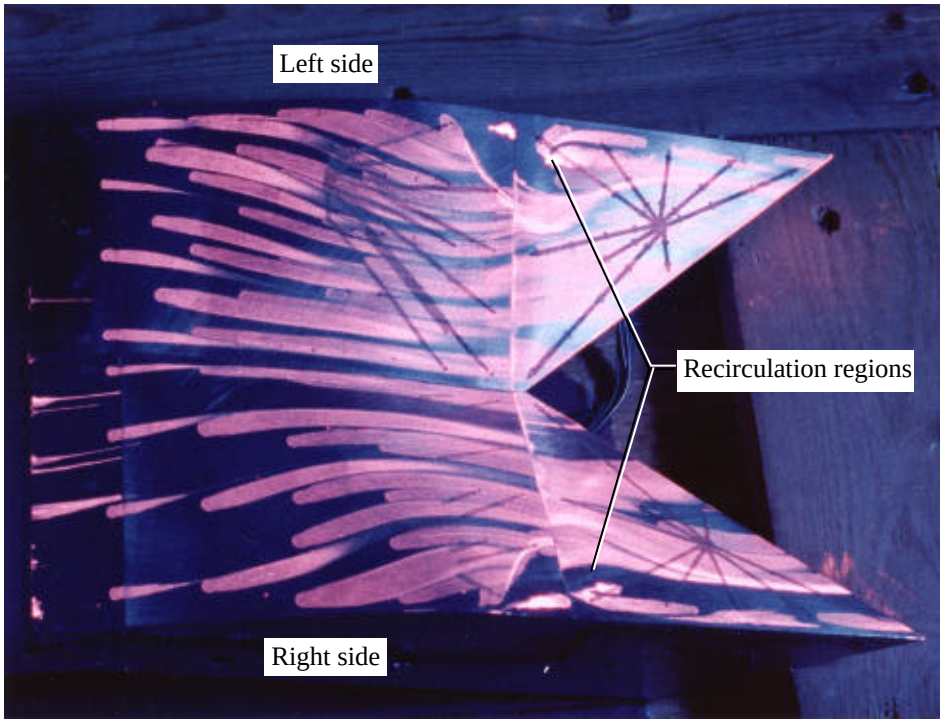

(b) Upper surface.

Figure 14. Oil flow visualization photographs of configuration 1-I. NPR = 4.

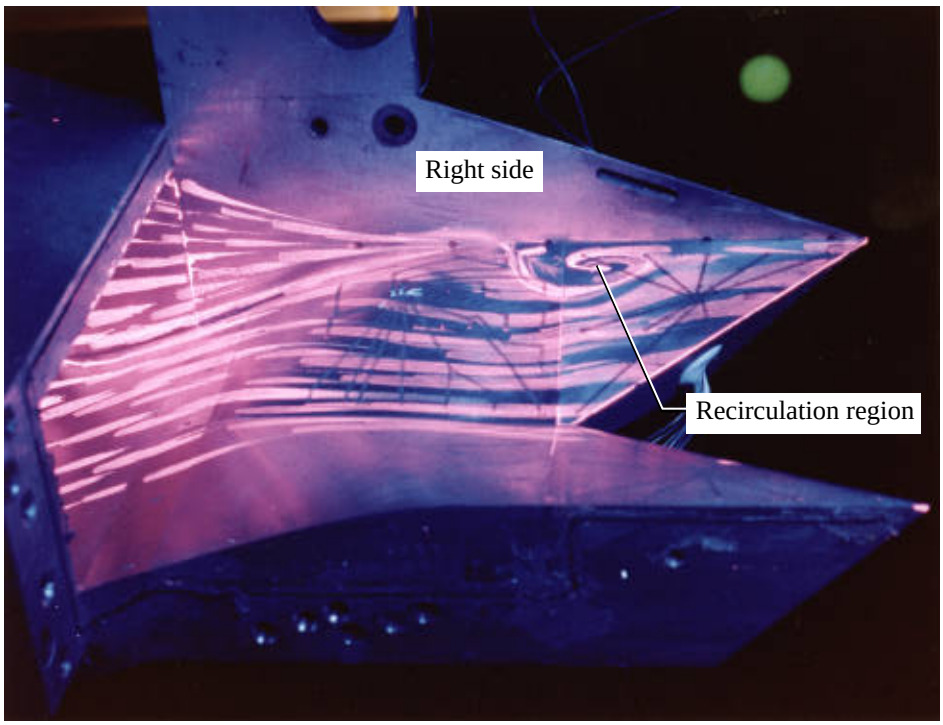

(c) Lower surface.

Figure 14. Concluded.

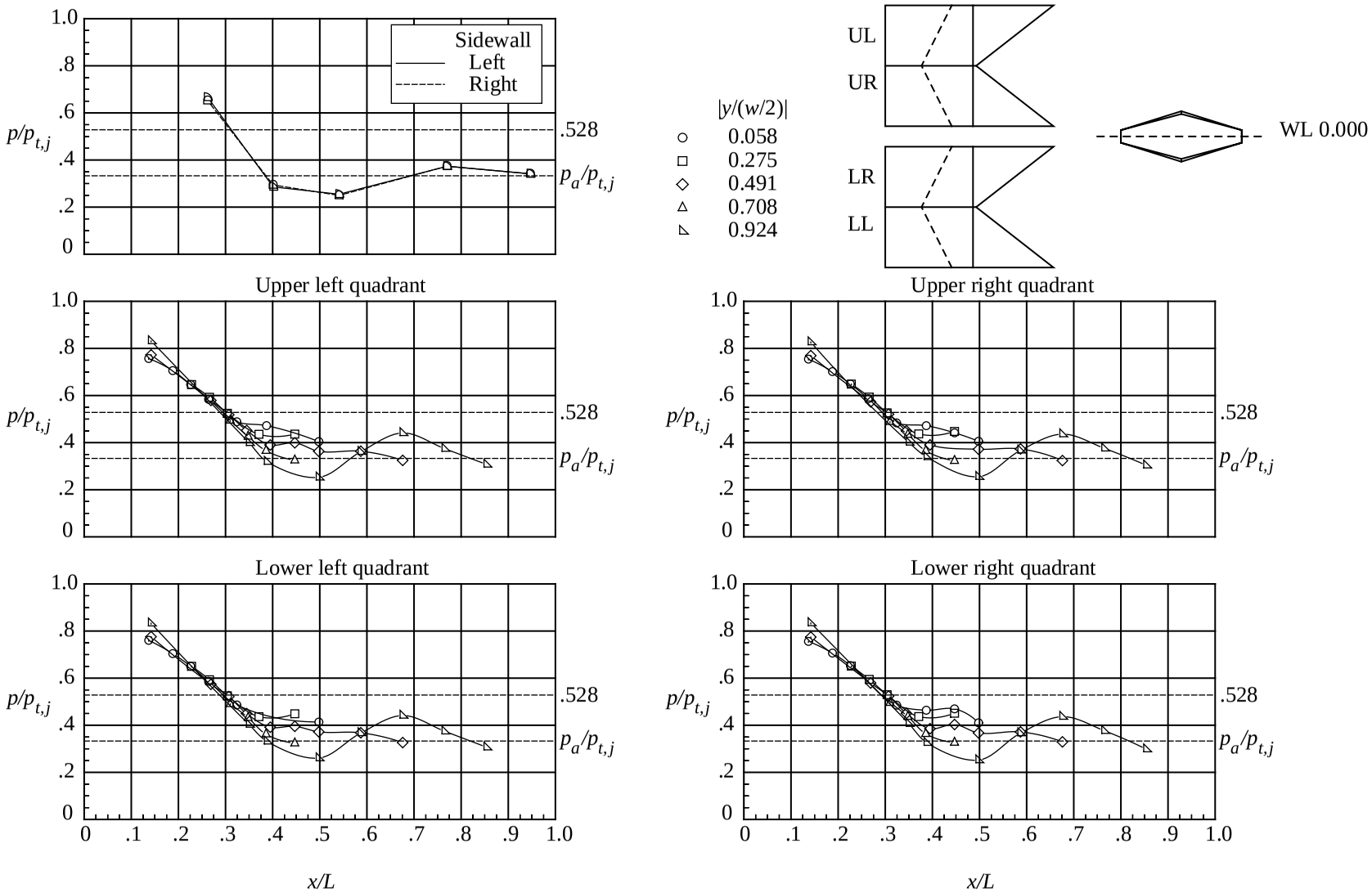

Figure 15. Internal static pressure distributions for configuration 2 at NPR = 3.00. L = 7.875 in.; w = 5.130 in.

	Configuration	I_{ul}	I_{ur}	I_{ll}	I_{lr}	D_u	D_l	T.E.	T.S.	I-F
○	3	3	3	3	3	Ext.	Ext.	a.h.	No	No
□	4	3	3	3	3	Ret.	Ret.	a.h.	No	No
◇	3-I	3	3	3	3	Ext.	Ext.	a.h.	No	Yes

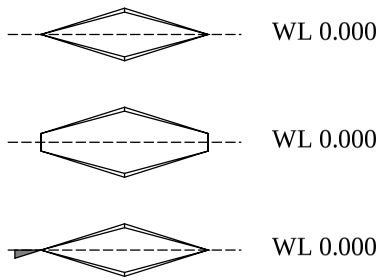

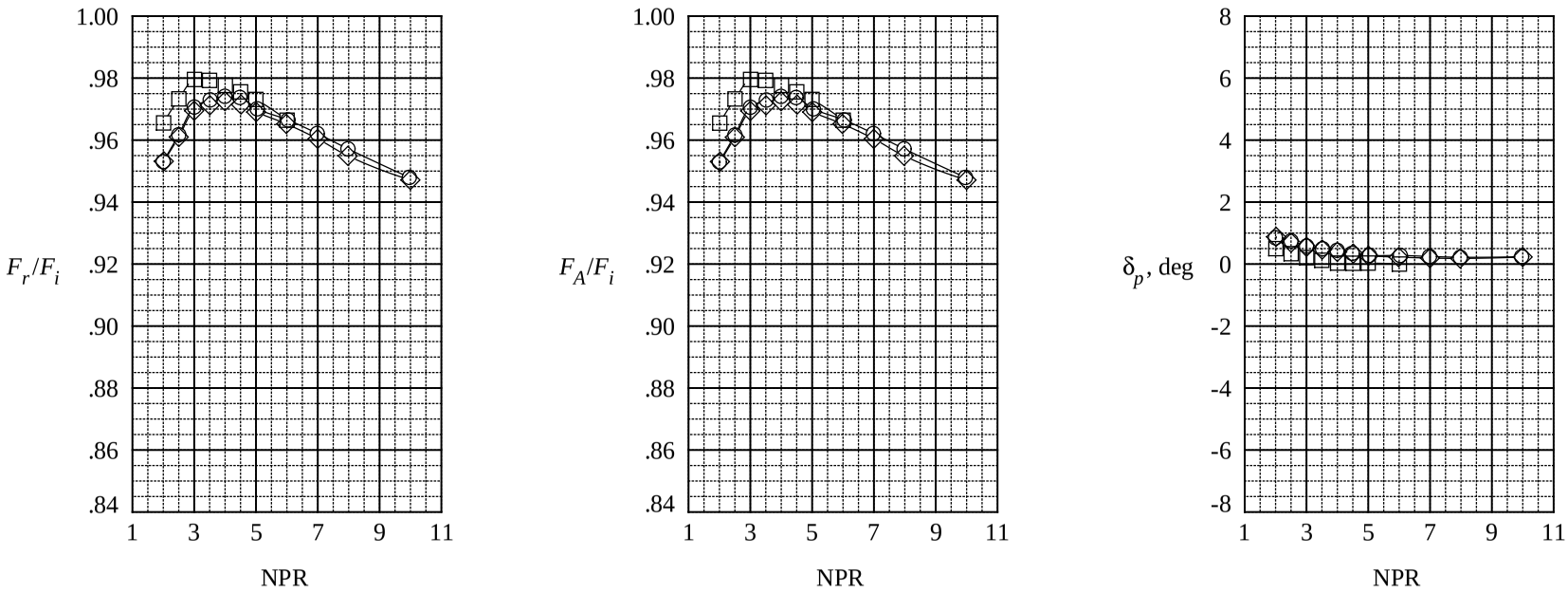

Figure 16. Effect of symmetric drawer retraction on internal performance of unvectored arrowhead configurations and effect of interfairing on internal performance.

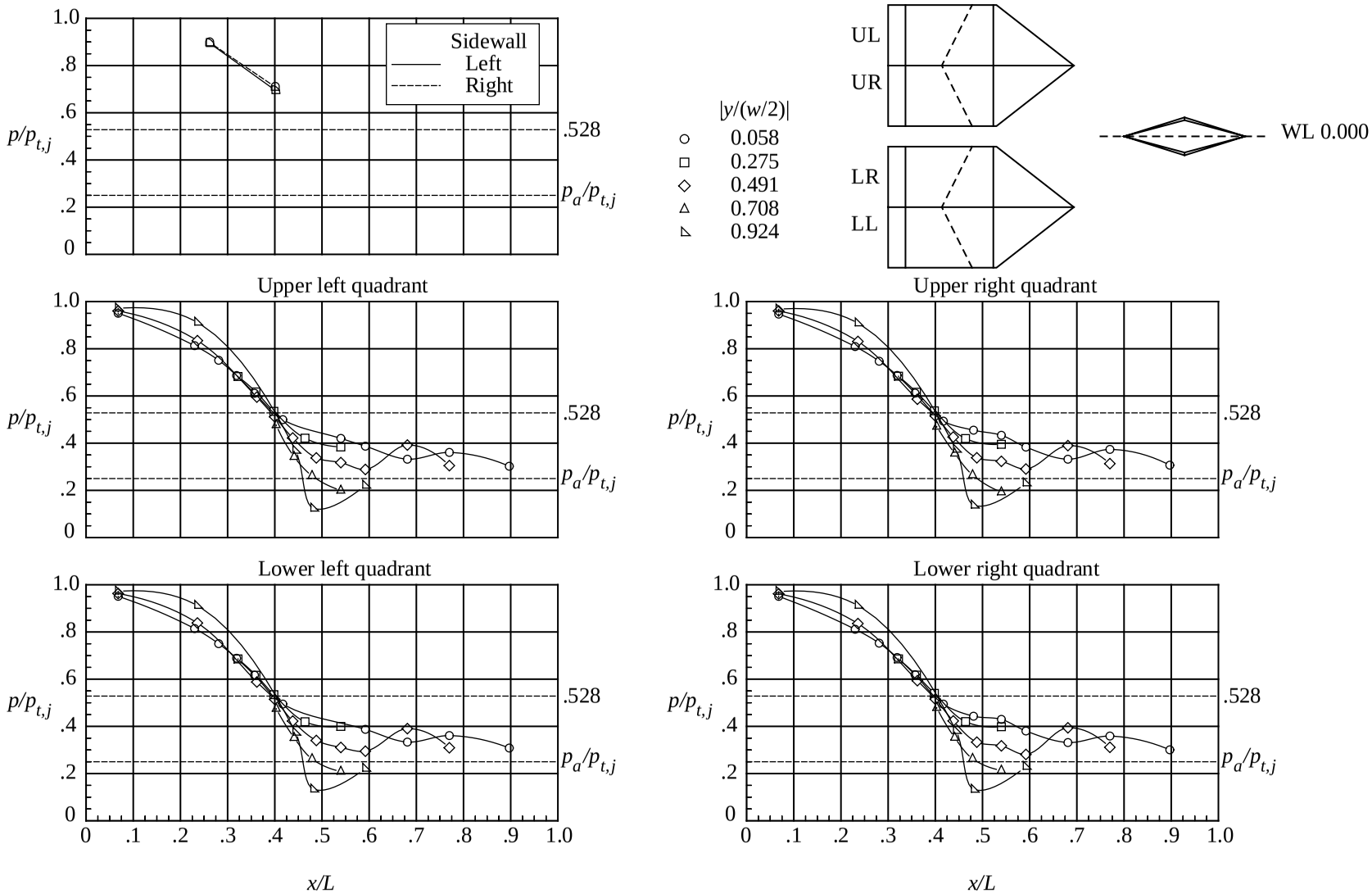

Figure 17. Internal static pressure distributions for configuration 3 at NPR = 3.99. L = 7.875 in.; w = 5.130 in.

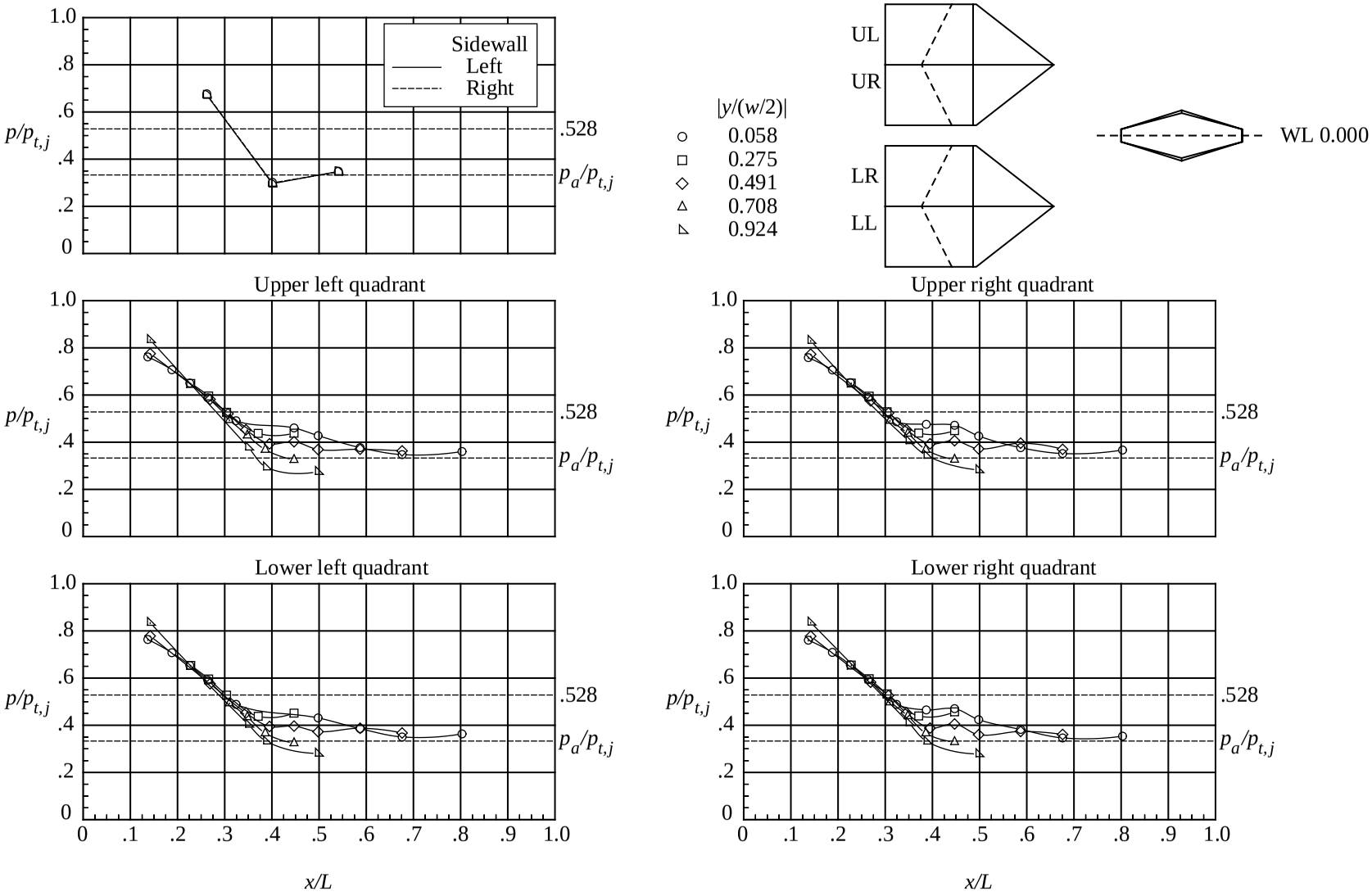

Figure 18. Internal static pressure distributions for configuration 4 at NPR = 3.01. L = 7.875 in.; w = 5.130 in.

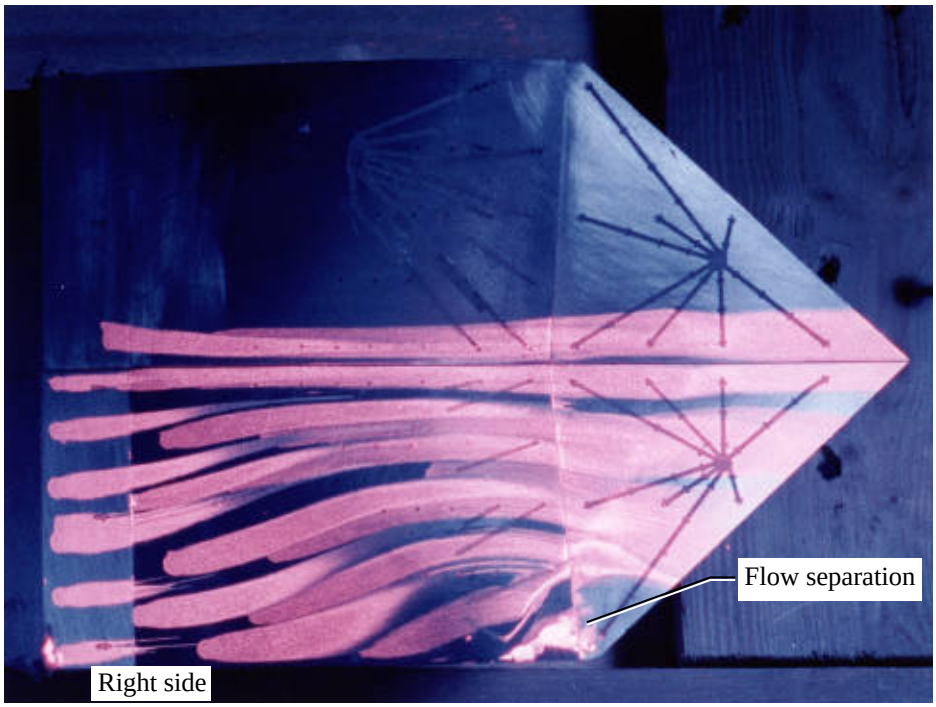

(a) Upper surface.

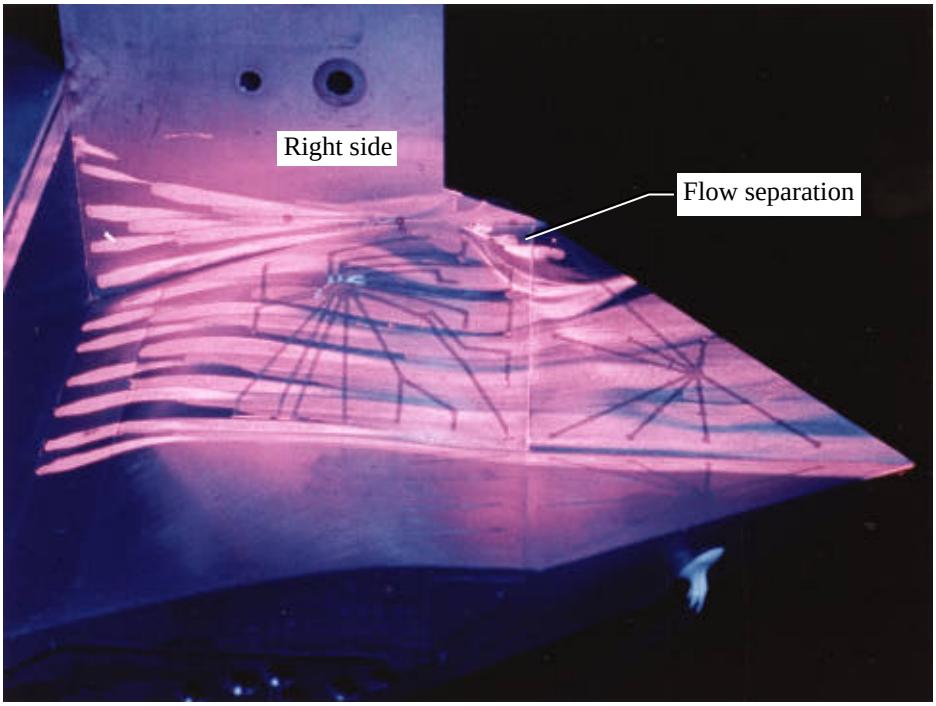

(b) Lower surface.

Figure 19. Oil flow visualization photographs of configuration 3 at NPR = 4.

	Configuration	I_{ul}	I_{ur}	I_{ll}	I_{lr}	D_u	D_l	T.E.	T.S.	I-F	
- - - - - - -	1	3	3	3	3	Ext.	Ext.	s.t.	No	No	WL 0.000
○———	5	2	2	3	3	Ext.	Ext.	s.t.	No	No	WL 0.000
□———	6	1	1	2	2	Ext.	Ext.	s.t.	Yes	No	WL 0.000

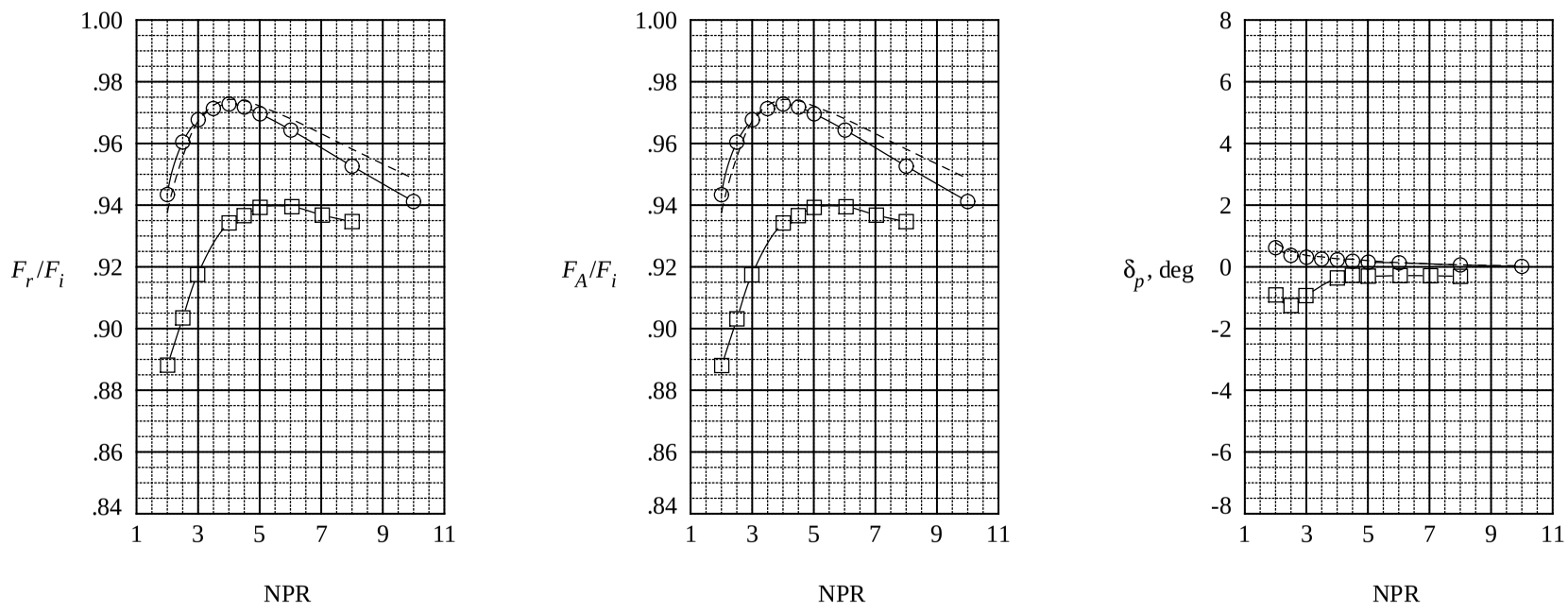

(a) Internal contouring concept.

Figure 20. Thrust and pitch thrust-vectoring performance resulting from two pitch thrust-vectoring techniques for swallowtail nozzle configurations.

Configuration	I_{ul}	I_{ur}	I_{ll}	I_{lr}	D_u	D_l	T.E.	T.S.	I-F
1	3	3	3	3	Ext.	Ext.	s.t.	No	No
7	3	3	3	3	Ext.	Par.	s.t.	No	No
8	3	3	3	3	Ext.	Ret.	s.t.	No	No

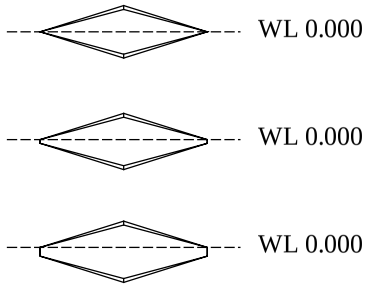

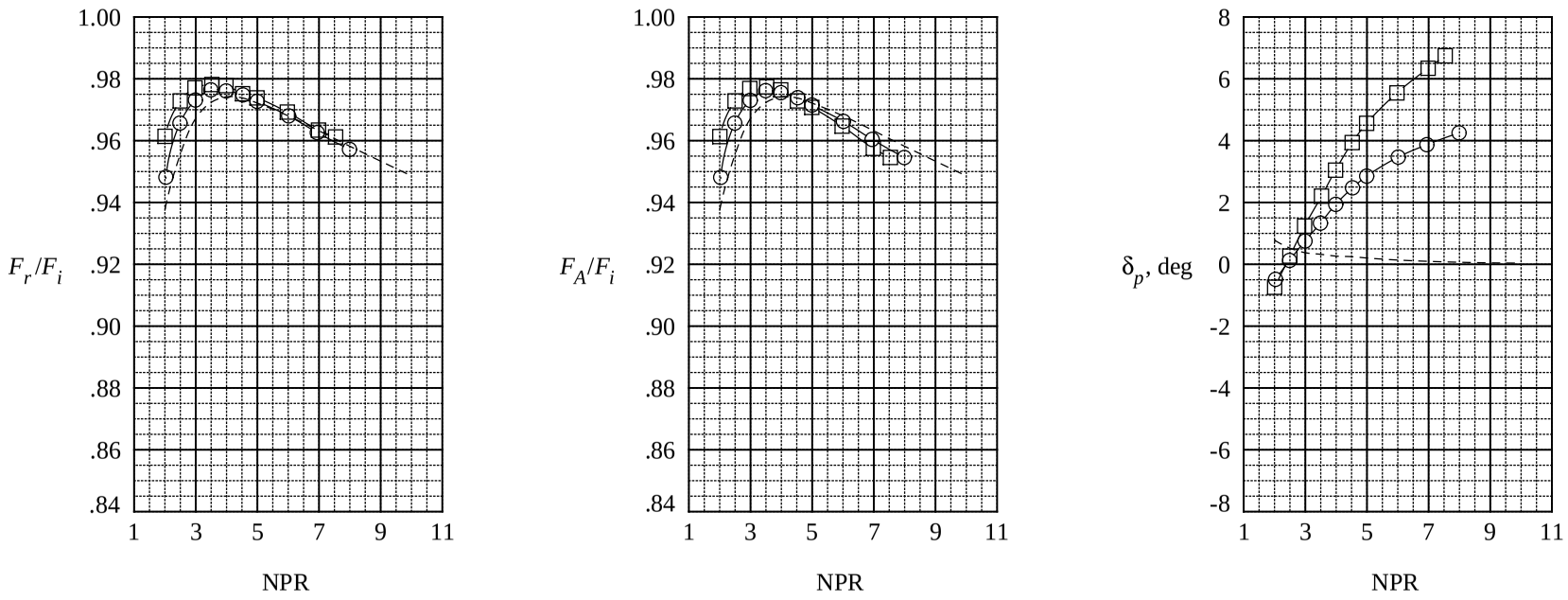

(b) Inclined-plane translation concept.

Figure 20. Concluded.

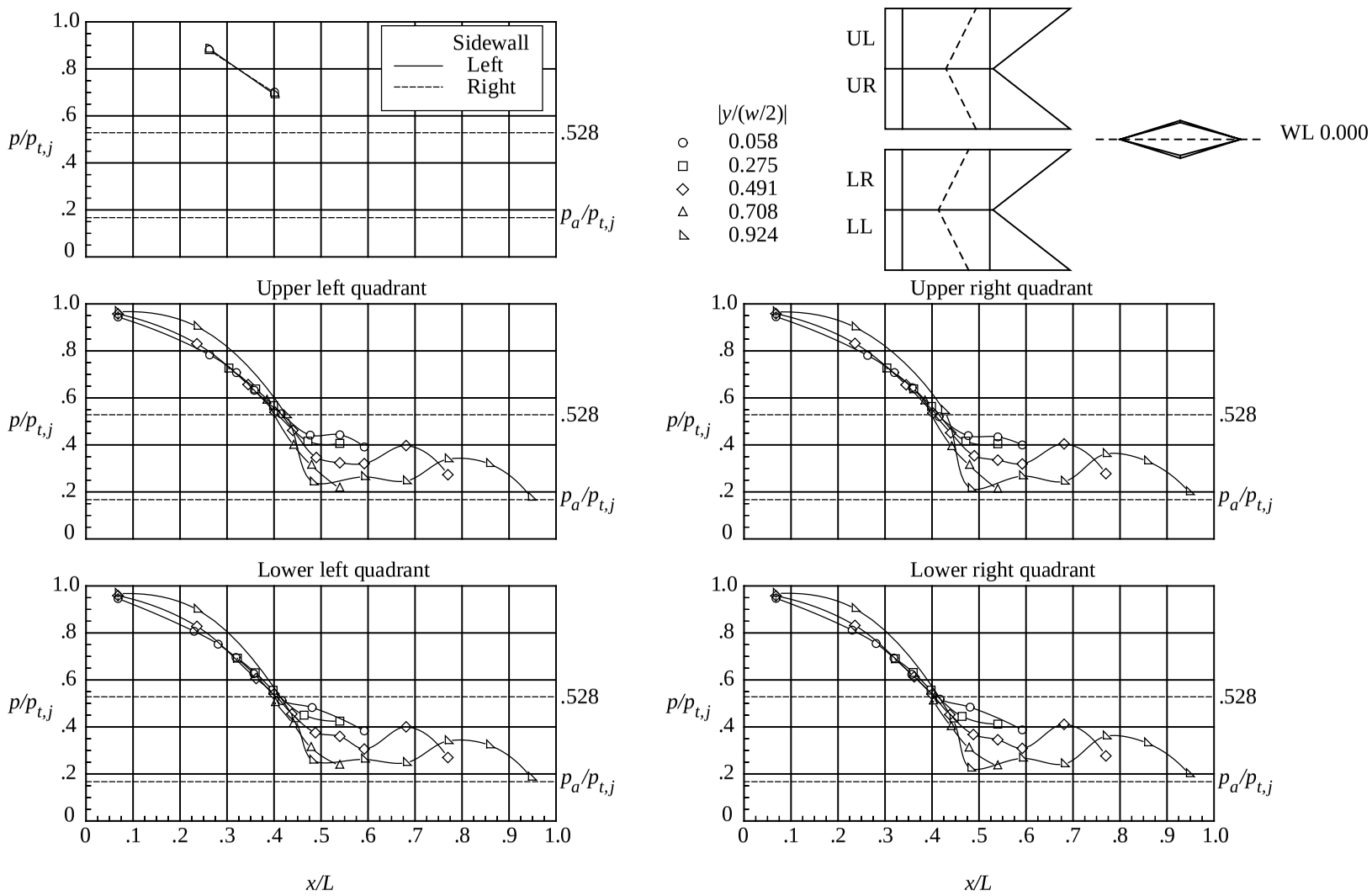

Figure 21. Internal static pressure distributions for configuration 5 at NPR = 6.02. L = 7.875 in.; w = 5.130 in.

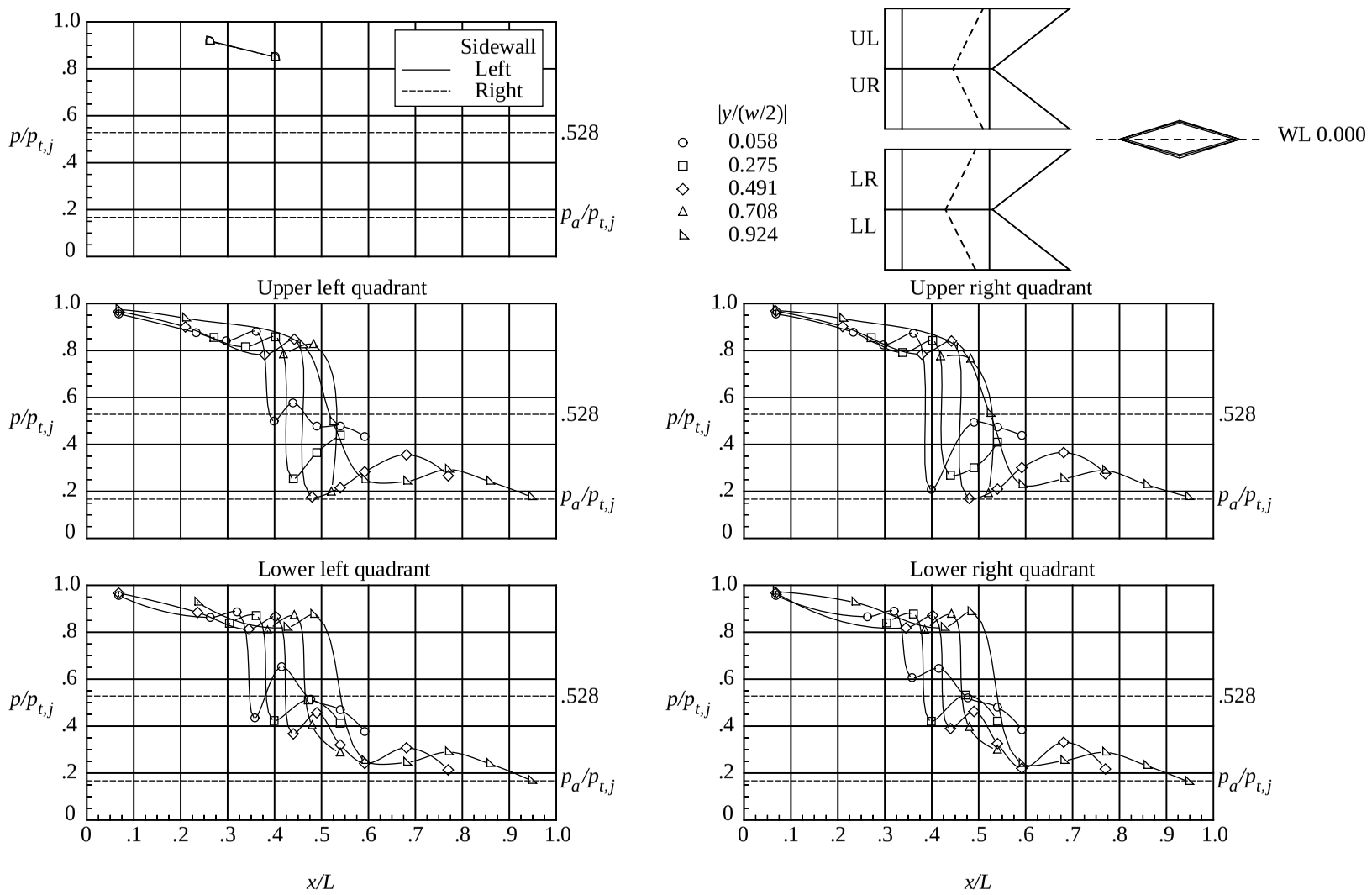

Figure 22. Internal static pressure distributions for configuration 6 at NPR = 6.05. L = 7.875 in.; w = 5.130 in.

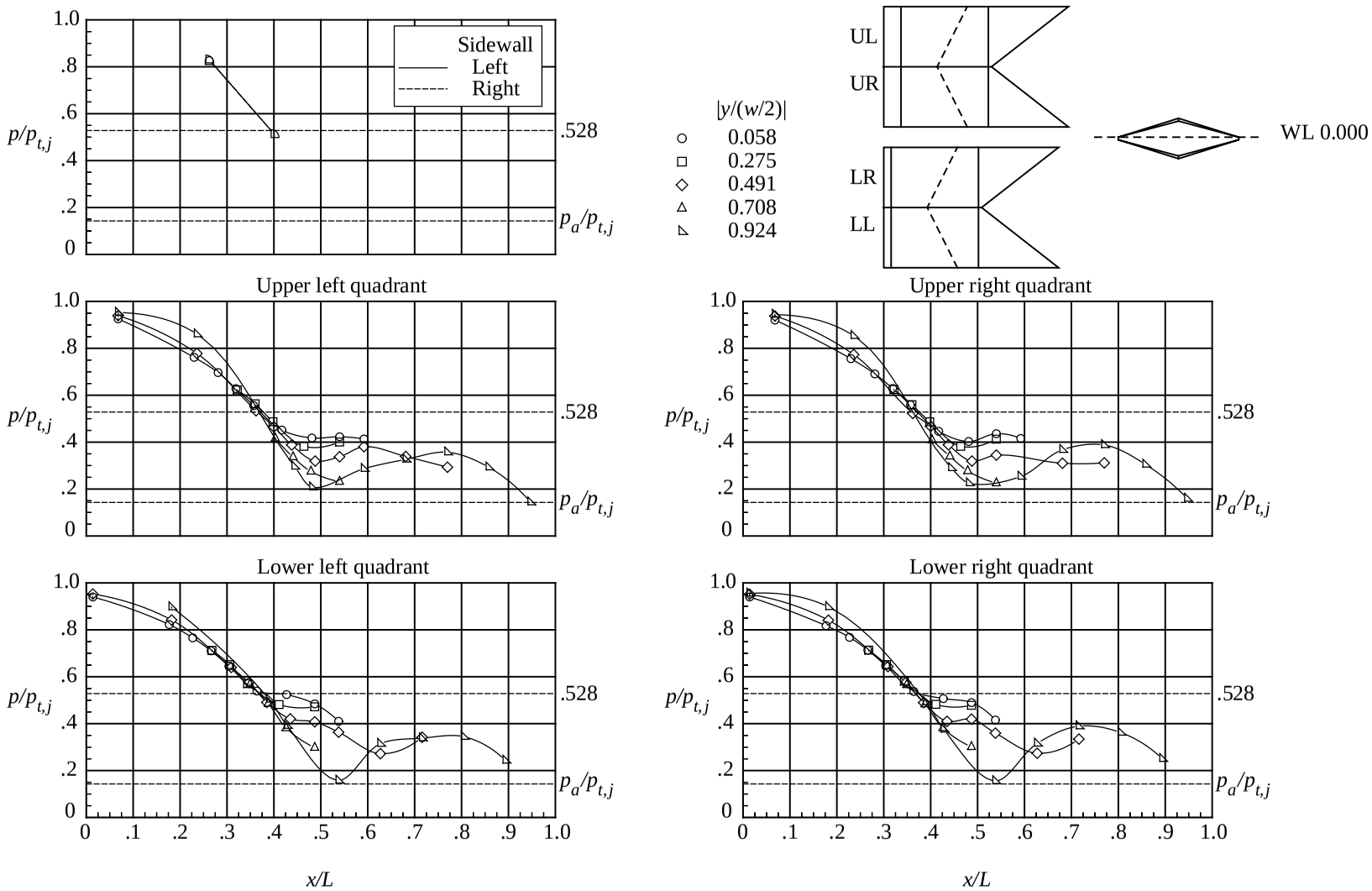

Figure 23. Internal static pressure distributions for configuration 7 at NPR = 6.94. L = 7.875 in.; w = 5.130 in.

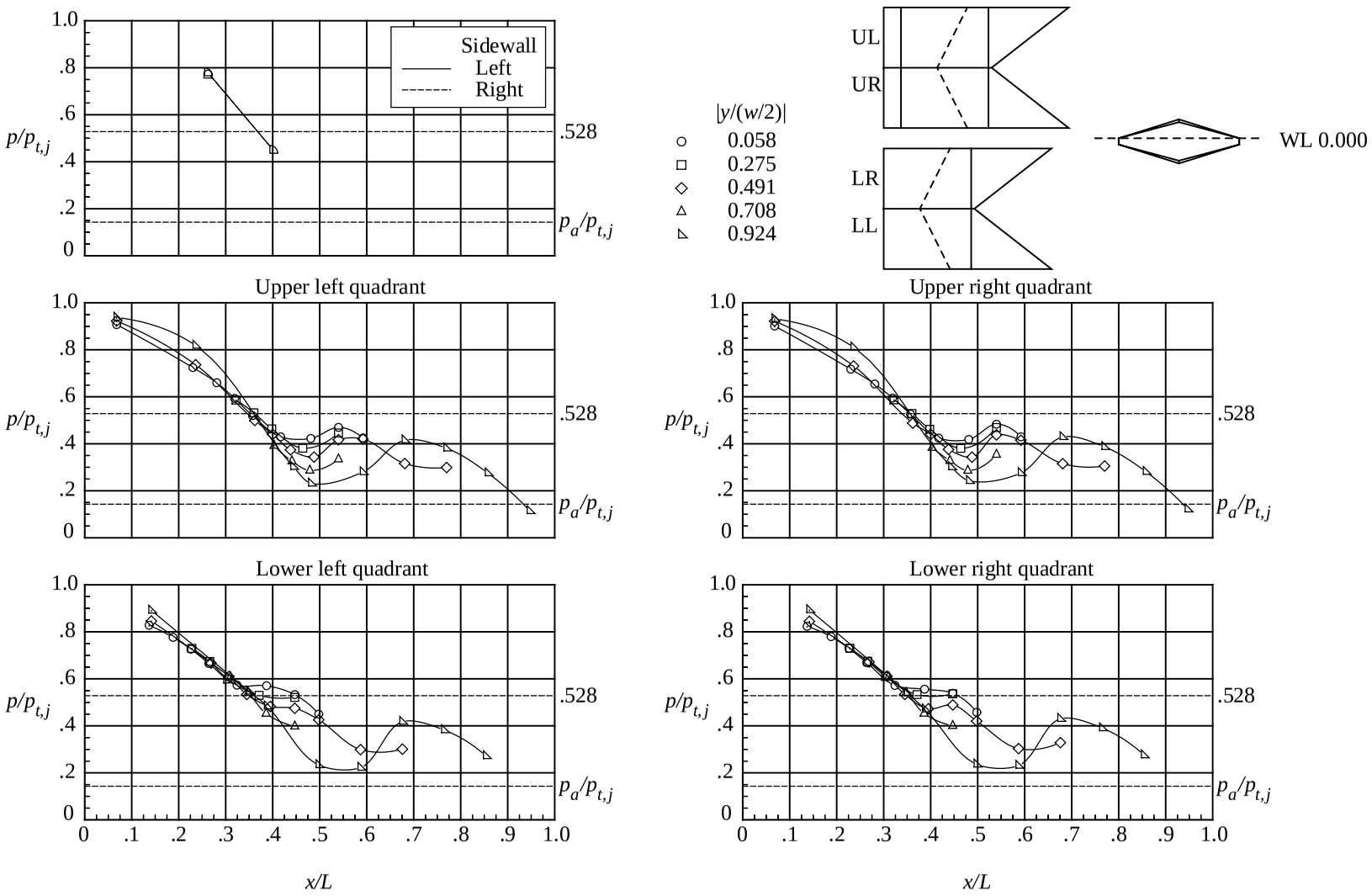

Figure 24. Internal static pressure distributions for configuration 8 at NPR = 6.98. L = 7.875 in.; w = 5.130 in.

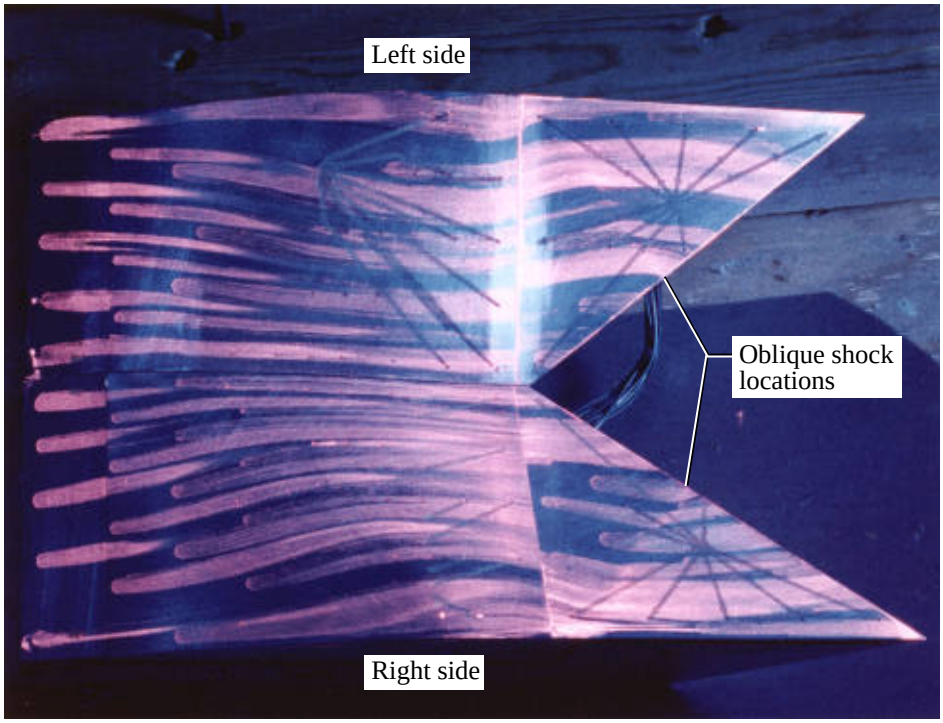

(a) Upper surface.

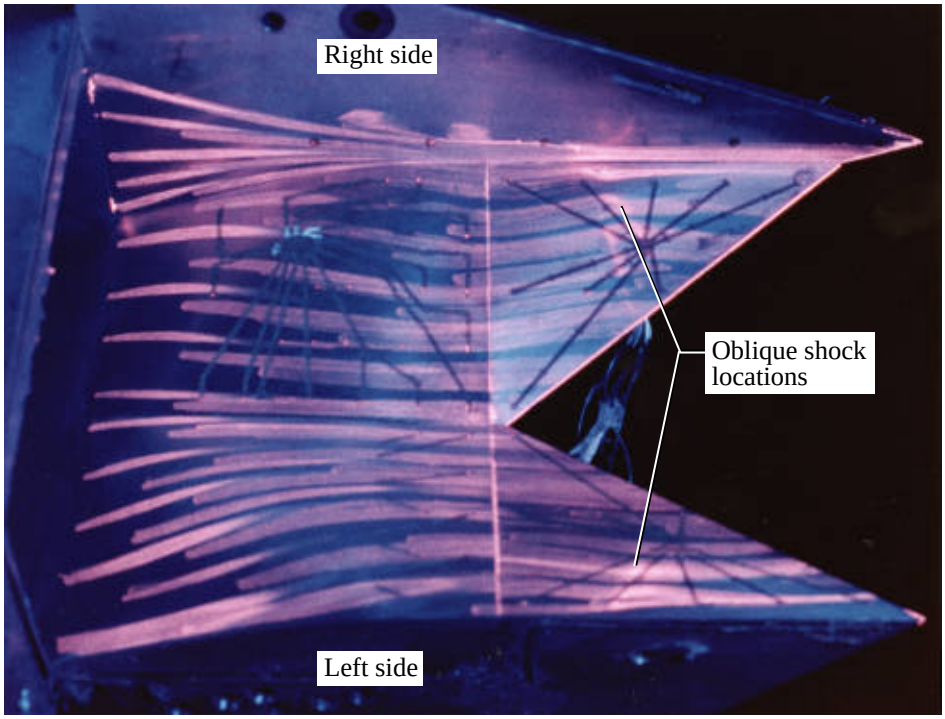

(b) Lower surface.

Figure 25. Oil flow visualization photographs of configuration 8 at NPR = 8.

Configuration	I_{ul}	I_{ur}	I_{ll}	I_{lr}	D_u	D_l	T.E.	T.S.	I-F
3	3	3	3	3	Ext.	Ext.	a.h.	No	No
9	3	3	3	3	Ext.	Par.	a.h.	No	No
10	3	3	3	3	Ext.	Ret.	a.h.	No	No

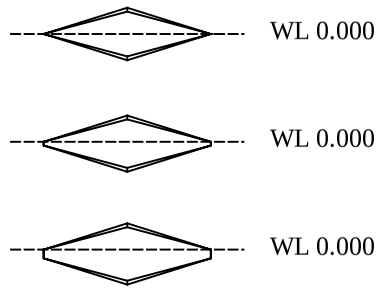

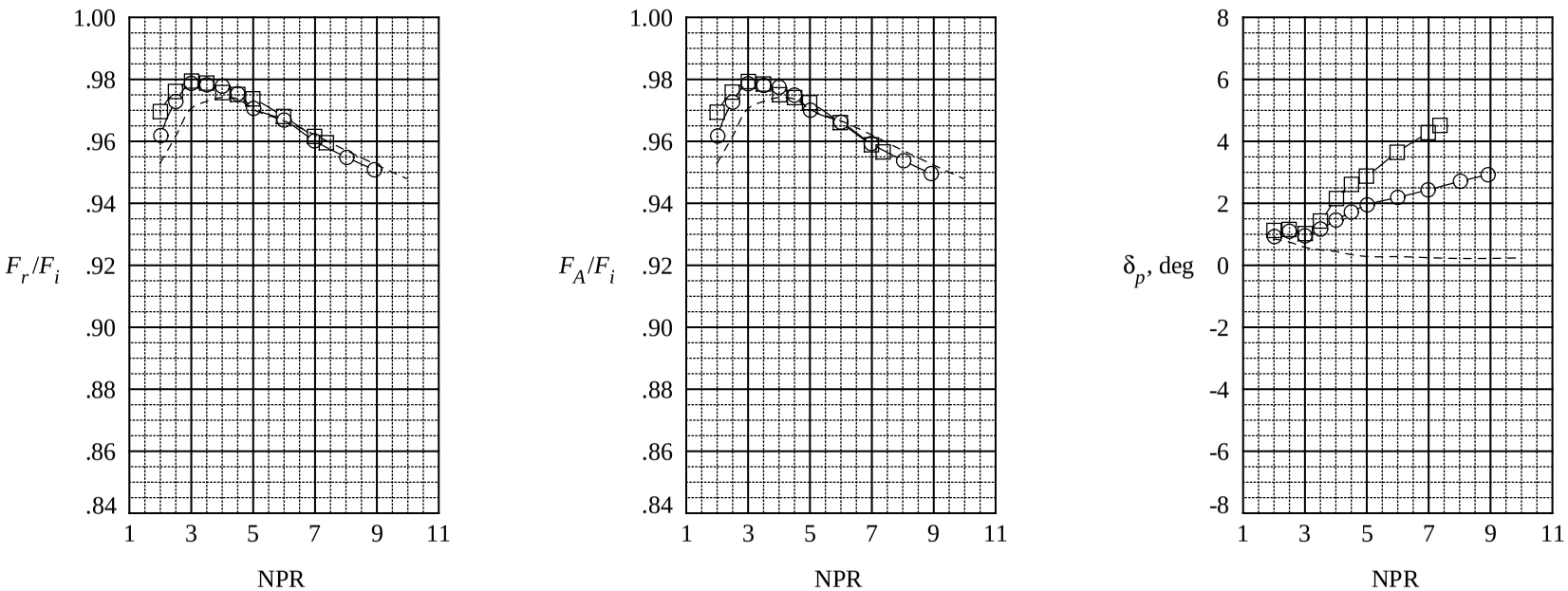

(a) Comparison with unvectored configuration.

Figure 26. Effect of drawer retraction on thrust and pitch thrust-vectoring performance of arrowhead nozzle configurations.

	Configuration	I_{ul}	I_{ur}	I_{ll}	I_{lr}	D_u	D_l	T.E.	T.S.	I-F
○	9	3	3	3	3	Ext.	Par.	a.h.	No	No
□	10	3	3	3	3	Ext.	Ret.	a.h.	No	No
●	7	3	3	3	3	Ext.	Par.	s.t.	No	No
■	8	3	3	3	3	Ext.	Ret.	s.t.	No	No

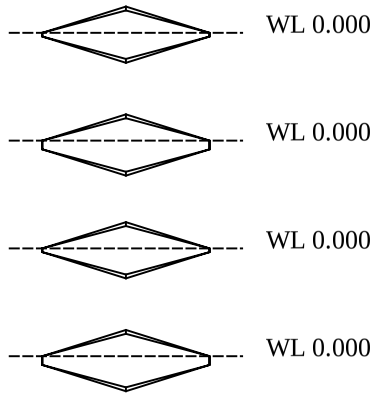

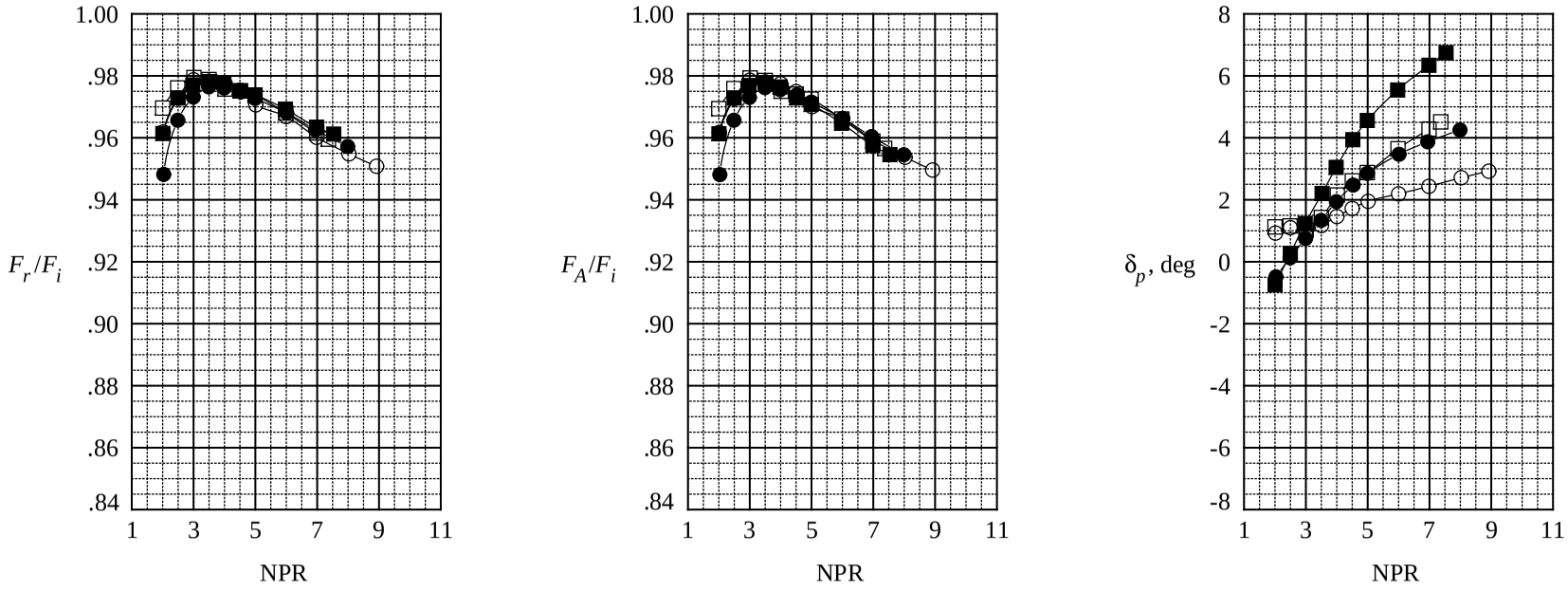

(b) Comparison with swallowtail configurations.

Figure 26. Concluded.

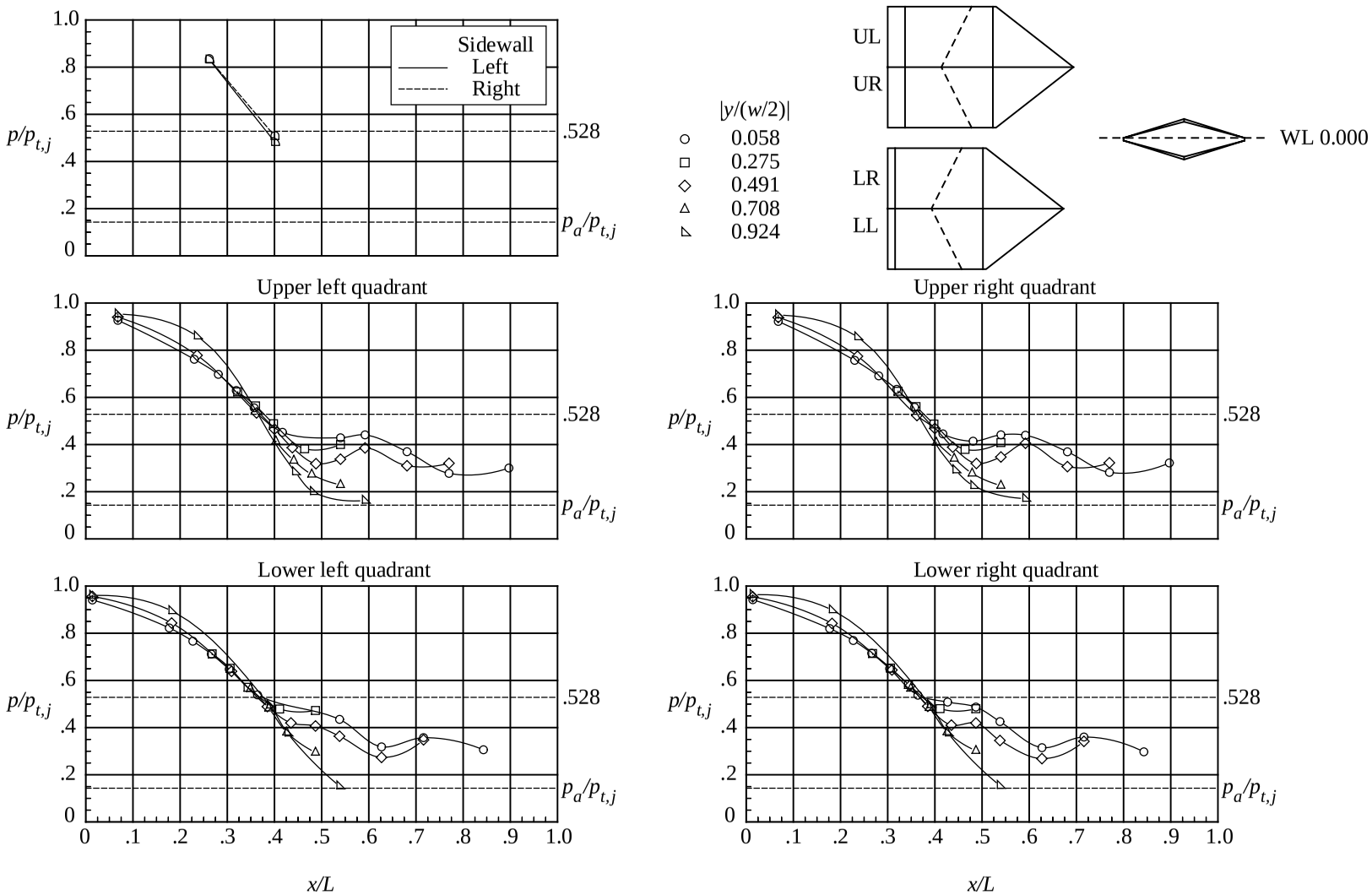

Figure 27. Internal static pressure distributions for configuration 9 at NPR = 6.98. L = 7.875 in.; w = 5.130 in.

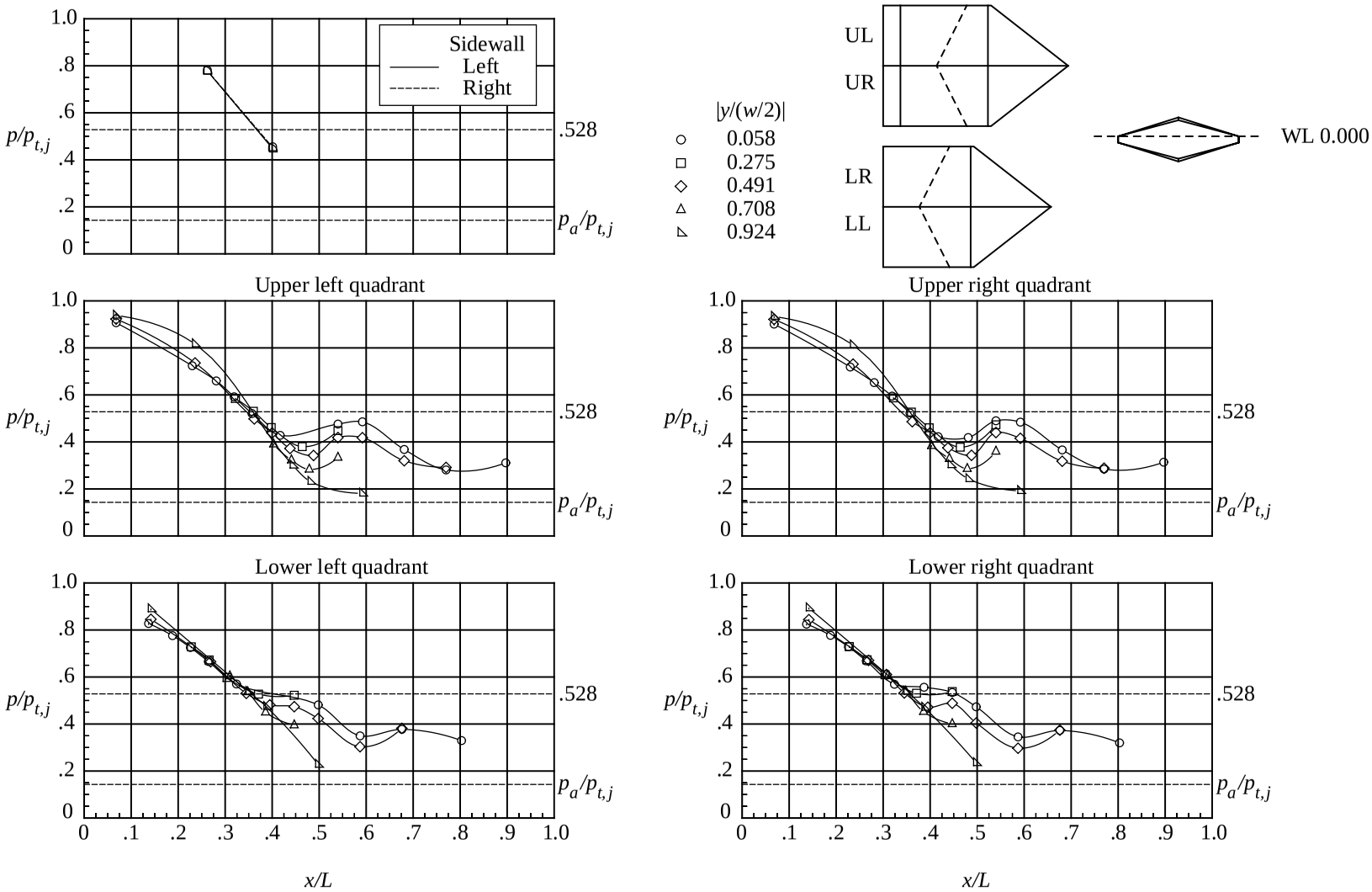

Figure 28. Internal static pressure distributions for configuration 10 at NPR = 6.99. L = 7.875 in.; w = 5.130 in.

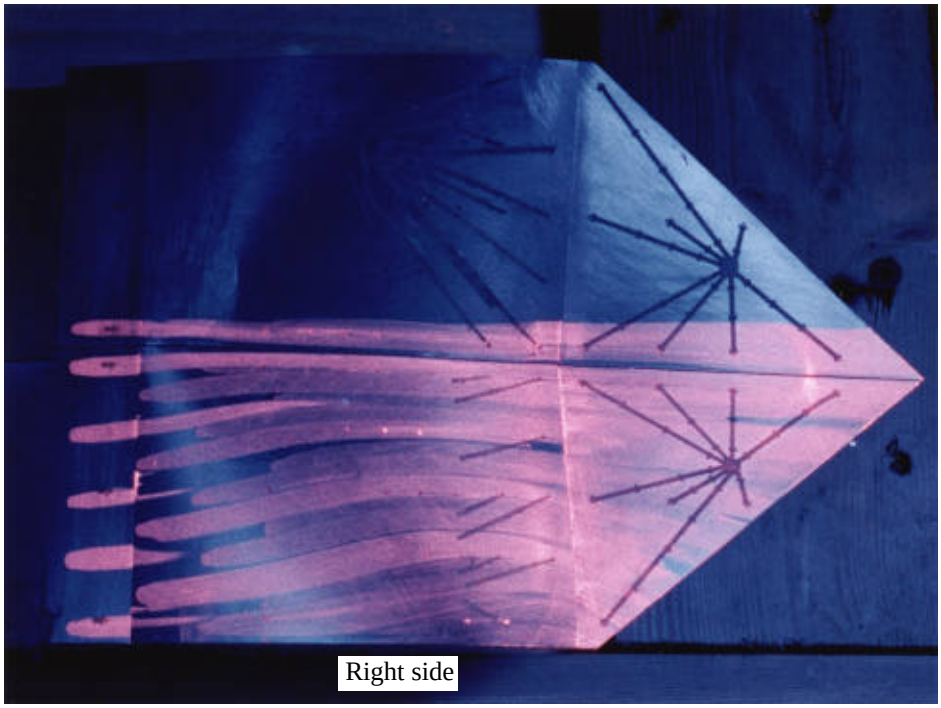

(a) Upper surface.

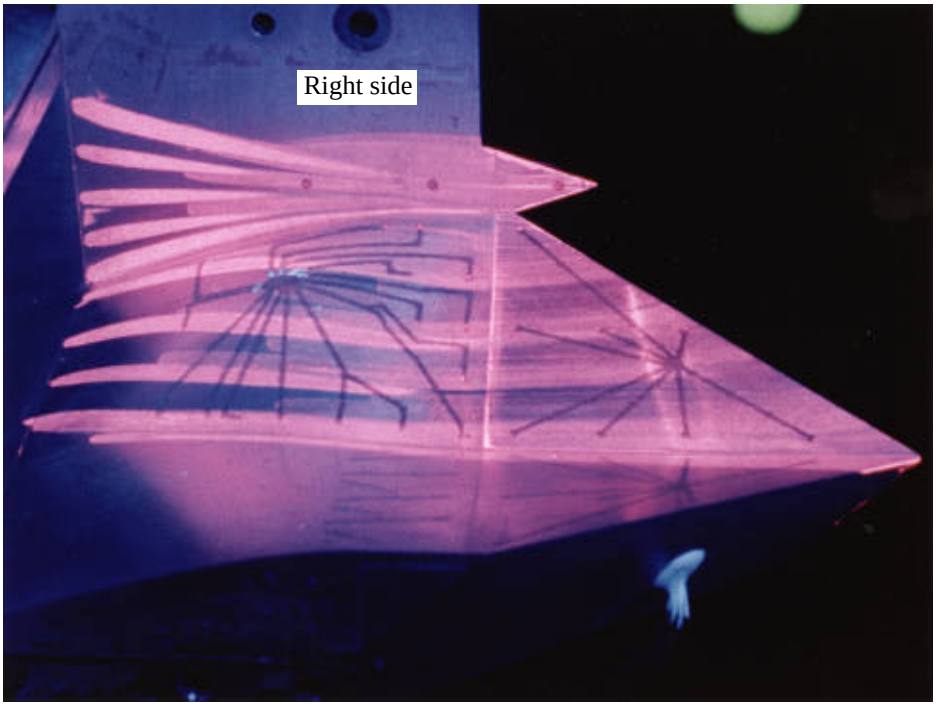

(b) Lower surface.

Figure 29. Oil flow visualization photographs of configuration 10 at NPR = 6.

Configuration	I_{ul}	I_{ur}	I_{ll}	I_{lr}	D_u	D_l	T.E.	T.S.	I-F
1	3	3	3	3	Ext.	Ext.	s.t.	No	No
11	5	1	5	1	Ext.	Ext.	s.t.	No	No
12	5	1	5	1	Ext.	Ext.	s.t.	Yes	No
11-I	5	1	5	1	Ext.	Ext.	s.t.	No	Yes
12-I	5	1	5	1	Ext.	Ext.	s.t.	Yes	Yes

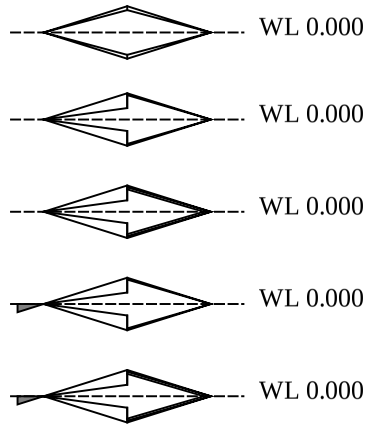

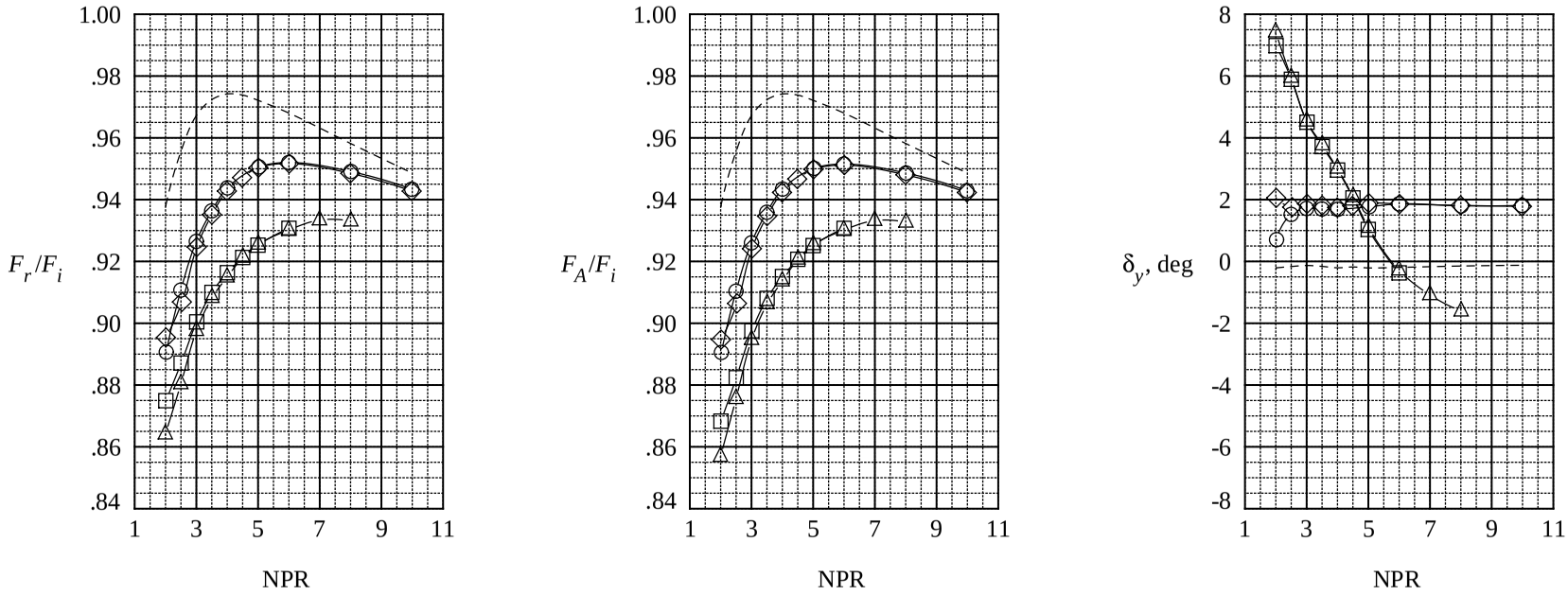

Figure 30. Effect of interfairing and throat ridge on internal thrust and yaw thrust-vectoring performance of swallowtail nozzle configurations.

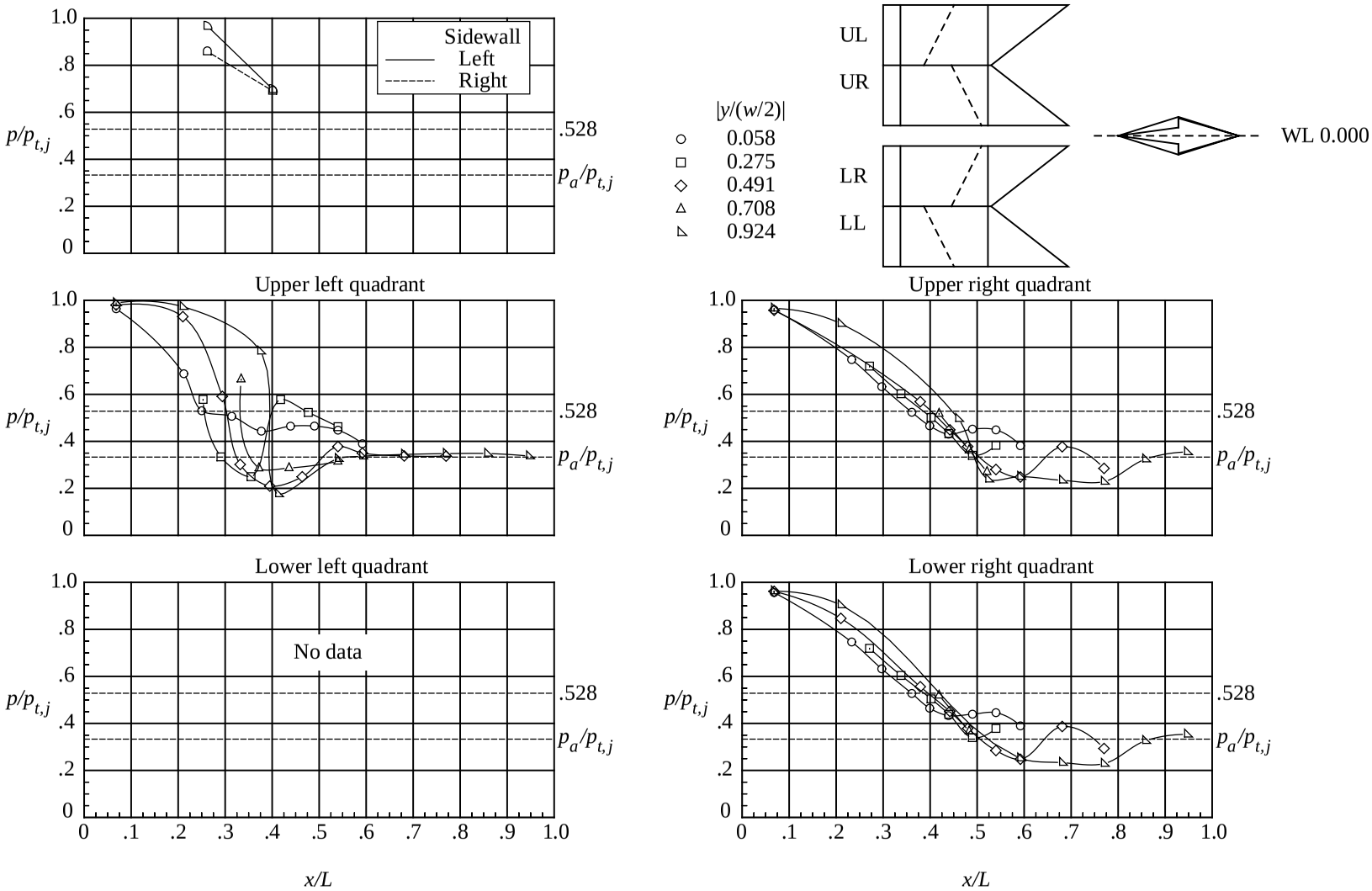

(a) NPR = 3.00.

Figure 31. Internal static pressure distributions for configuration 11. L = 7.875 in.; w = 5.130 in.

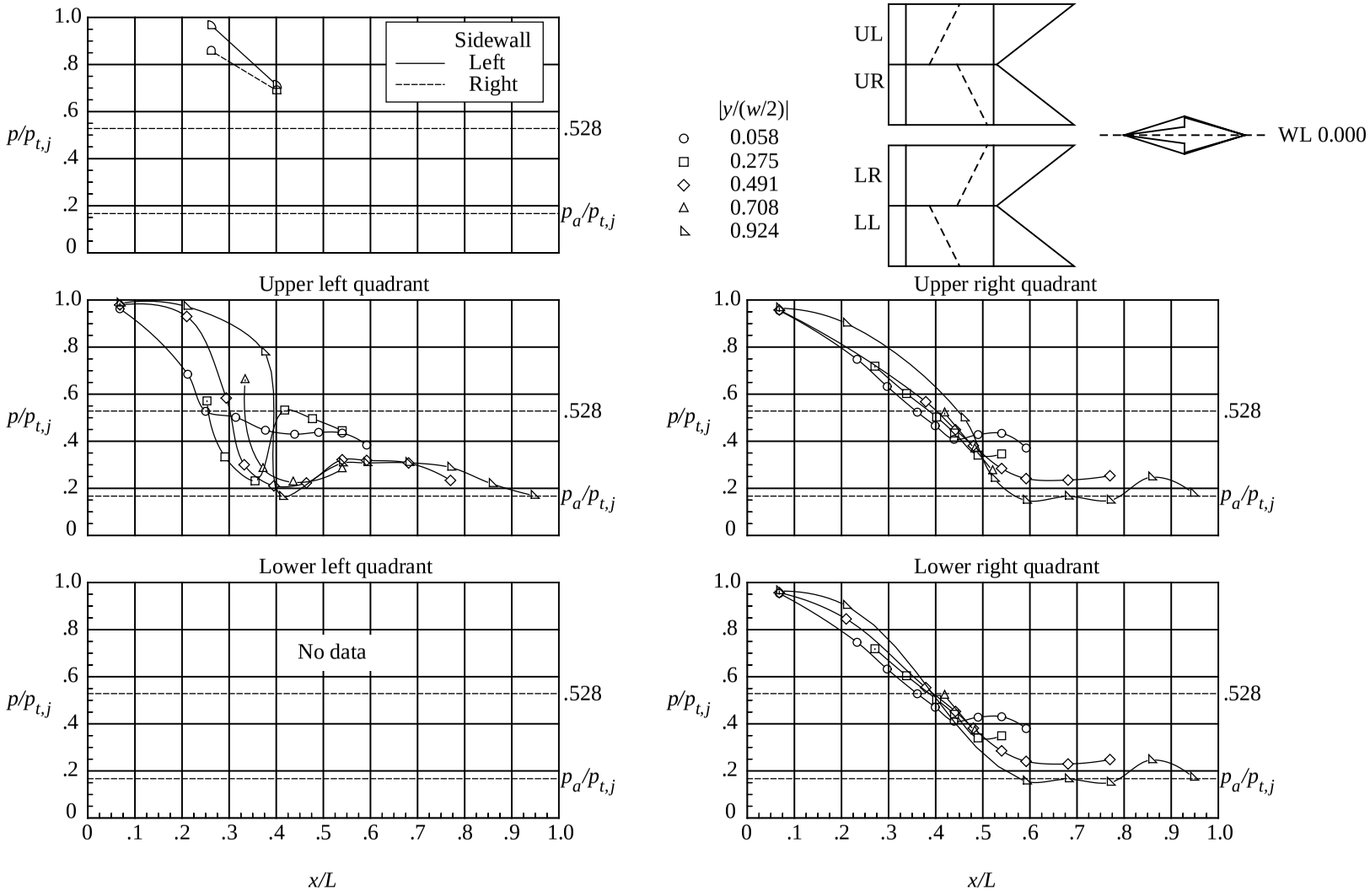

(b) NPR = 5.99.

Figure 31. Concluded.

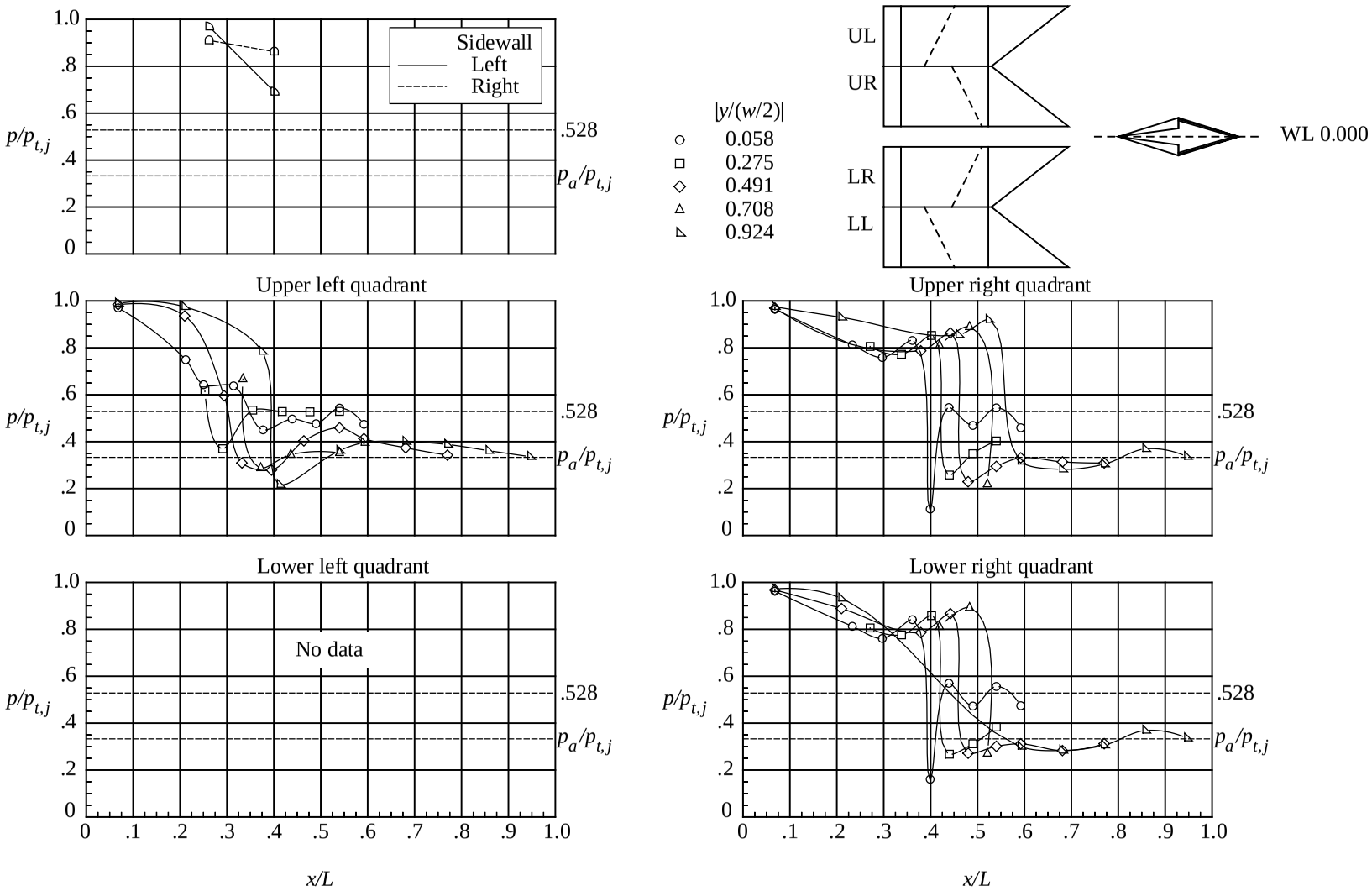

(a) NPR = 3.01.

Figure 32. Internal static pressure distributions for configuration 12. L = 7.875 in.; w = 5.130 in.

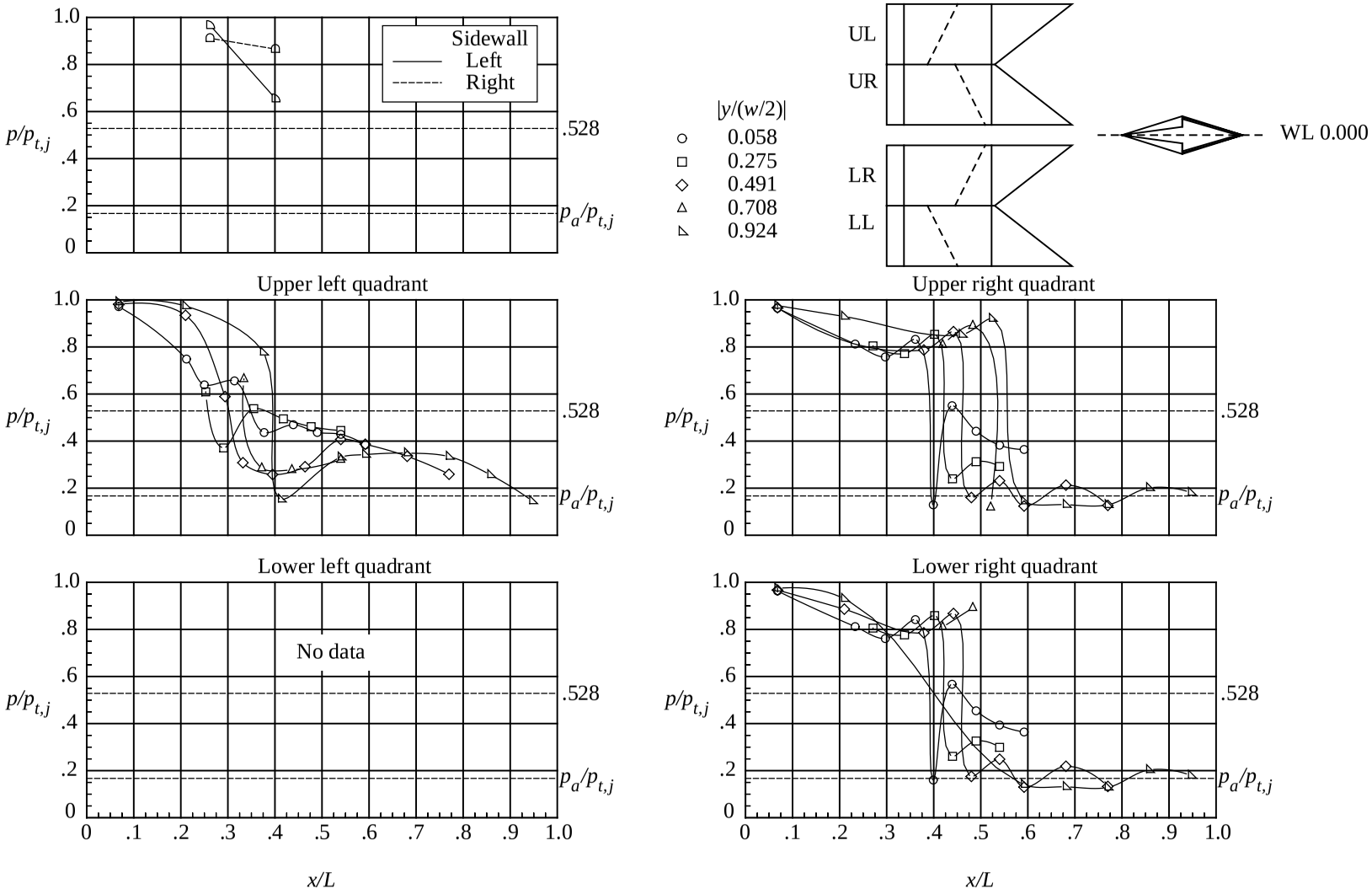

(b) NPR = 6.00.

Figure 32. Concluded.

Configuration	I_{ul}	I_{ur}	I_{ll}	I_{lr}	D_u	D_l	T.E.	T.S.	I-F	
1	3	3	3	3	Ext.	Ext.	s.t.	No	No	WL 0.000
13	4	2	4	2	Ext.	Ext.	s.t.	Yes	No	WL 0.000
14	4	1	4	1	Ext.	Ext.	s.t.	Yes	No	WL 0.000
12	5	1	5	1	Ext.	Ext.	s.t.	Yes	No	WL 0.000

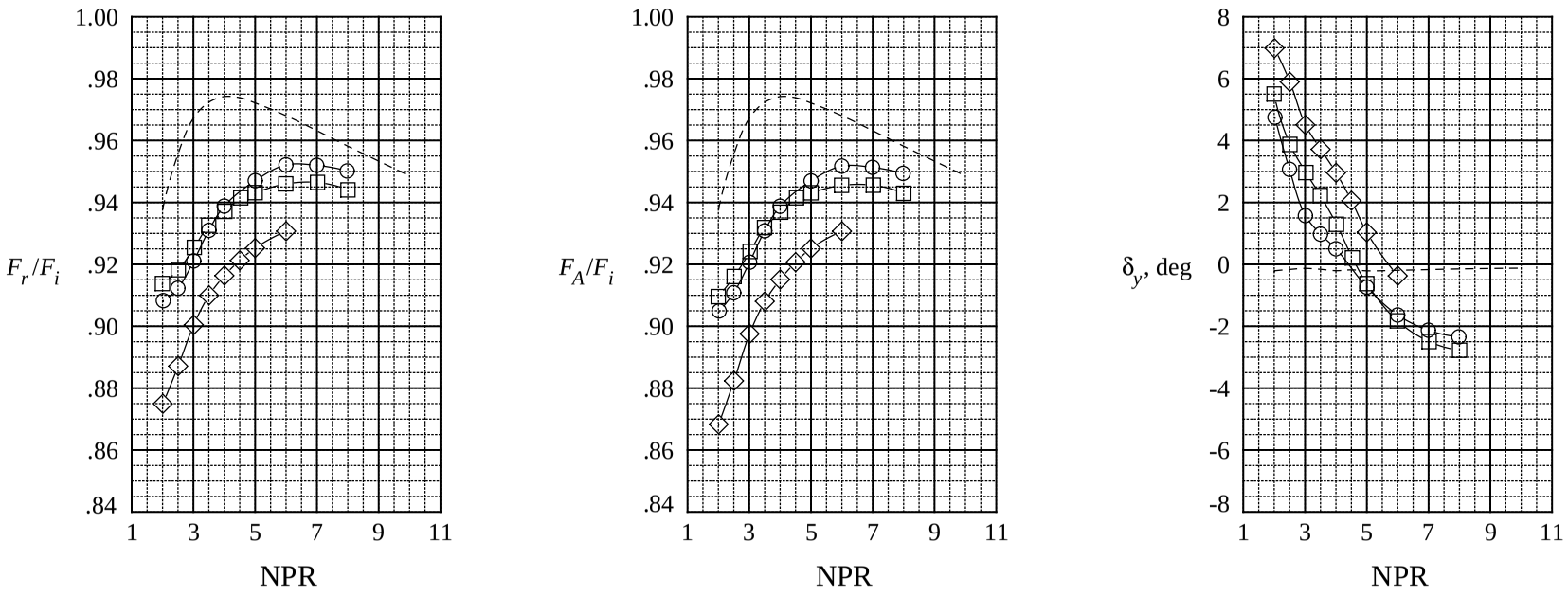

Figure 33. Effect of throat geometry on internal thrust and yaw thrust-vectoring performance of swallowtail nozzle configurations.

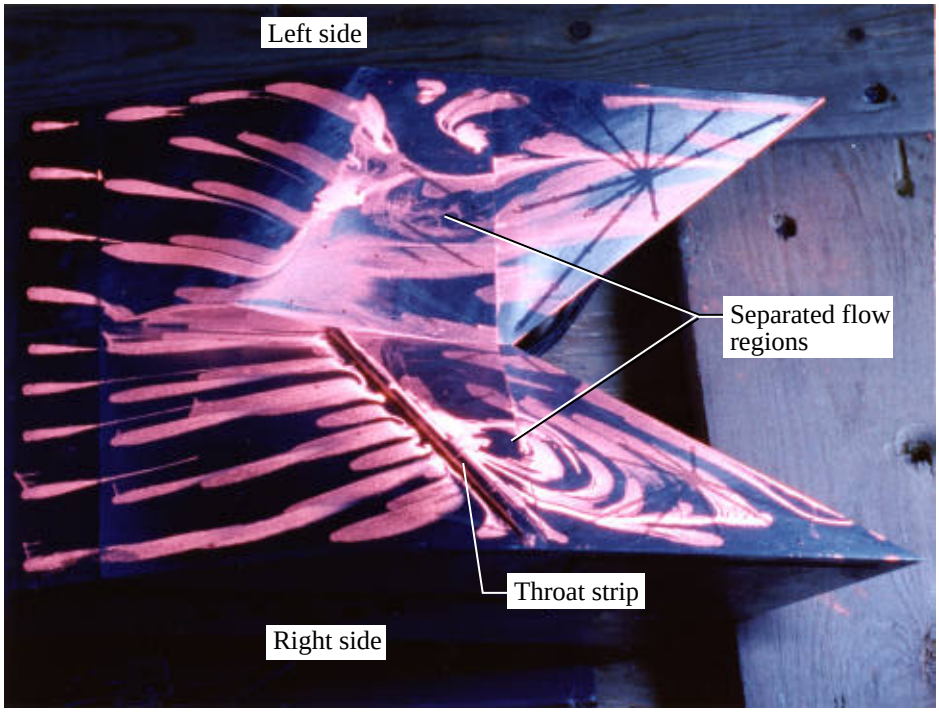

(a) Upper surface.

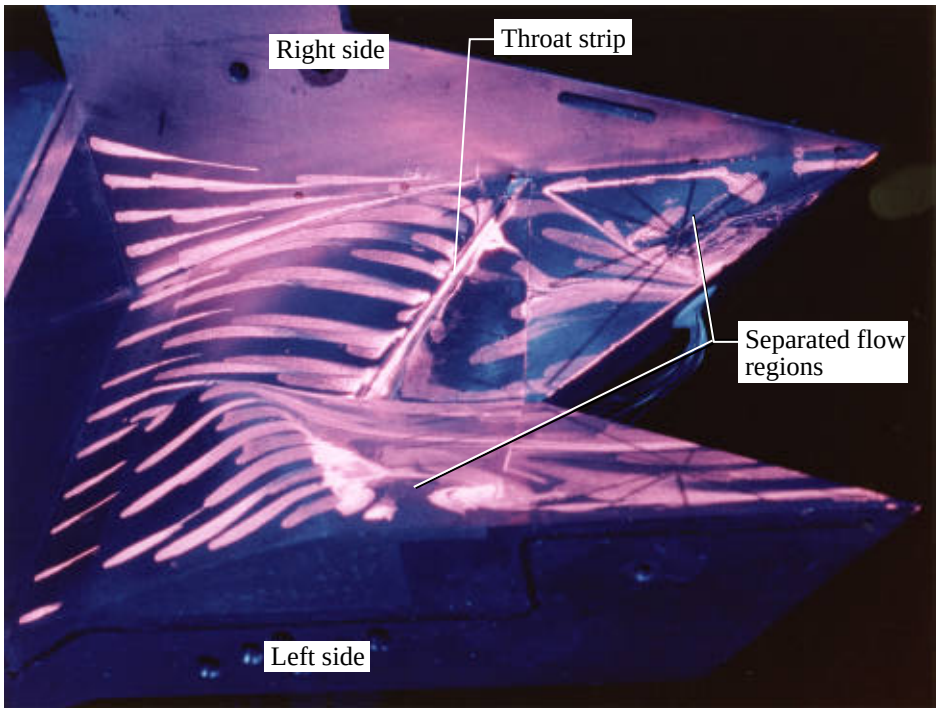

(b) Lower surface.

Figure 34. Oil flow visualization photographs of configuration 12 at NPR = 3.

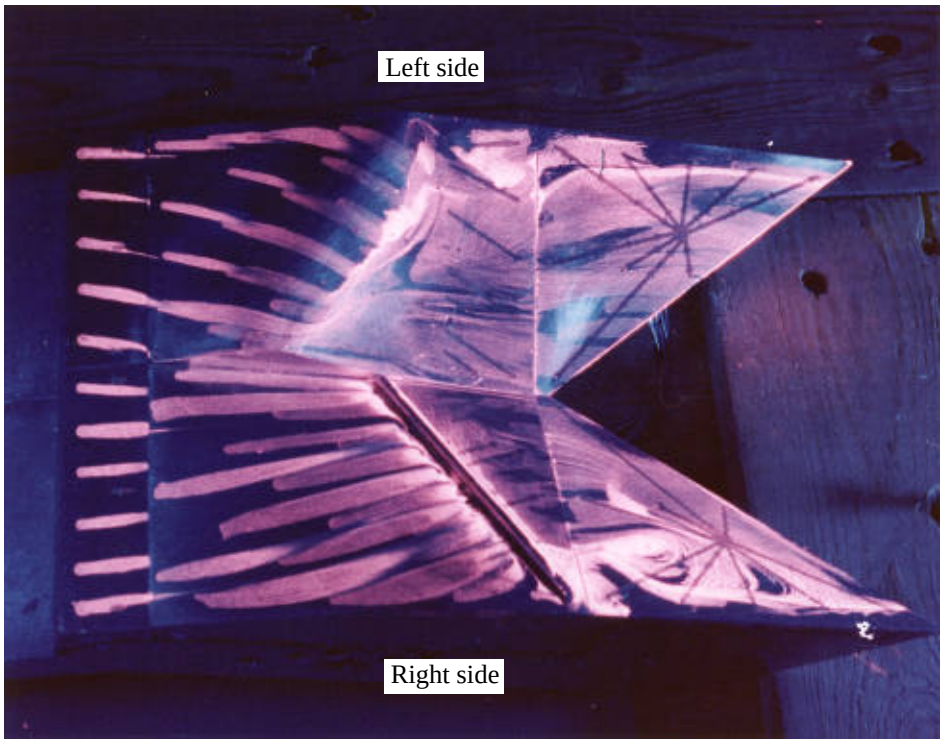

(a) Upper surface.

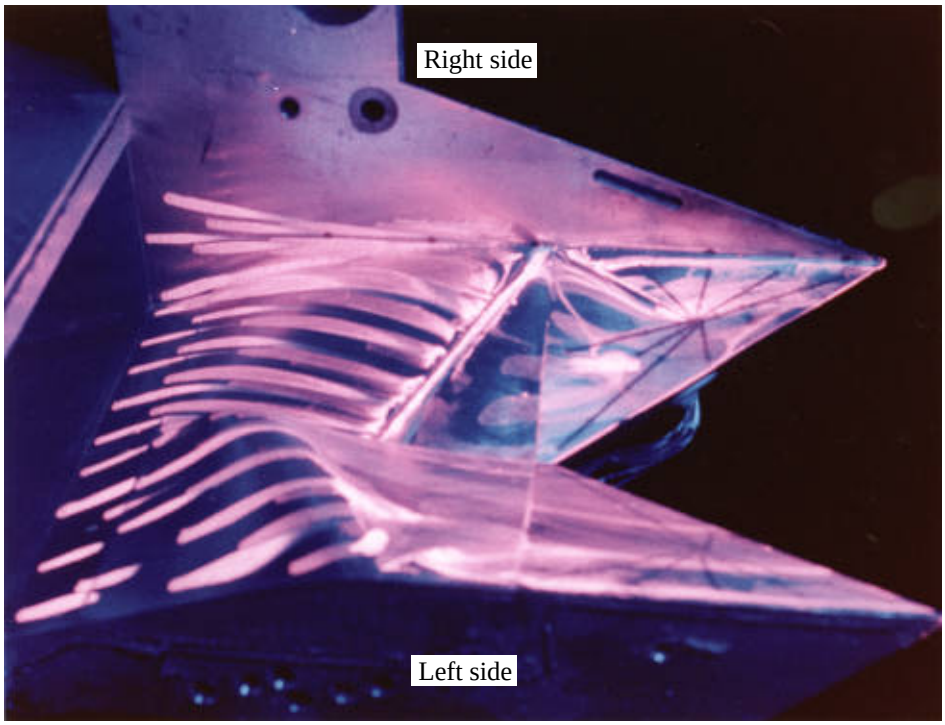

(b) Lower surface.

Figure 35. Oil flow visualization photographs of configuration 12 at NPR = 6.

Configuration	I_{ul}	I_{ur}	I_{ll}	I_{lr}	D_u	D_l	T.E.	T.S.	I-F	
3	3	3	3	3	Ext.	Ext.	a.h.	No	No	WL 0.000
15	4	1	4	1	Ext.	Ext.	a.h.	Yes	No	WL 0.000
16	5	1	5	1	Ext.	Ext.	a.h.	Yes	No	WL 0.000
15-I	4	1	4	1	Ext.	Ext.	a.h.	Yes	Yes	WL 0.000
16-I	5	1	5	1	Ext.	Ext.	a.h.	Yes	Yes	WL 0.000

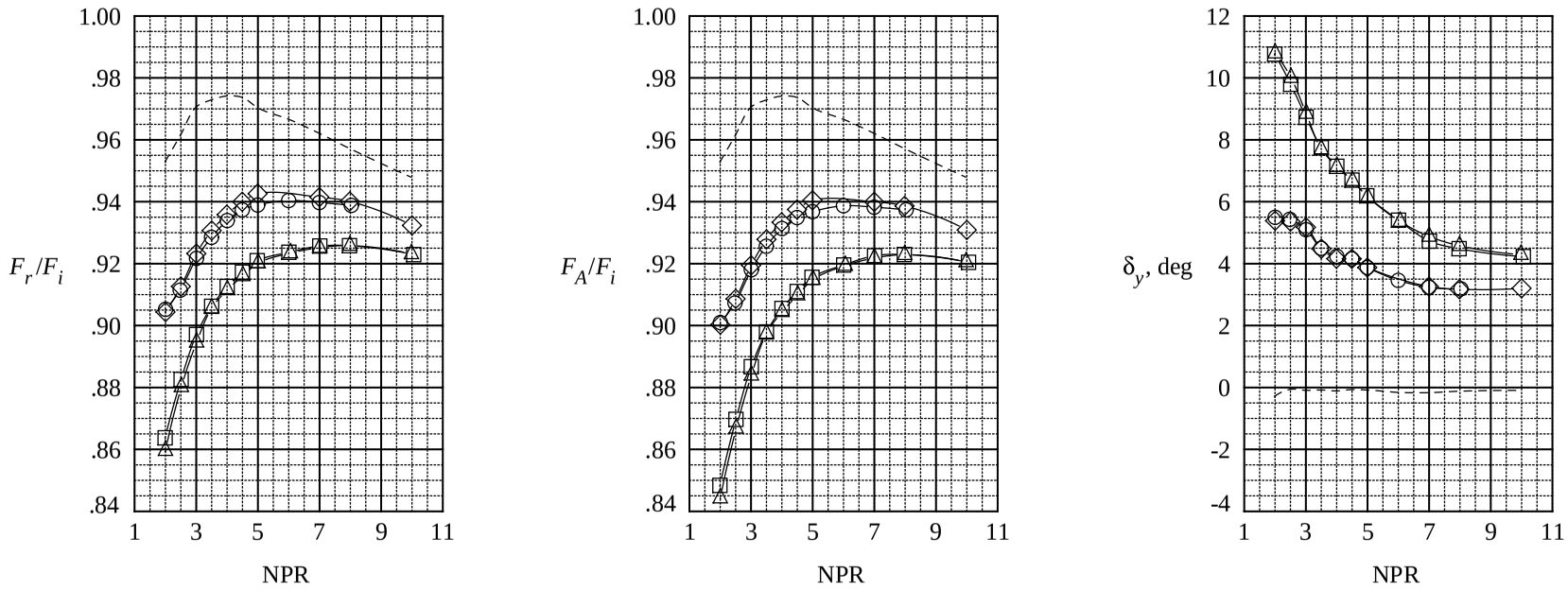

(a) Comparison with unvectored configuration.

Figure 36. Effect of interfairing and throat ridge on internal thrust and yaw thrust-vectoring performance of arrowhead nozzle configurations.

	Configuration	I_{ul}	I_{ur}	I_{ll}	I_{lr}	D_u	D_l	T.E.	T.S.	I-F	
○	15	4	1	4	1	Ext.	Ext.	a.h.	Yes	No	WL 0.000
□	16	5	1	5	1	Ext.	Ext.	a.h.	Yes	No	WL 0.000
●	14	4	1	4	1	Ext.	Ext.	s.t.	Yes	No	WL 0.000
■	12	5	1	5	1	Ext.	Ext.	s.t.	Yes	No	WL 0.000

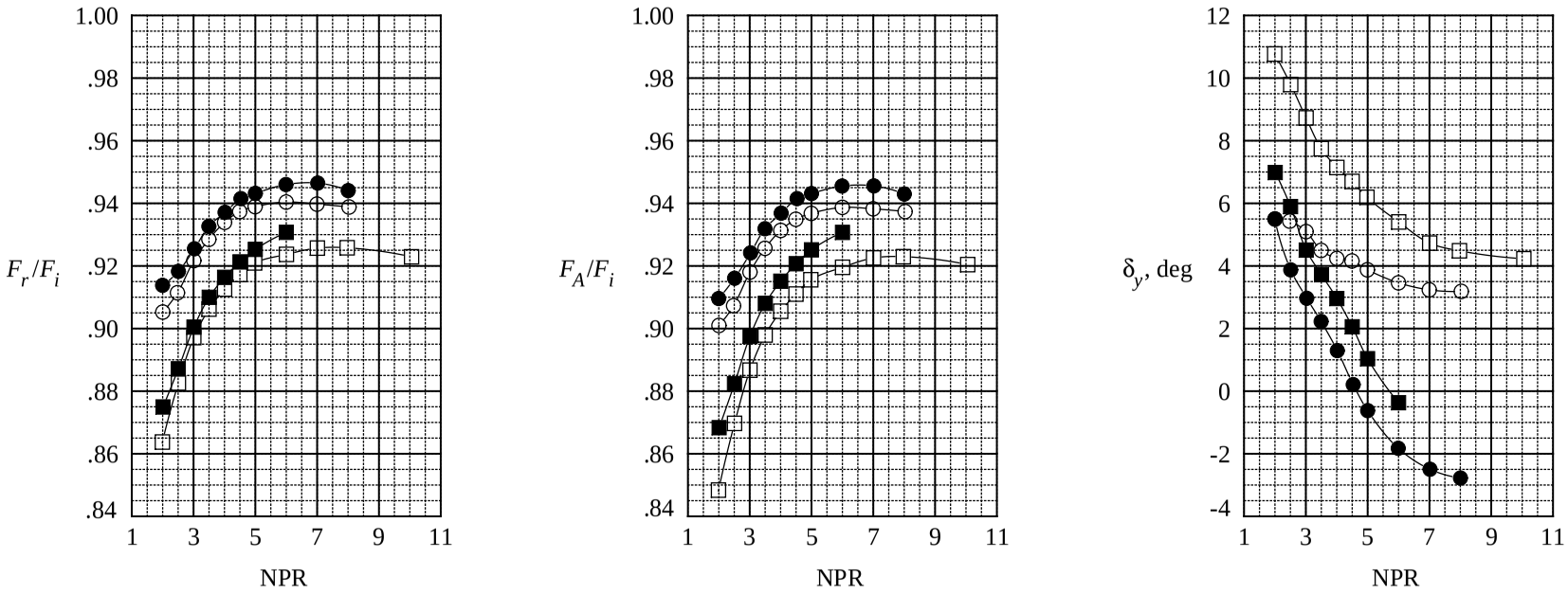

(b) Comparison with swallowtail configurations.

Figure 36. Concluded.

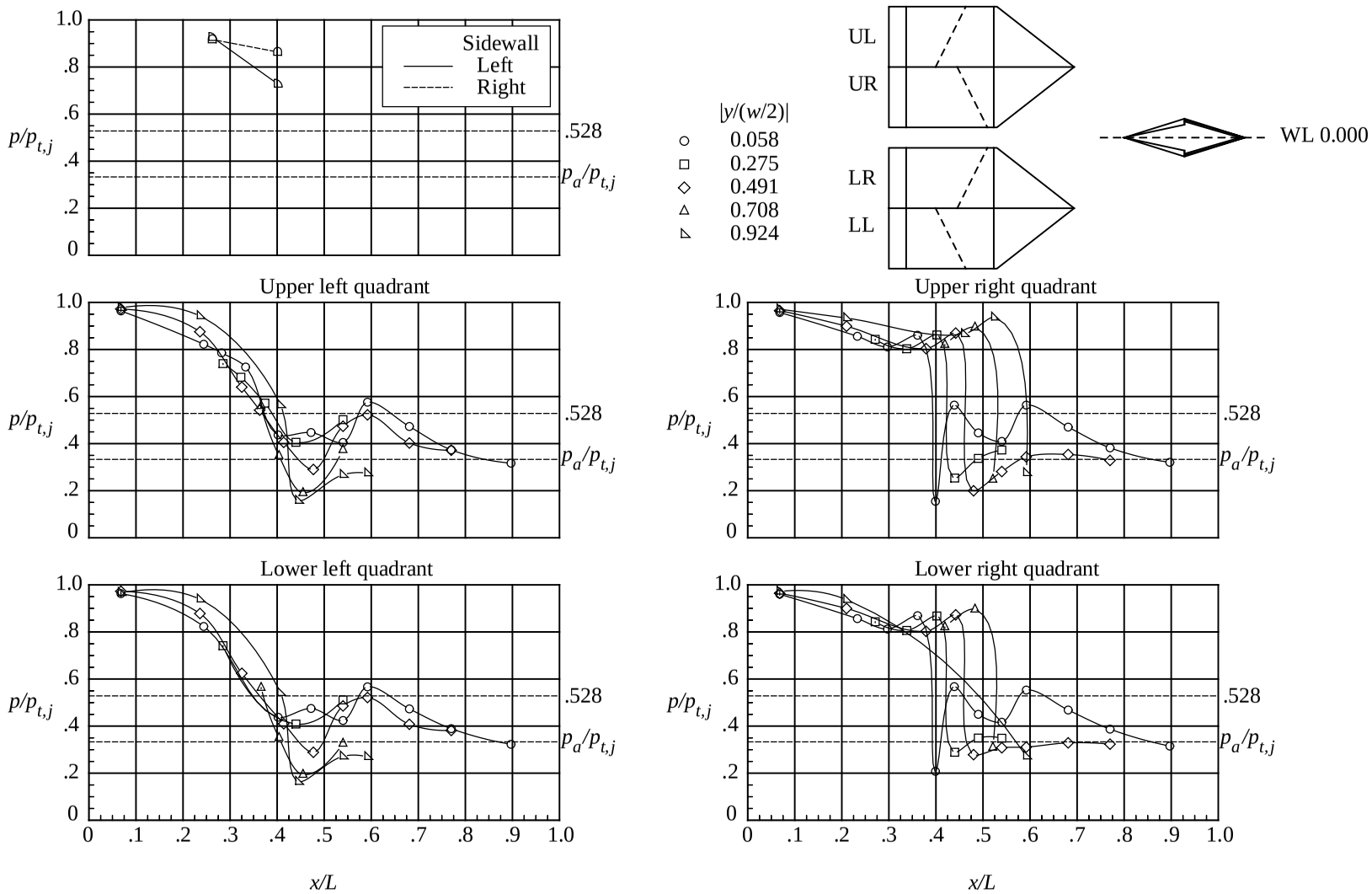

Figure 37. Internal static pressure distributions for configuration 15 at NPR = 3.01. L = 7.875 in.; w = 5.130 in.

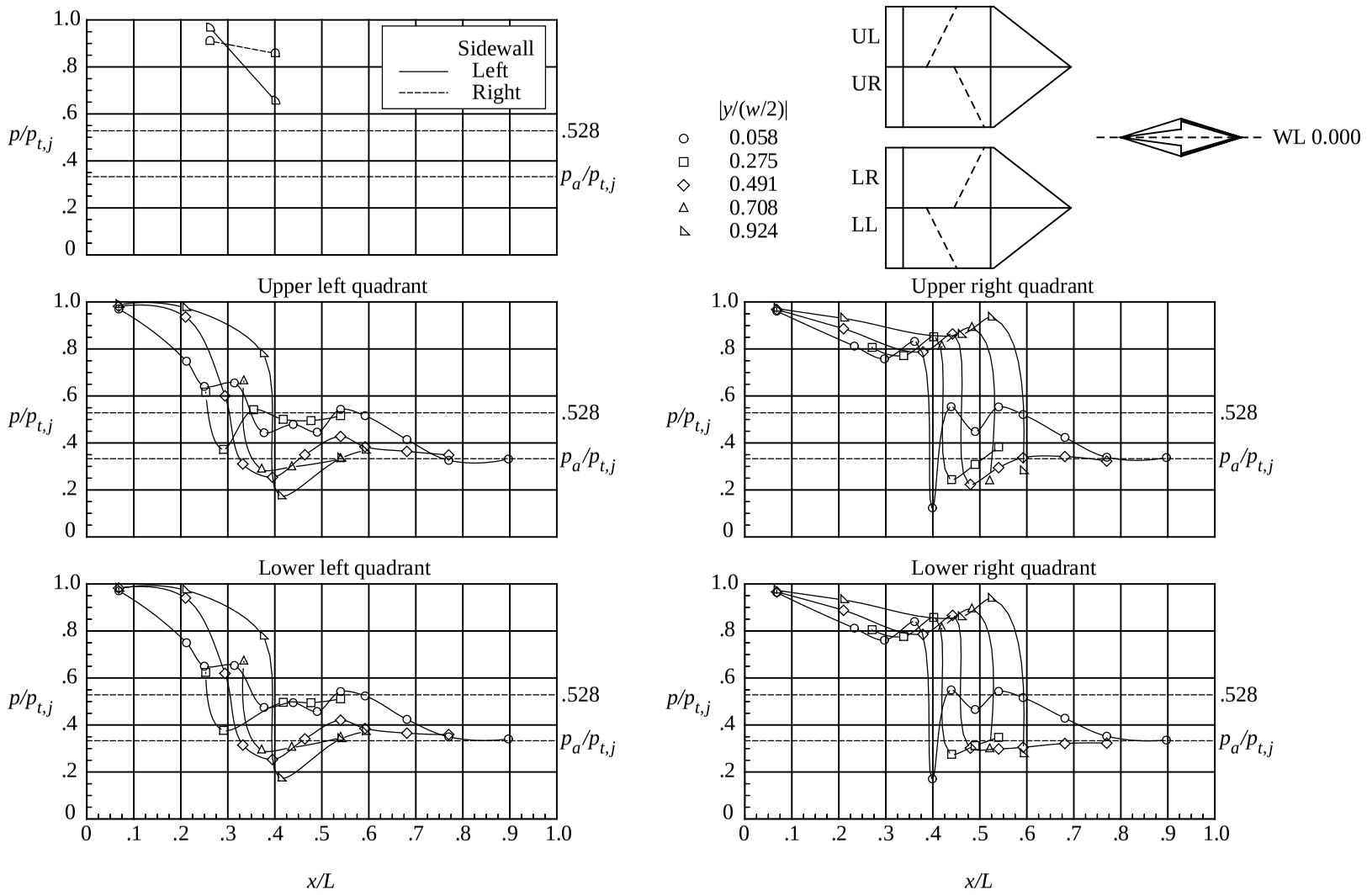

Figure 38. Internal static pressure distributions for configuration 16 at NPR = 3.01. L = 7.875 in.; w = 5.130 in.

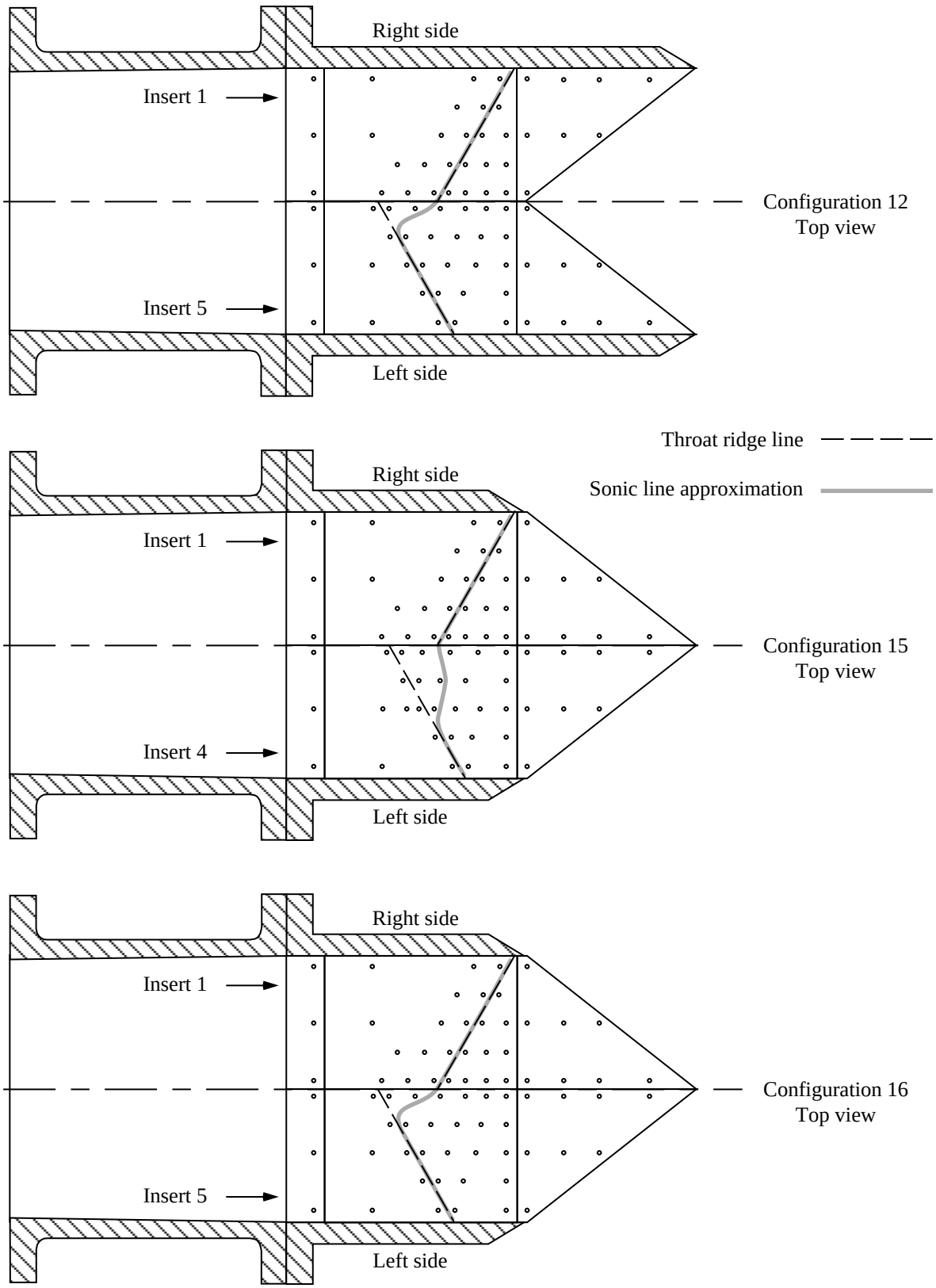

Figure 39. Approximate location of sonic line for configurations 12, 15, and 16 at NPR = 3.01. Actual pressure orifice locations for each configuration shown.

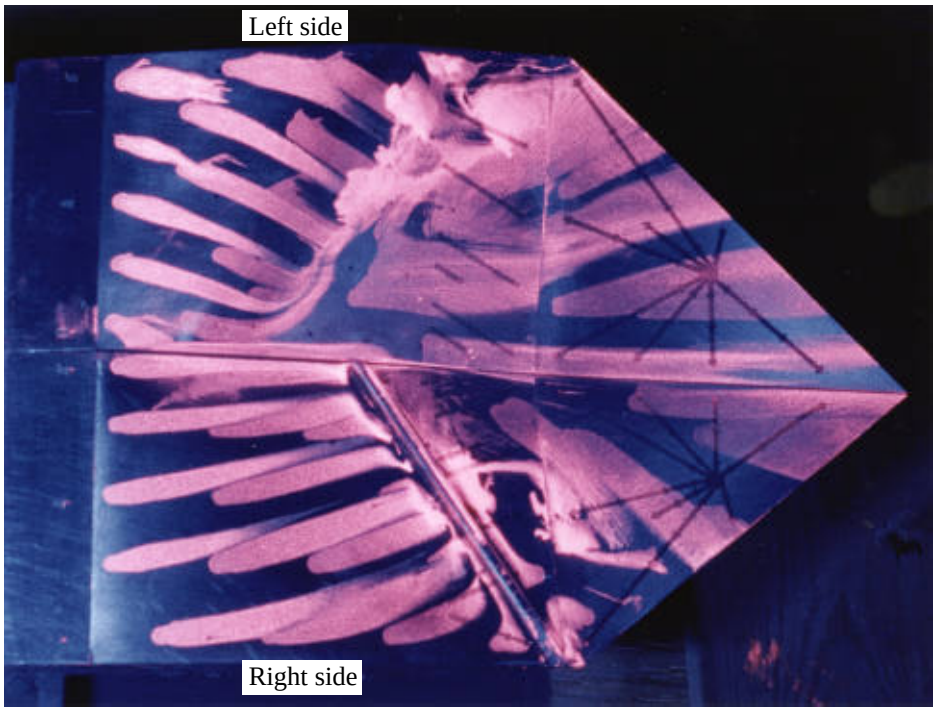

(a) Upper surface.

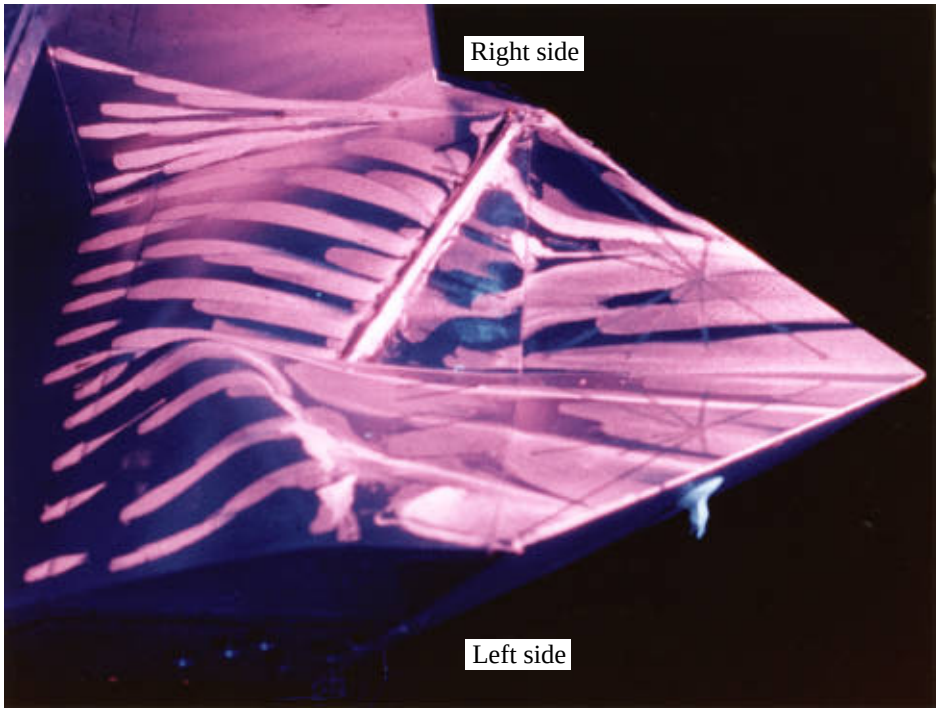

(b) Lower surface.

Figure 40. Oil flow visualization photographs of configuration 16 at NPR = 3.

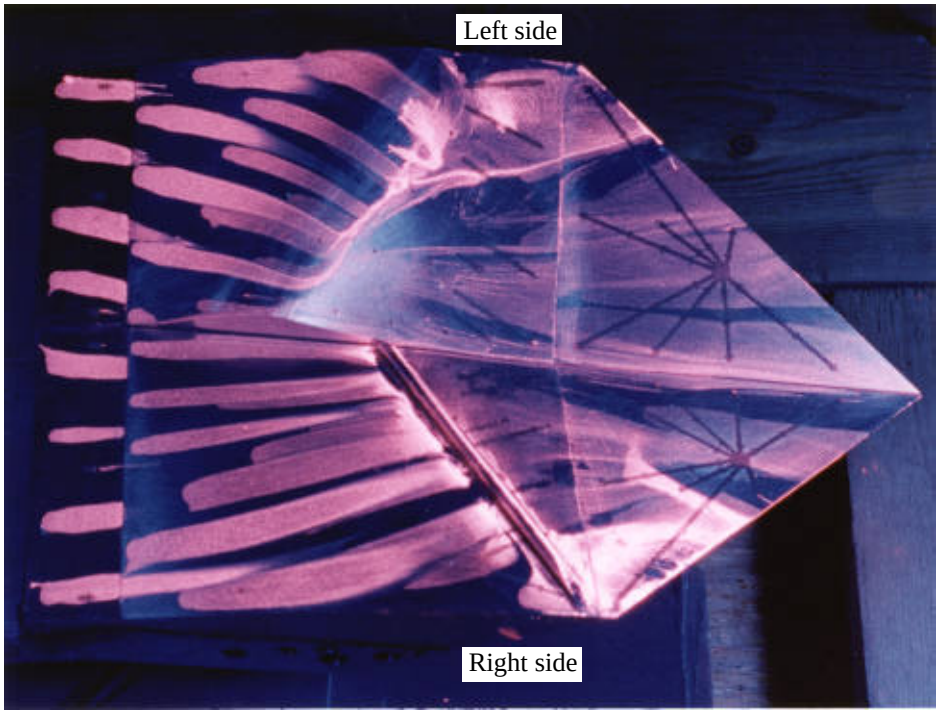

(a) Upper surface.

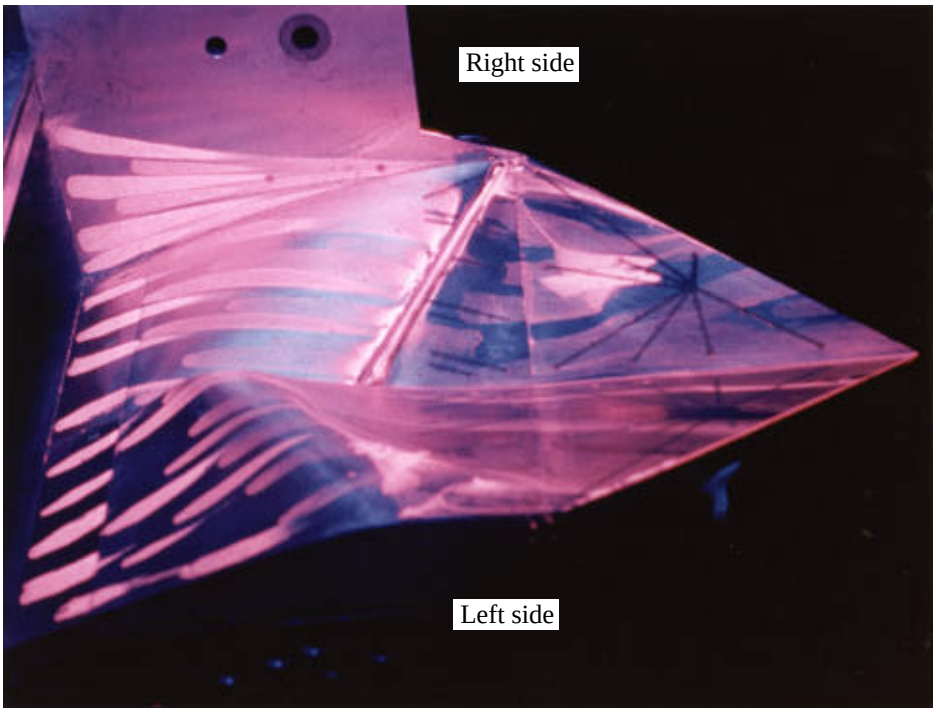

(b) Lower surface.

Figure 41. Oil flow visualization photographs of configuration 16 at NPR = 6.

REPORT DOCUMENTATION PAGE

Form Approved
OMB No. 0704-0188

1. AGENCY USE ONLY *(Leave blank)*

2. REPORT DATE
June 1997

3. REPORT TYPE AND DATES COVERED
Technical Paper

4. TITLE AND SUBTITLE
Static Investigation of a Multiaxis Thrust-Vectoring Nozzle With Variable Internal Contouring Ability

5. FUNDING NUMBERS
WU 505-59-30-24

6. AUTHOR(S)
David J. Wing, Charles T. L. Mills, and Mary L. Mason

7. PERFORMING ORGANIZATION NAME(S) AND ADDRESS(ES)
NASA Langley Research Center
Hampton, VA 23681-0001

8. PERFORMING ORGANIZATION REPORT NUMBER
L-17570

9. SPONSORING/MONITORING AGENCY NAME(S) AND ADDRESS(ES)
National Aeronautics and Space Administration
Washington, DC 20546-0001

10. SPONSORING/MONITORING AGENCY REPORT NUMBER
NASA TP-3628

11. SUPPLEMENTARY NOTES

12a. DISTRIBUTION/AVAILABILITY STATEMENT
Unclassified–Unlimited
Subject Category 02
Availability: NASA CASI (301) 621-0390

12b. DISTRIBUTION CODE

13. ABSTRACT *(Maximum 200 words)*
The thrust efficiency and vectoring performance of a convergent-divergent nozzle were investigated at static conditions in the model preparation area of the Langley 16-Foot Transonic Tunnel. The diamond-shaped nozzle was capable of varying the internal contour of each quadrant individually by using cam mechanisms and retractable drawers to produce pitch and yaw thrust vectoring. Pitch thrust vectoring was achieved by either retracting the lower drawers to incline the throat or varying the internal flow-path contours to incline the throat. Yaw thrust vectoring was achieved by reducing flow area left of the nozzle centerline and increasing flow area right of the nozzle centerline; a skewed throat deflected the flow in the lateral direction.

14. SUBJECT TERMS
Nozzle; Multiaxis thrust vectoring; Variable internal contour

15. NUMBER OF PAGES
147

16. PRICE CODE
A07

17. SECURITY CLASSIFICATION OF REPORT
Unclassified

18. SECURITY CLASSIFICATION OF THIS PAGE
Unclassified

19. SECURITY CLASSIFICATION OF ABSTRACT
Unclassified

20. LIMITATION OF ABSTRACT